1973

Studies Of Symmetrical And Asymmetrical Viscous Flows Past Impulsively Started Cylinders

Andrew Nigel Staniforth

CANADA

NATIONAL LIBRARY OF CANADA

CANADIAN THESES ON MICROFILM

BIBLIOTHÈQUE NATIONALE DU CANADA

THÈSES CANADIENNES SUR MICROFILM

NL-101(1/66)

STUDIES OF SYMMETRICAL AND ASYMMETRICAL VISCOUS FLOWS PAST IMPULSIVELY STARTED CYLINDERS

by

Andrew Nigel Staniforth
Department of Applied Mathematics

Submitted in partial fulfillment
of the requirements for the degree of
Doctor of Philosophy

Faculty of Graduate Studies
The University of Western Ontario
London, Canada
September 1972

ABSTRACT

This work concerns itself with the initial flow of a viscous incompressible fluid relative to a conformally-mappable cylinder which is impulsively started, and continues to move, with uniform velocity in a direction perpendicular to its axis. Two approaches for solving this class of problem are given, one semi-analytical in nature, the other fully-numerical. Common to both methods is a boundary-layer transformation of the Navier-Stokes equation and the equation of continuity, formulated in terms of the stream function and the vorticity, which are assumed to govern the motion. This removes the time-singularity at time zero, the start of the motion, which is indicated by boundary-layer theory.

In the semi-analytical approach the Reynolds number dependence R is removed from the problem by expanding the dependent variables in powers of $R^{-\frac{1}{2}}$ and equating coefficients. A further expansion in powers of t (the time measured from the start of the motion) is then made to remove the t-dependence. The resulting spatial equations are then solved subject to the appropriate initial and boundary conditions.

It is thought that this approach shows a more general structure than that noted by previous investigations, by extending boundary-layer theory to the finite Reynolds number for the general case in a way in which arbitrarily many

additional terms may be obtained with sufficient labour. For the case of an elliptic cylinder, the equations resulting from the above expansions have been further expanded in order to remove the angular dependence. The resulting ordinary differential equations in the remaining spatial variable are then solved numerically. This enables one to numerically determine terms of higher order than those given analytically.

In the fully-numerical approach the governing equations are solved by a step-by-step procedure in time. For a circular cylinder results are given for R=100,500,1000,10^4 and ∞, where R is based on the diameter of the cylinder. Results are also given for an elliptic cylinder of aspect ratio 0.6 inclined at an angle of 15° to the free stream at Reynolds numbers of 5,000 and ∞. Here R is based on twice the distance from the foci . These results are compared with those given by the semi-analytical approach, good agreement being found until times past the time of initial separation.

This work indicates that the manner in which separation occurs differs according to the range into which the value of R falls. It is thought that the fully-numerical method could prove useful in providing a starting solution for calculating the subsequent flow at higher times in the natural coordinate system for lower Reynolds numbers, thus circumventing the difficulty of finding accurate solutions at early times.

ACKNOWLEDGEMENTS

I would like to thank Dr. S.C.R. Dennis for initially suggesting the topic of this thesis, and for his continued interest and guidance throughout the investigation. I would also like to thank Miss D. MacDonald for her careful typing of the thesis, and the Computing Centre at this University for its cooperation. Finally, I would like to express my thanks to my wife Maureen for her encouragement and understanding throughout this study, particularly the time-consuming parts.

TABLE OF CONTENTS

LIST OF FIGURES

Figure

CHAPTER I

MATHEMATICAL FORMULATION OF THE PHYSICAL PROBLEM

1.1 INTRODUCTION

The problem to be considered is that of the initial flow past a cylinder of infinite length, which is impulsively started from rest normal to its axis in an infinite, viscous, incompressible fluid. The Navier-Stokes equations, which mathematically describe these and other flows in terms of non-linear differential equations, were formulated in the middle of the last century, and they have been investigated ever since with varying degrees of success. The non-linearity of these equations makes their exact solution impossible for all but a few very special cases, and the development of the subject has largely been one of obtaining successively better approximations under certain simplifying assumptions.

In 1883, Reynolds enunciated his principle of similarity, which states that any two flows that are geometrically similar are also dynamically similar, and will exhibit the same principle features, provided the dimensionless Reynolds number $R = \frac{2Ud}{\nu}$ is the same for both. Here U is a characteristic velocity (often that of the free stream at infinity), d is a characteristic length (usually a dimension of the body being studied) and ν is the coefficient of kinematic viscosity, a measure of the frictional effect of the fluid. This principle

is a consequence of the governing equations, and by solving them for a particular value of R, we are in fact solving all flows of that geometry having this value of R.

An immediate consequence of Reynolds principle of similarity is that the total force on a body immersed in a fluid can be characterised completely by two dimensionless coefficients, which are functions of R only, these being C_D and C_L, the drag and lift coefficients respectively. This property and the general principle enable scale models to be built and tested that will accurately predict the performance of the actual flow, minimising the possibility of building a costly prototype that fails to meet expectations. Aircraft design is an excellent example of its application to design problems.

It can be shown that the Reynolds number is a measure of the ratio of inertial to viscous forces, and this fact is exploited in the study of slightly viscous flows. In ideal fluid theory, the viscosity is assumed to be identically zero, and predicts that the fluid will slip along a boundary. However, it is observed physically that the fluid immediately adjacent to the boundary is in fact at rest. The reason for the breakdown of ideal fluid theory is that no matter how small the viscosity, which is physically always non-zero, there will exist a thin layer adjacent to the boundary in which the viscous effects cannot

be neglected.

Mathematically, the setting to zero of the viscosity reduces the order of the Navier-Stokes equations, resulting in its solution being intrinsically incapable of simultaneously satisfying all the boundary conditions. To resolve this difficulty Prandtl (1) postulated a two region theory. The first region is that of a thin boundary layer, immediately adjacent to the boundary, over which the tangential velocity changes from being zero on the boundary to a value at the outer edge predicted by the application of ideal fluid theory at the boundary itself. It is this region that produces a net drag force on an immersed body. The second region, external to the boundary layer, is then considered to be inviscid in nature, and is a slight displacement of the potential flow of ideal fluid theory to take account of the existence of the boundary layer.

Using this concept, and interpreting it mathematically, the Navier-Stokes equations may be approximated in a region close to the body by the Prandtl boundary-layer equations, which are to be solved subject to the conditions of no-slip on the cylinder surface and potential flow on the edge of the boundary-layer. These equations for impulsively started cylinders were first considered by Blasius (2) in 1908, and then thirty years later by Goldstein and Rosenhead (3). Blasius found the initial flow in terms of the first two terms of a power series of the time (measured non-dimensionally from the start of the motion), whilst Goldstein and Rosenhead extended the solution to include a third term. The first term is valid for all values of the

Reynolds number R, but subsequent terms hold only in the limit $R \to \infty$.

By using the first two terms of this series it is possible to obtain for both a circular and an elliptic cylinder, an approximation to the time at which the forward stream will first separate from the boundary and produce a recirculating region at the rear. A better estimate may be obtained by also including the third term. Properties of the flow obtained by these methods can only be considered valid until the time when separation first occurs, since thereafter the thickening of the boundary layer at the rear of the cylinder will interact with the assumed external potential flow and invalidate its use as a boundary condition of the problem. This is a major difficulty in the theory of time-dependent boundary layers.

To obtain the extension to finite Reynolds numbers, the Navier-Stokes equations should be solved, rather than their approximate counterpart, the boundary-layer equations; a more difficult task. In 1967, Wang (4,5) applied the method of matched asymptotic expansions to both circular and elliptic cylinder flows, and obtained a rather crude extension. He obtained the terms found by Blasius, together with a correction term for finite Reynolds number, but neglected the third term of the boundary layer as given by Goldstein and Rosenhead (3), and consequently his results are very much in error.

Since then, Collins and Dennis (6) have successfully extended the theory for flow around a circular cylinder, and for this case have shown a more general structure than had

hitherto been suspected. Their approach is systematic in marked contrast to previous methods, and arbitrarily many terms may be obtained with sufficient labour, four finite Reynolds number correction terms of different orders being given explicitly. They also calculated further terms numerically, and for the circular cylinder these results incorporate all the previous theoretical work for slightly viscous flows.

Whilst the circular cylinder theory is fairly well advanced for the small-time, high-but-finite Reynolds number régime, the elliptic cylinder case is not nearly as well understood, due in the main to its shape and the fact that the flow for a general orientation is no longer symmetric.

With the advent of the modern high-speed digital computer, an alternative approach is to use numerical methods. This was first considered by Payne (7) in 1958 for a circular cylinder, with most of the subsequent work being devoted to this case. Papers by Son and Hanratty (8), and Thoman and Szewczyk (9) have reviewed the literature on this problem, and no attempt will be made to list all the studies here. The elliptic cylinder problem has been considered recently by Lugt and Haussling (10).

The basic procedure, common to all these methods, and valid for all values of the Reynolds number, is to express the Navier-Stokes equations in terms of the stream function and vorticity, and then to integrate them by a step-by-step procedure in time. However for impulsively started cylinders one of the difficulties is the precise specification of the initial con-

ditions. Boundary-layer theory shows that the vorticity is initially infinite and confined to an infinitesimally thin region surrounding the cylinder surface. For this reason the direct application of finite-difference approximations to the equations will not give the initial flow correctly, and in practice, a finite initial vorticity distribution on the cylinder surface is obtained. Not only that, but any numerical scheme used to solve these equations will lose some accuracy due to the large gradients of the quantities concerned, particularly the vorticity. Ingham (11) has noted this difficulty, and illustrates how a small variance in the grid sizes can alter the solution appreciably in the small-time régime for a circular cylinder.

A re-examination of the early flow is thus desirable, since it is not known a priori how this initial error will propagate and affect the late-time solutions. Collins (12) recently detailed an alternative approach to the problem, employing a boundary-layer type transformation to remove the inherent singularity at time $t = 0$ in the Navier-Stokes equations for this problem. His early-time results for the case of the circular cylinder agree well with those of Dennis & Staniforth (13), who also used the same transformation but solved the resulting equations in a different manner.

In the present study, the singularity in the problem at $t = 0$ is removed in the same way, and the resulting equations solved by various methods to give an accurate description of the initial flow structure. One approach is to extend the

power-series solutions of Collins and Dennis (6) for the circular cylinder to the general case, with analytic results being given for both circular and elliptic cylinders. Further terms are then obtained numerically for the elliptic case. An alternative approach is also given which solves the transformed equations by fully-numerical techniques, with results being given for both circular and elliptic cases. These methods are in fact applicable to flow around any cylinder whose boundary can be mapped conformally onto a straight line, although the details may be more complicated. The main motivation for this work is to formulate a method of obtaining accurate initial solutions for this class of problem, which may then ultimately be integrated further to large times.

1.2 GOVERNING EQUATIONS

Consider a cylinder of infinite length and constant cross-section being impulsively started, and continuing to move, normal to its axis with uniform velocity U_0 in an infinite viscous incompressible fluid at time $t = 0$. Let us take a Cartesian coordinate system (X,Y,Z) fixed in the body (see Fig. 1), with the Z-axis being the axis of the cylinder. For convenience we will consider the following mathematically equivalent formulation, in which for time $t < 0$ the cylinder and fluid are moving with velocity U_0 inclined at an angle γ to the X-axis. At time $t = 0$, the cylinder is impulsively brought to rest and subsequently remains so. The fluid at large enough distances from the cylinder is assumed to move

with uniform velocity $(U_0\cos\gamma,\ U_0\sin\gamma, 0)$, for all t.

The equations which are assumed to govern the subsequent motion are the Navier-Stokes equation and the equation of continuity, which are coupled and to be solved subject to the boundary conditions of no-slip on the surface of the cylinder and uniform flow at infinity. The flow will also be assumed to remain two-dimensional within the X-Y plane.

The Navier-Stokes equation for viscous incompressible fluid flow may be written in dimensional form as follows [see Goldstein (14)];

$$\frac{\partial \underline{V}}{\partial t} - \underline{V} \times \underline{W} = -\underline{\nabla}\left(\frac{p}{\rho} + \frac{1}{2}\underline{V}^2\right) - \nu(\underline{\nabla} \times \underline{W}), \qquad (1.2.1)$$

where

$\underline{V} \equiv$ velocity vector of fluid,

$\underline{W} \equiv \underline{\nabla} \times \underline{V} \equiv$ vorticity vector,

$p \equiv$ actual pressure - hydrostatic pressure,

$\rho \equiv$ density of the fluid,

$\mu \equiv$ coefficient of viscosity of the fluid,

$\nu \equiv \mu/\rho \equiv$ coefficient of kinematic viscosity.

The equation of continuity is usually written as

$$\frac{D\rho}{Dt} + \rho\,\underline{\nabla}\cdot\underline{V} = 0 \ ,$$

which by definition of incompressibility reduces to

$$\underline{\nabla}\cdot\underline{V} = 0. \qquad (1.2.2)$$

We non-dimensionalise in the following manner:-

Let

$$\underline{V} = U_0\underline{V}' \ , \quad \underline{X} = d\underline{X}' \ , \quad p = \rho U_0^2 p' \ , \quad t = \frac{dt'}{U_0}, \qquad (1.2.3)$$

where U_0 is a representative velocity (chosen here to be that of the uniform flow at infinity), and d a representative length. For a circular cylinder d is chosen to be the radius, and for an elliptic cylinder to be $(a^2 - b^2)^{\frac{1}{2}}$, where a and b are the semi-major and semi-minor axes of the cross-section respectively. We thus obtain

$$\frac{\partial \underline{V}'}{\partial t'} - \underline{V}' \times \underline{W}' = - \underline{\nabla}'(p' + \frac{1}{2} \underline{V}'^2) - \frac{2}{R} \underline{\nabla}' \times \underline{W}' \ , \quad (1.2.4)$$

$$\underline{\nabla}' \cdot \underline{V}' = 0, \quad (1.2.5)$$

where

$$\underline{W}' = \underline{\nabla}' \times \underline{V}', \ R \equiv \frac{2U_0 d}{\nu} \ , \ \underline{\nabla}' = (\frac{\partial}{\partial X'}, \frac{\partial}{\partial Y'}, \frac{\partial}{\partial Z'}). \quad (1.2.6)$$

For convenience primes will be dropped, and all quantities are to be assumed non-dimensional unless otherwise stated. By taking the curl of equation (1.2.4) we may eliminate the pressure term and obtain the Helmholtz vorticity equation

$$\frac{\partial \underline{W}}{\partial t} - (\underline{W} \cdot \underline{\nabla}) \underline{V} + (\underline{V} \cdot \underline{\nabla}) \underline{W} = \frac{2}{R} \nabla^2 \underline{W}. \quad (1.2.7)$$

Since the flow is assumed two dimensional in the X-Y plane, equation (1.2.5) will reduce to

$$\frac{\partial V_1}{\partial X} + \frac{\partial V_2}{\partial Y} = 0 \ , \quad (1.2.8)$$

where $\underline{V} = (V_1, V_2, 0)$.
This may be identically satisfied by introducing the dimensionless stream function, $\psi(X,Y,t)$, related to the velocity components by

$$V_1(X,Y,t) = \frac{\partial \psi}{\partial Y} \quad , \quad V_2(X,Y,t) = - \frac{\partial \psi}{\partial X} \ . \quad (1.2.9)$$

As a consequence $\underline{W} = \underline{\nabla} \times \underline{V}$ only has the one component in the Z-direction, i.e. $\underline{W} = (0,0,-\zeta)$, where

$$\zeta = \frac{\partial V_1}{\partial Y} - \frac{\partial V_2}{\partial X} \ . \qquad (1.2.10)$$

Equations (1.2.9) and (1.2.10) then give the equivalent of the continuity equation in the form

$$\nabla^2 \psi = \zeta \ , \qquad (1.2.11)$$

where $\nabla^2 = \frac{\partial^2}{\partial X^2} + \frac{\partial^2}{\partial Y^2}$.

Returning to equation (1.2.7), we note that $(\underline{W}\cdot\underline{\nabla})\underline{V} = 0$, and the only non-zero component is in the Z-direction, yielding

$$\frac{\partial \zeta}{\partial t} = \frac{2}{R} \nabla^2 \zeta + \frac{\partial(\psi,\zeta)}{\partial(X,Y)} \ , \qquad (1.2.12)$$

where $$\frac{\partial(\psi,\zeta)}{\partial(X,Y)} \equiv \frac{\partial \psi}{\partial X}\frac{\partial \zeta}{\partial Y} - \frac{\partial \psi}{\partial Y}\frac{\partial \zeta}{\partial X} \ .$$

It remains to state explicitly the initial and boundary conditions to be imposed on ψ and ζ. It can be shown (see e.g. Goldstein and Rosenhead(3)) that impulsively bringing the cylinder to rest instantaneously creates an irrotational flow without circulation external to the cylinder. This flow is the well-known potential flow and may be calculated from equation (1.2.11) (with ζ set to zero since the flow is irrotational) together with the boundary condition of uniform flow at infinity. Equation (1.2.12) is identically satisfied by $\zeta = 0$. That the creation of this flow is instantaneous is reasonable on physical grounds since disturbances propogate with infinite velocity in an incompressible fluid.

However, the fluid must also obey the no-slip condition on the cylinder surface. Consequently at t=0 a boundary layer or vortex sheet of zero thickness is created at the surface. Across this sheet the tangential velocity changes from being zero on the boundary to that of the adjacent layer of fluid which is slipping past the sheet with a velocity determined by the external potential flow. Subsequently the vorticity created in this infinitesimal layer is diffused and convected further into the fluid, whilst the boundary-layer grows in thickness. Thus the initial flow at t=0 is potential, having zero vorticity external to an infinitesimally small boundary layer. Mathematically we need only specify that $\zeta=0$ external to the vortex sheet since the initial condition of potential flow is implicit in the governing equations together with uniform flow at infinity.

If c denotes the contour of the cylinder and D the infinite domain outside of it, then the conditions on ψ and ζ are:-

$$\left.\begin{array}{l} \text{For } t = 0 \quad \text{(i)} \ \zeta = 0 \text{ throughout D, } \zeta \neq 0 \text{ on C} \\ \text{For } t \geq 0 \quad \text{(ii)} \ \psi = \dfrac{\partial \psi}{\partial n} = 0 \text{ on C,} \\ \qquad\qquad \text{(iii)} \left.\begin{array}{l} V_1 = \dfrac{\partial \psi}{\partial Y} \to \cos\gamma \\ V_2 = -\dfrac{\partial \psi}{\partial X} \to \sin\gamma \end{array}\right\} \text{as } X^2 + Y^2 \to \infty \end{array}\right\} \quad (1.2.13)$$

Here $\frac{\partial}{\partial n}$ denotes differentiation in the normal direction to the cylinder.

Conditions (ii) and (iii) are the mathematical statements of no-slip on the boundary C and uniform flow at infinity respectively. The use of the condition of uniform flow at infinity for impulsively started motion can be justified on the basis that the vorticity generated on the surface of the cylinder is diffused and convected away at a finite rate. Thus after any finite interval of time, the uniform flow at infinity will remain undisturbed. Implicit in condition (iii) is that

$$\zeta(X,Y,t) \to 0 \text{ as } X^2 + Y^2 \to \infty \quad , \qquad (1.2.14)$$

which is obtained from the asymptotic form of the stream function at infinity

$$\psi = Y\cos\gamma - X\sin\gamma \ .$$

Let us consider a conformal transformation of the form

$$\xi + i\eta = F(X + iY) \ , \qquad (1.2.15)$$

which maps the region outside the cylinder on to the semi-infinite strip shown in Fig. 2. This approach follows that of Dennis & Chang (15) for steady-state solutions of symmetric motion, and is a preliminary transformation required in the present investigation.

The prime objective is to create a region which can be fitted exactly by a rectangular grid in order to facilitate the application of finite-difference methods, although it will also prove useful in the analytic investigation. A number of

such transformations can be written down explicitly and include the cases of circular and elliptic cylinders, finite-width flat plate and generalised Joukowski aerofoil. Transformations are chosen such that the surface of the cylinder (OABCD in Fig. 1) maps to $\xi = 0$ (OABCD in Fig. 2), with η varying from 0 to 2π and

$$\left.\begin{aligned} \psi(\xi,\eta,t) &= \psi(\xi,\eta+2n\pi,t) \ , \\ \zeta(\xi,\eta,t) &= \zeta(\xi,\eta+2n\pi,t) \ , \end{aligned}\right\} \qquad (1.2.16)$$

where n is an integer. This ensures the periodicity of the physical properties of the fluid.

After applying the transformation (1.2.15), equations (1.2.11) and (1.2.12) become

$$\frac{\partial \zeta}{\partial t} = H^2 \left[\frac{2}{R} \nabla_1^2 \zeta + \frac{\partial(\psi,\zeta)}{\partial(\xi,\eta)}\right] \quad , \qquad (1.2.17)$$

$$\nabla_1^2 \psi = \zeta / H^2 \quad , \qquad (1.2.18)$$

where

$$\left.\begin{aligned} \nabla_1^2 &= \frac{\partial^2}{\partial \xi^2} + \frac{\partial^2}{\partial \eta^2} \ , \\ H^2 &= \left(\frac{\partial \xi}{\partial X}\right)^2 + \left(\frac{\partial \xi}{\partial Y}\right)^2 = \left(\frac{\partial \eta}{\partial X}\right)^2 + \left(\frac{\partial \eta}{\partial Y}\right)^2 \ . \end{aligned}\right\} \qquad (1.2.19)$$

For the type of transformation (1.2.15) envisaged we find

$$\left.\begin{aligned} X &\sim K_0 \, e^{\xi} \cos\eta \\ Y &\sim K_0 \, e^{\xi} \sin\eta \end{aligned}\right\} \quad \text{as } \xi \to \infty \ , \qquad (1.2.20)$$

where K_0 is a geometry-dependent constant of the cylinder under consideration.

Transformations having the above mentioned properties have

been used extensively in the literature. For example, Dennis & Chang (15) and Collins (12) have considered the following transformations:-

(i) circular cylinder for which

$$\left.\begin{aligned} F(X + iY) &= \log(X + iY) \ , \\ H^2 &= e^{-2\xi} \ . \end{aligned}\right\} \qquad (1.2.21)$$

(ii) elliptic cylinder for which

$$\left.\begin{aligned} F(X + iY) &= \cosh^{-1}(X + iY) - \alpha \ , \\ H^2 &= 2/[\cosh 2(\xi + \alpha) - \cos 2\eta] \ . \end{aligned}\right\} \qquad (1.2.22)$$

Chang (16) has also considered the case of a generalized Joukowski aerofoil.

Payne (7), Kawaguti & Jain (17), Apelt (18), Keller & Takami (19), and Son & Hanratty (8) have all used variations of (i) for flow around a circular cylinder, whilst Lugt & Haussling (10) have considered (ii) for flow around an elliptic cylinder and Janssen (20) and Dennis & Dunwoody (21) have investigated the limiting case of (ii) for a flat plate. This list is far from complete, but is given as an indication of the widespread use of this type of transformation.

Examples of the values K_0 may take are

$$\left.\begin{aligned} &\text{(a)} \quad K_0 = 1 \text{ for circular cylinder,} \\ &\text{(b)} \quad K_0 = \tfrac{1}{2}e^{\alpha} \text{ for elliptic cylinder,} \\ &\text{(c)} \quad K_0 = \tfrac{1}{2} \text{ for finite-width flat plate.} \end{aligned}\right\} \qquad (1.2.23)$$

In specifying the boundary conditions in the transformed coordinate system we need the asymptotic relations (1.2.13) and (1.2.20) together with

$$\left.\begin{aligned} \frac{\partial\psi}{\partial\xi} &= \frac{\partial\psi}{\partial X}\frac{\partial X}{\partial\xi} + \frac{\partial\psi}{\partial Y}\frac{\partial Y}{\partial\xi} \quad , \\ \frac{\partial\psi}{\partial\eta} &= \frac{\partial\psi}{\partial X}\frac{\partial X}{\partial\eta} + \frac{\partial\psi}{\partial Y}\frac{\partial Y}{\partial\eta} \quad . \end{aligned}\right\} \tag{1.2.24}$$

Transforming the initial and boundary conditions into the (ξ,η) coordinate system we may then summarise the formulation as being the following:

For $t \leq 0$; $\zeta = 0$ throughout D, $\zeta \neq 0$ on C.

For $t \geq 0$; $$\frac{\partial\zeta}{\partial t} = H^2\left[\frac{2}{R}\nabla_1^2\zeta + \frac{\partial(\psi,\zeta)}{\partial(\xi,\eta)}\right] , \tag{1.2.17}$$

$$\nabla_1^2\psi = \zeta/H^2 \quad , \tag{1.2.18}$$

subject to the conditions

$$\left.\begin{aligned} \psi(\xi,\eta,t) &= \psi(\xi,\eta+2n\pi,t) \\ \zeta(\xi,\eta,t) &= \zeta(\xi,\eta+2n\pi,t) \end{aligned}\right\} \quad (n \text{ integer}) \tag{1.2.16}$$

$$\psi = \frac{\partial\psi}{\partial\xi} = 0 \quad \text{on } \xi = 0 \ , \tag{1.2.25}$$

$$\left.\begin{aligned} e^{-\xi}\frac{\partial\psi}{\partial\xi} &\to K_0 \sin(\eta - \gamma) \\ e^{-\xi}\frac{\partial\psi}{\partial\eta} &\to K_0 \cos(\eta - \gamma) \\ \zeta &\to 0 \end{aligned}\right\} \text{ as } \xi \to \infty \tag{1.2.26}$$

1.3 THE INTEGRAL BOUNDARY CONDITIONS FOR THE VORTICITY

All the boundary conditions of the problem, apart from those of the periodicity, can be considered as being imposed solely on the stream function ψ, since the third condition of (1.2.26) is a consequence of the other two. Conditions on ζ are contained implicitly in the non-linear coupling of the two equations (1.2.17) and (1.2.18). This formulation makes any uncoupling of the equations difficult.

We will proceed to derive additional conditions on ζ, to be subsequently referred to as the integral conditions, by making an asymmetric generalisation of a method first proposed by Dennis & Chang (15) for symmetric flows, and also used by Collins (12). In this method, the stream function is assumed to be represented by a Fourier sine series in the variable η. The generalisation to the present investigation is to assume the following Fourier expansion for the stream function

$$\psi(\xi,\eta,t) = \frac{G_0(\xi,t)}{2} + \sum_{n=1}^{\infty} [G_n(\xi,t)\cos n\eta + F_n(\xi,t)\sin n\eta]. \tag{1.3.1}$$

Term by term differentiation of this series with respect to η is justified (see e.g. Jeffreys & Jeffreys (22). Substitution of this series into equation (1.2.18) and the application of the standard methods for orthogonal functions yields

$$\frac{\partial^2 F_n}{\partial \xi^2} - n^2 F_n = \frac{1}{\pi}\int_0^{2\pi} \frac{\zeta \sin n\eta}{H^2}\, d\eta, \quad (n=1,2,\ldots), \tag{1.3.2}$$

$$\frac{\partial^2 G_n}{\partial \xi^2} - n^2 G_n = \frac{1}{\pi}\int_0^{2\pi} \frac{\zeta \cos n\eta}{H^2}\, d\eta, \quad (n=0,1,2,\ldots). \tag{1.3.3}$$

The boundary conditions (1.2.25) and (1.2.26) give

$$\left.\begin{aligned} F_n = \frac{\partial F_n}{\partial \xi} = 0 \quad &\text{on } \xi = 0 && (n=1,2,\ldots),\\ e^{-\xi}F_n = e^{-\xi}\frac{\partial F_n}{\partial \xi} = K_0 \cos\gamma\delta_{n,1}, \quad &\text{as } \xi \to \infty && (n=1,2,\ldots),\\ G_n = \frac{\partial G_n}{\partial \xi} = 0 \quad &\text{on } \xi = 0 && (n=0,1,2,\ldots),\\ e^{-\xi}G_n = e^{-\xi}\frac{\partial G_n}{\partial \xi} = -K_0 \sin\gamma\delta_{n,1}, \quad &\text{as } \xi \to \infty && (n=0,1,2,\ldots), \end{aligned}\right\} \tag{1.3.4}$$

where $\delta_{n,m}$, the Kronecker delta symbol, is defined by

$$\delta_{n,m} = 1 \text{ if } n = m,$$

$$\delta_{n,m} = 0 \text{ if } n \neq m.$$

Let p_n and q_n be defined by

$$\left.\begin{aligned} p_n &= \frac{\partial F_n}{\partial \xi} + nF_n \qquad (n=1,2,\ldots)\ , \\ q_n &= \frac{\partial G_n}{\partial \xi} + nG_n \qquad (n=0,1,2,\ldots)\ . \end{aligned}\right\} \tag{1.3.5}$$

We then obtain from equations (1.3.2) and (1.3.3)

$$\left.\begin{aligned} \frac{\partial}{\partial \xi}\left[e^{-n\xi}p_n\right] &= \frac{e^{-n\xi}}{\pi}\int_0^{2\pi} \frac{\zeta \sin n\eta}{H^2}\, d\eta \quad (n=1,2,\ldots), \\ \frac{\partial}{\partial \xi}\left[e^{-n\xi}q_n\right] &= \frac{e^{-n\xi}}{\pi}\int_0^{2\pi} \frac{\zeta \cos n\eta}{H^2}\, d\eta \quad (n=0,1,2,\ldots), \end{aligned}\right\} \tag{1.3.6}$$

together with

$$\left.\begin{aligned} &p_n = 0 \text{ on } \xi = 0,\ e^{-\xi}p_n \to 2K_0 \cos\gamma\ \delta_{n,1} \text{ as } \xi \to \infty \quad (n=1,2,\ldots), \\ &q_n = 0 \text{ on } \xi = 0,\ e^{-\xi}q_n \to -2K_0 \sin\gamma\ \delta_{n,1} \text{ as } \xi \to \infty \quad (n=0,1,2,\ldots), \end{aligned}\right\} \tag{1.3.7}$$

which are obtained from boundary conditions (1.3.4).

Integrating equations (1.3.6) from 0 to ξ yields (using conditions (1.3.7))

$$\left.\begin{aligned} e^{-n\xi}p_n &= \frac{1}{\pi}\int_0^{\xi} e^{-nx}\int_0^{2\pi} \frac{\zeta \sin n\eta}{H^2}\, d\eta\, dx \quad (n=1,2,\ldots), \\ e^{-n\xi}q_n &= \frac{1}{\pi}\int_0^{\xi} e^{-nx}\int_0^{2\pi} \frac{\zeta \cos n\eta}{H^2}\, d\eta\, dx \quad (n=0,1,2,\ldots). \end{aligned}\right\} \tag{1.3.8}$$

Taking the limit as $\xi \to \infty$, and using the asymptotic forms (1.3.7) we have finally

$$\frac{1}{\pi}\int_0^{\infty} e^{-n\xi}\int_0^{2\pi}\frac{\zeta \sin n\eta}{H^2}\,d\eta\,d\xi = 2K_0\cos\gamma\delta_{n,1} \quad (n=1,2,\ldots), \tag{1.3.9}$$

$$\frac{1}{\pi}\int_0^{\infty} e^{-n\xi}\int_0^{2\pi}\frac{\zeta \cos n\eta}{H^2}\,d\eta\,d\xi = -2K_0\cos\gamma\delta_{n,1} \quad (n=0,1,2,\ldots). \tag{1.3.10}$$

The third condition of (1.2.26) and equations (1.3.9) and (1.3.10) implicitly contain all the information of the first two of (1.2.26). The first two conditions of (1.2.26) may therefore be dropped. The re-specification of the boundary conditions in this manner will prove useful for several reasons. In the extension of boundary-layer theory to finite Reynolds number, one of the principle difficulties is in the specification of the external flow, which can no longer be considered potential due to its interaction with the thickening boundary layer. By using this formulation the displacement of the external flow need no longer be considered explicitly.

Another advantage is that by providing an extra condition on ζ it will enable us effectively to uncouple the two governing equations into two sets of infinite ones when we make a power-series analysis of these equations. These two infinite sets may then be solved explicitly in a criss-cross manner, alternating from one set to the other. In the fully-numerical solution, its application enables one to solve the equivalent of equation (1.2.18) in a more direct manner, rather than the usual time-consuming iterative methods for boundary-value problems.

1.4 THE BOUNDARY-LAYER TYPE TRANSFORMATION

It is known from the boundary-layer theory of this problem

(see e.g. Schlichting (23) p. 399), that the stream function and the boundary-layer thickness δ are proportional to k, whilst the vorticity ζ is inversely proportional to k, where $k = 2(2t/R)^{\frac{1}{2}}$.

Thus at time t = 0, there is an infinitesimally thin ring of vorticity of infinite magnitude generated on the surface of the cylinder. To illustrate how this behaviour affects the use of a numerical integration of the equations, consider the case of the flow around a circular cylinder. It can be shown (see Dennis & Chang (15)) that the initial solution for the vorticity at small times is

$$\zeta = \frac{4}{\pi^{\frac{1}{2}}} \frac{e^{-(\frac{\xi}{k})^2}}{k} \sin\eta \quad .$$

At t = 0 it is impossible to represent this solution numerically as required by numerical methods of integration, and even for small finite times this function cannot be represented accurately by any finite difference scheme. The same holds true for the general case. To obviate this difficulty the following transformation is used:

$$\xi = kz \ , \quad \psi = k\Psi \ , \quad \zeta = \frac{\omega}{k} \ , \qquad (1.4.1)$$

where

$$k = 2(2t/R)^{\frac{1}{2}} \ .$$

Under this transformation equations (1.2.17) and (1.2.18) become

$$H^2 \frac{\partial^2\omega}{\partial z^2} + 2z \frac{\partial\omega}{\partial z} + 2\omega = 4t\frac{\partial\omega}{\partial t} - \frac{8tH^2}{R} \frac{\partial^2\omega}{\partial\eta^2} + 4tH^2 \frac{\partial(\Psi,\omega)}{\partial(\eta,z)} \ , \qquad (1.4.2)$$

$$\frac{\partial^2\Psi}{\partial z^2} + k^2 \frac{\partial^2\Psi}{\partial\eta^2} = \omega H^{-2} \ . \qquad (1.4.3)$$

These are to be solved subject to

$$\left.\begin{aligned}\Psi(z,\eta,t) &= \Psi(z,\eta + 2n\pi,t)\\ \omega(z,\eta,t) &= \omega(z,\eta + 2n\pi,t)\end{aligned}\right\} \quad (n \text{ integer}) \ , \tag{1.4.4}$$

$$\Psi = \frac{\partial \Psi}{\partial z} = 0 \quad \text{on } z = 0 \ , \tag{1.4.5}$$

$$\omega \to 0 \quad \text{as } z \to \infty \ , \tag{1.4.6}$$

$$\int_0^\infty e^{-nkz} \int_0^{2\pi} \omega H^{-2} \sin n\eta \, d\eta \, dz = 2K_0 \pi \cos\gamma \delta_{n,1} \qquad (n=1,2,\ldots), \tag{1.4.7}$$

$$\int_0^\infty e^{-nkz} \int_0^{2\pi} \omega H^{-2} \cos n\eta \, d\eta \, dz = -2K_0 \pi \sin\gamma \delta_{n,1} \qquad (n=0,1,2\ldots), \tag{1.4.8}$$

obtained from equations (1.2.16), (1.2.25), (1.2.26), (1.3.9) and (1.3.10) respectively.

Equations (1.4.2) through (1.4.8) provide the complete formulation of the problem for $t \geq 0$.

The transformation (1.4.1) utilises the known boundary-layer structure of the initial flow, and removes the time singularity from the problem. In a numerical method of integration the solution can be started using a calculated finite distribution for ω consistent with boundary-layer theory, and since ω is a well-behaved function (in comparison to ζ, that is) it may be represented accuractely by finite-difference approximations in continuing the solution. This transformation also has the effect of stretching the coordinate normal to the body by placing more grid points close to the body, whilst at the same time taking account of the growth of the boundary layer. In the semi-analytical investigation it facilitates the formulation of a systematic procedure of solution and indicates a more general structure.

CHAPTER II

POWER SERIES EXPANSIONS FOR THE GENERAL CASE

2.1 SERIES EXPANSIONS IN POWERS OF K

In this chapter a method is given which extends the results of Collins and Dennis (6) for a circular cylinder to the general case of any conformally-mappable cylinder. It should be remarked here that a circular cylinder possesses infinitely many planes about which it is symmetrical, but for the general case this is not so. The mathematical manifestation of this property is that for a general cylinder, H is a function of both ξ and η in the (ξ,η) plane, whilst for the degenerate case of a circular cylinder it is independent of η.

For a circular cylinder this independence of η enables one to make a Fourier sine expansion of the dependent variables and ultimately obtain infinite sets of ordinary differential equations. Solutions for these may be built up explicitly by alternating from one set to the other. However for the general case, although this procedure will still lead to sets of ordinary differential equations, unfortunately they are implicitly given and cannot be solved explicitly in an alternating manner. In the present study this difficulty is circumvented by making a different representation of the dependent variables, which then leads to sets of differential equations which can be solved to some order explicitly. It is interesting to note that

it is a relatively easy matter to obtain the representation of Collins and Dennis (6) for the circular cylinder from the final form of the present analysis, giving a useful check on the work.

As previously noted, equations (1.4.2) through (1.4.8) provide the mathematical formulation for the problem. Equations (1.4.2) and (1.4.3) may be re-arranged to obtain

$$\frac{\partial^2\bar{\omega}}{\partial z^2} + 2H^{-2} z \frac{\partial\omega}{\partial z} + 2H^{-2}\omega = 4tH^{-2} \frac{\partial\omega}{\partial t} - k^2 \frac{\partial^2\bar{\omega}}{\partial\eta^2} + 4t \frac{\partial(\Psi,\omega)}{\partial(\eta,z)} , \tag{2.1.1}$$

$$\frac{\partial^2\Psi}{\partial z^2} + k^2 \frac{\partial^2\Psi}{\partial\eta^2} = H^{-2}\omega . \tag{2.1.2}$$

We note that the dependence of the problem on the parameter R can be considered to be isolated in the variable $k = (8t/R)^{\frac{1}{2}}$. Thus if we consider flows of low viscosity at small times, k will be small. Under these conditions we can remove the R-dependence from the problem by replacing the exponential in the integral conditions (1.4.7) and (1.4.8) by its power series expansion and making the further expansions

$$\omega = \sum_{n=0}^{\infty} \omega_n(z,\eta,t)k^n , \tag{2.1.3}$$

$$\Psi = \sum_{n=0}^{\infty} \Psi_n(z,\eta,t)k^n , \tag{2.1.4}$$

$$2H^{-2} = 2H_0^{-2} + \sum_{j=1}^{\infty} \beta_j (kz)^j , \tag{2.1.5}$$

where H_0^{-2} is the value of H^{-2} evaluated at $k = t = 0$. For a circular cylinder we have

$$H^{-2} = e^{2kz}\ ,\quad 2H_0^{-2} = 2,\quad \beta_j = \frac{2^{j+1}}{j!} \qquad (j=1,2,\ldots). \tag{2.1.6}$$

For an elliptic cylinder

$$\left.\begin{aligned} &2H^{-2} = \cosh 2(kz+\alpha) - \cos 2\eta,\quad 2H_0^{-2} = \cosh 2\alpha - \cos 2\eta,\\ &\beta_{2j-1} = \frac{2^{2j-1}\sinh 2\alpha}{(2j-1)!}\ ,\quad \beta_{2j} = \frac{2^{2j}\cosh 2\alpha}{(2j)!} \quad (j=1,2,\ldots). \end{aligned}\right\} \tag{2.1.7}$$

By making the above-mentioned expansions and equating coefficients of k^p we obtain the following two equations for $p = 0,1,2,\ldots$:-

$$\begin{aligned} \frac{\partial^2\omega_p}{\partial z^2} + 2H_0^{-2}\Big[z\frac{\partial\omega_p}{\partial z} + (1-p)\omega_p - 2t\frac{\partial\omega_p}{\partial t}\Big] &= -\sum_{\ell=0}^{p-1}\beta_{p-\ell}\, z^{p-\ell}\Big[z\frac{\partial\omega_\ell}{\partial z}\\ &+ (1-\ell)\omega_\ell - 2t\frac{\partial\omega_\ell}{\partial t}\Big] - \frac{\partial^2\omega_{p-2}}{\partial\eta^2} + 4t\sum_{\ell=0}^{p}\frac{\partial(\Psi_\ell,\omega_{p-\ell})}{\partial(\eta,z)}\ , \end{aligned} \tag{2.1.8}$$

$$2\frac{\partial^2\Psi_p}{\partial z^2} = -2\frac{\partial^2\Psi_{p-2}}{\partial\eta^2} + 2H_0^{-2}\omega_p + \sum_{\ell=1}^{p}\beta_\ell\, z^\ell\,\omega_{p-\ell}\ . \tag{2.1.9}$$

The boundary conditions for Ψ_p and ω_p are

$$\Psi_p = \frac{\partial\Psi_p}{\partial z} = 0 \quad \text{on } z = 0\ , \tag{2.1.10}$$

$$\omega_p \to 0 \quad \text{as } z \to \infty\ , \tag{2.1.11}$$

and the integral conditions can be written as

$$\begin{aligned} 2\int_0^\infty\int_0^{2\pi}\omega_p H_0^{-2}\sin n\eta\, d\eta\, dz &= 4K_0\pi\cos\gamma\,\delta_{n,1}\delta_{p,0}\\ &- \sum_{\ell=0}^{p-1}\int_0^\infty\int_0^{2\pi}\Big\{\frac{2H_0^{-2}(-nz)^{\ell+1}}{(\ell+1)!}\,\omega_{p-\ell-1}\\ &+ \frac{(-n)^\ell}{\ell!}\sum_{m=0}^{p-\ell-1}\beta_{p-m-\ell}\, z^{p-m}\omega_m\Big\}\sin n\eta\, d\eta\, dz \quad (n=1,2,\ldots), \end{aligned} \tag{2.1.12}$$

$$2\int_0^{\infty}\int_0^{2\pi} \omega_p H_0^{-2} \cos n\eta \, d\eta \, dz = -4K_0\pi\sin\gamma\,\delta_{n,1}\delta_{p,0} - \sum_{\ell=0}^{p-1} \int_0^{\infty}\int_0^{2\pi} \left\{ \frac{2H_0^{-2}(-nz)^{\ell+1}}{(\ell+1)!}\, \omega_{p-\ell-1} + \frac{(-n)^{\ell}}{\ell!} \sum_{m=0}^{p-\ell-1} \beta_{p-m-\ell} z^{p-m}\, \omega_m \right\} \cos n\eta \, d\eta \, dz \quad (n=0,1,2,\ldots). \tag{2.1.13}$$

In this chapter expressions having a negative subscript are assumed zero, and 0! is defined to have the value unity.

2.2 SERIES EXPANSIONS IN POWERS OF t

In order to isolate the t-dependence we make further expansions, valid for small t, as follows:-

$$\omega_p = \sum_{q=0}^{\infty} \omega_{p,q}(\eta,z)t^q \,, \tag{2.2.1}$$

$$\Psi_p = \sum_{q=0}^{\infty} \Psi_{p,q}(\eta,z)t^q \,. \tag{2.2.2}$$

Inserting these into equations (2.1.8) through (2.1.13) and equating powers of q yields for p = 0,1,2,... ; q = 0,1,2,...

$$\frac{\partial^2\omega_{p,q}}{\partial z^2} + 2H_0^{-2}\left[z\frac{\partial\omega_{p,q}}{\partial z} + (1-p-2q)\omega_{p,q}\right] = -\sum_{\ell=0}^{p-1}\left\{\beta_{p-\ell}z^{p-\ell}\left[z\frac{\partial\omega_{\ell,q}}{\partial z} + (1-\ell-2q)\omega_{\ell,q}\right]\right\} - \frac{\partial^2\omega_{p-2,q}}{\partial\eta^2} + 4\sum_{\ell=0}^{p}\sum_{n=1}^{q}\frac{\partial(\Psi_{\ell,q-n},\omega_{p-\ell,n-1})}{\partial(\eta,z)}, \tag{2.2.3}$$

$$2\frac{\partial^2\Psi_{p,q}}{\partial z^2} = -2\frac{\partial^2\Psi_{p-2,q}}{\partial\eta^2} + 2H_0^{-2}\omega_{p,q} + \sum_{\ell=1}^{p}\beta_\ell z^\ell \omega_{p-\ell,q} \,, \tag{2.2.4}$$

together with conditions similar to those of (2.1.10) through (2.1.13).

It is convenient when finding the solutions to these equations to make the transformation of variable

$$z = H_0 v \quad . \tag{2.2.5}$$

Finally, the system of equations for $p = 0,1,2,\ldots$; $q = 0,1,2,\ldots$ becomes

$$\frac{\partial^2 \omega_{p,q}}{\partial v^2} + 2v \frac{\partial \omega_{p,q}}{\partial v} + 2(1-p-2q)\omega_{p,q} = -\sum_{\ell=0}^{p-1} \left\{ \beta_{p-\ell} H_0^{p-\ell+2} v^{p-\ell} \left[v \frac{\partial \omega_{\ell,q}}{\partial v} + (1-\ell-2q)\omega_{\ell,q} \right] \right\} - L^2 \omega_{p-2,q} + 4H_0 \sum_{\ell=0}^{p} \sum_{n=1}^{q} \frac{\partial(\Psi_{\ell,q-n}, \omega_{p-\ell,n-1})}{\partial(\eta, v)} , \tag{2.2.6}$$

$$2 \frac{\partial^2 \Psi_{p,q}}{\partial v^2} = -2L^2 \Psi_{p-2,q} + 2\omega_{p,q} + \sum_{\ell=1}^{p} \beta_\ell H_0^{\ell+2} v^\ell \omega_{p-\ell,q}, \tag{2.2.7}$$

where

$$L^2 = H_0^2 \left(\frac{\partial}{\partial \eta} - v \frac{H_0'(\eta)}{H_0} \frac{\partial}{\partial v} \right)^2 . \tag{2.2.8}$$

These equations are to be solved subject to the conditions

$$\Psi_{p,q} = \frac{\partial \Psi_{p,q}}{\partial v} = 0 \quad \text{on } v = 0 , \tag{2.2.9}$$

$$\omega_{p,q} \to 0 \quad \text{as } v \to \infty , \tag{2.2.10}$$

$$2 \int_0^\infty \int_0^{2\pi} H_0^{-1} \omega_{p,q} \sin n\eta \, d\eta \, dv = 4K_0 \pi \cos\gamma \delta_{n,1} \delta_{p,0} \delta_{q,0} - \sum_{\ell=0}^{p-1} \int_0^\infty \int_0^{2\pi} \left\{ \frac{2H_0^\ell (-nv)^{\ell+1}}{(\ell+1)!} \omega_{p-\ell-1,q} + \frac{H_0 (-n)^\ell}{\ell!} \sum_{m=0}^{p-\ell-1} \beta_{p-m-\ell} (H_0 v)^{p-m} \omega_{m,q} \right\} \sin n\eta \, d\eta \, dv \quad (n=1,2,\ldots), \tag{2.2.11}$$

$$2\int_0^\infty\int_0^{2\pi} H_0^{-1}\omega_{p,q}\cos n\eta\, d\eta\, dv = -4K_0\pi\sin\gamma\delta_{n,1}\delta_{p,0}\delta_{q,0}$$
$$- \sum_{\ell=0}^{p-1}\int_0^\infty\int_0^{2\pi}\left\{\frac{2H_0^{\ell}(-nv)^{\ell+1}}{(\ell+1)!}\omega_{p-\ell-1,q}\right.$$
$$\left. + \frac{H_0(-n)^{\ell}}{\ell!}\sum_{m=0}^{p-\ell-1}\beta_{p-m-\ell}(H_0v)^{p-m}\omega_{m,q}\right\}\cos n\eta\, d\eta\, dv \quad (n=0,1,2,\ldots). \tag{2.2.12}$$

2.3 THE BOUNDARY LAYER SOLUTION

Consider the case of p = 0. Equations (2.2.6) through (2.2.12) then become for q = 0,1,2,....

$$\frac{\partial^2\omega_{0,q}}{\partial v^2} + 2v\frac{\partial\omega_{0,q}}{\partial v} + 2(1-2q)\omega_{0,q} = 4H_0\sum_{n=1}^{q}\frac{\partial(\Psi_{0,q-n},\omega_{0,n-1})}{\partial(\eta,v)}, \tag{2.3.1}$$

$$\frac{\partial^2\Psi_{0,q}}{\partial v^2} = \omega_{0,q}, \tag{2.3.2}$$

$$\Psi_{0,q} = \frac{\partial\Psi_{0,q}}{\partial v} = 0 \quad \text{on } v = 0, \tag{2.3.3}$$

$$\omega_{0,q} \to 0 \quad \text{as } v \to \infty, \tag{2.3.4}$$

$$\int_0^\infty\int_0^{2\pi} H_0^{-1}\omega_{0,q}\sin n\eta\, d\eta\, dv = 2K_0\pi\cos\gamma\delta_{n,1}\delta_{q,0} \quad (n=1,2,\ldots), \tag{2.3.5}$$

$$\int_0^\infty\int_0^{2\pi} H_0^{-1}\omega_{0,q}\cos n\eta\, d\eta\, dv = -2K_0\pi\sin\gamma\delta_{n,1}\delta_{q,0} \quad (n=0,1,2,\ldots), \tag{2.3.6}$$

These equations can now be solved explicitly to arbitrary order q, in the following way:-

(i) Set q = 0 and solve equation (2.3.1) subject to conditions (2.3.4), (2.3.5) and (2.3.6). Note that the right-hand side of equation (2.3.1) is zero.

(ii) Solve equation (2.3.2) with q = 0 subject to boundary conditions (2.3.3). Note that $\omega_{0,0}$ is now known explicitly.

(iii) Increment q by 1 and solve equation (2.3.1) subject to conditions (2.3.4), (2.3.5) and (2.3.6). Note that the right-hand side of equation (2.3.1) is known explicitly.

Solve equation (2.3.2) subject to boundary conditions (2.3.3). Note that the right-hand side of equation (2.3.2) is known explicitly.

(iv) Repeat (iii) to order required.

This is the alternating procedure of building up solutions previously mentioned, and it effectively uncouples the equations inasmuch as that in considering a particular equation the right-hand side and the boundary conditions are given explicitly.

Exact solutions have been found to the above system for values of q = 0,1,2 and are now given for q = 0,1. We find

$$\omega_{0,0} = U(\eta)\ A_0(v)\ , \tag{2.3.7}$$

$$\Psi_{0,0} = U(\eta)\ B_0(v)\ , \tag{2.3.8}$$

$$\omega_{0,1} = -H_0 U(\eta) U'(\eta)\ A_1(v)\ , \tag{2.3.9}$$

$$\Psi_{0,1} = -H_0 U(\eta) U'(\eta)\ B_1(v)\ , \tag{2.3.10}$$

where

$$U(\eta) = 2K_0 H_0(\eta)\sin(\eta-\gamma) ,$$

and the A_i and B_i $(i = 0,1)$ are defined in Appendix I.

Here $U(\eta)$ is the velocity in the direction of decreasing η on the surface of the cylinder as given by inviscid potential flow theory. In boundary-layer theory it is used as the boundary condition for the tangential velocity component on the edge of the boundary layer. The functions $B_0(v)$, $B_1(v)$ are just the functions ζ_0, ζ_1 of Blasius (see Schlichting (23), p. 399-400). Solutions with q set to 2 have been found but are not given here due to their length. The expressions found by setting $q = 0,1,2$ can be shown to be locally equivalent in a region close to the cylinder to those given by the method of Goldstein and Rosenhead (3). Wundt (24) made several corrections in the detail of this paper, one of which itself appears to be incorrect by a minus sign. For the function T, Wundt gives

$$T = \frac{1}{30\pi^{\frac{1}{2}}}[10\alpha\eta^3+(15\alpha-20)\eta-8\beta]e^{-\eta^2}+ \ldots ,$$

whereas this should read

$$T = \frac{1}{30\pi^{\frac{1}{2}}}[10\alpha\eta^3-(15\alpha-20)\eta-8\beta]e^{-\eta^2}+ \ldots .$$

Exact solutions were terminated with the t^2 coefficients due to their increasing complexity, although in principle one could solve to arbitrary order. In Chapter III a method for numerically determining the solutions to higher orders of t for an elliptic cylinder is outlined with results being given

as far as the t^7 coefficients. For the simpler case of a circular cylinder results by an analagous method have been given by Collins and Dennis (6).

2.4 HIGHER ORDER CORRECTIONS TO THE BOUNDARY-LAYER SOLUTIONS

Consider the case of p = 1. Equations (2.2.6) through (2.2.12) then reduce for q = 0,1,2,... to the equations

$$\frac{\partial^2 \omega_{1,q}}{\partial v^2} + 2v \frac{\partial \omega_{1,q}}{\partial v} - 4q\omega_{1,q} = -\beta_1 H_0^3 v[v \frac{\partial \omega_{0,q}}{\partial v} + (1-2q)\omega_{0,q}]$$

$$+ 4H_0 \sum_{n=1}^{q} [\frac{\partial(\Psi_{0,q-n}, \omega_{1,n-1})}{\partial(\eta, v)} + \frac{\partial(\Psi_{1,q-n}, \omega_{0,n-1})}{\partial(\eta, v)}] \ , \tag{2.4.1}$$

$$2 \frac{\partial^2 \Psi_{1,q}}{\partial v^2} = 2\omega_{1,q} + \beta_1 H_0^3 v \ \omega_{0,q} \ . \tag{2.4.2}$$

These must be solved subject to the conditions

$$\Psi_{1,q} = \frac{\partial \Psi_{1,q}}{\partial v} = 0 \quad \text{on } v = 0 \ , \tag{2.4.3}$$

$$\omega_{1,q} \to 0 \quad \text{as } v \to \infty \ , \tag{2.4.4}$$

$$2\int_0^\infty \int_0^{2\pi} H_0^{-1} \omega_{1,q} \sin n\eta \, d\eta \, dv = \int_0^\infty \int_0^{2\pi} v\omega_{0,q}(2n-\beta_1 H_0^2) \sin n\eta \, d\eta \, dv$$

$$(n=1,2,\ldots), \tag{2.4.5}$$

$$2 \int_0^\infty \int_0^{2\pi} H_0^{-1} \omega_{1,q} \cos n\eta \, d\eta \, dv = \int_0^\infty \int_0^{2\pi} v\omega_{0,q}(2n-\beta_1 H_0^2) \cos n\eta \, d\eta \, dv$$

$$(n=0,1,2,\ldots), \tag{2.4.6}$$

These equations can be solved in principle explicitly to arbitrary order q, in a manner similar to that outlined in Section 2.3. For p = 2, similar equations may be derived from equations (2.2.6) through (2.2.12) and solved in the same way. The following exact solutions have been found

$$\omega_{1,0} = \beta_1 H_0^3 U(\eta) A_2(v) + H_0 \sum_{n=1}^{\infty} (a_n \sin n\eta + b_n \cos n\eta) A_3(v), \tag{2.4.7}$$

$$\Psi_{1,0} = \beta_1 H_0^3 U(\eta) B_2(v) + H_0 \sum_{n=1}^{\infty} (a_n \sin n\eta + b_n \cos n\eta) B_3(v), \tag{2.4.8}$$

$$\begin{aligned}\omega_{1,1} = {} & \beta_1 H_0^4 U(\eta) U'(\eta) A_4(v) + H_0^2 U'(\eta) \sum_{n=1}^{\infty} (a_n \sin n\eta + b_n \cos n\eta) A_5(v) \\ & + \beta_1 H_0 U(\eta) \frac{d}{d\eta} [H_0^3 U(\eta)] A_6(v) + H_0 \sum_{n=1}^{\infty} (c_n \sin n\eta + d_n \cos n\eta) A_8(v) \\ & + H_0 U(\eta) \frac{d}{d\eta} [H_0 \sum_{n=1}^{\infty} (a_n \sin n\eta + b_n \cos n\eta)] A_7(v) ,\end{aligned} \tag{2.4.9}$$

$$\begin{aligned}\omega_{2,0} = {} & \beta_2 H_0^4 U(\eta) A_9(v) + \beta_1^2 H_0^6 U(\eta) A_{10}(v) + H_0^2 U(\eta) A_{13}(v) \\ & + \beta_1 H_0^4 \sum_{n=1}^{\infty} (a_n \sin n\eta + b_n \cos n\eta) A_{11}(v) + H_0^2 U''(\eta) A_{12}(v) \\ & + (H_0')^2 U(\eta) A_{14}(v) + H_0 \sum_{n=1}^{\infty} (C_n \sin n\eta + D_n \cos n\eta) A_{15}(v),\end{aligned} \tag{2.4.10}$$

where

$$a_n = \frac{n}{\pi} \int_0^{2\pi} U(\eta) \sin n\eta \, d\eta , \quad b_n = \frac{n}{\pi} \int_0^{2\pi} U(\eta) \cos n\eta \, d\eta,$$

$$c_n = \frac{n}{\pi} \left(\frac{3}{2} + \frac{2}{3\pi} - 2\sqrt{2}\right) \int_0^{2\pi} H_0 U(\eta) U'(\eta) \sin n\eta \, d\eta ,$$

$$d_n = \frac{n}{\pi}\left(\frac{3}{2} + \frac{2}{3\pi} - 2\sqrt{2}\right)\int_0^{2\pi} H_0 U(\eta)U'(\eta)\cos n\eta \, d\eta \ ,$$

$$C_n = -\frac{n^2}{\pi}\int_0^{2\pi} H_0 U(\eta)\sin n\eta \, d\eta - \frac{n\beta_1}{8\pi}\int_0^{2\pi} H_0{}^3 U(\eta)\sin n\eta \, d\eta$$

$$+ \frac{n}{\pi}\int_0^{2\pi} H_0 \sum_{m=1}^{\infty}(a_m \sin m\eta + b_m \cos m\eta)\sin n\eta \, d\eta \ ,$$

$$D_n = -\frac{n^2}{\pi}\int_0^{2\pi} H_0 U(\eta)\cos n\eta \, d\eta - \frac{n\beta_1}{8\pi}\int_0^{2\pi} H_0{}^3 U(\eta)\cos n\eta \, d\eta$$

$$+ \frac{n}{\pi}\int_0^{2\pi} H_0 \sum_{m=1}^{\infty}(a_m \sin m\eta + b_m \cos m\eta)\sin n\eta \, d\eta \ ,$$

and the $A_i(v)$, $(i=2,3,\ldots,15)$, $B_i(v)$, $(i=2,3)$, are defined in Appendix I.

In Chapter III a method for numerically determining the solutions of equations (2.4.1) through (2.4.6) is given for the case of an elliptic cylinder at varying angles of incidence. For the circular cylinder, results have already been given by Collins and Dennis (6).

It is found in practice that the right-hand side of equation (2.2.6) becomes increasingly more complicated the larger (p+q) becomes. The condition $p+q \leq 2$ was taken to be the restriction for finding exact solutions to these equations and no attempt was made to obtain expressions for terms of higher order. Using this means of specification Goldstein and Rosenhead's results (3) are equivalent to the conditions $p = 0$, $q \leq 2$, whilst Wang (4,5) used $p+q \leq 1$. The results given above for $p+q \leq 1$ agree with those of Wang's (5) inner expansion. For the case of a circular cylinder they are also in agree-

ment with those given by Collins and Dennis (6) for $p+q \leq 2$.

It is perhaps worth noting here that the analytic results given here are only true within the boundary-layer region close to the body. This is a consequence of replacing the exponential in the integral conditions (1.4.7) and (1.4.8) by its power-series expansion, and subsequently truncating the series. This assumption is very reasonable for small kz, which corresponds to a thin region surrounding the body. This region is of primary interest since outside of it the flow is virtually indistinguishable from the well-understood inviscid flow. Consequently the results are valid for moderate values of kz where the exponential can be well-approximated by the first few terms of its power series.

Collins and Dennis (6) noted this point and for a circular cylinder gave a first approximation to a uniformly valid expression. The expression

$$\Psi = \frac{K_0 \sin(\eta-\gamma)}{k(1+\operatorname{erf}\frac{kH_0}{2})} \left\{ e^{kz}\left[\operatorname{erf}\left(\frac{z}{H_0} - \frac{kH_0}{2}\right) + \operatorname{erf}\frac{kH_0}{2}\right] - e^{-kz}\left[\operatorname{erf}\left(\frac{z}{H_0} - \frac{3kH_0}{2}\right) + \operatorname{erf}\frac{3kH_0}{2}\right] \right\} , \qquad (2.4.11)$$

can be considered to be a first approximation to a uniformly valid one in the present case. It gives the following three regions:

(i) For $kz \ll 1$

$$\Psi \sim 2K_0 \sin(\eta-\gamma)\left[z \operatorname{erf}\frac{z}{H_0} + \frac{H_0}{\pi^{\frac{1}{2}}}\left(e^{-\frac{z^2}{H_0^2}} - 1\right)\right] = \Psi_{0,0} , \qquad (2.4.12)$$

i.e. flow within the boundary-layer region.

(ii) For $kz \sim 0(1)$

$$\Psi \sim \frac{2K_0}{k} \sinh kz \sin (\eta-\gamma) \ , \qquad (2.4.13)$$

i.e. potential flow outside the boundary layer.

(iii) For $kz \to \infty$

$$\Psi \sim \frac{K_0 e^{kz}}{k} \sin (\eta-\gamma) \ , \qquad (2.4.14)$$

i.e. uniform flow at infinity.

Although Wang (5) has given an expression for a uniformly valid solution it is incomplete since his $\Psi_2(\xi,\eta,t)$ was not given.

CHAPTER III

NUMERICAL INTEGRATION OF THE POWER SERIES EXPANSIONS FOR AN ELLIPSE

3.1 FOURIER EXPANSIONS OF THE BOUNDARY-LAYER POWER SERIES IN T

In this section we consider the Fourier expansion method of satisfying equations (2.3.1) through (2.3.6) for $q=0,1,2,\ldots$ for the case of an ellipse. In practice the infinite Fourier sums are approximated by a finite number of terms. This approach will enable us to eliminate the η-dependence from the equations and obtain ordinary differential equations in the variable v. In order to do this we make a preliminary transformation of dependent variables. An examination of the integral conditions (2.3.5) and (2.3.6) indicates that these conditions may be reduced to integral conditions on v alone by first making the transformation $\omega_{0,q} = H_0 \chi_{0,q}$, and then expanding $\chi_{0,q}$ in a Fourier series and evaluating the η part of the integrals. On making this transformation, a similar transformation for $\Psi_{0,q}$ is suggested by equation (2.3.2) in order to facilitate the subsequent Fourier analysis of this equation. Let

$$\omega_{0,q} = H_0 \chi_{0,q} \ , \quad \Psi_{0,q} = H_0 \Phi_{0,q} \ . \tag{3.1.1}$$

The equations (2.3.1) and (2.3.2) then become for $q=0,1,2,\ldots$

$$\frac{\partial^2 \chi_{0,q}}{\partial v^2} + 2v \frac{\partial \chi_{0,q}}{\partial v} + 2(1-2q)\chi_{0,q} = 4H_0^2 \sum_{n=1}^{q} \left[\frac{\partial(\Phi_{0,q-n}, \chi_{0,n-1})}{\partial(\eta, v)}\right]$$

$$- 4H_0 H_0'(\eta) \sum_{n=1}^{q} \left(\chi_{0,n-1} \frac{\partial \Phi_{0,q-n}}{\partial v} - \Phi_{0,q-n} \frac{\partial \chi_{0,n-1}}{\partial v}\right), \tag{3.1.2}$$

$$\frac{\partial^2 \Phi_{0,q}}{\partial v^2} = \chi_{0,q} \quad , \tag{3.1.3}$$

to be solved subject to the conditions

$$\Phi_{0,q} = \frac{\partial \Phi_{0,q}}{\partial v} = 0 \text{ on } v = 0 \quad , \tag{3.1.4}$$

$$\chi_{0,q} \to 0 \text{ as } v \to \infty \ , \tag{3.1.5}$$

$$\int_0^{\infty}\int_0^{2\pi} \chi_{0,q} \sin n\eta \, d\eta \, dv = 2K_0 \pi \cos\gamma \delta_{n,1}\delta_{q,0} \qquad (n=1,2,\ldots), \tag{3.1.6}$$

$$\int_0^{\infty}\int_0^{2\pi} \chi_{0,q} \cos n\eta \, d\eta \, dv = -2K_0 \pi \sin\gamma \delta_{n,1}\delta_{q,0} \qquad (n=0,1,2,\ldots), \tag{3.1.7}$$

where $H_0'(\eta) = \dfrac{dH_0}{d\eta}$.

The only difficulty in completing the Fourier analysis occurs in the handling of the right-hand side of equation (3.1.2). If we now restrict ourselves to the case of an elliptic cylinder then we know $H_0'(\eta)$ explicitly, i.e.

$$H_0'(\eta) = \frac{-H_0^{\,3} \sin 2\eta}{2} \quad ,$$

where $$H_0^{\,2} = \frac{2}{\cosh 2\alpha - \cos 2\eta} \ .$$

Using the above result for $H_0'(\eta)$ we may rewrite the right-

hand side of equation (3.1.2) as

$$4\sum_{n=1}^{q}\left[\frac{\partial\Phi_{0,q-n}}{\partial\eta}\frac{\partial}{\partial v}\left(H_0{}^2\chi_{0,n-1}\right)-\frac{\partial}{\partial v}\left(H_0{}^2\Phi_{0,q-n}\right)\frac{\partial\chi_{0,n-1}}{\partial\eta}\right]$$

$$+\,2\sum_{n=1}^{q}\left[\left(H_0{}^2\chi_{0,n-1}\right)\frac{\partial}{\partial v}\left(H_0{}^2\Phi_{0,q-n}\right)-\left(H_0{}^2\Phi_{0,q-n}\right)\frac{\partial}{\partial v}\left(H_0^2{}'\chi_{0,n-1}\right)\right],$$

which is now in a form that expedites the completion of the Fourier analysis.

If we now expand $H_0{}^2\chi$ and $H_0{}^2\Phi$ in Fourier series, we see that on applying the standard methods for orthogonal functions to equations (3.1.2) and (3.1.3) we obtain sets of ordinary differential equations in the variable v. This procedure effectively removes the η-dependence from the problem and reduces it to the solution of ordinary differential equations. It should be noted that the coefficients in the Fourier expansions for χ and $H_0{}^2\chi$ are related, and that from a knowledge of the coefficients for the expansion of χ we may deduce those for the expansion of $H_0{}^2\chi$. The expansions for Φ and $H_0{}^2\Phi$ are related in a similar manner. In obtaining these and other relations it is necessary to define the following coefficients for n=1 and 2;

$$I_n(r,s)=\frac{1}{\pi}\int_0^{2\pi}H_0{}^n\sin r\eta\,\sin s\eta\,d\eta\quad(r=1,2,\ldots\ ;\ s=1,2,\ldots),\tag{3.1.8}$$

$$J_n(r,s)=\frac{1}{\pi}\int_0^{2\pi}H_0{}^n\cos r\eta\,\cos s\eta\,d\eta\quad(r=1,2,\ldots\ ;\ s=1,2,\ldots).\tag{3.1.9}$$

Note that $I_n(r,s)$ and $J_n(r,s)$ are identically zero for

(r+s) odd, and that

$$\frac{1}{\pi}\int_0^{2\pi} H_0^n \sin r\eta \cos s\eta \, d\eta = 0 \quad (r=1,2,\ldots\ ;\ s=1,2,\ldots). \tag{3.1.10}$$

For n=2, $I_n(r,s)$ and $J_n(r,s)$ may be evaluated analytically in the case of an ellipse and are given below, where (r+s) is even and $r \geq s$, (this can always be arranged since I_n and J_n are both symmetric in r and s):

$$I_2(r,s) = \frac{4e^{-r\alpha}\sinh s\alpha}{\sinh 2\alpha}, \qquad J_2(r,s) = \frac{4e^{-r\alpha}\cosh s\alpha}{\sinh 2\alpha}. \tag{3.1.11}$$

For n=1 it is difficult, if not impossible, to evaluate $I_n(r,s)$ and $J_n(r,s)$ analytically, however they may be integrated numerically using Filon-type quadrature and they become exponentially small for increasing (r+s).

The notation used in this chapter for the functions in the Fourier expansions is not referred to elsewhere, and no confusion with other variables should arise. Let us make the following expansions for $\chi_{0,q}$ and $\Phi_{0,q}$ where q=0,1,2,...;

$$\chi_{0,q}(\eta,v) = \frac{1}{2}P^{(0)}_{0,q}(v) + \sum_{p=1}^{\infty}[P^{(0)}_{p,q}(v)\cos p\eta + Q^{(0)}_{p,q}(v)\sin p\eta],$$

$$\Phi_{0,q}(\eta,v) = \frac{1}{2}R^{(0)}_{0,q}(v) + \sum_{p=1}^{\infty}[R^{(0)}_{p,q}(v)\cos p\eta + S^{(0)}_{p,q}(v)\sin p\eta], \tag{3.1.12}$$

$$H_0^2\chi_{0,q}(\eta,v) = \tfrac{1}{2}\,T^{(0)}_{0,q}(v) + \sum_{p=1}^{\infty}[T^{(0)}_{p,q}(v)\cos p\eta + U^{(0)}_{p,q}(v)\sin p\eta],$$

$$H_0^2\Phi_{0,q}(\eta,v) = \tfrac{1}{2}\,V^{(0)}_{0,q}(v) + \sum_{p=1}^{\infty}[V^{(0)}_{p,q}(v)\cos p\eta + W^{(0)}_{p,q}(v)\sin p\eta].$$

(3.1.13)

The following relations, also true for v-derivatives, will then result;

$$T^{(0)}_{0,q} = \tfrac{1}{2}\,[I_2(1,1)+J_2(1,1)]P^{(0)}_{0,q} + \sum_{\ell=1}^{\infty}[I_2(\ell+1,1)+J_2(\ell+1,1)]P^{(0)}_{\ell,q},$$

$$V^{(0)}_{0,q} = \tfrac{1}{2}\,[I_2(1,1)+J_2(1,1)]R^{(0)}_{0,q} + \sum_{\ell=1}^{\infty}[I_2(\ell+1,1)+J_2(\ell+1,1)]R^{(0)}_{\ell,q},$$

(3.1.14)

$$\left.\begin{aligned} T^{(0)}_{p,q} &= \tfrac{1}{2}\,[I_2(p+1,1)+J_2(p+1,1)]P^{(0)}_{0,q} + \sum_{\ell=1}^{\infty}J_2(\ell,p)P^{(0)}_{\ell,q},\\ V^{(0)}_{p,q} &= \tfrac{1}{2}\,[I_2(p+1,1)+J_2(p+1,1)]R^{(0)}_{0,q} + \sum_{\ell=1}^{\infty}J_2(\ell,p)R^{(0)}_{\ell,q},\end{aligned}\right\} \quad (3.1.15)$$

$$\left.\begin{aligned} U^{(0)}_{p,q} &= \sum_{\ell=1}^{\infty} I_2(\ell,p)Q^{(0)}_{\ell,q},\\ W^{(0)}_{p,q} &= \sum_{\ell=1}^{\infty} I_2(\ell,p)S^{(0)}_{\ell,q}.\end{aligned}\right\} \quad (3.1.16)$$

Thus the expansions for χ and Φ immediately yield the expansions for $H_0^2\chi$ and $H_0^2\Phi$.

Using the above expansions and the usual methods for orthogonal functions we obtain the following sets of equations, where primes denote differentiation with respect to v, the Γ's and Δ's are defined in Appendix II, and p=1,2,...;

$q=0,1,2,\ldots$.

The functions $P^{(0)}_{0,q}$ satisfy

$$P^{(0)\prime\prime}_{0,q} + 2v\,P^{(0)\prime}_{0,q} + 2(1-2q)P^{(0)}_{0,q} = \Gamma^{(0)}_{0,q}(v), \qquad (3.1.17)$$

subject to

$$\left.\begin{aligned} &P^{(0)}_{0,q} \to 0 \text{ as } v \to \infty , \\ &\int_0^\infty P^{(0)}_{0,q}\,dv = 0 \ . \end{aligned}\right\} \qquad (3.1.18)$$

The equations for $P^{(0)}_{p,q}$ are

$$P^{(0)\prime\prime}_{p,q} + 2v\,P^{(0)\prime}_{p,q} + 2(1-2q)P^{(0)}_{p,q} = \Gamma^{(0)}_{p,q}(v), \qquad (3.1.19)$$

subject to

$$\left.\begin{aligned} &P^{(0)}_{p,q} \to 0 \quad \text{as} \quad v \to \infty , \\ &\int_0^\infty P^{(0)}_{p,q}\,dv = -2K_0 \sin\gamma\delta_{p,1}\delta_{q,0} \ . \end{aligned}\right\} \qquad (3.1.20)$$

The equations for $Q^{(0)}_{p,q}$ are

$$Q^{(0)\prime\prime}_{p,q} + 2v\,Q^{(0)\prime}_{p,q} + 2(1-2q)Q^{(0)}_{p,q} = \Delta^{(0)}_{p,q}(v), \qquad (3.1.21)$$

subject to

$$\left.\begin{aligned} &Q^{(0)}_{p,q} \to 0 \quad \text{as} \quad v \to \infty , \\ &\int_0^\infty Q^{(0)}_{p,q}\,dv = 2K_0 \cos\gamma\delta_{p,1}\delta_{q,0} \ . \end{aligned}\right\} \qquad (3.1.22)$$

Finally, the functions $R^{(0)}_{0,q}$, $R^{(0)}_{p,q}$ and $S^{(0)}_{p,q}$ satisfy

$$R^{(0)\prime\prime}_{0,q} = P^{(0)}_{0,q} \text{ with } R^{(0)}_{0,q} = R^{(0)\prime}_{0,q} = 0 \text{ on } v = 0, \qquad (3.1.23)$$

$$R^{(0)''}_{p,q} = P^{(0)}_{p,q} \text{ with } R^{(0)}_{p,q} = R^{(0)'}_{p,q} = 0 \text{ on } v = 0, \qquad (3.1.24)$$

$$S^{(0)''}_{p,q} = Q^{(0)}_{p,q} \text{ with } S^{(0)}_{p,q} = S^{(0)'}_{p,q} = 0 \text{ on } v = 0. \qquad (3.1.25)$$

The numerical techniques for solving these equations are described in Section 3.3. The general procedure is as follows:

(i) Set q = 0. From the exact expressions previously given for $\chi_{0,0}$ and $\Phi_{0,0}$ it is found that

$$P^{(0)}_{0,0} = 0 \ , \ P^{(0)}_{p,0} = \frac{4K_0}{\pi^{\frac{1}{2}}} \cos\gamma\delta_{p,1} e^{-v^2} \ , \ Q^{(0)}_{p,0} = \frac{-4K_0}{\pi^{\frac{1}{2}}} \sin\gamma\delta_{p,1} e^{-v^2} \qquad (3.1.26)$$

$$\left.\begin{aligned} R^{(0)}_{0,0} &= 0 \ , \ R^{(0)}_{p,0} = 2K_0 \cos\gamma\delta_{p,1} \left[v \operatorname{erf} v + \frac{1}{\pi^{\frac{1}{2}}} (e^{-v^2} - 1)\right], \\ S^{(0)}_{p,0} &= -2K_0 \sin\gamma\delta_{p,1} \left[v \operatorname{erf} v + \frac{1}{\pi^{\frac{1}{2}}} (e^{-v^2} - 1)\right]. \end{aligned}\right\} \qquad (3.1.27)$$

We then find $P^{(0)'}_{0,0}$, $R^{(0)'}_{0,0}$, $P^{(0)'}_{p,0}$, $Q^{(0)'}_{p,0}$, $R^{(0)'}_{p,0}$, $S^{(0)'}_{p,0}$, for $p=1,2,\ldots p_M$, and $T^{(0)}_{0,0}$, $V^{(0)}_{0,0}$, $T^{(0)}_{p,0}$, $U^{(0)}_{p,0}$, $V^{(0)}_{p,0}$, $W^{(0)}_{p,0}$ for $p=1,2,\ldots p_M$ using relations (3.1.14) through (3.1.16), where p_M is the value of p taken for the truncation of the Fourier series.

(ii) Increment q by 1. Solve equation (3.1.17) subject to conditions (3.1.18). Solve equations (3.1.19) and (3.1.21) subject to conditions (3.1.20) and (3.1.22) for $p=1,2,\ldots p_M$. Note that the right-hand sides of equations (3.1.17), (3.1.19) and (3.1.21) are known explicitly. We then find $T^{(0)}_{0,q}$, $V^{(0)}_{0,q}$, $T^{(0)}_{p,q}$, $U^{(0)}_{p,q}$, $V^{(0)}_{p,q}$, $W^{(0)}_{p,q}$ for $p=1,2,\ldots p_M$ using relations

(3.1.14) through (3.1.16) and all derivatives.

(iii) Repeat (ii) to order required.

3.2 FOURIER EXPANSIONS OF THE POWER SERIES IN T FOR THE K COEFFICIENTS

In this section we consider the Fourier expansion method of satisfying equations (2.4.1) through (2.4.6) for q=0,1,2,... for the case of an ellipse, in a similar manner to that outlined in Section 3.1.

Let

$$\omega_{1,q} = H_0 \chi_{1,q} \ , \ \Psi_{1,q} = H_0 \Phi_{1,q} . \tag{3.2.1}$$

Then equations (2.4.1) and (2.4.2) become for q=0,1,2,...

$$\frac{\partial^2 \chi_{1,q}}{\partial v^2} + 2v \frac{\partial \chi_{1,q}}{\partial v} - 4q\chi_{1,q} = - \beta_1 H_0^{\,3} v [v \frac{\partial \chi_{0,q}}{\partial v} + (1-2q)\chi_{0,q}]$$

$$+ 4H_0^{\,2} \sum_{n=1}^{q} [\frac{\partial(\Phi_{0,q-n}, \chi_{1,n-1})}{\partial(\eta, v)} + \frac{\partial(\Phi_{1,q-n}, \chi_{0,n-1})}{\partial(\eta, v)}]$$

$$+ 2H_0^{\,4} \sin 2\eta \sum_{n=1}^{q} [\chi_{1,n-1} \frac{\partial \Phi_{0,q-n}}{\partial v} - \Phi_{0,q-n} \frac{\partial \chi_{1,n-1}}{\partial v}$$

$$+ \chi_{0,n-1} \frac{\partial \Phi_{1,q-n}}{\partial v} - \Phi_{1,q-n} \frac{\partial \chi_{0,n-1}}{\partial v}] \ , \tag{3.2.2}$$

$$2 \frac{\partial^2 \Phi_{1,q}}{\partial v^2} = 2\chi_{1,q} + \beta_1 H_0^{\,3} v \chi_{0,q} \ , \tag{3.2.3}$$

to be solved subject to the conditions

$$\Phi_{1,q} = \frac{\partial \Phi_{1,q}}{\partial v} = 0 \text{ on } v = 0 \ , \tag{3.2.4}$$

$$\chi_{1,q} \to 0 \text{ as } v \to \infty \ , \tag{3.2.5}$$

$$2\int_0^{\infty}\int_0^{2\pi} \chi_{1,q} \sin n\eta \, d\eta \, dv = \int_0^{\infty}\int_0^{2\pi} H_0\chi_{0,q} v[2n-\beta_1 H_0^2]\sin n\eta \, d\eta \, dv, \tag{3.2.6}$$

$$2\int_0^{\infty}\int_0^{2\pi} \chi_{1,q} \cos n\eta \, d\eta \, dv = \int_0^{\infty}\int_0^{2\pi} H_0\chi_{0,q} v[2n-\beta_1 H_0^2]\cos n\eta \, d\eta \, dv . \tag{3.2.7}$$

Let

$$H_0\chi_{0,q} = \frac{1}{2} L_{0,q}^{(0)} + \sum_{p=1}^{\infty} (L_{p,q}^{(0)}\cos p\eta + M_{p,q}^{(0)} \sin p\eta), \tag{3.2.8}$$

$$H_0^3\chi_{0,q} = \frac{1}{2} N_{0,q}^{(0)} + \sum_{p=1}^{\infty} (N_{p,q}^{(0)}\cos p\eta + O_{p,q}^{(0)} \sin p\eta) . \tag{3.2.9}$$

Then the coefficients on the right sides may be determined from the equations

$$\begin{aligned}
L_{0,q}^{(0)} &= \tfrac{1}{2}[I_1(1,1)+J_1(1,1)]P_{0,q}^{(0)} + \sum_{\ell=1}^{\infty}[I_1(\ell+1,1)+J_1(\ell+1,1)]P_{\ell,q}^{(0)} , \\
L_{p,q}^{(0)} &= \tfrac{1}{2}[I_1(p+1,1)+J_1(p+1,1)]P_{0,q}^{(0)} + \sum_{\ell=1}^{\infty} J_1(\ell,p)P_{\ell,q}^{(0)} , \\
M_{p,q}^{(0)} &= \sum_{\ell=1}^{\infty} I_1(\ell,p)\, Q_{\ell,q}^{(0)} , \\
N_{0,q}^{(0)} &= \tfrac{1}{2}[I_1(1,1)+J_1(1,1]T_{0,q}^{(0)} + \sum_{\ell=1}^{\infty}[I_1(\ell+1,1)+J_1(\ell+1,1]T_{\ell,q}^{(0)} , \\
N_{p,q}^{(0)} &= \tfrac{1}{2}[I_1(p+1,1)+J_1(p+1)]T_{0,q}^{(0)} + \sum_{\ell=1}^{\infty} J_1(\ell,p)T_{\ell,q}^{(0)} , \\
O_{p,q}^{(0)} &= \sum_{\ell=1}^{\infty} I_1(\ell,p)U_{\ell,q}^{(0)} .
\end{aligned} \tag{3.2.10, 3.2.11}$$

Equations (3.2.8) and (3.2.9) are defined for use in equat-

ions (3.2.3), (3.2.6) and (3.2.7). It is assumed in the development of the present section that all the expansions of $\chi_{0,q}$ and $\Phi_{0,q}$ are known as the result of solving for the boundary-layer case to some order of q. It remains to define the expansions for $\chi_{1,q}$ and $\Phi_{1,q}$ and to substitute these expansions into the governing equations. Let us therefore make the expansions

$$\left.\begin{aligned} \chi_{1,q} &= \tfrac{1}{2} P_{0,q}^{(1)} + \sum_{p=1}^{\infty} [P_{p,q}^{(1)} \cos p\eta + Q_{p,q}^{(1)} \sin p\eta], \\ \Phi_{1,q} &= \tfrac{1}{2} R_{0,q}^{(1)} + \sum_{p=1}^{\infty} [R_{p,q}^{(1)} \cos p\eta + S_{p,q}^{(1)} \sin p\eta], \end{aligned}\right\} \qquad (3.2.12)$$

$$\left.\begin{aligned} H_0^{\,2}\chi_{1,q} &= \tfrac{1}{2} T_{0,q}^{(1)} + \sum_{p=1}^{\infty} [T_{p,q}^{(1)} \cos p\eta + U_{p,q}^{(1)} \sin p\eta], \\ H_0^{\,2}\Phi_{1,q} &= \tfrac{1}{2} V_{0,q}^{(1)} + \sum_{p=1}^{\infty} [V_{p,q}^{(1)} \cos p\eta + W_{p,q}^{(1)} \sin p\eta], \end{aligned}\right\} \qquad (3.2.13)$$

for $\chi_{1,q}$ and $\Phi_{1,q}$, where q = 0,1,2,... .

Relations similar to those of equations (3.1.14) through (3.1.16) will result, with superscript (1) replacing superscript (2), which enables us to calculate the expansions for $H_0^{\,2}\chi_{1,q}$ and $H_0^{\,2}\Phi_{1,q}$ from the expansions for $\chi_{1,q}$ and $\Phi_{1,q}$. The application of the previously defined expansions result in the following sets of equations, where primes denote differentiation with respect to v, the $\Gamma^{(1)}$'s and $\Delta^{(1)}$'s are defined in Appendix II, and p=1,2,...; q=0,1,2,... . The functions $P_{0,q}^{(1)}$ satisfy

$$P_{0,q}^{(1)''} + 2v\, P_{0,q}^{(1)'} - 4q\, P_{0,q}^{(1)} = \Gamma_{0,q}^{(1)}, \qquad (3.2.14)$$

subject to

$$\left.\begin{aligned} & P_{0,q}^{(1)} \to 0 \text{ as } v \to \infty \ , \\ & \int_0^\infty P_{0,q}^{(1)}\, dv = \frac{-\beta_1}{2} \int_0^\infty v\, N_{0,q}^{(0)}\, dv \ . \end{aligned}\right\} \tag{3.2.15}$$

The equations for $P_{p,q}^{(1)}$ are

$$P_{p,q}^{(1)"} + 2v\, P_{p,q}^{(1)'} - 4q\, P_{p,q}^{(1)} = \Gamma_{p,q}^{(1)}(v) \ , \tag{3.2.16}$$

subject to

$$\left.\begin{aligned} & P_{p,q}^{(1)} \to 0 \text{ as } v \to \infty \ , \\ & \int_0^\infty P_{p,q}^{(1)}\, dv = \int_0^\infty v[pL_{p,q}^{(0)} - \frac{\beta_1}{2} N_{p,q}^{(0)}]\, dv. \end{aligned}\right\} \tag{3.2.17}$$

The equations for $Q_{p,q}^{(1)}$ are

$$Q_{p,q}^{(1)"} + 2v\, Q_{p,q}^{(1)'} - 4q\, Q_{p,q}^{(1)} = \Delta_{p,q}^{(1)}(v) \ , \tag{3.2.18}$$

subject to

$$\left.\begin{aligned} & Q_{p,q}^{(1)} \to 0 \text{ as } v \to \infty \ , \\ & \int_0^\infty Q_{p,q}^{(1)}\, dv = \int_0^\infty v[pM_{p,q}^{(0)} - \frac{\beta_1}{2} O_{p,q}^{(0)}]\, dv. \end{aligned}\right\} \tag{3.2.19}$$

The equations for the functions $R_{0,q}^{(1)}$, $R_{p,q}^{(1)}$ and $S_{p,q}^{(1)}$ are

$$\begin{aligned} R_{0,q}^{(1)"} &= P_{0,q}^{(1)} + \frac{\beta_1 v}{2} N_{0,q}^{(0)} \quad \text{with } R_{0,q}^{(1)} = R_{0,q}^{(1)'} = 0 \text{ on } v = 0, \\ R_{p,q}^{(1)"} &= P_{p,q}^{(1)} + \frac{\beta_1 v}{2} N_{p,q}^{(0)} \quad \text{with } R_{p,q}^{(1)} = R_{p,q}^{(1)'} = 0 \text{ on } v = 0, \\ S_{p,q}^{(1)"} &= Q_{p,q}^{(1)} + \frac{\beta_1 v}{2} O_{p,q}^{(0)} \quad \text{with } S_{p,q}^{(1)} = S_{p,q}^{(1)'} = 0 \text{ on } v = 0 \ . \end{aligned} \tag{3.2.20}$$

The numerical techniques for solving these equations are described in Section 3.3, whilst the general procedure is similar to that described at the end of Section 3.1. Solutions to equations (3.1.17) through (3.1.25) must be known to the order of q required before solving equations (3.2.14) through (3.2.20).

3.3 NUMERICAL TECHNIQUES

The differential equations to be solved are all either of the form

$$y''(v) + 2v\, y'(v) + b\, y(v) = k(v) \ , \qquad (3.3.1)$$

subject to

$$y(v) \to 0 \text{ as } v \to \infty \ , \ \int_0^\infty y(v)\,dv = a \ ; \qquad (3.3.2)$$

or of the form

$$u''(v) = \ell(v) \ , \qquad (3.3.3)$$

subject to

$$u(v) = u'(v) = 0 \text{ on } v = 0 \ , \qquad (3.3.4)$$

where a,b are known constants.

In practice the infinite integral in condition (3.3.2) must be restricted to a finite domain $(0, v_M)$, where v_M is sufficiently large to ensure accurate evaluation of the integral. In fact we are writing the integral as

$$\int_0^\infty y\ dv = \int_0^{v_M} y\ dv + \int_{v_M}^\infty y\ dv \ , \qquad (3.3.5)$$

and assuming that $\int_{v_M}^\infty y\ dv$ can be neglected. This is reasonable since the y represents a component of vorticity which decays exponentially to zero.

To obtain an accurate method of solution to equation

(3.3.1) we remove the first derivative by the transformation

$$y = g(v)e^{-\frac{v^2}{2}} . \tag{3.3.6}$$

This gives the equation

$$g''(v) - m(v)g(v) = n(v) , \tag{3.3.7}$$

to be solved subject to

$$g(v_M) = 0 , \int_0^{v_M} g(v)e^{-\frac{v^2}{2}} dv = a, \tag{3.3.8}$$

where $m(v) = v^2 + 1 - b$, $n(v) = k(v)e^{\frac{v^2}{2}}$.

Since equation (3.3.7) is a second order linear differential equation we may write g as the sum of the homogeneous solution and a particular solution.

Let

$$g = \lambda g_H + g_P , \tag{3.3.9}$$

where

$$g_H'' - m(v)g_H = 0 \text{ with } g_H(0) = 1, \; g_H(v_M) = 0, \tag{3.3.10}$$

$$g_P'' - m(v)g_P = n(v) \text{ with } g_P(0) = 1, g_P(v_M) = 0. \tag{3.3.11}$$

To evaluate the constant λ we use the integral condition (3.3.8) to obtain

$$\lambda = \frac{a - \int_0^{v_M} g_P e^{-\frac{v^2}{2}} dv}{\int_0^{v_M} g_H e^{-\frac{v^2}{2}} dv} . \tag{3.3.12}$$

A finite-difference approximation to equation (3.3.7) correct to order h^6 (see Fox (25), p.68) is

$$g_{i-1}(1 - \frac{h^2}{12} m_{i-1}) - g_i(2 + \frac{5h^2}{6} m_i) + g_{i+1}(1 - \frac{h^2}{12} m_{i+1}) = \frac{h^2}{12}(n_{i-1} + 10n_i + n_{i+1}), \qquad (3.3.13)$$

where i-1,i,i+1 denote three successive points of a uniform grid of size $h = v_i - v_{i-1}$.

Using the finite-difference approximation (3.3.13), equations (3.3.10) and (3.3.11) may be solved as matrix problems, from which λ may then be calculated using Simpson quadrature to evaluate the integrals and finally obtain y, the solution of equation (3.3.1). A direct method of solving the matrix problems was used, rather than an iterative procedure, details being given in Appendix III. This method of solution is very accurate.

As an illustration of this a typical equation, given below, was solved with two grid sizes $h = 0.05$, $h = 0.025$ with y_M taken to be 7. The equation considered was

$$y'' + 2vy' - 2y = 16e^{-v^2}[(1+2v^2)\operatorname{erf} v + \frac{2v}{\pi^{\frac{1}{2}}}(e^{-v^2} - 1)], \qquad (3.3.14)$$

subject to

$$\int_0^\infty y\, dx = 0, \quad y \to 0 \text{ as } v \to \infty .$$

This equation occurs in the exact solution for the function $\omega_{0,1}$ and its solution is $y = 2\pi^{\frac{1}{2}} A_1$, where A_1 is defined in Appendix I.

We are particularly interested in the solution on $v = 0$, since many of the properties of the fluid may be calculated from the surface solutions. A comparison of the exact solution of equation (3.3.14) and that obtained from the

numerical method using grid values of h = 0.050 and 0.025 respectively, is given in Table (3.3.1).

v	Exact	h=0.050	h=0.025
0	0.5697653 E+01	0.5697655 E+01	0.5697653 E+01
1	-0.1365999 E+01	-0.1366000 E+01	-0.1365999 E+01
2	-0.2689796 E+00	-0.2689796 E+00	-0.2689796 E+00
4	-0.6478746 E-05	-0.6478747 E-05	-0.6478745 E-05
6	-0.3056275 E-13	-0.3056205 E-13	-0.3056263 E-13

TABLE (3.3.1)

In all the subsequent calculations h was taken to be 0.05 and v_M to be 7. As the above results suggest, these values are more than adequate, and the method is indeed accurate.

To solve equation (3.3.3) subject to conditions (3.3.4) the following well known step-by-step method was used; u_1 is calculated from the one-step formula

$$u_1 = \frac{h^2}{6}[2\ell_0 + \ell_1] + 0(h4) \ , \qquad (3.3.15)$$

whilst u_{n+1} for n=1,2,3,... is calculated from the two-step formula

$$u_{n+1} = 2u_n - u_{\ell-1} + \frac{h^2}{12}[\ell_{n-1}+10\ell_n+\ell_{n-1}]+0(R^6), \qquad (3.3.16)$$

where h, as before, is the uniform grid size $v_{n+1} - v_n$.

All derivatives required for the evaluation of the right-hand side of equation (3.3.1) were calculated using six-point formulae accurate to order h^6.

3.4 RESULTS FOR THE BOUNDARY-LAYER EXPANSIONS

Two elliptic cylinders of aspect ratios $\tau_1 = 0.3$ and $\tau_1 = 0.6$ respectively, were considered at various angles of inclination. For $\tau_1 = 0.6$, calculations were made at angles of incidence $\gamma = 0°, 15°, 30°, 45°$ and $90°$, whilst for $\tau_1 = 0.3$ only the case $\gamma = 15°$ was studied.

Table (3.4.1) displays the values of the parameters used, where:-

p_M is the value taken for the truncation of the Fourier Series,

q_M is the value taken for the truncation of the polynomial series in t^q,

v_M is the value taken for the upper limit of integration of the integral boundary conditions (3.1.18), (3.1.20), (3.1.22) and

h is the grid size taken in the solution of the ordinary differential equations.

	p_M	q_M	v_M	h
$\tau_1=0.3$	81	6	7	0.05
$\tau_1=0.6$	41	7	7	0.05

TABLE (3.4.1)

It can be shown that

$$\chi_{0,1} = \sum_{p=1}^{\infty} [P_{p,1}^{(0)} \cos p\eta + Q_{p,1}^{(0)} \sin p\eta], \qquad (3.4.1)$$

where

$$P_{p,1}^{(0)} = 4K_0^2 \sin 2\gamma \, A_1(v) \, p \, e^{-p\alpha} \quad \text{for p even,}$$

$$= 0 \quad \text{for p odd,}$$

$$Q_{p,1}^{(0)} = 4K_0^2 \frac{(1-\cos 2\gamma \cosh 2\alpha)}{\sinh 2\alpha} A_1(v) p\, e^{-p\alpha} \quad \text{for p even,}$$

$$= 0 \quad \text{for p odd.}$$

The error E in truncating this series to p_M terms can then be shown for large p_M to behave as $(p_M+1)e^{-(p_M+1)\alpha}$, where p_M is assumed odd, to within a multipluative constant independent of p_M.

For $\tau_1=0.3$ and $p_M = 81$, this gives $E \sim 0(10^{-9})$, whilst for $\tau_1=0.6$ and $p_M = 41$, this gives $E \sim 0(10^{-11})$.

It can be seen that the number of terms required in the Fourier Series to describe adequately the quantities increases as the ellipse becomes thinner. It should also be noted that a doubling of p_M results in a quadrupling of the computation time, as indicated by the form of the Γ's and Δ's, and the number of equations to be solved in which they appear, i.e. the computation time is proportional to p_M^2.

It is found that the truncation error incurred by the Fourier series expansions becomes progressively worse the larger the power of t. Throughout the calculations the order of the first term omitted divided by the largest term was always better than 10^{-3}. It is thought that the values of Φ and χ calculated from these coefficients are accurate to three significant figures provided t is sufficiently small to ensure that truncation of the t-series also meets this criterion.

Various properties of the fluid may be calculated from a knowledge of the values of the coefficients and their

v-derivatives on the surface of the cylinder (i.e. v=0). Further details of the calculation of these properties (including the extension to finite Reynolds number) are given in Appendix IV. Due to the large amount of data involved, only coefficients for the one case, viz. τ_1=0.6 at γ=15°, are given explicitly, although calculated properties are given for all cases. Tables (3.4.2) through (3.4.9) give the values of $P^{(0)}_{p,q}(v)$, $Q^{(0)}_{p,q}(v)$, $P^{(0)'}_{p,q}$, $Q^{(0)'}_{p,q}(v)$ on v=0, where p refers to the Fourier series expansion, and q to the polynomial expansion in t. It can be seen from the analysis that $P^{(0)}_{p,q} = Q^{(0)}_{p,q} = P^{(0)'}_{p,q} = Q^{(0)'}_{p,q} = 0$ for (p+q) even, and consequently these coefficients have been omitted from the tables.

As previously mentioned, the coefficients for q=1 are known analytically, [see equation (3.4.1)], and generally give six-figure agreement with the numerical results, confirming the belief that the only significant error is due to the truncation of the series in t, rather than the accuracy of the numerical methods. Further checks consolidate this view, and the truncation of the power series in t does not generally become significant until quite some time after the fluid has first separated from the ellipse.

Separation of the fluid from the cylinder (i.e. the existence of a recirculatory region behind the cylinder) first occurs for the smallest (positive) value of t satisfying $\chi = \frac{\partial \chi}{\partial \eta} = 0$ on $v = 0$, and at a corresponding value of η. Goldstein and Rosenhead (3) gave the expression

	t^0 q=0	t^2 q=2	t^4 q=4	t^6 q=6
$P^{(0)}_{1,q}$	-0.5841 E+00	0.1243 E+00	0.3572 E-01	-0.4936 E-01
$P^{(0)}_{3,q}$	0.	0.3846 E+00	0.2233 E-01	-0.1068 E+00
$P^{(0)}_{5,q}$	0.	0.4071 E+00	-0.1075 E+00	-0.1526 E+00
$P^{(0)}_{7,q}$	0.	0.2702 E+00	-0.2577 E+00	-0.9452 E-01
$P^{(0)}_{9,q}$	0.	0.1411 E+00	-0.3106 E+00	0.4831 E-01
$P^{(0)}_{11,q}$	0.	0.6368 E-01	-0.2682 E+00	0.1772 E+00
$P^{(0)}_{13,q}$	0.	0.2608 E-01	-0.1878 E+00	0.2295 E+00
$P^{(0)}_{15,q}$	0.	0.9962 E-02	-0.1137 E+00	0.2109 E+00
$P^{(0)}_{17,q}$	0.	0.3610 E-02	-0.6181 E-01	0.1578 E+00
$P^{(0)}_{19,q}$	0.	0.1256 E-02	-0.3089 E-01	0.1023 E+00
$P^{(0)}_{21,q}$	0.	0.4228 E-03	-0.1444 E-01	0.5930 E-01
$P^{(0)}_{23,q}$	0.	0.1386 E-03	-0.6390 E-02	0.3146 E-01
$P^{(0)}_{25,q}$	0.	0.4441 E-04	-0.2701 E-02	0.1550 E-01
$P^{(0)}_{27,q}$	0.	0.1396 E-04	-0.1100 E-02	0.7168 E-02
$P^{(0)}_{29,q}$	0.	0.4320 E-05	-0.4321 E-03	0.3135 E-02
$P^{(0)}_{31,q}$	0.	0.1318 E-05	-0.1651 E-03	0.1304 E-02
$P^{(0)}_{33,q}$	0.	0.3969 E-06	-0.6152 E-04	0.5182 E-03
$P^{(0)}_{35,q}$	0.	0.1183 E-06	-0.2241 E-04	0.1970 E-03
$P^{(0)}_{37,q}$	0.	0.3491 E-07	-0.7999 E-05	0.7106 E-04
$P^{(0)}_{39,q}$	0.	0.1021 E-07	-0.2787 E-05	0.2121 E-04
$P^{(0)}_{41,q}$	0.	0.2974 E-08	-0.8755 E-06	-0.8571 E-05

TABLE (3.4.2) Values of $P^{(0)}_{p,q}(v)$ on v=0 for τ_1=0.6 at γ=15°.

	t^1 q=1	t^3 q=3	t^5 q=5	t^7 q=7
$P^{(0)}_{0,q}$	0.2913 E-12	0.2570 E-01	0.4668 E-01	-0.8961 E-01
$P^{(0)}_{2,q}$	0.1607 E+01	-0.2145 E-01	0.6637 E-01	-0.1217 E+00
$P^{(0)}_{4,q}$	0.8036 E+00	-0.1087 E+00	0.1288 E+00	-0.2440 E+00
$P^{(0)}_{6,q}$	0.3014 E+00	-0.1123 E+00	0.1747 E+00	-0.4748 E+00
$P^{(0)}_{8,q}$	0.1005 E+00	-0.6949 E-01	0.1368 E+00	-0.7217 E+00
$P^{(0)}_{10,q}$	0.3139 E-01	-0.3155 E-01	0.4408 E-01	-0.8392 E+00
$P^{(0)}_{12,q}$	0.9418 E-02	-0.1103 E-01	-0.3713 E-01	-0.7743 E+00
$P^{(0)}_{14,q}$	0.2747 E-02	-0.2730 E-02	-0.7494 E-01	-0.5896 E+00
$P^{(0)}_{16,q}$	0.7848 E-03	-0.1760 E-03	-0.7564 E-01	-0.3820 E+00
$P^{(0)}_{18,q}$	0.2207 E-03	0.3181 E-03	-0.5852 E-01	-0.2150 E+00
$P^{(0)}_{20,q}$	0.6131 E-04	0.2672 E-03	-0.3857 E-01	-0.1064 E+00
$P^{(0)}_{22,q}$	0.1686 E-04	0.1507 E-03	-0.2271 E-01	-0.4639 E-01
$P^{(0)}_{24,q}$	0.4598 E-05	0.7196 E-04	-0.1227 E-01	-0.1765 E-01
$P^{(0)}_{26,q}$	0.1245 E-05	0.3114 E-04	-0.6195 E-02	-0.5646 E-02
$P^{(0)}_{28,q}$	0.3353 E-06	0.1260 E-04	-0.2956 E-02	-0.1347 E-02
$P^{(0)}_{30,q}$	0.8981 E-07	0.4849 E-05	-0.1345 E-02	-0.1019 E-03
$P^{(0)}_{32,q}$	0.2395 E-07	0.1795 E-05	-0.5881 E-03	0.1273 E-03
$P^{(0)}_{34,q}$	0.6362 E-08	0.6434 E-06	-0.2482 E-03	0.1022 E-03
$P^{(0)}_{36,q}$	0.1684 E-08	0.2246 E-06	-0.1017 E-03	0.5517 E-04
$P^{(0)}_{38,q}$	0.4444 E-09	0.7674 E-07	-0.4063 E-04	0.3425 E-04
$P^{(0)}_{40,q}$	0.1170 E-09	0.2602 E-07	-0.1602 E-04	0.2620 E-04

TABLE (3.4.3) Values of $P^{(0)}_{p,q}(v)$ on $v=0$ for $\tau_1=0.6$ at $\gamma=15°$.

	t^0 q=0	t^2 q=2	t^4 q=4	t^6 q=6
$Q^{(0)}_{1,q}$	0.2180 E+00	0.3594 E-02	-0.7703 E-01	0.9586 E-02
$Q^{(0)}_{3,q}$	0.	-0.6697 E-01	-0.2129 E+00	0.6470 E-01
$Q^{(0)}_{5,q}$	0.	-0.9593 E-01	-0.2868 E+00	0.1871 E+00
$Q^{(0)}_{7,q}$	0.	-0.7058 E-01	-0.2854 E+00	0.3256 E+00
$Q^{(0)}_{9,q}$	0.	-0.3880 E-01	-0.2319 E+00	0.3948 E+00
$Q^{(0)}_{11,q}$	0.	-0.1807 E-01	-0.1615 E+00	0.3622 E+00
$Q^{(0)}_{13,q}$	0.	-0.7556 E-02	-0.9967 E-01	0.2637 E+00
$Q^{(0)}_{15,q}$	0.	-0.2929 E-02	-0.5581 E-01	0.1552 E+00
$Q^{(0)}_{17,q}$	0.	-0.1073 E-02	-0.2887 E-01	0.7228 E-01
$Q^{(0)}_{19,q}$	0.	-0.3766 E-03	-0.1398 E-01	0.2322 E-01
$Q^{(0)}_{21,q}$	0.	-0.1277 E-03	-0.6403 E-02	0.5516 E-03
$Q^{(0)}_{23,q}$	0.	-0.4207 E-04	-0.2798 E-02	-0.6719 E-02
$Q^{(0)}_{25,q}$	0.	-0.1355 E-04	-0.1174 E-02	-0.7036 E-02
$Q^{(0)}_{27,q}$	0.	-0.4276 E-05	-0.4759 E-03	-0.5180 E-02
$Q^{(0)}_{29,q}$	0.	-0.1327 E-05	-0.1870 E-03	-0.3235 E-02
$Q^{(0)}_{31,q}$	0.	-0.4061 E-06	-0.1651 E-03	-0.1821 E-02
$Q^{(0)}_{33,q}$	0.	-0.1227 E-06	-0.6152 E-04	-0.9505 E-03
$Q^{(0)}_{35,q}$	0.	-0.3663 E-07	-0.2241 E-04	-0.4684 E-03
$Q^{(0)}_{37,q}$	0.	-0.1083 E-07	-0.7999 E-05	-0.2208 E-03
$Q^{(0)}_{39,q}$	0.	-0.3175 E-08	-0.2787 E-05	-0.1013 E-03
$Q^{(0)}_{41,q}$	0.	-0.9416 E-09	-0.8755 E-06	-0.4818 E-04

TABLE (3.4.4) Values of $Q^{(0)}_{p,q}(v)$ on $v=0$ for $\tau_1=0.6$ at $\gamma=15°$.

	t^1 q=1	t^3 q=3	t^5 q=5	t^7 q=7
$Q^{(0)}_{2,q}$	-0.1441 E+01	-0.8199 E-01	-0.2349 E-01	-0.6208 E-01
$Q^{(0)}_{4,q}$	-0.7203 E+00	-0.2879 E-01	-0.6351 E-01	-0.1200 E+00
$Q^{(0)}_{6,q}$	-0.2701 E+00	0.1974 E-01	-0.1516 E+00	-0.1157 E+00
$Q^{(0)}_{8,q}$	-0.9004 E-01	0.3068 E-01	-0.2608 E+00	0.2461 E-01
$Q^{(0)}_{10,q}$	-0.2814 E-01	0.2330 E-01	-0.3277 E+00	0.2889 E+00
$Q^{(0)}_{12,q}$	-0.8441 E-02	0.1356 E-01	-0.3233 E+00	0.5645 E+00
$Q^{(0)}_{14,q}$	-0.2462 E-02	0.6782 E-02	-0.2656 E+00	0.7334 E+00
$Q^{(0)}_{16,q}$	-0.7034 E-03	0.3065 E-02	-0.1895 E+00	0.7524 E+00
$Q^{(0)}_{18,q}$	-0.1978 E-03	0.1287 E-02	-0.1210 E+00	0.6543 E+00
$Q^{(0)}_{20,q}$	-0.5496 E-04	0.5109 E-03	-0.7055 E-01	0.5016 E+00
$Q^{(0)}_{22,q}$	-0.1511 E-04	0.1940 E-03	-0.3820 E-01	0.3479 E+00
$Q^{(0)}_{24,q}$	-0.4122 E-05	0.7105 E-04	-0.1943 E-01	0.2224 E+00
$Q^{(0)}_{26,q}$	-0.1116 E-05	0.2524 E-04	-0.9376 E-02	0.1327 E+00
$Q^{(0)}_{28,q}$	-0.3005 E-06	0.8743 E-05	-0.4323 E-02	0.7471 E-01
$Q^{(0)}_{30,q}$	-0.8050 E-07	0.2963 E-05	-0.1915 E-02	0.4001 E-01
$Q^{(0)}_{32,q}$	-0.2147 E-07	0.9850 E-06	-0.8197 E-03	0.2050 E-01
$Q^{(0)}_{34,q}$	-0.5702 E-08	0.3220 E-06	-0.3402 E-03	0.1011 E-01
$Q^{(0)}_{36,q}$	-0.1509 E-08	0.1037 E-06	-0.1373 E-03	0.4817 E-02
$Q^{(0)}_{38,q}$	-0.3982 E-09	0.3291 E-07	-0.5399 E-04	0.2218 E-02
$Q^{(0)}_{40,q}$	-0.1045 E-09	0.1008 E-07	-0.2054 E-04	0.9703 E-03

TABLE (3.4.5) Values of $Q^{(0)}_{p,q}(v)$ on $v=0$ for $\tau_1=0.6$ at $\gamma=15°$.

	t^0 q=0	t^2 q=2	t^4 q=4	t^6 q=6
$P^{(0)'}_{1,q}$	0.	-0.2944 E-04	0.1840 E-03	-0.4609 E-03
$P^{(0)'}_{3,q}$	0.	0.1670 E-03	0.2142 E-03	-0.6164 E-03
$P^{(0)'}_{5,q}$	0.	0.2375 E-03	0.8879 E-04	-0.6478 E-03
$P^{(0)'}_{7,q}$	0.	0.1732 E-03	-0.8305 E-04	-0.1994 E-03
$P^{(0)'}_{9,q}$	0.	0.9466 E-04	-0.1556 E-03	0.5657 E-03
$P^{(0)'}_{11,q}$	0.	0.4391 E-04	-0.1363 E-03	0.1160 E-02
$P^{(0)'}_{13,q}$	0.	0.1831 E-04	-0.8678 E-04	0.1324 E-02
$P^{(0)'}_{15,q}$	0.	0.7082 E-05	-0.4492 E-04	0.1137 E-02
$P^{(0)'}_{17,q}$	0.	0.2591 E-05	-0.1979 E-04	0.8082 E-03
$P^{(0)'}_{19,q}$	0.	0.9080 E-06	-0.7504 E-05	0.4987 E-03
$P^{(0)'}_{21,q}$	0.	0.3075 E-06	-0.2400 E-05	0.2747 E-03
$P^{(0)'}_{23,q}$	0.	0.1012 E-06	-0.5829 E-06	0.1373 E-03
$P^{(0)'}_{25,q}$	0.	0.3257 E-07	-0.5054 E-07	0.6292 E-04
$P^{(0)'}_{27,q}$	0.	0.1027 E-07	0.5604 E-07	0.2654 E-04
$P^{(0)'}_{29,q}$	0.	0.3184 E-08	0.5092 E-07	0.1028 E-04
$P^{(0)'}_{31,q}$	0.	0.9724 E-09	0.3001 E-07	0.3607 E-05
$P^{(0)'}_{33,q}$	0.	0.2927 E-09	0.1493 E-07	0.1105 E-05
$P^{(0)'}_{35,q}$	0.	0.8722 E-10	0.6736 E-08	0.2626 E-06
$P^{(0)'}_{37,q}$	0.	0.2523 E-10	0.2848 E-08	0.1671 E-07
$P^{(0)'}_{39,q}$	0.	0.7439 E-11	0.1166 E-08	-0.5526 E-07
$P^{(0)'}_{41,q}$	0.	0.4369 E-11	0.5884 E-09	-0.1583 E-06

TABLE (3.4.6) Values of $P^{(0)'}_{p,q}(v)$ on v=0 for τ_1=0.6 at γ=15°/

	t^1 q=1	t^3 q=3	t^5 q=5	t^7 q=7
$P^{(0)'}_{0,q}$	0.1143 E-11	-0.4875 E-04	-0.9118 E-04	0.8414 E-04
$P^{(0)'}_{2,q}$	-0.4000 E+01	-0.1079 E-03	0.3344 E-04	0.8247 E-04
$P^{(0)'}_{4,q}$	-0.2000 E+01	-0.7993 E-04	0.4485 E-03	-0.1817 E-03
$P^{(0)'}_{6,q}$	-0.7500 E+00	0.5228 E-04	0.8637 E-03	-0.1118 E-02
$P^{(0)'}_{8,q}$	-0.2500 E+00	0.1295 E-03	0.8844 E-03	-0.2438 E-02
$P^{(0)'}_{10,q}$	-0.7813 E-01	0.1263 E-03	0.5636 E-03	-0.3274 E-02
$P^{(0)'}_{12,q}$	-0.2344 E-01	0.8844 E-04	0.1907 E-03	-0.3149 E-02
$P^{(0)'}_{14,q}$	-0.6836 E-02	0.5123 E-04	-0.5052 E-04	-0.2311 E-02
$P^{(0)'}_{16,q}$	-0.1953 E-02	0.2613 E-04	-0.1414 E-03	-0.1302 E-02
$P^{(0)'}_{18,q}$	-0.5493 E-03	0.1216 E-04	-0.1396 E-03	-0.5116 E-03
$P^{(0)'}_{20,q}$	-0.1526 E-03	0.5270 E-05	-0.1031 E-03	-0.5221 E-04
$P^{(0)'}_{22,q}$	-0.4196 E-04	0.2161 E-05	-0.6486 E-04	0.1389 E-03
$P^{(0)'}_{24,q}$	-0.1144 E-04	0.8466 E-06	-0.3660 E-04	0.1737 E-03
$P^{(0)'}_{26,q}$	-0.3099 E-05	0.3195 E-06	-0.1905 E-04	0.1427 E-03
$P^{(0)'}_{28,q}$	-0.8345 E-06	0.1168 E-06	-0.9296 E-05	0.9726 E-04
$P^{(0)'}_{30,q}$	-0.2235 E-06	0.4158 E-07	-0.4305 E-05	0.5907 E-04
$P^{(0)'}_{32,q}$	-0.5960 E-07	0.1446 E-07	-0.1908 E-05	0.3303 E-04
$P^{(0)'}_{34,q}$	-0.1583 E-07	0.4928 E-08	-0.8146 E-06	0.1733 E-04
$P^{(0)'}_{36,q}$	-0.4191 E-08	0.1646 E-08	-0.3367 E-06	0.8677 E-05
$P^{(0)'}_{38,q}$	-0.1106 E-08	0.5406 E-09	-0.1357 E-06	0.4267 E-05
$P^{(0)'}_{40,q}$	-0.2915 E-09	0.1753 E-09	-0.5450 E-07	0.2166 E-05

TABLE (3.4.7) Values of $P^{(0)'}_{p,q}(v)$ on $v=0$ for $\tau_1=0.6$ at $\gamma=15°$.

	t^0 q=0	t^2 q=2	t^4 q=4	t^6 q=6
$Q^{(0)'}_{1,q}$	0.	0.1001 E-03	-0.4145 E-04	0.1545 E-04
$Q^{(0)'}_{3,q}$	0.	0.6211 E-04	-0.1812 E-03	0.1759 E-03
$Q^{(0)'}_{5,q}$	0.	-0.8187 E-05	-0.2645 E-03	0.6023 E-03
$Q^{(0)'}_{7,q}$	0.	-0.2483 E-04	-0.2193 E-03	0.1056 E-02
$Q^{(0)'}_{9,q}$	0.	-0.1827 E-04	-0.1203 E-03	0.1125 E-02
$Q^{(0)'}_{11,q}$	0.	-0.9713 E-05	-0.4102 E-04	0.7200 E-03
$Q^{(0)'}_{13,q}$	0.	-0.4382 E-05	-0.6859 E-06	0.1153 E-03
$Q^{(0)'}_{15,q}$	0.	-0.1784 E-05	0.1187 E-04	-0.3691 E-03
$Q^{(0)'}_{17,q}$	0.	-0.6767 E-06	0.1167 E-04	-0.5952 E-03
$Q^{(0)'}_{19,q}$	0.	-0.2436 E-06	0.7980 E-05	-0.5986 E-03
$Q^{(0)'}_{21,q}$	0.	-0.8420 E-07	0.4584 E-05	-0.4829 E-03
$Q^{(0)'}_{23,q}$	0.	-0.2818 E-07	0.2357 E-05	-0.3379 E-03
$Q^{(0)'}_{25,q}$	0.	-0.9190 E-08	0.1120 E-05	-0.2131 E-03
$Q^{(0)'}_{27,q}$	0.	-0.2933 E-08	0.5006 E-06	-0.1238 E-03
$Q^{(0)'}_{29,q}$	0.	-0.9181 E-09	0.2131 E-06	-0.6734 E-04
$Q^{(0)'}_{31,q}$	0.	-0.2816 E-09	0.8707 E-07	-0.3463 E-04
$Q^{(0)'}_{33,q}$	0.	-0.8369 E-10	0.3438 E-07	-0.1700 E-04
$Q^{(0)'}_{35,q}$	0.	-0.2373 E-10	0.1319 E-07	-0.7994 E-05
$Q^{(0)'}_{37,q}$	0.	-0.5635 E-11	0.4937 E-08	-0.3634 E-05
$Q^{(0)'}_{39,q}$	0.	-0.1060 E-11	0.1819 E-08	-0.1616 E-05
$Q^{(0)'}_{41,q}$	0.	0.1776 E-13	0.6526 E-09	-0.7534 E-06

TABLE (3.4.8) Values of $Q^{(0)}_{p,q}(v)$ on v=0 for τ_1=0.6 at γ=15°.

	t^1 q=1	t^3 q=3	t^5 q=5	t^7 q=7
$Q^{(0)'}_{2,q}$	0.3585 E+01	0.6911 E-04	0.2462 E-03	-0.3872 E-03
$Q^{(0)'}_{4,q}$	0.1793 E+01	0.1568 E-03	0.2593 E-03	-0.9800 E-03
$Q^{(0)'}_{6,q}$	0.6722 E+00	0.1717 E-03	-0.6730 E-04	-0.1441 E-02
$Q^{(0)'}_{8,q}$	0.2241 E+00	0.1306 E-03	-0.5547 E-03	-0.1162 E-02
$Q^{(0)'}_{10,q}$	0.7003 E-01	0.7998 E-04	-0.9096 E-03	-0.5335 E-04
$Q^{(0)'}_{12,q}$	0.2101 E-01	0.4236 E-04	-0.9927 E-03	0.1294 E-02
$Q^{(0)'}_{14,q}$	0.6127 E-02	0.2023 E-04	-0.8569 E-03	0.2207 E-02
$Q^{(0)'}_{16,q}$	0.1751 E-02	0.8936 E-05	-0.6288 E-03	0.2426 E-02
$Q^{(0)'}_{18,q}$	0.4924 E-03	0.3715 E-05	-0.4085 E-03	0.2107 E-02
$Q^{(0)'}_{20,q}$	0.1368 E-03	0.1471 E-05	-0.2411 E-03	0.1556 E-02
$Q^{(0)'}_{22,q}$	0.3761 E-04	0.5593 E-06	-0.1317 E-03	0.1014 E-02
$Q^{(0)'}_{24,q}$	0.1026 E-04	0.2057 E-06	-0.6744 E-04	0.5965 E-03
$Q^{(0)'}_{26,q}$	0.2778 E-05	0.7355 E-07	-0.3270 E-04	0.3217 E-03
$Q^{(0)'}_{28,q}$	0.7480 E-06	0.2566 E-07	-0.1514 E-04	0.1605 E-03
$Q^{(0)'}_{30,q}$	0.2003 E-06	0.8768 E-08	-0.6731 E-05	0.7458 E-04
$Q^{(0)'}_{32,q}$	0.5343 E-07	0.2945 E-08	-0.2889 E-05	0.3234 E-04
$Q^{(0)'}_{34,q}$	0.1419 E-07	0.9698 E-09	-0.1202 E-05	0.1306 E-04
$Q^{(0)'}_{36,q}$	0.3757 E-08	0.3167 E-09	-0.4862 E-06	0.4866 E-05
$Q^{(0)'}_{38,q}$	0.9914 E-09	0.1005 E-09	-0.1917 E-06	0.1605 E-05
$Q^{(0)'}_{40,q}$	0.2598 E-09	0.3289 E-10	-0.7342 E-07	0.3048 E-06

TABLE (3.4.9) Values of $Q^{(0)'}_{p,q}(v)$ on v=0 for τ_1=0.6 at γ=15°.

$$\frac{1}{t} = -0.7122\ U' + \sqrt{(0.7271\ U'^2 + 0.05975\ UU'')}\ , \quad (3.4.2)$$

(where $U(\eta)$ is the velocity on the surface of the cylinder as predicted by inviscid potential theory), to be solved in conjunction with t taking its minimum value, as the condition for the onset of separation. This expression is entirely equivalent to that given by considering the roots of

$$\omega_{0,0} + \omega_{0,1} t + \omega_{0,2} t^2 = 0\ ,$$

and gives a useful check on the accuracy of the numerical time-series method, by comparing this with that given by truncating the numerical time-series after the t^2 term.

Tables (3.4.10) and (3.4.11) give the values for t_s and η_s, the time and angle for the onset of separation, in the case $\tau_1=0.6$ at various angles of incidence, γ, as calculated by using

(i) the numerical time-series to t^7,

(ii) the numerical time-series to t^2,

(iii) the Goldstein-Rosenhead result.

Table (3.4.12) gives the same information for the case $\tau_1=0.3$ at $\gamma=15°$.

Tables (3.4.10), (3.4.11) and (3.4.12) show good agreement between the results of the analytical boundary-layer method of Goldstein and Rosenhead, and the numerical time-series to t^2, as indeed they should.

Table (3.4.13) gives results for $\tau_1=0.6$ at $\gamma=15°$ for various levels of truncation of the time-series, and indicates that at the time of separation the time-series is convergent

γ	0°	15°	30°	45°	90°
(i) Time series to t^7	0.1811	0.1815	0.1838	0.1903	0.2690
(ii) Time series to t^2	0.1797	0.1801	0.1823	0.1886	0.2653
(iii) Goldstein-Rosenhead	0.1797	0.1801	0.1823	0.1885	0.2652

TABLE (3.4.10) Separation time, t_s, at various angles of incidence for $\tau_1=0.6$.

γ	0°	15°	30°	45°	90°
(i) Time series to t^7	0.	0.09064[c]	0.1743[c]	0.2496[c]	0.4667[c]
(ii) Time series to t^2	0.	0.09183[c]	0.1764[c]	0.2523[c]	0.4676[c]
(iii) Goldstein-Rosenhead	0.	0.09185[c]	0.1764[c]	0.2523[c]	0.4676[c]

TABLE (3.4.11) Separation angle, η_s, at various angles of incidence for $\tau_1=0.6$.

	t_s	η_s
(i) Time series to t^6	0.04418	0.06576[c]
(ii) Time series to t^2	0.04380	0.06702[c]
(iii) Goldstein-Rosenhead	0.04379	0.06703[c]

TABLE (3.4.12) Separation time, t_s, and separation angle, η_s, for $\tau_1=0.3$ at $\gamma=15°$.

since the approximations difference well. This is also true of the other cases considered.

	Separation time, t_s	1st difference	Separation angle, η_s	1st difference
Time series to t^1	0.197888		0.088189^c	
		-0.017774		0.003645^c
Time series to t^2	0.180114		0.091834^c	
		0.000599		0.000294^c
Time series to t^3	0.180713		0.092128^c	
		0.000730		-0.001085^c
Time series to t^4	0.181443		0.091043^c	
		0.000090		-0.000517^c
Time series to t^5	0.181533		0.090526^c	
		-0.000018		0.000029^c
Time series to t^6	0.181515		0.090555^c	
		-0.000005		0.000082^c
Time series to t^7	0.181510		0.090637^c	

TABLE (3.4.13) Separation time and angle and differences at various truncations for $\tau_1=0.6$ at $\gamma=15°$.

Figs. 3 through 8 show the temporal development of $R^{-\frac{1}{2}}\zeta$ on the surface of the cylinder for the cases considered. It should be noted that the convergence of the time-series in the case $\tau_1=0.3$ is found to be restricted to lower values of t than for the case of $\tau_1=0.6$, but this is to be expected since the development of the boundary layer is more rapid for the former case as indicated by a much earlier non-dimensional time of separation. Equations (1.4.1), (2.2.1), (3.1.1) and (3.1.12) were used to obtain the expression

$$R^{-\frac{1}{2}}\zeta = \frac{H_0}{2\sqrt{2t}} \sum_{q=0}^{q_M} t^q \{\frac{1}{2} P_{0,q}(v=0) + \sum_{p=1}^{p_M} [P_{p,q}(v=0)\cos p\eta + Q_{p,q}(v=0)\sin p\eta]\},$$

from which $R^{-\frac{1}{2}}\zeta$ was graphed for the various cases.

Fig. 9 shows the movement of the separation points with respect to time after separation has commenced for an ellipse of aspect ratio $\tau_1=0.6$ at various angles of incidence, γ. The lowest minima of the curves corresponds to the initial time at which separation commences, and the curve itself shows the growth of the recirculatory region thereafter. For $\gamma=\frac{\pi}{2}$ it can be seen that the two symmetrical bubbles behind the ellipse join along the axis of symmetry ($\eta=0$) at a time close to 0.5. The form of these curves is similar to those given by Wang (5) (his Fig. 2) for a finite value of the Reynolds number R, although they are of course quantitatively different. No attempt has been made to go to higher values of t than those given, since it is considered that for these higher values of t, the t-series has insufficient terms to give meaningful results.

Fig. 10 shows the streamline pattern that results at t=0.5, with the Reynolds number having been set to 100, for the case $\tau_1=0.6$ at $\gamma=15°$. For this case the fluid initially commences separation at time t=0.182 at an angle of $\eta=0.091^c$ (5.19°). The bubble then grows until it reaches the separating streamline at $\gamma=15°$ at a time t=0.203, whereupon a second bubble commences on the opposite side of the separating streamline and both bubbles continue to grow. At time t=0.5 the extent to which the recirculatory bubbles have grown can be seen from Fig. 10. The lower bubble has an anticlockwise rotation whilst the upper one rotates clockwise, and their growth can be followed with the aid of Fig. 9.

For the symmetric cases of $\gamma=0°$ and $\gamma=90°$, it is interesting to see how the general asymmetric case degenerates. In both cases the two bubbles commence separation simultaneously; for $\gamma=0$ both bubbles commence separation at $\eta=0°$ in a manner similar to that of flow around a circular cylinder; for $\gamma=90°$, the bubbles commence separation at $\eta=26.7°$ and $\eta=180°-26.7°$ and grow until they join at $\eta=0°$.

3.5 RESULTS FOR HIGHER-ORDER CORRECTIONS

The cases considered in the previous section are reconsidered here, with additional terms in the polynomial series in k being included. Specifically, the coefficients associated with k^1 are calculated as outlined in Section 3.2, and in the calculation of the various properties of the fluid the t^0 term in k^2 is also included, as given by the analytic expression (2.4.10).

The values of the parameters used to calculate the k^1 coefficients are as in Table (3.4.1), with the exception of q_M, the value taken for the truncation of the polynomial series in t^q. For $\tau_1=0.3$, q_M is taken to be 4, whilst for $\tau_1=0.6$, q_M is taken to be 6.

As noted in the previous section, various properties of the fluid may be calculated from the surface values of the coefficients. Again, coefficients are only given explicitly for the one case, viz. $\tau_1=0.6$ at $\gamma=15°$, although calculated properties are given for all cases. Tables (3.5.1) through (3.5.8) give the values of $P^{(1)}_{p,q}(v)$, $Q^{(1)}_{p,q}(v)$, $P^{(1)'}_{p,q}(v)$, $Q^{(1)'}_{p,q}(v)$ on $v=0$, where p refers to the Fourier Series expansion, and

	t^0 q=0 (F-N)	t^0 q=0 (Analytic)	t^2 q=2	t^4 q=4
$P^{(1)}_{1,q}$	-0.2092 E+00	-0.2092 E+00	-0.2048 E+01	-0.2231 E+01
$P^{(1)}_{3,q}$	-0.1017 E+00	-0.1017 E+00	-0.6585 E+01	-0.5542 E+01
$P^{(1)}_{5,q}$	-0.3422 E-01	-0.3422 E-01	-0.7067 E+01	-0.5199 E+01
$P^{(1)}_{7,q}$	-0.1034 E-01	-0.1034 E-01	-0.4835 E+01	0.4729 E+00
$P^{(1)}_{9,q}$	-0.2968 E-02	-0.2968 E-02	-0.2594 E+01	0.8141 E+01
$P^{(1)}_{11,q}$	-0.8273 E-03	-0.8273 E-03	-0.1195 E+01	0.1326 E+02
$P^{(1)}_{13,q}$	-0.2262 E-03	-0.2262 E-03	-0.4960 E+00	0.1413 E+02
$P^{(1)}_{15,q}$	-0.6103 E-04	-0.6103 E-04	-0.1906 E+00	0.1189 E+02
$P^{(1)}_{17,q}$	-0.1630 E-04	-0.1630 E-04	-0.6903 E-01	0.8520 E+01
$P^{(1)}_{19,q}$	-0.4320 E-05	-0.4320 E-05	-0.2385 E-01	0.5410 E+01
$P^{(1)}_{21,q}$	-0.1138 E-05	-0.1138 E-05	-0.7929 E-02	0.3126 E+01
$P^{(1)}_{23,q}$	-0.2983 E-06	-0.2983 E-06	-0.2551 E-02	0.1673 E+01
$P^{(1)}_{25,q}$	-0.7789 E-07	-0.7789 E-07	-0.7978 E-03	0.8406 E+00
$P^{(1)}_{27,q}$	-0.2026 E-07	-0.2027 E-07	-0.2434 E-03	0.4004 E+00
$P^{(1)}_{29,q}$	-0.5257 E-08	-0.5257 E-08	-0.7262 E-04	0.1821 E+00
$P^{(1)}_{31,q}$	-0.1360 E-08	-0.1360 E-08	-0.2122 E-04	0.7965 E-01
$P^{(1)}_{33,q}$	-0.3511 E-09	-0.3512 E-09	-0.6083 E-05	0.3364 E-01
$P^{(1)}_{35,q}$	-0.9045 E-10	-0.9050 E-10	-0.1711 E-05	0.1378 E-01
$P^{(1)}_{37,q}$	-0.2328 E-10	-0.2336 E-10	-0.4713 E-06	0.5499 E-02
$P^{(1)}_{39,q}$	-0.5940 E-11	-0.5984 E-11	-0.1227 E-06	0.2157 E-02
$P^{(1)}_{41,q}$	-0.1400 E-11	-0.1415 E-11	-0.8209 E-08	0.8966 E-03

TABLE (3.5.1) Values of $P^{(1)}_{p,q}(v)$ on v=0 for τ_1=0.6 at γ=15°. γ=15°.

	t^1 q=1 (F-N)	t^1 q=1 (Analytic)	t^3 q=3	t^5 q=5
$P^{(1)}_{0,q}$	-0.2080 E+00	-0.2080 E+00	-0.2954 E+00	-0.1145 E+01
$P^{(1)}_{2,q}$	-0.3693 E+01	-0.3693 E+01	-0.4469 E+01	-0.2580 E+01
$P^{(1)}_{4,q}$	-0.4297 E+01	-0.4297 E+01	-0.8022 E+01	-0.1424 E+01
$P^{(1)}_{6,q}$	-0.2757 E+01	-0.2757 E+01	-0.5932 E+01	0.5559 E+01
$P^{(1)}_{8,q}$	-0.1364 E+01	-0.1364 E+01	-0.1035 E+01	0.1495 E+02
$P^{(1)}_{10,q}$	-0.5822 E+00	-0.5822 E+00	0.2402 E+01	0.2137 E+02
$P^{(1)}_{12,q}$	-0.2261 E+00	-0.2261 E+00	0.3361 E+01	0.2277 E+02
$P^{(1)}_{14,q}$	-0.8220 E-01	-0.8217 E-01	0.2824 E+01	0.2023 E+02
$P^{(1)}_{16,q}$	-0.2845 E-01	-0.2844 E-01	0.1881 E+01	0.1583 E+02
$P^{(1)}_{18,q}$	-0.9487 E-02	-0.9480 E-02	0.1082 E+01	0.1123 E+02
$P^{(1)}_{20,q}$	-0.3070 E-02	-0.3067 E-02	0.5614 E+00	0.7348 E+01
$P^{(1)}_{22,q}$	-0.9700 E-03	-0.9684 E-03	0.2692 E+00	0.4492 E+01
$P^{(1)}_{24,q}$	-0.3033 E-03	-0.3000 E-03	0.1213 E+00	0.2585 E+01
$P^{(1)}_{26,q}$	-0.9144 E-04	-0.9116 E-04	0.5195 E-01	0.1411 E+01
$P^{(1)}_{28,q}$	-0.2744 E-04	-0.2733 E-04	0.2132 E-01	0.7340 E+00
$P^{(1)}_{30,q}$	-0.8133 E-05	-0.8090 E-05	0.8440 E-02	0.3658 E+00
$P^{(1)}_{32,q}$	-0.2385 E-05	-0.2368 E-05	0.3239 E-02	0.1754 E+00
$P^{(1)}_{34,q}$	-0.6925 E-06	-0.6866 E-06	0.1210 E-02	0.8118 E-01
$P^{(1)}_{36,q}$	-0.1994 E-01	-0.1973 E-06	0.4415 E-03	0.3639 E-01
$P^{(1)}_{38,q}$	-0.5696 E-07	-0.5624 E-07	0.1579 E-03	0.1584 E-01
$P^{(1)}_{40,q}$	-0.1605 E-07	-0.1592 E-07	0.5665 E-04	0.6800 E-02

TABLE (3.5.2) Values of $P^{(1)}_{p,q}(v)$ on $v=0$ for $\tau_1=0.6$ at $\gamma=15°$.

	t^0 q=0 (F-N)	t^0 q=0 (Analytic)	t^2 q=2	t^4 q=4
$Q^{(1)}_{1,q}$	0.1053 E+01	0.1053 E+01	0.6090 E+00	0.2217 E+01
$Q^{(1)}_{3,q}$	0.3381 E+00	0.3381 E+00	0.3385 E+01	0.8411 E+01
$Q^{(1)}_{5,q}$	0.9971 E-01	0.9971 E-01	0.3983 E+01	0.1415 E+02
$Q^{(1)}_{7,q}$	0.2821 E-01	0.2821 E-01	0.2836 E+01	0.1847 E+02
$Q^{(1)}_{9,q}$	0.7787 E-02	0.7787 E-02	0.1563 E+01	0.2063 E+02
$Q^{(1)}_{11,q}$	0.2114 E-02	0.2114 E-02	0.7372 E+00	0.1978 E+02
$Q^{(1)}_{13,q}$	0.5674 E-03	0.5674 E-03	0.3128 E+00	0.1638 E+02
$Q^{(1)}_{15,q}$	0.1509 E-03	0.1509 E-03	0.1229 E+00	0.1193 E+02
$Q^{(1)}_{17,q}$	0.3987 E-04	0.3987 E-04	0.4559 E-01	0.7784 E+01
$Q^{(1)}_{19,q}$	0.1048 E-04	0.1048 E-04	0.1615 E-01	0.4633 E+01
$Q^{(1)}_{21,q}$	0.2740 E-05	0.2740 E-05	0.5516 E-02	0.2553 E+01
$Q^{(1)}_{23,q}$	0.7139 E-06	0.7139 E-06	0.1827 E-02	0.1318 E+01
$Q^{(1)}_{25,q}$	0.1854 E-06	0.1854 E-06	0.5900 E-03	0.6434 E+00
$Q^{(1)}_{27,q}$	0.4803 E-07	0.4804 E-07	0.1864 E-03	0.2993 E+00
$Q^{(1)}_{29,q}$	0.1241 E-07	0.1241 E-07	0.5777 E-04	0.1336 E+00
$Q^{(1)}_{31,q}$	0.3202 E-08	0.3202 E-08	0.1761 E-04	0.5745 E-01
$Q^{(1)}_{33,q}$	0.8237 E-09	0.8237 E-09	0.5290 E-05	0.2393 E-01
$Q^{(1)}_{35,q}$	0.2123 E-09	0.2122 E-09	0.1568 E-05	0.9683 E-02
$Q^{(1)}_{37,q}$	0.5372 E-10	0.5364 E-10	0.4574 E-06	0.3818 E-02
$Q^{(1)}_{39,q}$	0.1499 E-10	0.1499 E-10	0.1256 E-06	0.1468 E-02
$Q^{(1)}_{41,q}$	0.3006 E-11	0.2922 E-11	0.6138 E-08	0.5381 E-03

TABLE (3.5.3) Values of $Q^{(1)}_{p,q}(v)$ on v=0 for τ_1=0.6 at γ=15°.

	t^1 q=1 (F-N)	t^1 q=1 (Analytic)	t^3 q=3	t^5 q=5
$Q^{(1)}_{2,q}$	0.1882 E+01	0.1882 E+01	0.3206 E+01	0.5949 E+01
$Q^{(1)}_{4,q}$	0.2824 E+01	0.2824 E+01	0.6904 E+01	0.1501 E+02
$Q^{(1)}_{6,q}$	0.1986 E+01	0.1986 E+01	0.8310 E+01	0.2306 E+02
$Q^{(1)}_{8,q}$	0.1031 E+01	0.1031 E+01	0.7314 E+01	0.2860 E+02
$Q^{(1)}_{10,q}$	0.4539 E+00	0.4538 E+00	0.5246 E+01	0.3169 E+02
$Q^{(1)}_{12,q}$	0.1800 E+00	0.1800 E+00	0.3251 E+01	0.3201 E+02
$Q^{(1)}_{14,q}$	0.6644 E-01	0.6642 E-01	0.1804 E+01	0.2926 E+02
$Q^{(1)}_{16,q}$	0.2327 E-01	0.2326 E-01	0.9178 E+00	0.2412 E+02
$Q^{(1)}_{18,q}$	0.7832 E-02	0.7826 E-02	0.4356 E+00	0.1802 E+02
$Q^{(1)}_{20,q}$	0.2554 E-02	0.2551 E-02	0.1952 E+00	0.1231 E+02
$Q^{(1)}_{22,q}$	0.8119 E-03	0.8105 E-03	0.8342 E-01	0.7767 E+01
$Q^{(1)}_{24,q}$	0.2527 E-03	0.2521 E-03	0.3422 E-01	0.4569 E+01
$Q^{(1)}_{26,q}$	0.7729 E-04	0.7704 E-04	0.1356 E-01	0.2529 E+01
$Q^{(1)}_{28,q}$	0.2328 E-04	0.2318 E-04	0.5209 E-02	0.1327 E+01
$Q^{(1)}_{30,q}$	0.6925 E-05	0.6886 E-05	0.1949 E-02	0.6637 E+00
$Q^{(1)}_{32,q}$	0.2036 E-05	0.2022 E-05	0.7125 E-03	0.3184 E+00
$Q^{(1)}_{34,q}$	0.5929 E-06	0.5875 E-06	0.2550 E-03	0.1472 E+00
$Q^{(1)}_{36,q}$	0.1711 E-06	0.1692 E-06	0.8957 E-04	0.6582 E-01
$Q^{(1)}_{38,q}$	0.4903 E-07	0.4836 E-07	0.3089 E-04	0.2862 E-01
$Q^{(1)}_{40,q}$	0.1379 E-07	0.1365 E-07	0.1037 E-04	0.1233 E-01

TABLE (3.5.4) Values of $Q^{(1)}_{p,q}(v)$ on $v=0$ for $\tau_1=0.6$ at $\gamma=15°$.

	t^0 q=0	t^2 q=2	t^4 q=4
$P^{(1)'}_{1,q}$	0.6684 E+00	0.4824 E+01	0.6357 E+01
$P^{(1)'}_{3,q}$	0.2666 E+00	0.1741 E+02	0.2044 E+02
$P^{(1)'}_{5,q}$	0.8498 E-01	0.1629 E+02	0.2218 E+02
$P^{(1)'}_{7,q}$	0.2503 E-01	0.9025 E+01	0.5264 E+01
$P^{(1)'}_{9,q}$	0.7081 E-02	0.3560 E+01	-0.2003 E+02
$P^{(1)'}_{11,q}$	0.1955 E-02	0.9884 E+00	-0.3831 E+02
$P^{(1)'}_{13,q}$	0.5310 E-03	0.1134 E+00	-0.4301 E+02
$P^{(1)'}_{15,q}$	0.1425 E-03	-0.8158 E-01	-0.3717 E+02
$P^{(1)'}_{17,q}$	0.3792 E-04	-0.7943 E-01	-0.2706 E+02
$P^{(1)'}_{19,q}$	0.1002 E-04	-0.4648 E-01	-0.1737 E+02
$P^{(1)'}_{21,q}$	0.2633 E-05	-0.2247 E-01	-0.1012 E+02
$P^{(1)'}_{23,q}$	0.6887 E-06	-0.9748 E-02	-0.5449 E+01
$P^{(1)'}_{25,q}$	0.1795 E-06	-0.3933 E-02	-0.2751 E+01
$P^{(1)'}_{27,q}$	0.4663 E-07	-0.1504 E-02	-0.1315 E+01
$P^{(1)'}_{29,q}$	0.1208 E-07	-0.5523 E-03	-0.6002 E+00
$P^{(1)'}_{31,q}$	0.3122 E-08	-0.1961 E-03	-0.2632 E+00
$P^{(1)'}_{33,q}$	0.8056 E-09	-0.6777 E-04	-0.1114 E+00
$P^{(1)'}_{35,q}$	0.2076 E-09	-0.2288 E-04	-0.4574 E-01
$P^{(1)'}_{37,q}$	0.5364 E-10	-0.7576 E-05	-0.1829 E-01
$P^{(1)'}_{39,q}$	0.1380 E-10	-0.2482 E-05	-0.7196 E-02
$P^{(1)'}_{41,q}$	0.3385 E-11	-0.8801 E-06	-0.3032 E-02

TABLE (3.5.5) Values of $P^{(1)'}_{p,q}(v)$ on v=0 for τ_1=0.6 at γ=15°.

	t^1 q=1	t^3 q=3	t^5 q=5
$P^{(1)'}_{0,q}$	-0.2165 E-04	0.2457 E-03	0.2533 E-02
$P^{(1)'}_{2,q}$	0.7657 E+01	0.1637 E+02	0.6301 E+01
$P^{(1)'}_{4,q}$	0.9236 E+01	0.3085 E+02	0.3093 E+00
$P^{(1)'}_{6,q}$	0.5988 E+01	0.2385 E+02	-0.3110 E+02
$P^{(1)'}_{8,q}$	0.2976 E+01	0.5824 E+01	-0.7136 E+02
$P^{(1)'}_{10,q}$	0.1274 E+01	-0.7225 E+01	-0.9673 E+02
$P^{(1)'}_{12,q}$	0.4958 E+00	-0.1126 E+02	-0.9947 E+02
$P^{(1)'}_{14,q}$	0.1805 E+00	-0.9721 E+01	-0.8578 E+02
$P^{(1)'}_{16,q}$	0.6253 E-01	-0.6550 E+01	-0.6534 E+02
$P^{(1)'}_{18,q}$	0.2086 E-01	-0.3794 E+01	-0.4527 E+02
$P^{(1)'}_{20,q}$	0.6756 E-02	-0.1976 E+01	-0.2906 E+02
$P^{(1)'}_{22,q}$	0.2135 E-02	-0.9503 E+00	-0.1748 E+02
$P^{(1)'}_{24,q}$	0.6614 E-03	-0.4290 E+00	-0.9928 E+01
$P^{(1)'}_{26,q}$	0.2014 E-03	-0.1840 E+00	-0.5362 E+01
$P^{(1)'}_{28,q}$	0.6047 E-04	-0.7559 E-01	-0.2767 E+01
$P^{(1)'}_{30,q}$	0.1793 E-04	-0.2995 E-01	-0.1370 E+01
$P^{(1)'}_{32,q}$	0.5257 E-05	-0.1150 E-01	-0.6536 E+00
$P^{(1)'}_{34,q}$	0.1527 E-05	-0.4299 E-02	-0.3013 E+00
$P^{(1)'}_{36,q}$	0.4398 E-06	-0.1569 E-02	-0.1347 E+00
$P^{(1)'}_{38,q}$	0.1256 E-06	-0.5617 E-03	-0.5848 E-01
$P^{(1)'}_{40,q}$	0.3541 E-07	-0.2018 E-03	-0.2500 E-01

TABLE (3.5.6) Values of $P^{(1)'}_{p,q}(v)$ on v=0 for τ_1=0.6 at γ=15°.

	t^0 q=0	t^2 q=2	t^4 q=4
$Q^{(1)'}_{1,q}$	-0.1936 E+01	-0.2061 E+01	-0.4056 E+01
$Q^{(1)'}_{3,q}$	-0.6800 E+00	-0.1160 E+02	-0.2184 E+02
$Q^{(1)'}_{5,q}$	-0.2077 E+00	-0.1309 E+02	-0.4078 E+02
$Q^{(1)'}_{7,q}$	-0.5986 E-01	-0.8799 E+01	-0.5581 E+02
$Q^{(1)'}_{9,q}$	-0.1672 E-01	-0.4524 E+01	-0.6420 E+02
$Q^{(1)'}_{11,q}$	-0.4575 E-02	-0.1965 E+01	-0.6280 E+02
$Q^{(1)'}_{13,q}$	-0.1235 E-02	-0.7566 E+00	-0.5276 E+02
$Q^{(1)'}_{15,q}$	-0.3299 E-03	-0.2650 E+00	-0.3880 E+02
$Q^{(1)'}_{17,q}$	-0.8744 E-04	-0.8556 E-01	-0.2551 E+02
$Q^{(1)'}_{19,q}$	-0.2304 E-04	-0.2553 E-01	-0.1527 E+02
$Q^{(1)'}_{21,q}$	-0.6039 E-05	-0.6990 E-02	-0.8452 E+01
$Q^{(1)'}_{23,q}$	-0.1577 E-05	-0.1709 E-02	-0.4378 E+01
$Q^{(1)'}_{25,q}$	-0.4102 E-06	-0.3446 E-03	-0.2143 E+01
$Q^{(1)'}_{27,q}$	-0.1064 E-06	-0.3950 E-04	-0.9994 E+00
$Q^{(1)'}_{29,q}$	-0.2753 E-07	0.1054 E-04	-0.4468 E+00
$Q^{(1)'}_{31,q}$	-0.7109 E-08	0.1058 E-04	-0.1925 E+00
$Q^{(1)'}_{33,q}$	-0.1830 E-08	0.5532 E-05	-0.8029 E-01
$Q^{(1)'}_{35,q}$	-0.4716 E-09	0.2383 E-05	-0.3253 E-01
$Q^{(1)'}_{37,q}$	-0.1204 E-09	0.9365 E-06	-0.1284 E-01
$Q^{(1)'}_{39,q}$	-0.3158 E-10	0.3702 E-06	-0.4938 E-02
$Q^{(1)'}_{41,q}$	-0.6526 E-11	0.2466 E-06	-0.1804 E-02

TABLE (3.5.7) Values of $Q^{(1)'}_{p,q}(v)$ on $v=0$ for $\tau_1=0.6$ at $\gamma=15°$.

	t^1 q=1	t^3 q=3	t^5 q=5
$Q^{(1)'}_{2,q}$	-0.3390 E+01	-0.8456 E+01	-0.1943 E+02
$Q^{(1)'}_{4,q}$	-0.5648 E+01	-0.2260 E+02	-0.5613 E+02
$Q^{(1)'}_{6,q}$	-0.4103 E+01	-0.2936 E+02	-0.8890 E+02
$Q^{(1)'}_{8,q}$	-0.2165 E+01	-0.2670 E+02	-0.1086 E+03
$Q^{(1)'}_{10,q}$	-0.9622 E+00	-0.1945 E+02	-0.1169 E+03
$Q^{(1)'}_{12,q}$	-0.3841 E+00	-0.1214 E+02	-0.1153 E+03
$Q^{(1)'}_{14,q}$	-0.1425 E+00	-0.6756 E+01	-0.1039 E+03
$Q^{(1)'}_{16,q}$	-0.5009 E-01	-0.3441 E+01	-0.8512 E+02
$Q^{(1)'}_{18,q}$	-0.1690 E-01	-0.1633 E+01	-0.6350 E+02
$Q^{(1)'}_{20,q}$	-0.5525 E-02	-0.7315 E+00	-0.4342 E+02
$Q^{(1)'}_{22,q}$	-0.1760 E-02	-0.3122 E+00	-0.2745 E+02
$Q^{(1)'}_{24,q}$	-0.5486 E-03	-0.1279 E+00	-0.1620 E+02
$Q^{(1)'}_{26,q}$	-0.1680 E-03	-0.5060 E-01	-0.8988 E+01
$Q^{(1)'}_{28,q}$	-0.5067 E-04	-0.1942 E-01	-0.4727 E+01
$Q^{(1)'}_{30,q}$	-0.1509 E-04	-0.7257 E-02	-0.2771 E+01
$Q^{(1)'}_{32,q}$	-0.4440 E-05	-0.2649 E-02	-0.1140 E+01
$Q^{(1)'}_{34,q}$	-0.1294 E-05	-0.9470 E-01	-0.5281 E+00
$Q^{(1)'}_{36,q}$	-0.3737 E-06	-0.3322 E-03	-0.2366 E+00
$Q^{(1)'}_{38,q}$	-0.1072 E-06	-0.1144 E-03	-0.1031 E+00
$Q^{(1)'}_{40,q}$	-0.3013 E-07	-0.3819 E-04	-0.4459 E-01

TABLE (3.5.8) Values of $Q^{(1)'}_{p,q}(v)$ on v=0 for τ_1=0.6 at γ=15°.

q to the polynomial expansion in t. From the analysis it can be seen that $P^{(1)}_{p,q} = Q^{(1)}_{p,q} = P^{(1)'}_{p,q} = Q^{(1)'}_{p,q} = 0$ for (p+q) even.

It is also found that the magnitude of the coefficients of t^2 increases as q becomes larger, although ultimately they should die away. However, for small times the t^q part of the series ensures reasonable convergence of the truncated series.

Since $\omega_{1,0}$ and $\omega_{1,1}$ are known analytically from expressions (2.4.7) and (2.4.8), we may compare the values on the surface with those given numerically. This comparison is included in Tables (3.5.1) through (3.5.4), and also indirectly checks $P^{(0)}_{p,1}$ and $Q^{(0)}_{p,1}$, since the calculation for $P^{(1)}_{p,1}$ and $Q^{(1)}_{p,1}$ uses their previously computed values. Expanding $\omega_{1,0}$ we find that

$$P^{(1)}_{p,0} = -2K_0 \sin\gamma [\beta_1 A_2(v) J_3(1,p) + pA_3(v) J_1(1,p)], \quad (3.5.1)$$

$$Q^{(1)}_{p,0} = 2K_0 \cos\gamma [\beta_1 A_2(v) I_3(1,p) + pA_3(v) I_1(1,p)]. \quad (3.5.2)$$

$P^{(1)}_{p,0}$ and $Q^{(1)}_{p,0}$ on v=0 were calculated in the check from equations (3.5.1) and (3.5.2), where $I_1(1,p)$, $J_1(1,p)$, $I_3(1,p)$, and $J_3(1,p)$ were evaluated numerically using Filon-type quadrature.

$P^{(1)}_{p,1}$ and $Q^{(1)}_{p,1}$ on v=0 were calculated directly from $\omega_{1,1}$ by using Filon quadrature to evaluate

$$P^{(1)}_{p,1} = \frac{1}{\pi} \int_0^{2\pi} \frac{\omega_{1,1}}{H_0} \cos p\eta \, d\eta \, , \quad (3.5.3)$$

$$Q^{(1)}_{p,1} = \frac{1}{\pi} \int_0^{2\pi} \frac{\omega_{1,1}}{H_0} \sin p\eta \, d\eta \, . \quad (3.5.4)$$

The agreement between the fully-numerical results and

and those obtained from the corresponding analysis can be seen to be very adequate, with part of the discrepancy for large values of p being the result of difficulties associated with the Filon quadrature of the integrals. The agreement in fact often goes beyond the four figures indicated, six-figure agreement not being unusual.

The cases for an elliptic cylinder of aspect ratio τ_1=0.6 at various angles of incidence were studied with R being set to 5,000, whilst for τ_1=0.3 the Reynolds number was taken to be 50,000. Figs. 11 through 15 show the temporal development of the surface vorticity ζ at various angles of incidence for τ_1=0.6, as calculated from the expression

$$\zeta(v=0) = \frac{H_0}{k} \sum_{q=0}^{7} t^q \{\tfrac{1}{2} P_{0,q}^{(0)}(v=0) + \sum_{p=1}^{p_M} [P_{p,q}^{(0)}(v=0)\cos p\eta + Q_{p,q}^{(0)}(v=0)\sin p\eta]\} + H_0 \sum_{q=0}^{5} t^q \{\tfrac{1}{2} P_{0,q}^{(1)}(v=0) + \sum_{p=1}^{p_M} [P_{p,q}^{(1)}(v=0)\cos p\eta + Q_{p,q}^{(1)}(v=0)\sin p\eta]\} + k\omega_{2,0}(v=0), \qquad (3.5.5)$$

where p_M = 41.

Fig. 16 shows the temporal development of the surface-vorticity for τ_1=0.3 at γ=15° using the above expression with the first sum over q being to 6, the second to 4, and p_M taking the value 81. Note that the t^0 term in k^2, calculated from the analytic result (2.4.10), has been included in the above calculations.

The times and angles of separation are given by finding

the roots of $\chi = \frac{\partial \chi}{\partial \eta} = 0$ on v=0, the surface of the cylinder. Figs. 17 through 22 show the times of separation versus the Reynolds number for the two ellipses at various angles of incidence, whilst Figs. 23 through 27 show the angles of separation versus Reynolds number. For the symmetric case of τ_1=0.6 at γ=0°, separation occurs at η=0°, the rear stagnation point, throughout the whole domain of R.

In the following discussion it should be realised that the truncation of the k and t series makes the predictions of this method become increasingly less valid for larger values of the time and smaller values of the Reynolds number. The approximate domain of validity of this method is discussed in more detail in Section 5.3, where the results of a calculation at R=5,000 using a fully-numerical method are compared with those of the present method. From these results a crude estimate can be made with regard to the domain of validity.

Let us consider in more detail the case τ_1=0.6 at γ=15°, and the manner in which the onset of separation occurs. The curves labelled I,II,III and IV in Fig. 18, which give the times of separation at various Reynolds numbers, correspond to curves of the same label in Fig. 23, which give the angle at which this separation will occur. For example, at R=100,000 separation first occurs at a time t=0.185 as given by curve I of Fig. 18, and at an angle of η=0.102^c as given by curve I of Fig. 23.

The schematic way in which separation occurs for Reynolds numbers in excess of approximately 13,000 is shown in Fig. 28.

The dividing streamline close to the ellipse starts to move slowly downward at the rear of the cylinder soon after motion commences. A separated region then commences on the lower side of the dividing streamline (Fig. 28b) and grows until it reaches the dividing streamline (Fig. 28c), at which time a second region of separation commences immediately above the zero streamline. (Fig. 28d). Some time thereafter a third bubble commences higher up on the rear side of the ellipse (Fig. 28e) which then proceeds to coalesce with the second bubble (Fig. 28f). Much later a fourth bubble appears on the lower part of the ellipse (Fig. 28g) within the first bubble. The existence of this fourth bubble is far from certain, since it develops at times outside the range of the validity of the time-series. The predicted time at which it occurs is certainly not accurate, although the phenomena itself may or may not exist.

As $R\to\infty$ it is found that the second and third bubbles which coalesce, commence to separate at closer times and angles of separation, and in the limiting case degenerate into just one bubble which commences separation at the zero streamline. The above manner in which separation will occur is somewhat similar to that inferred by Wang (5) for the case $\tau_1=0.5$, $R\approx 115$ at an angle of incidence of 54°. However, it is found in the present study that the coalescing of the two bubbles did not cause any significant changes in the lift when R=100,000, which continues to increase. This is probably due to the fact that the time-series method is inaccurate at

these values of t, and possibly because the bubbles are insufficiently developed, and in fact Wang (5) does not indicate that he has made any calculations for the lift to bear out his inference.

The schematic way in which separation occurs in the present case for R in the approximate range 1,700 to 13,000 is shown in Fig. 29. Again the dividing streamline close to the ellipse begins to move down the rear side, only at a faster rate (Fig. 29b). Separation then occurs above the dividing streamline at the rear (Fig. 29c) rather than below as was the case for R > 13,000. The first region of separation starts to grow, and the dividing streamline continues to move downward until a second region of separation commences below the first region, but above the dividing streamline (Fig. 29d). For R = 5,000 at a time t=0.5, the streamline pattern is shown in Fig. 31, corresponding to the schematic Fig. 29c. The inset of Fig. 31 is of the separated region which has been magnified in a direction normal to the ellipse.

The schematic manner in which separation occurs in the present case for R < 1700 is shown in Fig. 30. Again the dividing streamline close to the rear of the ellipse begins to move downward (Fig. 30b), but this time separation commences below the dividing streamline (Fig. 30c), followed sometime thereafter by a separated region above the dividing streamline (Fig. 30d)

Thus we see that there are three different ranges of R, in which separation occurs in distinct ways. In the drawing

of these schematic figures, use was made of print-outs of the vorticity which facilitated the interpretation of the graphs for time and angle of separation. The time to which the time-series remains accurate becomes progressively more restrictive the lower the value of R. For this reason it would appear that Wang (5), in choosing a Reynolds number equivalent to 115 in the present study, made an unfortunate choice. In his calculations he has used the equivalent of the first two terms ($\omega_{0,0}$ and $\omega_{0,1}$) in the boundary-layer case, and the first term only ($\omega_{1,0}$) of the higher order corrections; a total of three terms. These would not appear to be sufficient in number to adequately describe the flow pattern, and even the thirteen terms considered in this study will produce some quantitative discrepancy for Reynolds numbers this small. This was also found by Collins (12) in his study of the circular cylinder, when making a comparison of the times of separation as predicted by the time-series and those found by fully numerical procedures at Reynolds numbers of this order.

The pressure coefficient $P^*(\eta,t)$ is defined in Appendix IV and is given by expression (IV.4). For the present case of an ellipse this reduces to

$$P^*(\eta,t) = \frac{1}{2t}\int_{\eta}^{\pi+\gamma} \left(\frac{\partial \chi}{\partial v}\right)_{v=0} d\eta, \qquad (3.5.6)$$

where η_0, the point taken for the base pressure, has been arbitrarily set to $\pi+\gamma$, γ being the angle of inclination of the ellipse to the free stream. For the various cases considered equation (3.5.6) was used to plot $P^*(\eta,t)$ in Figs. 32 through 37 for Reynolds numbers of 5,000 and 50,000.

C_D and C_L, the drag and lift coefficients are defined in terms of C_x,C_y and γ by equations (IV.7) and (IV.8) of Appendix IV. Equations (IV.11) and (IV.12) of the same appendix become for the present case

$$C_x = -\frac{\sinh \alpha}{2}\int_0^{2\pi} P^*\cos\eta \, d\eta + \frac{2\cosh \alpha}{Rk}\int_0^{2\pi} H_0(\chi)_{v=0}\sin\eta \, d\eta \, , \tag{3.5.7}$$

$$C_y = -\frac{\cosh \alpha}{2}\int_0^{2\pi} P^*\sin\eta \, d\eta - \frac{2\sinh \alpha}{Rk}\int_0^{2\pi} H_0(\chi)_{v=0}\cos\eta \, d\eta \, . \tag{3.5.8}$$

The coefficients of drag and lift, C_D and C_L, for the case τ_1=0.6 at various angles of incidence are plotted against time in Figs. 38 and 39 respectively with R taken to be 5,000 whilst Fig. 40 plots C_D and C_L against time for the case τ_1=0.3 at γ=15° with R set at 50,000.

CHAPTER IV

THE FULLY-NUMERICAL METHOD OF INTEGRATING THE GOVERNING EQUATIONS FOR FLOW PAST A GENERAL CYLINDER

4.1 THE GENERAL METHOD OF SOLUTION

In this chapter, we propose an alternative method of solution of equations (1.4.2) through (1.4.8). The approach taken is to solve these equations by fully numerical methods, by which means the solutions may be advanced to higher times than by the previously given time-series method. It also provides a means of ascertaining the approximate domain of validity of the time-series method, and also serves as an accuracy check by making comparisons at early times of results given by the two methods.

The governing equations are

$$H^2 \frac{\partial^2 \omega}{\partial z^2} + 2z \frac{\partial \omega}{\partial z} + 2\omega = 4t \frac{\partial \omega}{\partial t} - \frac{8tH^2}{R} \frac{\partial^2 \omega}{\partial \eta^2} + 4tH^2 \frac{\partial(\Psi,\omega)}{\partial(\eta,z)}, \quad (4.1.1)$$

and

$$\frac{\partial^2 \Psi}{\partial z^2} + k^2 \frac{\partial^2 \Psi}{\partial \eta^2} = \omega H^{-2} . \quad (4.1.2)$$

Let us define $r_n(z,t)$ and $s_n(z,t)$ as follows:-

$$r_n(z,t) = \frac{1}{\pi} \int_0^{2\pi} \omega H^{-2} \sin n\eta \, d\eta \qquad (n=1,2,3,\ldots), \quad (4.1.3)$$

$$s_n(z,t) = \frac{1}{\pi}\int_0^{2\pi} \omega H^{-2} \cos n\eta \, d\eta \qquad (n=0,1,2,\ldots). \qquad (4.1.4)$$

Now let us make a Fourier expansion of $\Psi(z,\eta,t)$, viz.

$$\Psi(z,\eta,t) = \frac{g_0(z,t)}{2} + \sum_{n=1}^{\infty} [g_n(z,t)\cos n\eta + f_n(z,t)\sin n\eta]. \qquad (4.1.5)$$

Term by term differentiation of this series with respect to η is justified [see e.g. Jeffreys and Jeffreys (22)]. Substitution of this series in equation (4.1.12) and the standard use of orthogonal functions yields the pair of equations

$$\frac{\partial^2 f_n(z,t)}{\partial z^2} - n^2k^2 f_n(z,t) = r_n(z,t) \quad (n=1,2,3,\ldots), \qquad (4.1.6)$$

$$\frac{\partial^2 g_n(z,t)}{\partial z^2} - n^2k^2 g_n(z,t) = s_n(z,t) \quad (n=0,1,2,\ldots). \qquad (4.1.7)$$

From equations (1.4.5), (4.1.5) and the uniform flow at infinity condition (1.2.26), the above equations will have boundary conditions

$$\left.\begin{aligned} &f_n = \frac{\partial f_n}{\partial z} = 0 \text{ on } z = 0, \\ &\left.\begin{aligned} &kf_n(z,t)e^{-kz} \to K_0\cos\gamma\delta_{n,1} \\ &\frac{\partial f_n(z,t)}{\partial z}\, e^{-kz} \to K_0 \cos\gamma\delta_{n,1} \end{aligned}\right\} \text{as } z\to\infty \end{aligned}\right\} (n=1,2,3\ldots), \qquad (4.1.8)$$

and

$$\left.\begin{aligned} & g_n = \frac{\partial g_n}{\partial z} = 0 \text{ on } z = 0 \ , \\ & k\bar{g}_n(z,t)e^{-kz} \to -K_0 \sin\gamma\delta_{n,1} \\ & \frac{\partial \bar{g}_n(z,t)}{\partial z} e^{-kz} \to -K_0 \sin\gamma\delta_{n,1} \end{aligned}\right\} \text{as } z \to \infty \Bigg\} \ (n=0,1,2,\ldots) \qquad (4.1.9)$$

The solution of equation (4.1.2) can now be considered to be replaced by the solution of equations (4.1.6) and (4.1.7), subject to the boundary conditions (4.1.8) and (4.1.9). Further, at a particular instant in time, these equations may be considered to be ordinary differential equations in the variable z. This property facilitates their numerical solution.

The remaining boundary conditions to be imposed are given by [rewriting conditions (1.4.4), (1.4.6), (1.4.7) and (1.4.8)]

$$\omega \to 0 \quad \text{as } z \to \infty \ , \qquad (4.1.10)$$

$$\int_0^\infty e^{-nkz} r_n(z,t)\,dz = 2K_0 \cos\gamma\delta_{n,1} \quad (n=1,2,3,\ldots), \qquad (4.1.11)$$

$$\int_0^\infty e^{-nkz} s_n(z,t)\,dz = -2K_0 \sin\gamma\delta_{n,1} \quad (n=0,1,2,\ldots), \qquad (4.1.12)$$

$$\left.\begin{aligned} & \Psi(z,\eta,t) = \Psi(z,\eta+2\pi,t) \ , \\ & \omega(z,\eta,t) = \omega(z,\eta+2\pi,t). \end{aligned}\right\} \qquad (4.1.13)$$

Inversion of expressions (4.1.3) and (4.1.4) yields

$$\omega(z,\eta,t) = H^2\{\sum_{n=1}^{\infty} [r_n(z,t)\sin n\eta + s_n(z,t)\cos n\eta] + \frac{s_0(z,t)}{2}\}. \qquad (4.1.14)$$

Let us assume that all quantities are known at a particular time t, and that we wish to advance the solution to a time $t + \Delta t$. The method, essentially, consists of solving equations (4.1.1) and (4.1.2) in an implicit manner to convergence. In more detail, we perform the following steps, where k is the iteration counter:

(i) Solve (4.1.1) for $\omega^{(k)}(z,\eta,t+\Delta t)$ everywhere except on the surface of the cylinder (z=0), using boundary conditions (4.1.10) and (4.1.13).

(ii) Calculate $r_n^{(k)}(z,t+\Delta t)$, $s_n^{(k)}(z,t+\Delta t)$ from equations (4.1.3) and (4.1.4) respectively, for $z \neq 0$.

(iii) Calculate $r_n^{(k)}(0,t+\Delta t)$, $s_n^{(k)}(0,t+\Delta t)$ by using equations (4.1.11) and (4.1.12) respectively, from which $\omega^{(k)}(0,\eta,t+\Delta t)$ may be computed using the expression (4.1.14).

(iv) Solve equations (4.1.6) and (4.1.7) for $f_n^{(k)}(z,t+\Delta t)$, $g_n^{(k)}(z,t+\Delta t)$ using boundary conditions (4.1.7) and (4.1.8).

(v) Calculate $\psi^{(k)}(z,\eta,t+\Delta t)$ everywhere from the expression (4.1.5), and also its spatial derivatives.

(vi) Repeat steps (i) - (v) to convergence, incrementing k by 1 for each complete iteration (i) - (v).

The scheme used to approximate equation (4.1.1) in order to find $\omega^{(k)}(z,\eta,t+\Delta t)$ is very similar to the Crank-Nicholson implicit procedure. Equation (4.1.1) may be rewritten in the form

$$t\,\frac{\partial \omega}{\partial t} = q(z,\eta,t)\ , \qquad (4.1.15)$$

where

$$q(z,\eta,t) = [\frac{2tH^2}{R}\frac{\partial^2}{\partial\eta^2} + tH^2(\frac{\partial\Psi}{\partial z}\frac{\partial}{\partial\eta} - \frac{\partial\Psi}{\partial\eta}\frac{\partial}{\partial z}) + \frac{1}{4}(H^2\frac{\partial^2}{\partial z^2} + 2z\frac{\partial}{\partial z} + 2)]\omega(z,\eta,t).$$

It is the finite-difference approximation to the time derivative that enables us to advance the solution step-by-step in time, provided that we know the complete solution at the previous time stage. Let us integrate both sides of equation (4.1.15) from t to t + Δt, keeping z and η fixed and the left hand side being integrated by parts, to obtain

$$[\omega\tau]_t^{t+\Delta t} - \int_t^{t+\Delta t} \omega\, d\tau = \int_t^{t+\Delta t} q(z,\eta,\tau)d\tau\ , \qquad (4.1.16)$$

where Δt is the time increment.

By approximating the integrals using the trapezoidal rule, we obtain

$$\omega(z,\eta,t+\Delta t) = \omega(z,\eta,t) + \frac{\Delta t}{(2t+\Delta t)}[q(z,\eta,t+\Delta t) + q(z,\eta,t)] + E, \qquad (4.1.17)$$

where

$$E = \frac{-(\Delta t)^3}{6(2t+\Delta t)}[\frac{\partial^2\omega(\tau_1)}{\partial t^2} + \frac{\partial^2 q(\tau_2)}{\partial t^2}],\ t<\tau_1<t+\Delta t,\ t<\tau_2<t+\Delta t\ .$$

Since $q(z,\eta,t+\Delta t)$ is itself dependent on $\omega(z,\eta,t+\Delta t)$ and its derivatives, equation (4.1.17) gives $\omega(z,\eta,t+\Delta t)$ implicitly. We solve these equations iteratively using the Gauss-Seidel procedure. This solution in turn must be otained iteratively in conjunction with the finite-difference analogues of

equations (4.1.6) and (4.1.7), since $q(z,\eta,t+\Delta t)$ is also dependent on $\Psi(z,\eta,t+\Delta t)$. An explicit method of solution for equation (4.1.1) is not practical, since the time increment Δt would have to be extremely small in order that the integrations should remain stable, resulting in too much computational time being required.

To start the integration procedure, t is set to zero. Since ω and Ψ are both known at t=0 from Chapter II to be

$$\omega|_{t=0} = \omega_{0,0} = \frac{4K_0H_0}{\pi^{\frac{1}{2}}} e^{-z^2/H_0^2} \sin(\eta-\gamma),$$

$$\Psi|_{t=0} = \Psi_{0,0} = 2K_0 \sin(\eta-\gamma)\left[z \operatorname{erf}\frac{z}{H_0} + \frac{H_0}{\pi^{\frac{1}{2}}}\left(e^{-z^2/H_0^2} - 1\right)\right], \tag{4.1.18}$$

then q at t=0 can also be computed.

The time-series method indicates that the second time-derivatives of ω and Ψ behave as $R^{-1/2}\, t^{-3/2}$ for small t. Consequently, Δt must be taken to be very small when starting the integrations in order that the error term E in equation (4.1.17) be negligible. This problem does not arise in the starting procedure for the boundary-layer case, since the time-derivatives in this instance do not exhibit the same singular behaviour near t=0.

The usual approach taken by most authors to the solution of equations (4.1.1) and (4.1.2), (expressed in the (ξ,η) coordinate system in their formulations) is to solve both equations iteratively at a particular time step, using time-consuming boundary value techniques. One of the advantages of the present formulation is that the elliptic boundary

value problem for equation (4.1.2) has been reduced to a step-by-step integration, since at a particular iterate r_n is known at all values of z.

4.2 NUMERICAL TECHNIQUES USED IN THE INTEGRATIONS

The way in which the time derivative in equation (4.1.1) is approximated has been given in the previous section. In approximating the spatial derivatives, a uniform grid size h is taken in the z-direction. This is shown in Fig. 41, together with the convention for labelling the grid points around some given point 0, located at $z = nh$, $\eta = mh_1$, where m and n are positive integers. Both first and second derivatives are approximated by using three point central-difference formulae. The two following are typical approximations to derivatives at the grid point 0, from which the others may be inferred:-

$$\left.\begin{aligned} \left.\frac{\partial \omega_0}{\partial z}\right|_t &= \left.\left(\frac{\omega_1 - \omega_3}{2h}\right)\right|_t + O(h^2) \ , \\ \left.\frac{\partial^2 \omega_0}{\partial \eta^2}\right|_{t+\Delta t} &= \left.\left(\frac{\omega_2 - 2\omega_0 + \omega_4}{h_1^2}\right)\right|_{t+\Delta t} + O(h_1^2) . \end{aligned}\right\} \qquad (4.2.1)$$

By using these approximations and rearranging terms we obtain the following expression for ω_0 at time $t+\Delta t$:

$$\left.\omega_0\right|_{t+\Delta t} = \left.f\{a\omega_1 + b\omega_2 + c\omega_3 + d\omega_4\}\right|_{t+\Delta t} + \left.H^2\right|_t \left.H^{-2}\right|_{t+\Delta t} e(t) f, \qquad (4.2.2)$$

where

$$a(\tau) = \left.[1 + hzH^{-2} - 2\tau h \frac{\partial \Psi}{\partial \eta}]\right|_\tau \ ,$$

$$b(\tau) = \left.[\frac{8\tau h^2}{Rh_1^2} + \frac{2\tau h^2}{h_1}\frac{\partial \Psi}{\partial z}]\right|_\tau \ ,$$

$$c(\tau) = \left[1 - hzH^{-2} + 2\tau h \frac{\partial \Psi}{\partial \eta}\right]\Big|_{\tau} \quad ,$$

$$d(\tau) = \left[\frac{8\tau h^2}{Rh_1^2} - \frac{2\tau h^2}{h_1}\frac{\partial \Psi}{\partial z}\right]\Big|_{\tau} \quad ,$$

$$e(\tau) = \left\{a\omega_1 + b\omega_2 + c\omega_3 + d\omega_4 + \left[2h^2\left(3 + \frac{4\tau}{\Delta t}\right)H^{-2} - \left(2 + \frac{16h^2\tau}{Rh_1^2}\right)\right]\omega_0\right\}\Big|_{\tau},$$

$$f = \left\{H^{-2}\Big|_{t+\Delta t}\left[2h^2\left(1 + \frac{4t}{\Delta t}\right)\right] + \left[2 + \frac{16h^2(t+\Delta t)}{Rh_1^2}\right]\right\}^{-1} .$$

Finite-difference approximations for $\frac{\partial \Psi}{\partial \eta}$ and $\frac{\partial \Psi}{\partial z}$ are not given above since they are calculated separately in the solution of equation (4.1.2) as described later. Equation (4.2.2) defines a matrix problem which, as previously mentioned, is solved by Gauss-Seidel iteration. In this procedure, the field is systematically swept using equation (4.2.2) at each interior grid point, and at each application the right-hand side is computed using the most recent iterate available for $\omega_i\Big|_{t+\Delta t}$ where i=1,2,3,4.

The boundary conditions used in the above matrix problem are now described. Insteady of the condition (4.1.10) that $\omega \to 0$ as $z \to \infty$, we impose the condition

$$\omega = 0 \text{ on } z = z_M \quad , \tag{4.2.3}$$

where $z = z_M$ defines the maximum value taken for z.

The value $z = z_M$ is chosen to be sufficiently large to ensure that taking any larger value for z_M will result in no significant change being observed in the solutions. The values chosen in this study were found to be quite adequate.

The most recent iterate for ω on $z = 0$ in the alternating procedure of finding solutions to equations (4.1.1) and (4.1.2) is used as the boundary condition to be applied on $z = 0$. After solving the above matrix problem this is replaced by the iterate as calculated by step (iii) of the procedure outline. The other boundary condition to be imposed is that of periodicity, i.e.,

$$\omega(z,\eta,t+\Delta t) = \omega(z,\eta+2\pi,t+\Delta t). \qquad (4.2.4)$$

Difficulties arise in the numerical evaluation of the integrals in equations (4.1.3) and (4.1.4) for large values of n, since the integrand possesses many zeros. The application of Simpson quadrature to the integrand thus requires an extremely small choice of the grid size to give reasonable results. This was pointed out by Filon (26), who proposed approximation of the non-periodic part of the integrand, rather than of the whole integrand, by a parabola over three successive grid points η_{m-1},η_m and η_{m+1} of a grid of size h_1, where $\eta_m = mh_1$. The integrals are then integrated by parts to yield the following

$$\int_{\eta_{m-1}}^{\eta_{m+1}} f(\eta)\sin n\eta\, d\eta = -\frac{1}{n}(f_{m+1}\cos n\eta_{m+1} - f_{m-1}\cos n\eta_{m-1})$$

$$+ \frac{1}{h_1^2 n^3}(f_{m-1} - 2f_m + f_{m+1})(\cos n\eta_{m+1} - \cos n\eta_{m-1})$$

$$+ \frac{1}{2h_1 n^2}[(3f_{m+1} - 4f_m + f_{m-1})\sin n\eta_{m+1} - (4f_m - f_{m+1}$$

$$- 3f_{m-1})\sin n\eta_{m-1}] \qquad (4.2.5)$$

$$\int_{\eta_{m-1}}^{\eta_{m+1}} f(\eta)\cos n\eta\, d\eta = \frac{1}{n}\left(f_{m+1}\sin n\eta_{m+1} - f_{m-1}\sin n\eta_{m-1}\right)$$

$$- \frac{1}{h_1^2 n^3}\left(f_{m-1} - 2f_m + f_{m+1}\right)\left(\sin n\eta_{m+1} - \sin n\eta_{m-1}\right)$$

$$+ \frac{1}{2h_1 n^2}\left[\left(3f_{m+1} - 4f_m + f_{m-1}\right)\cos n\eta_{m+1} - \left(4f_m - f_{m+1}\right.\right.$$

$$\left.\left. - 3f_{m-1}\right)\cos n\eta_{m-1}\right] \qquad (4.2.6)$$

where f_m denotes the value of f at $\eta = \eta_m$.

The integrals (4.1.3) and (4.1.4) can be calculated using expressions (4.2.3) and (4.2.4) and summing over the equally spaced intervals of length $2h_1$, where $f(\eta) = \omega H^{-2}$, z being assumed fixed. These integrals are calculated for all values of $z \neq 0$. The infinite sum in expression (4.1.5) is assumed to be replaced by the finite sum from n = 1 to $n = n_M$, the value taken for truncation of the series for Ψ. Consequently, the integrals defined by equation (4.1.3) and (4.1.4) are calculated for values of n up to and including n_M. The values for $r_n(z,t)$ and $s_n(z,t)$ on the boundary may now be found from the integral conditions (4.1.11) and (4.1.12). The infinite integral is assumed replaceable by the finite integral from 0 to z_M and is approximated by Simpson quadrature from which we obtain

$$r_n(0,t) = \frac{6K_0\cos\gamma\delta_{n,1}}{\ell_M h} - 4r_n(z_1)e^{-nkz_1} - r_n(z_2)e^{-nkz_2}$$
$$- \sum_{\ell=2}\left[r_n(z_{2\ell})e^{-nkz_{2\ell}} + 4r_n(z_{2\ell-1})e^{-nkz_{2\ell-1}}\right.$$

$$\left. + r_n(z_{2\ell-2})e^{-nkz_{2\ell-2}}\right], \qquad (4.2.7)$$

$$s_n(0,t) = -\frac{6K_0 \sin\gamma\delta_{n,1}}{h} - 4s_n(z_1)e^{-nkz_1} - s_n(z_2)e^{-nkz_2}$$

$$- \sum_{\ell=2}^{\ell_M} [s_n(z_{2\ell})e^{-nkz_{2\ell}} + 4s_n(z_{2\ell-1})e^{-nkz_{2\ell-1}}$$

$$+ s_n(z_{2\ell-2})e^{-nkz_{2\ell-2}}] , \qquad (4.2.8)$$

where $2\ell_M h = z_M$, $z_{2\ell} = 2\ell h$.
Equation (4.1.14), with the infinite sum replaced by the finite sum from n = 1 to $n = n_M$, can then be used to calculate the values for ω on z = 0.

In the actual computations it was found to be necessary to "smooth" $r_n(0,t)$ and $s_n(0,t)$ in the following manner in order to obtain sequences of convergent iterates Ψ and ω. If $r_n^{(k)}(0,t)$ is the kth iterate for $r_n(0,t)$ and $\tilde{r}_n(0,t)$ is the most recent value calculated from equation (4.2.7), then $r_n^{(k+1)}(0,t)$, the (k+1)th iterate for $r_n(0,t)$, is given by

$$r_n^{(k+1}(0,t) = \kappa\tilde{r}_n(0,t) + (1-\kappa)r_n^{(k)}(0,t), \qquad (4.2.9)$$

where $0 < \kappa \leq 1$.

This technique of smoothing to obtain convergence of the iterates has been noted before in the literature (see e.g. Thom and Apelt (27) and Dennis and Chang (15)), and is only an aid to convergence and should not affect the validity of the final solutions. If the condition

$$\left| r_n^{(k+1)}(0,t) - r_n^{(k)}(0,t) \right| < \varepsilon \qquad (4.2.10)$$

is taken to be the criterion for convergence of the process,

then

$$\left|\tilde{r}_n(0,t) - r_n^{(k)}(0,t)\right| < \frac{\varepsilon}{\kappa} . \qquad (4.2.11)$$

Equation (4.2.11) indicates that true convergence for $r_n(0,t)$ is likely to be of order $\frac{\varepsilon}{\kappa}$ rather than ε.

Equations (4.1.6) and (4.1.7) are of the form, at some fixed value of t,

$$f''(z) - \beta^2 f(z) = r(z) , \qquad (4.2.12)$$

subject to the boundary conditions

$$f = f' = 0 \quad \text{on } z = 0 . \qquad (4.2.13)$$

For small values of β, equation (4.2.12) may be solved by the well known step-by-step formulae given below. The integration is started using

$$f_1 = \frac{h^2}{6-\beta^2h^2}[2r_0 + r_1] + 0(h^4) . \qquad (4.2.14)$$

Here function subscripts (0,1,2,...) are used to denote the value of the function at x = 0,h,2h .... . The procedure is then continued in a step-by-step manner, successively using for n=1,2,3,... the formula

$$f_{n+1} = \frac{24 + 10\beta^2h^2}{12 - \beta^2h^2} f_n - f_{n-1} + \frac{h^2}{12 - \beta^2h^2}[r_{n+1} + 10r_n + r_{n-1}] + 0(h^6) . \qquad (4.2.15)$$

f_n' for n=1,2,3,... is then given by

$$f_n' = \frac{6 - \beta^2h^2}{12h}[f_{n+1} - f_{n-1}] - \frac{h}{12}[r_{n+1} - r_{n-1}] + 0(h^4) . \qquad (4.2.16)$$

Equations of the form of equation (4.2.12) were solved by the above method for values of $\beta \leq 1$. However, it has been noted by Dennis and Chang (15) that most step-by-step procedures become increasingly unstable as β becomes large. For values of $\beta \geq 1$ the following step-by-step method, attributable to the above authors, was used.

Theoretically, the boundary conditions (4.2.13) are sufficient for the solution of equation (4.2.12). However, we have additional conditions available from equations (4.1.8) and (4.1.9) which have been used to derive the integral conditions (4.1.11) and (4.1.12) and use is made of these latter conditions in the numerical procedure, as will be described below. It is these additional conditions that facilitates the numerical solution of equation (4.2.12). Let us define functions p and q by

$$\left.\begin{aligned} p &= f' + \beta f \ , \\ q &= f' - \beta f \ . \end{aligned}\right\} \qquad (4.2.17)$$

Equation (4.2.12) then yields the equations

$$p' - \beta p = r \ , \qquad (4.2.18)$$

$$q' + \beta q = r. \qquad (4.2.19)$$

Equation (4.2.19) may be integrated step-by-step from z=0 by first using

$$q_1 = \gamma q_0 + \frac{1}{\beta}(r_1 - \gamma r_0) - \frac{1}{2h\beta^2}[r_2 - r_0 - \gamma(4r_1 - 3r_0 - r_2)] + \frac{1}{h^2\beta^3}(r_0 - 2r_1 + r_2)(1 - \gamma) \ , \qquad (4.2.20)$$

to start the procedure, and then continuing the integrations

for j=1,2,3,... by the formula

$$q_{i+1} = \gamma^2 q_{i-1} + \frac{1}{\beta}(r_{i+1} - \gamma^2 r_{i-1}) - \frac{1}{2h\beta^2}[(3r_{i+1} - 4r_i + r_{i-1}) - \gamma^2(4r_i - 3r_{i-1} - r_{i+1})] + \frac{1}{h^2\beta^3}(r_{i-1} - 2r_i + r_{i+1})(1-\gamma^2), \tag{4.2.21}$$

where $\gamma = e^{-\beta h}$.

In starting the integration, the condition $q_0 = 0$ is used, obtained from conditions (4.2.13). The error growth for the integration of equation (4.2.19) is acceptable (see Dennis and Chang (15)). However, if this method is attempted for the solution of equation (4.2.18), this is no longer the case. This difficulty is obviated by setting $z' = z_M - z$, where z_M is the field length, yielding

$$\frac{dp}{dz'} + \beta p = -r(z_M - z') \ . \tag{4.2.22}$$

This is now of the form (4.2.19), and may be integrated in the same manner with a knowledge of p at $z' = 0$, i.e. p at $z = z_M$. The functions f and f' are then found from the relations

$$\left.\begin{aligned} f &= \frac{(p-q)}{2\beta} \ , \\ f' &= \frac{p+q}{2} \ . \end{aligned}\right\} \tag{4.2.23}$$

To complete the outline of the method, we require only to specify p on $z = z_M$. This may be obtained by integrating equation (4.2.18) from $z = z_M$ to $z = \infty$ and using the asymptotic conditions (4.1.8) and (4.1.9) to obtain

$$e^{-\beta z_M} p(z = z_M) = 2c\delta_{n,1} - \int_{z_M}^{\infty} re^{-\beta z} dz, \qquad (4.2.24)$$

where $c = 2K_0 \cos\gamma$ when solving equation (4.1.6),

and $c = -2K_0 \sin\gamma$ when solving equation (4.1.7).

For z_M sufficiently large, the integral on the right-hand side may be assumed zero. Indeed, in our previous analysis we assumed r=0 for all values of $z \geq z_M$, since ω is assumed zero on $z = z_M$.

Thus, in integrating equation (4.2.22) we use the condition

$$p(z = z_M) = 2ce^{\beta z_M}\delta_{n,1} \qquad (4.2.25)$$

to initiate the integration.

4.3 RESULTS FOR FLOW PAST A CIRCULAR CYLINDER

In this section the method outlined in the two previous sections is applied to the case of flow past a circular cylinder. The angle of inclination γ is arbitrarily assumed zero for convenience, and the flow is further assumed to be symmetrical about $\eta = 0$. Thus only the region $0 \leq \eta \leq \pi$ need be considered, with

$$\Psi = \omega = 0 \quad \text{on} \quad \eta = 0, \pi. \qquad (4.3.1)$$

The details of the transformation (1.2.15) are

$$\left.\begin{aligned} \xi + i\eta &= \log (X + iY), \\ H^2 &= e^{-2\xi} = e^{-2kz}, \\ K_0 &= 1, \end{aligned}\right\} \qquad (4.3.2)$$

and the representative dimension d is chosen to be the radius of the cylinder.

A consequence of the assumption of symmetry about $\eta = 0$ is that $s_n(z,t)$ and $g_n(z,t)$ are identically zero for all arguments and do not enter into the calculations. Calculations were carried out for R = 100,500,10^3,10^4 and ∞.

There are several parameters of the calculations which may be varied, including:- (i) z_M, the length of the field, (ii) h, the grid-size in the z-direction, (iii) h_1, the grid-size in the η-direction, (iv) κ, the smoothing factor, (v) ε, the convergence tolerance, (vi) n_M, the value taken for truncation of the Fourier series, and (vii) Δt, the time increment. To check whether a choice of parameter is adequate for each value of R is not practical, due to the large amount of computer time required. However, each parameter was checked for some Reynolds number by comparing the results of two calculations performed at two different values of that parameter, and verifying that there was no significant difference. The indication from the checks is that the solutions are reliable as far in time as they were considered. For the results given here, the values of the parameters are displayed in Table (4.3.1). These are considered adequate for all values of R, with the possible exception of R= ∞, for which z_M was extended to 8.

z_M	h	h_1	κ	ε	n_M	Δt
5	0.05	$\pi/30$	10^{-1}	10^{-4}	29	0.025

TABLE (4.3.1) Values for the parameters used in the calculations.

A time increment of Δt =0.025 was chosen, except in the

first interval in which smaller steps were taken as previously mentioned. That $z_M = 5$ is satisfactory, at least for early times, can be seen from the initial solution for the vorticity

$$\omega(z,\eta,0) = \frac{4}{\pi^{\frac{1}{2}}} e^{-z^2} \sin\eta. \qquad (4.3.3)$$

From equation (4.3.3) it can be seen that at time t=0,

$$r_n(z,0) = \frac{4}{\pi^{\frac{1}{2}}} e^{-z^2} \delta_{1,n} . \qquad (4.3.4)$$

Also, the initial solution for the stream function yields

$$f_n(z,0) = 2[z \text{ erf } z + \frac{1}{\pi^{\frac{1}{2}}} (e^{-z^2} - 1)]\delta_{1,n}. \qquad (4.3.5)$$

Thus at t=0, the series for ω and Ψ consist of only one term each and build up slowly as t increases, only a few terms being necessary for small values of t.

It was found convenient throughout the calculations to work in terms of $\Omega(z,\eta,t)$, a perturbation from the initial vorticity $\omega(z,\eta,0)$, i.e.

$$\omega(z,\eta,t) = \frac{4}{\pi^{\frac{1}{2}}} e^{-z^2} \sin\eta + \Omega(z,\eta,t). \qquad (4.3.6)$$

The method of solution remains unchanged, and the alterations in the detail of the equations are trivial and will not be given here.

For R=100 and 500, at no time did the vorticity in the vicinity of $z = z_M$ exceed 10^{-5}. For the larger Reynolds numbers this was not the case, with values of order 10^{-3} being observed. However, by using a more powerful computer for the case $R=\infty$, extension of the field length to $z_M = 8$

produced very little change in the values of the surface vorticity, and it was concluded that whilst an extended field is desirable, it does not adversely affect the solutions to any great degree. The check on the surface vorticity is a fairly sensitive one, since these values are essentially computed from sums of the vorticity throughout the field. Thus any significant changes in the field will cause corresponding significant changes in the vorticity on the boundary.

In the procedure, most of the computer time is spent in solving the boundary-value problem for ω. This means that an increase in the value of n_M will not result in a very large increase in computer time, and the value $n_M = 29$ was found to be more than adequate. A value of say 19, would probably give as good results for most cases, certainly for early times, the value of 29 being chosen since it did not appreciably alter the compute time anyway. This cannot be said for a refining of the parameters h and h_1. In fact, at the time of computation of these results, a further refinement was not feasible due to the size of the machine available. This, however, was subsequently checked when a larger machine became available, and it was found that a halving of either of these two parameters resulted in a near quadrupling of the time required, due to their influence on the matrix problem.

Collins (12), has studied this problem of flow around a circular cylinder using two different methods. The first approach is that of a time-series, the generalisation of which was given in Chapters II and III, and the second a fully-

numerical scheme in which the η-dependence is removed from the problem. His results for R=100,500,1000 and ∞ have been compared with the present ones, and are generally in good agreement. The largest discrepancy occurs in a comparison of the surface vorticity in the wake region. This is to be expected, since in the present method with a grid-size of $h_1 = \pi/30$, there will only be a few points within the wake region. Unfortunately, a substantial reduction in h_1 was not considered feasible due to the large increase in computer size and time required. As previously mentioned, the grid-size h_1 was halved for one particular case as a check on the accuracy, and in this case results were obtained which were in closer agreement with those of Collins (12). However, the results with a step-size of $h_1 = \pi/30$ were considered satisfactory and did not warrant the increased computer time required in a refinement. Three or four figure agreement was not uncommon in the upstream region, in which the vorticity diffuses more slowly.

Separation, if it occurs, will commence at the rear stagnation point $\eta = 0$, at a time t_s, given by

$$\left.\frac{\partial \omega}{\partial \eta}\right|_{z=0,\eta=0} = \sum_{n=1}^{n_M} n\, r_n(0,t_s) = 0. \qquad (4.3.7)$$

The time of separation, t_s, was calculated by using a linear interpolation between results given at the time immediately preceding separation and those given at the time immediately following. This gives

$$t_s = t_0 + \frac{\sigma(t_0)\Delta t}{\sigma(t_0) - \sigma(t_0+\Delta t)}, \qquad (4.3.8)$$

where t_0 is the time immediately preceding separation, Δt is the time step, and

$$\sigma(t) \doteq \sum_{n=1}^{n_M} n r_n(0,t).$$

A quadratic interpolation shows no difference in the first three figures of the results. Fig. 42 graphically shows t_s as a function of R using the present results, and includes a calculation at $R = 10^6$. At $R = \infty$ there is good agreement with the value $t_s = .320$ calculated by Goldstein and Rosenhead (3). Table (3.4.2) shows the comparison of the time of separation between the present results, the time-series method of Collins and the fully-numerical method of Collins, for various Reynolds numbers. As can be seen, the agreement between the fully-numerical results of Collins and the present is good.

R	100	500	10^3	10^4	10^6	∞
Collins time-series	0.589	0.396	0.371	0.337	0.323	0.322
Collins fully-numerical	0.513	0.394	0.371	--	--	0.322
Present	0.515	0.395	0.373	0.338	0.324	0.321

TABLE (4.3.2) Comparison of t_s, as given by three different methods.

The temporal development of surface vorticity is given in Figs. 43 through 46 for the four finite values of R. It is initially infinite but rapidly decreases until eventually separation occurs at the rear stagnation point. At some time

thereafter, the surface vorticity starts to fluctuate in the separated region, starting at an earlier time the higher the values of R. It is barely noticeable at t=2 for R=100, but well-advanced at t=1.5 for $R=10^4$. This type of behaviour for high Reynolds number has been noted by Son and Hanratty (8) for R=200 and 500, by Thoman and Szewczyk (9) for R=40,000 and by Collins (12) for R=100,500,1000 and 5000. For $R=10^4$ the present method breaks down shortly after the more violent fluctuations set in, due to the iterations failing to converge.

The temporal development of $R^{-\frac{1}{2}}\zeta$ for R=∞ is given in Fig. 47 as far as t=1.0. For this case it was not possible to go beyond t=1.1, despite several varied attempts to do so. Again the iterations failed to converge. Collins (12) experienced the same difficulty, the solution terminating at t=1.25. It is thought possible that R=∞ may be a singular case, since there is no evidence of fluctuation of the surface vorticity as is apparent in the cases of finite R. It is certain that the fluctuations are increased by the presence of the R^{-1} term in equation (4.1.1).

Some properties of the R=∞ solution are given in Fig. 48. The friction drag coefficient C_f is calculated from

$$R^{\frac{1}{2}}C_f = \left(\frac{2}{t}\right)^{\frac{1}{2}} \int_0^{\pi} \omega(0,\eta,t)\sin\eta \, d\eta \ . \qquad (4.3.9)$$

The quantity η_s is the angle of separation. The quantity A is the magnitude of $R^{\frac{1}{2}} \frac{\partial C_f}{\partial \eta}$ at $\eta=\pi$, where c_f is the local coefficient of skin friction on the cylinder given by

$c_f = 4\zeta(0,\eta,t)/R$. This is known to have the value A = 9.86 from steady boundary-layer theory with external potential flow.

The pressure coefficient on the cylinder is calculated from

$$P^*(\eta,t) = \frac{1}{2t}\int_{\eta}^{\pi} \left(\frac{\partial\omega}{\partial z}\right)_{z=0} d\eta, \qquad (4.3.10)$$

which is derived from equation (IV.4) of Appendix IV, with $\eta_0=\pi$ being chosen as the base point on the cylinder. The temporal development of this coefficient is shown in Figs. 49, 50 and 51 for R=100,500 and 1000 respectively.

Fig. 52 gives the variation of the total drag coefficient $C_D = D/(\rho U_0^2 a)$ where D is the drag and ρ the density. This was calculated from

$$C_D = \frac{d}{dt}\left\{\int_0^{\infty}\int_0^{\pi} 2\omega e^{3kz}\sin\eta\, d\eta\, dz\right\} . \qquad (4.3.11)$$

This result for C_D is derived in Appendix IV from a result given by Phillips (28). At lower values of R, C_D was found to fluctuate slightly with time shortly after separation has occurred, and the dotted curves are mean curves in this region. This phenomenon is attributed to the fact that the calculation of the time derivative involves the difference of two quantities which have nearly the same value. Consequently an inaccuracy in the fourth significant figure of the original quantities becomes an inaccuracy in the second significant figure for C_D.

Streamlines for R=100,500 and 1,000 at times t=1 and t=2 are shown in Figs. 53 through 58.

CHAPTER V

CALCULATED FLOW PAST AN ELLIPTIC CYLINDER USING THE FULLY NUMERICAL METHOD

5.1 A FURTHER TRANSFORMATION FOR THE BOUNDARY LAYER CASE

For the boundary layer case, $R \to \infty$, and the following equations, obtained from equations (4.1.1) and (4.1.2) govern the flow:

$$H_0^2 \frac{\partial^2 \omega}{\partial z^2} + 2z \frac{\partial \omega}{\partial z} + 2\omega = 4t \frac{\partial \omega}{\partial t} + 4t H_0^2 \frac{\partial(\Psi,\omega)}{\partial(\eta,z)} , \qquad (5.1.1)$$

$$\frac{\partial^2 \Psi}{\partial z^2} = H_0^{-2} \omega . \qquad (5.1.2)$$

These are to be solved subject to the following conditions:-

$$\omega \to 0 \text{ as } z \to \infty , \qquad (5.1.3)$$

$$\left.\begin{aligned} \int_0^{\infty}\int_0^{2\pi} \omega H_0^{-2} \sin n\eta \, d\eta \, dz &= 2K_0 \pi \cos\gamma\delta_{n,1}, \quad (n=1,2,\ldots) \\ \int_0^{\infty}\int_0^{2\pi} \omega H_0^{-2} \cos n\eta \, d\eta \, dz &= -2K_0 \pi \sin\gamma\delta_{n,1}, \quad (n=0,1,2..) \end{aligned}\right\} \qquad (5.1.4)$$

$$\Psi = \frac{\partial \Psi}{\partial z} = 0 \text{ on } z = 0 , \qquad (5.1.5)$$

$$\left.\begin{aligned} \Psi(z,\eta,t) &= \Psi(z,\eta+2\pi,t) , \\ \omega(z,\eta,t) &= \omega(z,\eta+2\pi,t) , \end{aligned}\right\} \qquad (5.1.6)$$

where

$$H_0^2 = 2/(\cosh 2\alpha - \cos 2\eta) .$$

It is convenient to make the changes of variable

$$z = H_0 v \quad ; \quad \omega = H_0 \chi \quad ; \quad \Psi = H_0 \Phi \ . \tag{5.1.7}$$

Equations (5.1.1) through (5.1.6) then become

$$\frac{\partial^2 \chi}{\partial v^2} + 2v \frac{\partial \chi}{\partial v} + 2\chi = 4t \frac{\partial \chi}{\partial t} + 4tH_0^2 [\frac{\partial(\Phi,\chi)}{\partial(\eta,v)} + \frac{H_0^2 \sin 2\eta}{2}(\chi \frac{\partial \Phi}{\partial v} - \Phi \frac{\partial \chi}{\partial v})], \tag{5.1.8}$$

$$\frac{\partial^2 \Phi}{\partial v^2} = \chi \ , \tag{5.1.9}$$

$$\chi \to 0 \text{ as } v \to \infty \ , \tag{5.1.10}$$

$$\left.\begin{aligned} \int_0^\infty \int_0^{2\pi} \chi \sin n\eta \, d\eta \, dv &= 2K_0 \pi \cos\gamma \delta_{n,1} \ , \quad (n=1,2,\ldots) \\ \int_0^\infty \int_0^{2\pi} \chi \cos n\eta \, d\eta \, dv &= -2K_0 \pi \sin\gamma \delta_{n,1} \ , \quad (n=0,1,2,\ldots) \end{aligned}\right\} \tag{5.1.11}$$

$$\Phi = \frac{\partial \Phi}{\partial v} = 0 \text{ on } v = 0 \ , \tag{5.1.12}$$

$$\left.\begin{aligned} \Phi(v,\eta,t) &= \Phi(v,\eta+2\pi,t) \ , \\ \chi(v,\eta,t) &= \chi(v,\eta+2\pi,t) \ . \end{aligned}\right\} \tag{5.1.13}$$

The initial solutions required to start off the integrations are

$$\left.\begin{aligned} \chi(v,\eta,0) &= \frac{4K_0}{\pi^{\frac{1}{2}}} e^{-v^2} \sin(\eta-\gamma) \ , \\ \Phi(v,\eta,0) &= 2K_0 \sin(\eta-\gamma)[v \operatorname{erf} v + \frac{1}{\pi^{\frac{1}{2}}}(e^{-v^2}-1)] . \end{aligned}\right\} \tag{5.1.14}$$

Let us make the following definitions for r_n^*, s_n^* and Φ:-

$$\left.\begin{aligned} r_n^*(v,t) &= \frac{1}{\pi} \int_0^{2\pi} \chi \sin n\eta \, d\eta, \quad (n=1,2,\ldots) \\ s_n^*(v,t) &= \frac{1}{\pi} \int_0^{2\pi} \chi \cos n\eta \, d\eta, \quad (n=0,1,2,\ldots) \end{aligned}\right\} \tag{5.1.15}$$

$$\Phi(v,\eta,t) = \frac{g_0^*(v,t)}{2} + \sum_{n=1}^{\infty} [g_n^*(v,t)\cos n\eta + f_n^*(v,t)\sin n\eta]. \qquad (5.1.16)$$

With these definitions the following ensue, which are analagous to equations (4.1.6), (4.1.7), (4.1.11), (4.1.12) and (4.1.14) respectively:-

$$\frac{\partial^2 f_n(v,t)}{\partial v^2} = r_n^*(v,t) \quad , \qquad (n=1,2,\ldots) \qquad (5.1.17)$$

$$\frac{\partial^2 g_n(v,t)}{\partial v^2} = s_n^*(v,t) \quad , \qquad (n=0,1,2,\ldots) \qquad (5.1.18)$$

$$\int_0^{\infty} r_n^*(v,t)\,dv = 2K_0\cos\gamma\delta_{n,1} \quad , \qquad (n=1,2,\ldots) \qquad (5.1.19)$$

$$\int_0^{\infty} s_n^*(v,t)\,dv = -2K_0\sin\gamma\delta_{n,1} \quad , \qquad (n=0,1,2,\ldots) \qquad (5.1.20)$$

$$\chi(v,\eta,t) = \sum_{n=1}^{\infty} [r_n^*(v,t)\sin n\eta + s_n^*(v,t)\cos n\eta] + \frac{s_0^*(v,t)}{2}. \qquad (5.1.21)$$

The above equations resulting from the changes of variable are solved in a manner similar to that outlined in Chapter IV. Equations (5.1.17) and (5.1.18) are solved using the step-by-step procedures (4.2.14) and (4.2.15) with β set to zero. Along a line of constant η, equation (5.1.9) can be considered to be of the same form as equation (5.1.17). An alternative method of solution to equation (5.1.9) is to integrate this equation outwards along a line of constant η in the same manner as for the solution of equation (5.1.17), rather than expanding Φ in a Fourier series and solving

the component equations. It should be noted that this alternative is only possible in the limit $R\to\infty$, since in this case the η-derivative term is absent.

The principal advantage of this formulation for the boundary-layer case is that the initial solutions (5.1.14) give rise to very simple expressions for r_n^*, s_n^*, f_n^* and g_n^*, i.e.

$$\left.\begin{aligned} r_n^*(v,0) &= \frac{4K_0}{\pi^{\frac{1}{2}}} e^{-v^2}\cos\gamma\delta_{1,n} \\ s_n^*(v,0) &= 2K_0\cos\gamma[v\ \mathrm{erf}\ v + \frac{1}{\pi^{\frac{1}{2}}}(e^{-v^2}-1)]\delta_{1,n} \end{aligned}\right\}(n=1,2,..)$$

$$\left.\begin{aligned} s_n^*(v,0) &= -\frac{4K_0}{\pi^{\frac{1}{2}}} e^{-v^2}\sin\gamma\delta_{1,n} \\ g_n^*(v,0) &= -2K_0\sin\gamma[v\ \mathrm{erf}\ v + \frac{1}{\pi^{\frac{1}{2}}}(e^{-v^2}-1)]\delta_{1,n} \end{aligned}\right\}(n=0,1,2,..)$$

(5.1.22)

Thus initially the expansions for χ and Φ consist of two terms each, similar to the circular cylinder problem considered in the previous chapter, and suggests that the expansions for early times in this formulation will be rapidly convergent. Again, in the actual solution it is convenient to express χ as a perturbation $\Omega(v,\eta,t)$ from the initial solution,

$$\text{i.e.}\quad \chi(v,\eta,t) = \frac{4K_0 e^{-v^2}}{\pi^{\frac{1}{2}}}\sin(\eta-\gamma)+\Omega(v,\eta,t). \qquad (5.1.23)$$

In the computations it is of course necessary to replace the infinite sums in equations (5.1.16) and (5.1.21) by the finite sum 1 to n_M, where n_M is the value taken for truncation of the series.

It should be noted that results for the boundary-layer

flow past a circular cylinder using the transformations of this section, have in fact already been given in Chapter IV. This is a consequence of the fact that for a circular cylinder H_0 takes the value 1, and the transformation (5.1.7) reduces in this case to an identity transformation.

5.2 RESULTS FOR THE BOUNDARY-LAYER FLOW PAST AN ELLIPSE

For the case of flow past an elliptic cylinder it is found that the series (5.1.21) is not as rapidly convergent as in the circular case. Consequently n_M, the value taken for the truncation of this series, must be increased in the present case. This, however, presents difficulties in the evaluation of the integrals (5.1.15) for the larger values of n, due to the previously-noted rapid oscillation of the trigonometric part of the integrands. In practice it is found that for a fixed grid size of h_1 in the η-direction, that there is a maximum value of n for which the previously outlined method of Filon quadrature gives good results, and above which they become increasingly less accurate.

One way of circumventing this difficulty would be to reduce the grid-size h_1 accordingly, but this is impractical for two reasons. The primary reason is that a halving of grid-size usually results in a quadrupling of the computation time required for the solution of the matrix problem, and the secondary reason is that an increase in grid points gives rise to the problem of limited machine core-storage. A more efficient way to achieve the accurate evaluation of an integral of this kind is to double the number of grid points by inter-

polation and then calculate the value of the integral. This is equivalent to a halving of the grid size for the purpose of evaluating the integrals, but has the advantage of not requiring any additional computation time in the solution of the matrix problem for the vorticity. Since the interpolatedvorticity is only required to be stored at the evaluation of a particular integral, the increase in computer storage is negligible. In fact, since storage arrays are multi-purpose in nature, there should in practice be no increase in storage requirements. The interpolation formula used in the present work was the four point Lagrangian formula

$$\chi(\eta_m + \frac{h_1}{2}) = \frac{1}{16}[-\chi(\eta_{m-1})+9\chi(\eta_m)+9\chi(\eta_{m+1})-\chi(\eta_{m+2})],$$

where $\eta_m = mh_1$.

This is accurate to order h^4 and was found in practice to be very satisfactory.

Results are given in this section for the case of an elliptic cylinder of aspect ratio $\tau_1=0.6$, impulsively started at an angle of 15° to its major axis. The values taken for the parameters are given in Table (5.2.1). These are: (i) v_M, the length of the field, (ii) h, the grid-size in the v-direction, (iii)h_1, the grid size in the η-direction, (iv) κ, the smoothing factor, (v) ε, the convergence tolerance, (vi) n_M, the value taken for the truncation of the Fourier series, and (vii) Δt, the time increment.

v_M	h	h_1	κ	ϵ	n_M	Δt
7	0.05	$\pi/48$	10^{-1}	10^{-4}	40	0.025

TABLE (5.2.1) Values for the parameters used in the calculation.

Calculations were carried out using the above parameters to a dimensionless time of t=0.6. At this time it was found that the number of iterations required to solve the equations were significantly increased over that required at the previous time-step, and it was decided to discontinue the integrations. The reasons for this are two-fold. Firstly, it was found in the case of the circular cylinder that this behaviour was a premonition of the breakdown of the scheme within a few time increments, and this was thought to be the situation in the present case. The second reason was one of cost, since this type of problem requires large amounts of computer time.

Table (5.2.2) gives a comparison of the time of separation t_s, and angle of separation, η_s, as computed by (i) the time-series using terms to order t^7, (ii) the present method using linear interpolation methods, and (iii) the present method using quadratic interpolation procedures. As can be seen from this table the discretisation of the functions causes some difficulty in the estimation of the angle of separation, but this could be circumvented by sufficiently reducing the time-step in the vicinity of the time of separation. The time of separation does not seem to be as sensitive to this discretisation as the angle of separation. The agree-

ment between the values calculated by the time-series and those calculated by the fully-numerical method using quadratic interpolations is considered good.

	t_s	η_s
(i) Time-series to t^7	0.1815	0.091[c]
(ii) Fully numerical (linear interpolation)	0.1820	0.101[c]
(iii) Fully numerical (quadratic interpolation)	0.1819	0.093[c]

TABLE (5.2.2) Comparison of the separation values as calculated by different methods.

One of the purposes of solving the boundary-layer equations numerically is to estimate the approximate time-domain of validity of the time series. A comparison of values of the surface vorticity, ω, as calculated by the time-series method to order t^7 and the fully-numerical method for this case, is given in Table (5.2.3) for a dimensionless time of $t=0.5$ at intervals of $\frac{\pi}{24}$. As previously mentioned, a comparison of the values of the surface vorticity is a fairly sensitive check on the accuracy of the results generally, since the calculation of these is effectively a weighted sum of values throughout the field. The agreement at this time is considered good, and it is inferred from this that results for an elliptic cylinder of aspect ratio $\tau_1=0.6$ as calculated from the time series are valid until times of this order for the number of terms considered. The agreement at time $t=0.6$ is not quite so good, although still acceptable.

The results on the upstream side of the ellipse (corres-

Time-series from $\eta=0$ to $\eta=\pi$	F-N from $\eta=0$ to $\eta=\pi$	Time-series from $\eta=\pi$ to $\eta=2\pi$	F-N from $\eta=\pi$ to $\eta=2\pi$
1.413	1.402	2.207	2.248
0.721	0.708	1.126	1.125
0.000	0.000	0.000	0.000
-0.398	-0.400	-0.882	-0.884
-0.413	-0.420	-1.463	-1.464
-0.188	-0.193	-1.796	-1.797
0.113	0.111	-1.970	-1.970
0.405	0.404	-2.056	-2.056
0.661	0.660	-2.099	-2.099
0.875	0.875	-2.124	-2.124
1.055	1.054	-2.140	-2.140
1.205	1.205	-2.152	-2.153
1.335	1.335	-2.160	-2.161
1.452	1.452	-2.161	-2.161
1.563	1.563	-2.149	-2.150
1.678	1.679	-2.116	-2.117
1.813	1.814	-2.050	-2.051
1.986	1.986	-1.927	-1.928
2.222	2.219	-1.715	-1.717
2.540	2.532	-1.363	-1.366
2.909	2.906	-0.805	-0.815
3.232	3.242	0.026	0.028
3.376	3.355	1.034	1.155
3.055	3.048	1.636	1.618
2.207	2.248	1.413	1.402

TABLE (5.2.3) Comparison of the values of the surface vorticity, ω, at intervals of $\pi/24$, as computed by (i) the time-series method, (ii) the fully numerical method at t=0.5.

ponding approximately to $\frac{7\pi}{6} < \eta < \frac{11\pi}{6}$), show the best agreement since physically the flow, and consequently the functions, undergo the least change in this region. The downstream side exhibits less agreement, although it is still quite acceptable, this being attributed to two factors. Firstly, in both approaches the Fourier series do not converge too quickly for values of η close to $\eta = n\pi$, (n=0 1,2,...) and secondly in the fully numerical method the gradients of the functions in the wake region are larger, resulting in less accuracy when using finite differences to approximate the equations.

The temporal development of $R^{-\frac{1}{2}}\zeta$ for the case considered using the present method is given in Fig. 59, whilst the streamlines are given in Figs. 60 through 63 for times of t=0.15,0.25,0.45 and 0.60 respectively, R being set to 100 for the latter results. The movement of the separation points is in close agreement with the results given in Chapter 3 which are graphically illustrated in Fig. 9, and will not be given here.

5.3 RESULTS AT A FINITE REYNOLDS NUMBER

For flow past an elliptic cylinder at a finite value of the Reynolds number, we apply here the formulation of Chapter IV. The details of transformation (1.2.15) are

$$\left.\begin{aligned} \xi + i\eta &= \cosh^{-1}(X+iY) - \alpha, \\ H^2 &= 2/[\cosh 2(\xi+\alpha) - \cos 2\eta] , \\ K_o &= \frac{1}{2} e^{\alpha} \quad . \end{aligned}\right\} \qquad (5.3.1)$$

The representative length d is taken to be $(a^2-b^2)^{\frac{1}{2}}$, where a

and b are the lengths of the semi-major and semi-minor axes respectively.

As previously noted, the evaluation of the trigonometric integrals (4.1.3) and (4.1.4) for large values of n can cause difficulties. In the present section this problem is circumvented as in Section 5.2, by first interpolating and then using Filon quadrature.

In Section 3.4 results were given in some detail for the case of flow past an ellipse of aspect ratio 0.6 inclined at an angle of 15° to the free stream. The time-series method predicted that for $R < 13{,}000$ separation would occur in a radically different manner than for $R > 13{,}000$. However, it is possible that this behaviour could prove to be incorrect if the time-series were invalid at the predicted times for Reynolds numbers of this order. It is the purpose of the present section to re-solve the above case using fully-numerical techniques in order to obtain an approximate domain of validity for the time series and to verify the conclusions of Section 3.4. For this comparison a Reynolds number of 5,000 was chosen.

The values taken for the parameters are given in Table (5.3.1). These are: (i) z_M, the length of the field, (ii) h, the grid-size in the z-direction, (iii) h_1, the grid-size in the η-direction, (iv) κ, the smoothing factor, (v) ε, the convergence criterion, (vi) n_M, the value taken for the truncation of the Fourier series, and (vii) Δt, the time increment.

z_M	h	h_1	κ	ε	n_M	Δt
7	0.05	$\pi/48$	10^{-1}	10^{-4}	40	0.025

TABLE (5.3.1) Values for the parameters used in the calculation.

The solutions were advanced to t=0.025 by taking five steps of $\Delta t=0.001$ and then four steps with $\Delta t=0.005$. This is to restrict the truncation error incurred by the approximation of the time derivative at very small times, as mentioned in Section 4.2. Calculations were carried out using the above parameters to a dimensionless time t=1.0. Shortly before this time, it was observed that the number of iterations required for a converged solution at a particular time-step was beginning to slowly increase over that required at previous time-steps. It was felt that the calculations were approaching their ultimate breakdown, and that the solutions would not continue to be reliable for too much further in time. Since the problem had already consumed large amounts of computer time, it was decided to terminate the calculations at this point.

The temporal development of the surface vorticity ω for the case considered using the present method is given in Fig. 64, whilst the temporal development of the pressure coefficient is given in Fig. 65. The variation of the drag and lift coefficients C_D and C_L with respect to time are given in Fig. 66. These are calculated from expression (IV.7) and (IV.8) of Appendix IV, where

$$\left.\begin{aligned} C_X &= \frac{d}{dt}\left\{\int_0^{\infty}\int_0^{2\pi} \sinh(kz+\alpha)\ \omega H^{-2}\ \sin\eta\ d\eta\ dz\right\}, \\ C_Y &= -\frac{d}{dt}\left\{\int_0^{\infty}\int_0^{2\pi} \cosh(kz+\alpha)\ \omega H^{-2}\ \cos\eta\ d\eta\ dz\right\}. \end{aligned}\right\} \qquad (5.3.2)$$

The streamlines at t=0.2,0.6 and 1.0 are given in Figs. 67, 68 and 69 respectively.

A comparison of the values of the surface vorticity ω, as calculated from the time-series to order t^7 in k^0, t^5 in k^1 and t^0 in k^2, and by the fully-numerical method for this case is given in Table (5.3.2) at a dimensionless time of t=0.4 at intervals of $\pi/24$. The agreement at this time is considered quite good, and it is inferred from this that results for an elliptic cylinder of aspect ratio $\tau_1=0.6$ as calculated from the time series at a Reynolds number of 5,000 are valid until times of this order for the number of terms considered. The agreement at time t=0.5 is not quite so good, although it is still considered to be acceptable. As before, the results on the upstream side of the ellipse show the best agreement, with less agreement being found on the downstream side, particularly in the separated region. This is thought to be primarily due to the fact that in this region the surface vorticity as calculated from the time series is of two orders of magnitude less than the quantities used in its calculation. Consequently the truncation of the time-series becomes more significant in this region and less quantitative agreement can be expected.

Time-series from $\eta=0$ to $\eta=\pi$	F-N from $\eta=0$ to $\eta=\pi$	Time-series from $\eta=\pi$ to $\eta=2\pi$	F-N from $\eta=\pi$ to $\eta=2\pi$
28.6	28.8	77.2	76.9
20.6	17.3	39.2	38.5
2.5	2.1	- 0.2	- 0.0
- -3.0	- -4.5	- 30.8	- 30.8
- -0.7	- -2.1	- 51.5	- 51.6
6.3	5.6	- 64.0	- 64.2
15.6	15.3	- 71.2	- 71.3
24.9	24.9	- 75.2	- 75.4
33.5	33.5	- 77.6	- 77.8
40.8	40.8	- 79.3	- 79.5
47.0	47.1	- 80.5	- 80.7
52.3	52.4	- 81.5	- 81.7
56.9	57.0	- 82.2	- 82.4
61.1	61.1	- 82.6	- 82.8
65.0	65.1	- 82.5	- 82.6
68.9	69.1	- 81.5	- 81.7
73.4	73.6	- 79.2	- 79.5
78.9	79.1	- 75.0	- 75.3
86.2	86.4	- 67.6	- 68.1
95.7	95.7	- 55.6	- 56.5
106.4	106.3	- 37.9	- 39.3
114.7	115.1	- 16.2	- 16.8
116.2	116.7	2.1	6.8
104.1	104.8	14.4	24.3
77.2	76.9	28.6	28.8

TABLE (5.3.2) Comparison of the values of the surface vorticity ω at intervals of $\pi/24$, as computed by (i) the time-series method (ii) the fully-numerical method at t=0.4.

	t_s	η_s
(i) Time-series	0.31	0.36^c
(ii) Fully-numerical	0.29	0.34^c

TABLE (5.3.3) Comparison of the separation values as calculated by different methods for R=5,000.

Table (5.3.3) gives a comparison of the estimates for the time t_s, and angle η_s, of separation as computed by (i) the time-series method to t^7 in k^0, t^5 in k^1 and t^0 in k^2, (ii) the fully-numerical method using quadratic interpolation. The agreement is considered adequate for the following reasons. The time of separation for R=5,000 occurs at a much later value than in the limiting case $R\to\infty$ (0.31 as compared to 0.18), and consequently the error incurred in truncating the time-series in the region of the time of separation is far greater. The fully-numerical calculations verify the prediction of the time-series that the free streamline starts to move very rapidly down the rearside of the ellipse shortly before separation occurs, and consequently gradients of the vorticity become large in this region. This affects both the truncation error of the fully-numerical solutions and the estimates of the separation values. It is also found that the Fourier series for ω in the (z,η) coordinate system for R=5,000 converges more slowly than that for χ in the (v,η) coordinate system, employed in the limit $R\to\infty$, adding to the truncation error. It is difficult therefore to ascertain which is more accurate, the time-series of the fully-numerical

procedure, since some error can be expected to occur in both methods. However, it seems probable that the true time of separation lies somewhere in the region $t_s=0.30\pm0.01$ at a corresponding angle of separation $\eta_s=0.35^c\pm0.01^c$.

As noted in the previous paragraph, the onset of separation occurs in exactly the same manner as that predicted by the time-series and also gives estimates for the time and angle of separation which are also in good quantitative agreement. The time-series also predicts the existence of a second separated region occurring at $t=0.56$ and $\eta=-0.16^c$. However, it would appear that the time-series fails to converge at values of t this large since its existence had not been detected by the fully-numerical method at a time of $t=1.0$. Nevertheless, as can be seen from Fig. 64, a kink in the surface vorticity is fairly well-developed in the region of $\eta=-0.16^c$ and its previous temporal development makes it appear likely that this second separated region does in fact exist, although it occurs at a far later time than predicted by the time-series. Thus although the time-series will definitely give a quantitatively incorrect result for the second separated region, its development may in fact be qualitatively correct. This remains to be seen.

It is hoped that in the not-too-distant future a calculation for some value of R less than 1,700 will be undertaken in order to determine whether or not a third regime for R exists as predicted by the time-series, for which separation should occur in yet another manner.

CHAPTER VI

SUMMARY AND CONCLUSION

The primary objective of this thesis is to consider an asymmetrical viscous fluid flow past an impulsively started cylinder in an unbounded incompressible fluid, and to examine the manner in which the onset of separation occurs. For this purpose the case of an ellipse of aspect ratio 0.6, inclined at an angle of 15° to its direction of motion, is studied in some detail by two different methods.

The analytical results of the time-series method given in Chapter II extends the existing theory for finite Reynolds number to a higher order than that given previously, the given solutions holding true in the general case. This latter property gives a useful check on the work, agreement being found with previous results for the special case of a circular cylinder. Two elliptic cylinders of different aspect ratios at various angles of incidence are then examined in Chapter III by numerically determining the coefficients in the time-series to higher order. The fully-numerical method leads one to believe that for an ellipse of aspect ratio 0.6 that the time series is valid until times of order t=0.5 for the boundary-layer case and until $t \approx 0.4$ when R=5,000. The time-series method also predicts that the manner in which separation will occur for this case is dependent on the value

of R. For R > 13,000 separation will occur in a similar manner to that predicted by boundary-layer theory. However, for R < 13,000 this is no longer true, and shows that for this particular configuration even the qualitative results of boundary-layer theory (valid in the limit $R\to\infty$) break down at relatively high values of the Reynolds number. This restriction on the application of time-dependent boundary-layer theory is thought to be of possible significance.

The fully-numerical method is described in Chapter IV and tested by applying it to the case of a circular cylinder. Good agreement is found between these results and those of a similar study by Collins. The method is also applied to an elliptic cylinder of aspect ratio 0.6 at an angle of 15°, giving good agreement with the results of the time-series method until sometime after separation commences. Solutions are given as far as t=1.0 for R=5,000 and to t=0.6 when 1/R=0. The method also indicates the approximate domain of validity of the time-series approach for these two cases. It is hoped at some future date to consider the case of a lower value of the Reynolds number (for which the domain of validity of the time series is more restricted) and then to continue the calculations to higher times by switching over to the more natural (ξ,η) coordinate system.

Both the numerical time-series and the fully-numerical method require more terms in the Fourier series as the aspect ratio of the ellipse decreases. This is a drawback, although satisfactory results should still be obtainable for early times.

Experimental studies related to the general area of this thesis include those of Schwabe (31), Sarpkaya (32), Taneda and Honji (33,34) and Honji (35). The most relevant of these studies to the present investigation is that of Honji (35). However, there are extreme difficulties encountered experimentally in starting the motion, and data for times of the order of this study are generally not given due to the difficulties of measurement. Consequently, it was not possible to make any comparisons with experiment in the investigation.

APPENDIX I

The A_i,(i=0,1,2,...,15), and B_i, (i=0,1,2,3), referred to in Chapter II are defined below, where

$$\text{erf } v = \frac{2}{\pi^{\frac{1}{2}}} \int_0^v e^{-w^2}\, dw.$$

$$A_0 = \frac{2}{\pi^{\frac{1}{2}}} e^{-v^2}$$

$$A_1 = 2v(\text{erf } v)^2 + \frac{(1-2v^2)}{\pi^{\frac{1}{2}}} \text{erf } v\, e^{-v^2} + \frac{2v\, e^{-v^2}}{\pi} \left(\frac{4}{3} - e^{-v^2}\right) + 2\left(1 + \frac{4}{3\pi}\right)\left(v \text{ erf } v + \frac{e^{-v^2}}{\pi^{\frac{1}{2}}}\right) - 4\left(1 + \frac{2}{3\pi}\right)v$$

$$A_2 = -\frac{1}{8}\left[(1 - \text{erf } v) + \frac{2}{\pi^{\frac{1}{2}}} (v + 2v^3) e^{-v^2}\right]$$

$$A_3 = 1 - \text{erf } v$$

$$A_4 = -\frac{1}{4}\left(\frac{1}{8} + \frac{1}{3\pi} + \sqrt{2}\right)\left[(1 + 2v^2)(\text{erf } v - 1) + \frac{2v\, e^{-v^2}}{\pi^{\frac{1}{2}}}\right] - \frac{v\, e^{-v^2} \text{erf } v}{2\pi^{\frac{1}{2}}} \left[\frac{3}{4} + \frac{5v^2}{3} + v^4\right] + \frac{e^{-v^2}}{\pi} \left[\frac{2}{15} + \frac{\pi^{\frac{1}{2}} v}{8} + \frac{v}{3\pi^{\frac{1}{2}}} + \frac{2v^2}{5} + \frac{2v^4}{3}\right] - \frac{e^{-2v^2}}{\pi} \left[\frac{1}{3} + \frac{7v^2}{12} + \frac{v^4}{2}\right]$$

$$A_5 = \frac{5v\, e^{-v^2}}{2\pi^{\frac{1}{2}}} + \frac{3}{4} (1 + 2v^2)(\text{erf } v - 1)$$

$$A_6 = \frac{1}{4}\left(\frac{5}{16} - \sqrt{2}\right)\left[(1 + 2v^2)(\text{erf } v - 1) + \frac{2v\, e^{-v^2}}{\pi^{\frac{1}{2}}}\right] - \frac{v^2 (\text{erf } v)^2}{4} \frac{\text{erf } v}{4\pi^{\frac{1}{2}}} \left[\frac{5v\, e^{-v^2}}{2} + \frac{v^3\, e^{-v^2}}{3} + \frac{\pi^{\frac{1}{2}}}{2}\right] + \frac{1}{8} (1+2v^2) - \frac{e^{-v^2}}{4\pi^{\frac{1}{2}}} \left(\frac{v}{4} + \frac{v^3}{3}\right)$$

$$- \frac{e^{-2v^2}}{3\pi} (1 + \frac{v^2}{4})$$

$$A_7 = 2v^2 (\text{erf } v)^2 + \text{erf } v[\frac{11}{8} + \frac{3v^2}{4} + \frac{3v\, e^{-v^2}}{\pi^{\frac{1}{2}}} - \frac{2v^3 e^{-v^2}}{3\pi^{\frac{1}{2}}}]$$
$$- \frac{11}{8} (1 + 2v^2) + \frac{e^{-v^2}}{\pi}[\frac{8}{15} + \frac{5\pi^{\frac{1}{2}}v}{4} + \frac{8v^2}{5} + \frac{2\pi^{\frac{1}{2}}v^3}{3}]$$
$$+ \frac{2e^{-2v^2}}{3\pi} [2 - v^2]$$

$$A_8 = (1 + 2v^2)(\text{erf } v - 1) + \frac{2v\, e^{-v^2}}{\pi^{\frac{1}{2}}}$$

$$A_9 = - (\frac{1}{8} + \frac{v^2}{4} + \frac{v^4}{3}) \frac{e^{-v^2}}{\pi^{\frac{1}{2}}}$$

$$A_{10} = (\frac{7}{128} + \frac{7v^2}{64} + \frac{7v^4}{96} + \frac{v^6}{16}) \frac{e^{-v^2}}{\pi^{\frac{1}{2}}}$$

$$A_{11} = - (1 + 2v^2) \frac{e^{-v^2}}{8\pi^{\frac{1}{2}}}$$

$$A_{12} = 2v(1 - \text{erf } v) + (2v^3 - 5) \frac{e^{-v^2}}{4\pi^{\frac{1}{2}}}$$

$$A_{13} = v(1 - \text{erf } v) + \frac{(2v^2 - 3)e^{-v^2}}{4\pi^{\frac{1}{2}}}$$

$$A_{14} = 2v(1 - \text{erf } v) + \frac{e^{-v^2}}{\pi^{\frac{1}{2}}}[- \frac{7}{4} + \frac{v^2}{2} + \frac{2v^4}{3}]$$

$$A_{15} = v(\text{erf } v - 1) + \frac{e^{-v^2}}{\pi^{\frac{1}{2}}}$$

$$B_0 = v \text{ erf } v + \frac{1}{\pi^{\frac{1}{2}}}(e^{-v^2} - 1)$$

$$B_1 = \frac{1}{6}(2v^3 - 3v)(\text{erf} v)^2 + \frac{1}{6}(1 + \frac{4}{3\pi})(2v^3 + 3v)\text{erf } v + \frac{1}{6\pi^{\frac{1}{2}}}\text{erf } v[(4v^2 - 11)e^{-v^2}$$
$$-4] + \frac{4}{3}(\frac{2}{\pi})^{\frac{1}{2}} \text{erf}(2^{\frac{1}{2}}v) + \frac{v}{3\pi} e^{-2v^2} + \frac{1}{3\pi^{\frac{1}{2}}}(1 + \frac{4}{3\pi})(1 + v^2)e^{-v^2} - \frac{2}{3}(1 + \frac{2}{3\pi})v^3$$
$$- \frac{2v}{3\pi} - \frac{1}{3\pi^{\frac{1}{2}}}(1 + \frac{4}{3\pi})$$

$$B_2 = \frac{1}{32}\left[(1 + 2v^2)\,\mathrm{erf}\ v - 2v^2 - \frac{2v\, e^{-v^2}}{\pi^{\frac{1}{2}}}\right]$$

$$B_3 = \frac{1}{4}\left[2v^2 - (1 + 2v^2)\ \mathrm{erf}\ v + \frac{2v}{\pi^{\frac{1}{2}}}\ (2 - e^{-v^2})\right]$$

APPENDIX II

The functions defined here are referenced in Chapter III. For q=0, the sums over n are taken to be identically zero.

Let

$$\Gamma^{(0)}_{0,q}(v) = \sum_{n=1}^{q} \left\{ \sum_{m=1}^{\infty} [4m(F_1(m,m)+F_2(m,m))+F_3(m+2,m)-F_3(m,m+2)] + \sum_{m=1}^{2} F_3(m,2-m) \right\} ,$$

$$\Gamma^{(0)}_{p,q}(v) = 2\sum_{n=1}^{q} \left\{ \sum_{m=1}^{\infty} (m+p)[F_1(m+p,m)+F_2(m+p,m)] + (1-\delta_{p,1}) \sum_{m=1}^{p-1} (p-m) [F_1(p-m,m)-F_2(p-m,m)] + \sum_{m=p+1}^{\infty} (m-p)[F_1(m-p,m)+F_2(m-p,m)] + pF_1(p,0) \right\}$$

$$+ \frac{1}{2}\sum_{n=1}^{q} \left\{ \sum_{m=1}^{\infty} F_3(p+m+2,m) + \sum_{m=1}^{p+1} F_3(p-m+2,m) + \sum_{m=\max(1,p-1)}^{\infty} F_3(m-p+2,m) - \sum_{m=p+3}^{\infty} F_3(m-p-2,m) - (1-\delta_{p,1}-\delta_{p,2}-\delta_{p,3}) \sum_{m=1}^{p-3} F_3(p-m-2,m) - \sum_{m=\max(1,3-p)}^{\infty} F_3(m+p-2,m) + F_3(p+2,0) - (1-\delta_{p,1}-\delta_{p,2})F_3(p-2,0) + \delta_{p,1}F_3(1,0) \right\} ,$$

$$\Delta^{(0)}_{p,q}(v) = 2 \sum_{n=1}^{q} \Bigg\{ \sum_{m=1}^{p} F_4(m+p,m) + (1-\delta_{p,1}) \sum_{m=1}^{p-1} F_4(p-m,m)$$

$$- \sum_{m=p+1}^{\infty} F_4(m-p,m) + p\left(P_{p,n-1}V'_{0,q-n} - T'_{0,n-1}R_{p,q-n}\right) \Bigg\}$$

$$+ \frac{1}{2} \sum_{n=1}^{\infty} \Bigg\{ (1-\delta_{p,1}-\delta_{p,2}-\delta_{p,3}) \sum_{m=1}^{p-3} [F_5(p-m-2,m) - F_6(p-m-2,m)]$$

$$- \sum_{m=p+3}^{\infty} [F_5(m-p-2,m) + F_6(m-p-2,m)]$$

$$+ \sum_{m=\max(1,3-p)}^{\infty} [F_5(m+p-2,m) + F_6(m+p-2,m)]$$

$$- \sum_{m=1}^{\infty} [F_5(m+p+2,m) + F_6(m+p+2,m)]$$

$$- \sum_{m=1}^{p+1} [F_5(p-m+2,m) - F_6(p-m+2,m)]$$

$$+ \sum_{m=\max(1,p-1)}^{\infty} [F_5(m-p+2,m) + F_6(m-p+2,m)]$$

$$- [F_5(0,p+2) + F_5(p+2,0)]$$

$$+ (1-\delta_{p,1}-\delta_{p,2}) [F_5(0,p-2) + F_5(p-2,0)]$$

$$+ \delta_{p,1} [F_5(0,1) + F_5(1,0)] + \delta_{p,2} F_5(0,0) \Bigg\} \quad ,$$

where

$$F_1(\ell,m) = S^{(0)}_{\ell,q-n} T^{(0)'}_{m,n-1} - Q^{(0)}_{\ell,n-1} V^{(0)'}_{m,q-n} \quad ,$$

$$F_2(\ell,m) = P^{(0)}_{\ell,n-1} W^{(0)'}_{m,q-n} - R^{(0)}_{\ell,q-n} U^{(0)'}_{m,n-1} \quad ,$$

$$F_3(\ell,m) = T^{(0)}_{m,n-1} W^{(0)'}_{\ell,q-n} - W^{(0)}_{\ell,q-n} T^{(0)'}_{m,n-1} + U^{(0)}_{\ell,n-1} V^{(0)'}_{m,q-n} - V^{(0)}_{m,q-n} U^{(0)'}_{\ell,n-1} \quad ,$$

$$F_4(\ell,m) = \ell[P^{(0)}_{\ell,n-1}V^{(0)\prime}_{m,q-n} - R^{(0)}_{\ell,q-n}T^{(0)\prime}_{m,n-1}] + m(S^{(0)}_{m,q-n}U^{(0)\prime}_{\ell,n-1} - Q^{(0)}_{m,n-1}W^{(0)\prime}_{\ell,q-n}) \quad ,$$

$$F_5(\ell,m) = T^{(0)}_{m,n-1}V^{(0)\prime}_{\ell,q-n} - V^{(0)}_{\ell,q-n}T^{(0)\prime}_{m,n-1} \quad ,$$

$$F_6(\ell,m) = U^{(0)}_{m,n-1}W^{(0)\prime}_{\ell,q-n} - W^{(0)}_{\ell,q-n}U^{(0)\prime}_{m,n-1} \quad ,$$

$$\max(\ell,m) = \begin{cases} \ell \text{ if } \ell \geq m \\ m \text{ if } \ell < m \end{cases} \quad .$$

The functions associated with k' are defined as

$$\Gamma^{(1)}_{0,q} = -\beta_1 v[vN^{(0)\prime}_{0,q} + (1-2q)N^{(0)}_{0,q}]$$

$$+ \sum_{n=1}^{q} \left\{ \sum_{m=1}^{\infty} [4F_7(m,m) + 4F_8(m,m) + F_9(m+2,m) - F_9(m,m+2)] + \sum_{m=1}^{2} F_9(m,2-m) \right\} \quad ,$$

$$\Gamma^{(1)}_{p,q} = -\beta_1 v[vN^{(0)\prime}_{p,q} + (1-2q)N^{(0)}_{p,q}]$$

$$+2 \sum_{n=1}^{q} \left\{ \sum_{m=1}^{\infty} [F_7(m+p,m) + F_8(m+p,m)] + F_7(p,0) \right.$$

$$+ \sum_{m=p+1}^{\infty} [F_7(m-p,m) + F_8(m-p,m)]$$

$$\left. + (1-\delta_{p,1}) \sum_{m=1}^{p-1} [F_7(p-m,m) - F_8(p-m,m)] \right\}$$

$$+ \frac{1}{2} \sum_{n=1}^{q} \left\{ \sum_{m=1}^{\infty} F_9(p+m+2,m) + \sum_{m=\max(1,p-1)}^{\infty} F_9(m-p+2,m) \right.$$

$$- \sum_{m=p+3}^{\infty} F_9(m-p-2,m) - \sum_{m=\max(1,3-p)}^{\infty} F_9(m+p-2,m)$$

$$- (1-\delta_{p,1}-\delta_{p,2}-\delta_{p,3}) \sum_{m=1}^{p-3} F_9(p-m-2,m)$$

$$+ F_9(p+2,0) - (1-\delta_{p,1}-\delta_{p,2}) F_9(p-2,0) + \delta_{p,1} F_9(1,0) \Big\} ,$$

$$\Delta_{p,q}^{(1)}(v) = -\beta_1 v [v O_{p,q}^{(0)\prime} + (1-2q) O_{p,q}^{(0)}]$$

$$+ 2 \sum_{n=1}^{q} \Big\{ \sum_{m=1}^{\infty} F_{10}(m+p,m) + (1-\delta_{p,1}) \sum_{m=1}^{p-1} F_{10}(p-m,m)$$

$$- \sum_{m=p+1}^{\infty} F_{10}(m-p,m) + p [P_{p,n-1}^{(1)} V_{0,q-n}^{(0)\prime} - R_{p,q-n}^{(0)} T_{0,n-1}^{(1)\prime}$$

$$+ P_{p,n-1}^{(0)} V_{0,q-n}^{(1)\prime} - R_{p,q-n}^{(1)} T_{0,n-1}^{(0)\prime}] \Big\}$$

$$+ \frac{1}{2} \sum_{n=1}^{q} \Big\{ (1-\delta_{p,1}-\delta_{p,2}-\delta_{p,3}) \sum_{m=1}^{p-3} [F_{11}(p-m-2,m)$$

$$- F_{12}(p-m-2,m)] - \sum_{m=p+3}^{\infty} [F_{11}(m-p-2,m) + F_{12}(m-p-2,m)]$$

$$+ \sum_{m=\max(1,3-p)}^{\infty} [F_{11}(m+p-2,m) + F_{12}(m+p-2,m)]$$

$$- \sum_{m=1}^{\infty} [F_{11}(m+p+2,m) + F_{12}(m+p+2,m)]$$

$$- \sum_{m=1}^{p+1} [F_{11}(p-m+2,m) - F_{12}(p-m+2,m)]$$

$$+ \sum_{m=\max(1,p-1)}^{\infty} [F_{11}(m-p+2,m) + F_{12}(m-p+2,m)]$$

$$- [F_{11}(p+2,0) + F_{11}(0,p+2)]$$

$$+ \delta_{p,2}F_{11}(0,0)+\delta_{p,1}[F_{11}(1,0)+F_{11}(0,1)]$$

$$+ (1-\delta_{p,1}-\delta_{p,2})[F_{11}(p-2,0)+F_{11}(0,p-2)]\Big\} \quad ,$$

where

$$F_7(\ell,m) = \ell[S^{(0)}_{\ell,q-n}T^{(1)'}_{m,n-1}-V^{(0)'}_{m,q-n}Q^{(1)}_{\ell,n-1}+S^{(1)}_{\ell,q-n}T^{(0)'}_{m,n-1}$$

$$-Q^{(0)}_{\ell,n-1}V^{(1)'}_{m,q-n}] \quad ,$$

$$F_8(\ell,m) = \ell[P^{(1)}_{\ell,n-1}W^{(0)'}_{m,q-n}-R^{(0)}_{\ell,q-n}U^{(1)'}_{m,n-1}+W^{(1)'}_{m,q-n}P^{(0)}_{\ell,n-1}$$

$$-R^{(1)}_{\ell,q-n}U^{(0)'}_{m,n-1}] \quad ,$$

$$F_9(\ell,m) = U^{(1)}_{\ell,n-1}V^{(0)'}_{m,q-n}-V^{(0)}_{m,q-n}U^{(1)'}_{\ell,n-1}+T^{(1)}_{m,n-1}W^{(0)'}_{\ell,q-n}$$

$$-W^{(0)}_{\ell,q-n}T^{(1)'}_{m,n-1}+U^{(0)}_{\ell,n-1}V^{(1)'}_{m,q-n}-V^{(1)}_{m,q-n}U^{(0)'}_{\ell,n-1}$$

$$+T^{(0)}_{m,n-1}W^{(1)'}_{\ell,q-n}-W^{(1)}_{\ell,q-n}T^{(0)'}_{m,n-1}$$

$$F_{10}(\ell,m) = \ell[P^{(1)}_{\ell,n-1}V^{(0)'}_{m,q-n}-R^{(0)}_{\ell,q-n}T^{(1)'}_{m,n-1}+P^{(0)}_{\ell,n-1}V^{(1)'}_{m,q-n}$$

$$-R^{(1)}_{\ell,q-n}T^{(0)'}_{m,n-1}]+m[S^{(0)}_{m,q-n}U^{(1)'}_{\ell,n-1}$$

$$-Q^{(1)}_{m,n-1}W^{(0)'}_{\ell,q-n}+S^{(1)}_{m,q-n}U^{(0)'}_{\ell,n-1}-Q^{(0)}_{m,n-1}W^{(1)'}_{\ell,q-n}],$$

$$F_{11}(\ell,m) = T^{(1)}_{m,n-1}V^{(0)'}_{\ell,q-n}-V^{(0)}_{\ell,q-n}T^{(1)'}_{m,n-1}+T^{(0)'}_{m,n-1}V^{(1)'}_{\ell,q-n}$$

$$-V^{(1)}_{\ell,q-n}T^{(0)'}_{m,n-1} \quad ,$$

$$F_{12}(\ell,m) = U^{(1)}_{m,n-1}W^{(0)'}_{\ell,q-n}-W^{(0)}_{\ell,q-n}U^{(1)'}_{m,n-1}+U^{(0)}_{m,n-1}W^{(1)'}_{\ell,q-n}$$

$$-W^{(1)}_{\ell,q-n}U^{(0)'}_{m,n-1} \quad .$$

APPENDIX III

The matrix problem

$$A_i g_{i-1} + B_i g_i + C_i g_{i+1} = D_i, \quad (i=1,2,\ldots,i_{max}-1)$$

where

$$g_0 = 1, \; g_{i_{max}} = 0 \; ,$$

and A_i, B_i, C_i and D_i are known explicitly, can be solved by a direct method given by Varga (29), p. 196. The proof of stability is given by Rosser (30).

Define $F_0 = 0, \quad \delta_0 = g_0 \; ,$

$$F_{i+1} = - \frac{C_{i+1}}{B_{i+1}+A_{i+1}F_i} \; ,$$

$$\delta_{i+1} = \frac{D_{i+1}-A_{i+1}\delta_i}{B_{i+1}+A_{i+1}F_i} \; . \qquad (i=0,1,\ldots,i_{max}-2)$$

The solution is then given by

$$g_i = F_i g_{i+1} + \delta_i \; . \qquad (i=i_{max}-1, i_{max}-2, \ldots, 2, 1)$$

To find the g_H and g_p referred to in Chapter III, take

$$A_i = 1 - \frac{h^2}{12} m_{i-1} \; , \quad B_i = -(2 + \frac{5h^2}{6} m_i), \; C_i = (1 - \frac{h^2}{12} m_{i+1}),$$

together with

$$D_i = 0 \; ,$$

for the case of g_H and

$$D_i = \frac{h^2}{12} (n_{i+1}+10n_i+n_{i-1}),$$

for the case of g_p.

APPENDIX IV

The dimensionless pressure coefficient $P^*(\eta,t)$ on the surface of the cylinder is defined to be

$$P^*(\eta,t)=\frac{p(\eta,t)-p(\eta_0,t)}{\frac{1}{2}\rho U^2} = 2[p'(\eta,t)-p'(\eta_0,t)], \quad \text{(IV.1)}$$

where $p(\eta,t)$ and $p'(\eta,t)$ are respectively the dimensional and non-dimensional pressures on the surface of the cylinder, and η_0 is some base point on the surface.

If we now take the component of equation (1.2.1) in the η-direction on the surface of the cylinder (where $\underline{V}=0$), we can show that

$$\frac{\partial p'(\eta,t)}{\partial \eta} = -\frac{2}{R}\left(\frac{\partial \zeta}{\partial \xi}\right)_{\xi=0} . \quad \text{(IV.2)}$$

Integrating equation (IV.2) along the surface of the cylinder then gives

$$p'(\eta,t)-p'(\eta_0,t) = -\frac{2}{R}\int_{\eta_0}^{\eta}\left(\frac{\partial \zeta}{\partial \xi}\right)_{\xi=0} d\eta \quad . \quad \text{(IV.3)}$$

Hence combining equations (IV.1) and (IV.3) gives the following expression for the dimensionless pressure coefficient

$$P^*(\eta,t) = -\frac{4}{R}\int_{\eta_0}^{\eta}\left(\frac{\partial \zeta}{\partial \xi}\right)_{\xi=0} d\eta \quad . \quad \text{(IV.4)}$$

Let us non-dimensionlise the body forces with respect to $\rho U_0^2 d$, where for a circular cylinder we take d to be the radius of the cylinder, and for an elliptic cylinder d is

taken to be $(a^2-b^2)^{\frac{1}{2}}$, a and b being the lengths of the semi-major and semi-minor axes respectively. Then the dimensionless forces C_X and C_Y, in the Cartesian X and Y directions respectively, exerted by the fluid on the cylinder are given by

$$C_X = - \oint_C \left(\frac{P^*}{2}\, dY + \frac{2}{R}\zeta\, dX\right) , \qquad \text{(IV.5)}$$

$$C_Y = \oint_C \left(\frac{P^*}{2}\, dX - \frac{2}{R}\zeta\, dY\right) , \qquad \text{(IV.6)}$$

where C denotes integration around the cylinder ($\xi=0$) in the anti-clockwise sense, and X and Y are non-dimensional Cartesian coordinates.

The first part of the integrals gives the pressure contribution to the force, whilst the second gives the frictional contribution. If we now define C_D and C_L to be the forces parallel and normal to the direction of the free stream respectively, then we obtain the following relations in terms of C_X, C_Y and the angle of incidence, γ,

$$C_D = C_X\cos\gamma + C_Y\sin\gamma , \qquad \text{(IV.7)}$$

$$C_L = C_Y\cos\gamma - C_X\sin\gamma . \qquad \text{(IV.8)}$$

C_D and C_L are usually referred to as the coefficients of drag and lift respectively. For symmetrical flows (e.g. a circular cylinder), we have $\gamma=0$ and also find $C_Y=0$. Consequently

$$C_D = C_X , \qquad \text{(IV.9)}$$

$$C_L = 0 . \qquad \text{(IV.10)}$$

For an elliptic cylinder equations (IV.5) and (IV.6) become in the (ξ,η) coordinate system

$$C_X = -\frac{\sinh\alpha}{2}\int_0^{2\pi} P^*\cos\eta\, d\eta + \frac{2\cosh\alpha}{R}\int_0^{2\pi}\zeta|_{\xi=0}\sin\eta\, d\eta, \quad \text{(IV.11)}$$

$$C_Y = -\frac{\cosh\alpha}{2}\int_0^{2\pi} P^*\sin\eta\, d\eta - \frac{2\sinh\alpha}{R}\int_0^{2\pi}\zeta|_{\xi=0}\cos\eta\, d\eta, \quad \text{(IV.12)}$$

from which C_D and C_L may be calculated using expressions (IV.7) and (IV.8).

We now consider a method for deriving expressions for C_X and C_Y by total momentum considerations. The total momentum of the fluid in the X-direction (see Fig. 1) is given by

$$M_X = \int_D\int \zeta U_1 dXdY \quad , \quad \text{(IV.13)}$$

where D is the infinite domain outside of the cylinder and U_1 is the component of velocity $\underline{V}$ in the X-direction.

If we now work in terms of the non-dimensional quantities X', Y', U_1' and t' defined in equation (1.2.3) we obtain

$$M_X = d^2\rho U_0\int_D\int U_1' dX'dY' \quad . \quad \text{(IV.14)}$$

It has been shown by Phillips (28) that this can be further reduced to

$$M_X = -d^2\zeta U_0\int_D\int Y'\zeta' dX'dY' \quad , \quad \text{(IV.15)}$$

where $$\zeta' = \frac{\partial U_1'}{\partial Y'} - \frac{\partial U_2'}{\partial X'} \quad .$$

Hence

$$\frac{dM_X}{dt} = -d\rho U_0^2 \frac{d}{dt'} \left\{ \iint_D Y'\zeta' dX' dY' \right\} .$$

Thus we obtain the expression for C_X given by

$$C_X = -\frac{1}{\rho U_0^2 d} \frac{dM_X}{dt} = \frac{d}{dt'} \left\{ \iint_D Y'\zeta' dX' dY' \right\} . \qquad \text{(IV.16)}$$

Let us now drop primes for convenience and assume all quantities are non-dimensionalised, giving

$$C_X = \frac{d}{dt} \left\{ \iint_D Y\zeta dX dY \right\} . \qquad \text{(IV.17)}$$

For the type of conformal transformation that we have employed we find that

$$Y = e(\xi)\sin\eta ,$$

$$X = f(\xi)\cos\eta ,$$

where for a circular cylinder $e(\xi) = f(\xi) = e^{\xi}$ and for an elliptic cylinder $e(\xi) = \sinh(\xi+\alpha)$, $f(\xi) = \cosh(\xi+\alpha)$.

Hence, under the conformal transformation employed expression (IV.17) becomes

$$C_X = \frac{d}{dt} \left\{ \int_0^{\infty} \int_0^{2\pi} e(\xi)\zeta H^{-2} \sin\eta \, d\eta \, d\xi \right\}. \qquad \text{(IV.18)}$$

In the (z,η) plane equation (IV.18) then becomes

$$C_X = \frac{d}{dt} \left\{ \int_0^{\infty} \int_0^{2\pi} e(kz)\omega H^{-2} \sin\eta \, d\eta \, dz \right\} , \qquad \text{(IV.19)}$$

and in a similar manner we obtain

$$C_Y = \frac{d}{dt} \left\{ \int_0^{\infty} \int_0^{2\pi} f(kz)\omega H^{-2} \cos\eta \, d\eta \, dz \right\} . \qquad \text{(IV.20)}$$

REFERENCES

(1) Prandtl, L., Über Flüssigkeitsbewegung bei sehr kleiner Reibung, Proceedings 3rd. Intern. Math. Congr., Heidelberg (1904) 484; reprinted in "Vier Abhandlungen zur Hydrodynamik und Aerodynamik" Göttingen (1927); NACA TM 452 (1928).

(2) Blasius, H., Grenzschichten in Flüssigkeiten mit kleiner Reibung, Zeit. f. Math u. Phys. 56 (1908) 1; English Translation NACA TM 1256.

(3) Goldstein, S. and Rosenhead, L., Boundary Layer Growth, Proc. Camb. Phil. Soc. 32 (1936) 392.

(4) Wang, C.-Y., The Flow Past a Circular Cylinder which is Started Impulsively from Rest, J. Math. Phys. 46 (1967) 195.

(5) Wang, C.-Y., Separation and Stall of an Impulsively Started Elliptic Cylinder, J. Appl. Mech. 34 (1967) 823.

(6) Collins, W.M. and Dennis, S.C.R., The Initial Flow Past an Impulsively Started Circular Cylinder, Quart. J. Mech. Appl. Math. (1972), to appear.

(7) Payne, R.B., Calculations of Unsteady Viscous Flow Past a Circular Cylinder, J. Fluid Mech. 4 (1958) 81.

(8) Son, J.S. and Hanratty, T.J., Numerical Solution for the Flow around a Cylinder at Reynolds Numbers of 40,200 and 500, J. Fluid Mech. 35 (1969) 369.

(9) Thoman, D.C., Szewczyk, A.A., Time-Dependent Viscous Flow over a Circular Cylinder, Phys. Fluids Suppl. II, (1969) 76.

(10) Lugt, H.J. and Haussling, H.J., Laminar Flows Past a Flat Plate at Various Angles of Attack, Lecture Notes in Physics, Springer-Verlag, 8 (1971) 78.

(11) Ingham, D.B., Note on the Numerical Solution for Unsteady Viscous Flow Past a Circular Cylinder, J. Fluid Mech. 31 (1968) 815.

(12) Collins, W.M., Ph.D. Thesis, University of Western Ontario, London, Canada (1971).

(13) Dennis, S.C.R. and Staniforth, A.N., A Numerical Method for Calculating the Initial Flow Past a Cylinder in a Viscous Fluid, Lecture Notes in Physics, Springer-Verlag, 8 (1971) 343.

(14) Goldstein, S. (Ed.), Modern Developments in Fluid Dynamics, Clarendon Press, Oxford, (1938), Vol. I, p. 100.

(15) Dennis, S.C.R. and Chang, G.-Z., Numerical Integration of the Navier-Stokes Equations in Two-Dimensions, University of Wisconsin, MRC Summary Report No. 859 (1969).

(16) Chang, G.-Z., Ph.D. Thesis, University of Western Ontario, London, Canada (1969).

(17) Kawaguti, M. and Jain, P., Numerical Study of a Viscous Fluid Past a Circular Cylinder, University of Wisconsin, MRC Summary Report No. 590, (1965).

(18) Apelt, C.J., Aeronautical Research Council Reports and Memoranda No. 3175, London, (1961).

(19) Keller, H.B. and Takami, H., Numerical Solution of Non-Linear Differential Equations,(Ed., Greenspan, D.), John Wiley and Sons, New York, (1966) 115.

(20) Janssen, E., Flow Past a Flat Plate at Low Reynolds Numbers, J. Fluid Mech. 3 (1957) 329.

(21) Dennis, S.C.R. and Dunwoody, J., The Steady Flow of a Viscous Fluid Past a Flat Plate, J. Fluid Mech., 24 (1966) 577.

(22) Jeffreys, H. and Jeffreys, B.S., Methods of Mathematical Physics, 3rd ed. Cambridge University Press, (1962) 411.

(23) Schlichting, H., Boundary Layer Theory (6th ed.), McGraw-Hill, New York (1968).

(24) Wundt, H., Wachstum der Laminaren Grenzschicht an schräg Angeströmtem Zylindern bei An fahrt aus der Ruhe, Ing. Arch. 23 (1955) 212.

(25) Fox, L., The Numerical Solution of Two-Point Boundary Problems in Ordinary Differential Equations, Oxford (1957).

(26) Filon, L.N.G., On a Quadrature Formula for Trigonometric Integrals, Proc. Roy. Soc. Edin. 49 (1928) 38.

(27) Thom, A. and Apelt, C.J., Aeronautical Research Council Reports and Memoranda No. 3061, London (1958).

(28) Phillips, O.M., The Intensity of Aeolian Tones, J. Fluid Mech. 1 (1956) 607.

(29) Varga, R.S., Matrix Iterative Analysis, Prentice-Hall, London (1962).

(30) Rosser, J.B., The Direct Solution of Difference Analogs of Poisson's Equation, Technical Summary Report No. 797, Mathematics Research Center, Madison, Wisconsin (1967).

(31) SchWabe, M., Pressure Distribution in Non-uniform Two-Dimensional Flow, Ing. Arch. 6 (1935) 1; English Translation, NACA TM1039.

(32) Sarpkaya, T., Separate Flow about Lifting Bodies and Impulsive Flow about Cylinders, AIAA Journal 4 No. 3 (1966).

(33) Taneda, S., Honji, H., Unsteady Flow Past a Circular Cylinder, J. Phys. Soc. Japan, 27 (1969) 1668.

(34) Taneda, S., Honji, H., Unsteady Flow Past a Flat Plate Normal to the Direction of Motion, J. Phys. Soc. Japan, 30, (1971) 262.

(35) Honji, H., Report No. 65 of Research Institute for Applied Mechanics, Kyushu University, XIX (1972).

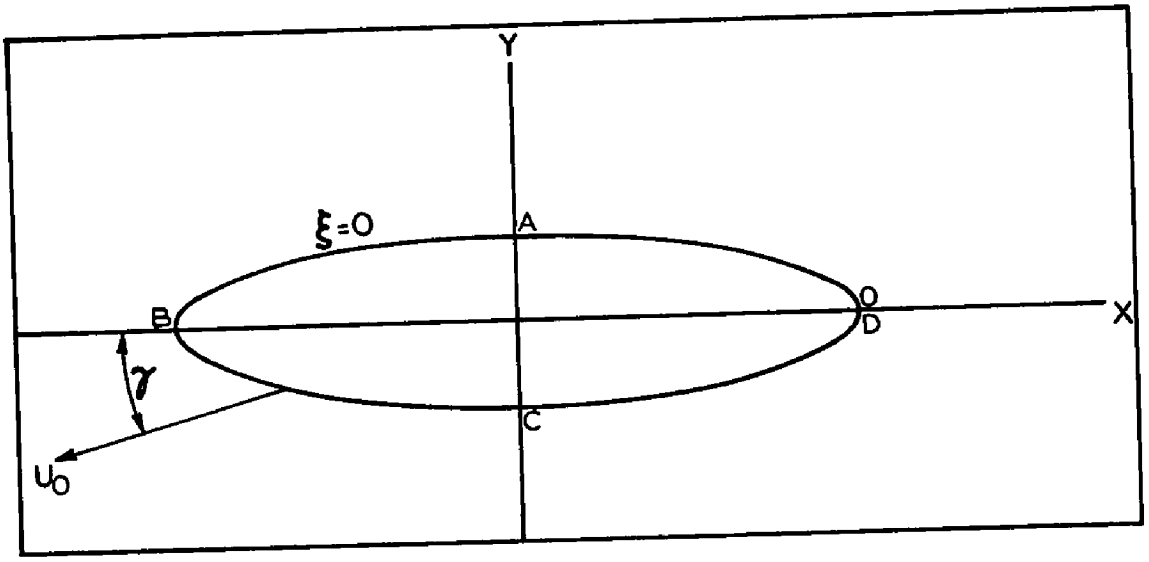

Fig. 1 Orientation of Cartesian Axes.

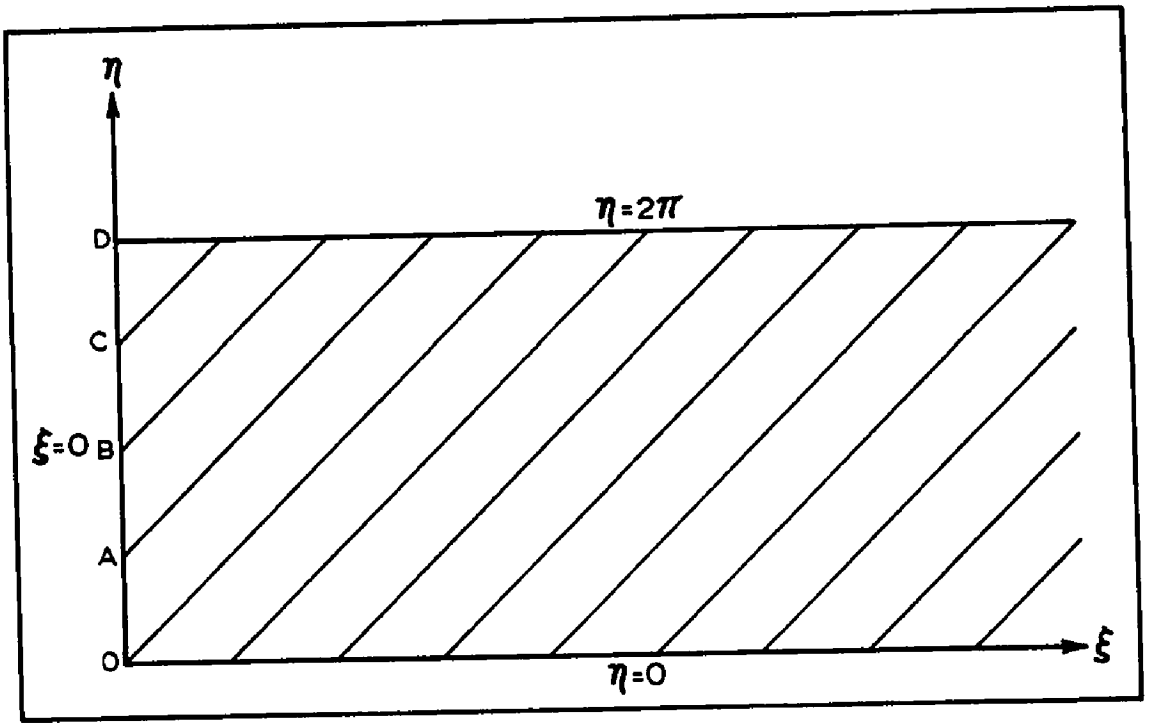

Fig. 2 Transformed Domain.

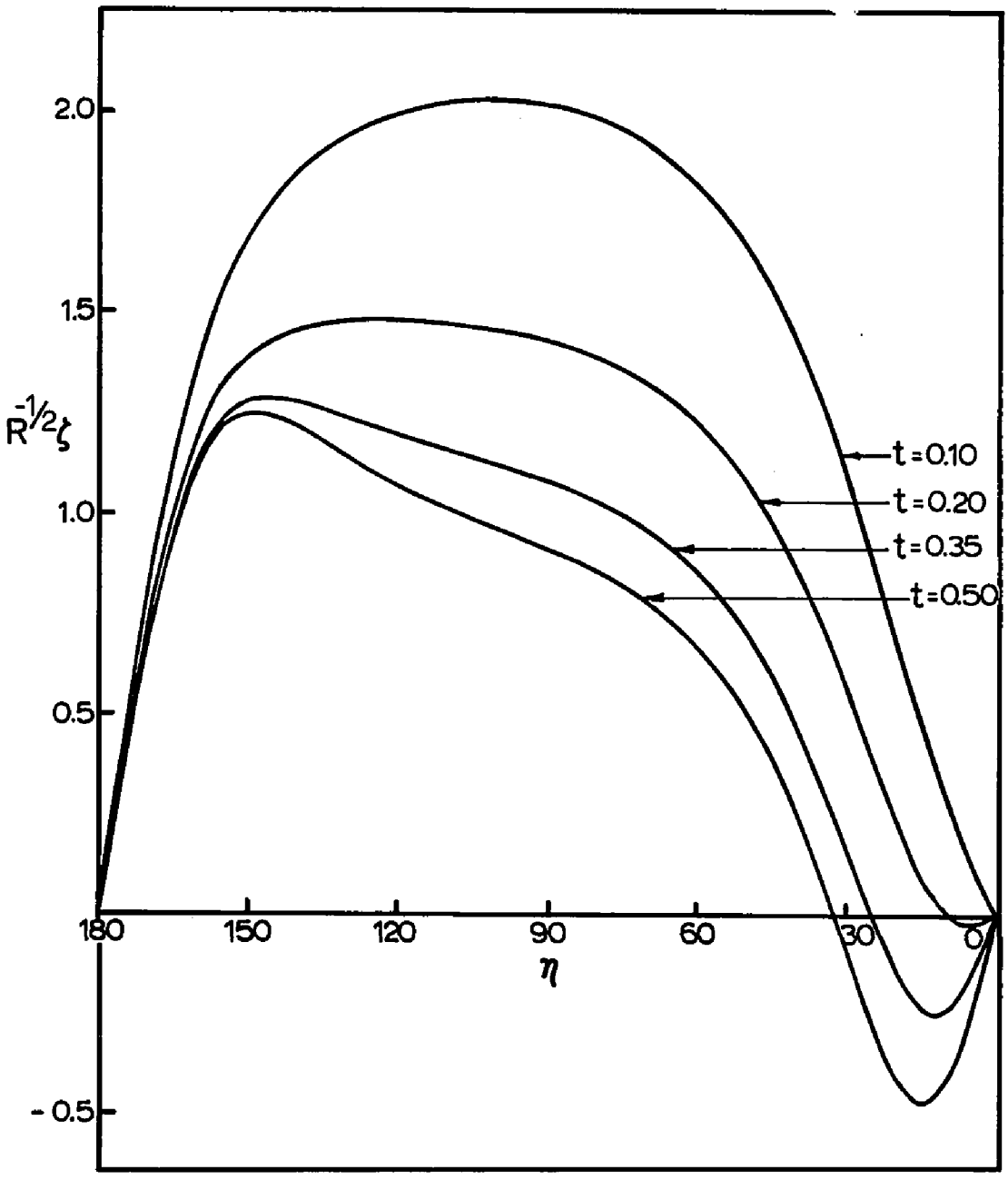

Fig. 3 $R^{-\frac{1}{2}}\zeta$ on the Surface of an Elliptic Cylinder of Aspect Ratio 0.6 at $\gamma=0°$, using the Time-Series to t^7 for the Boundary-Layer Case.

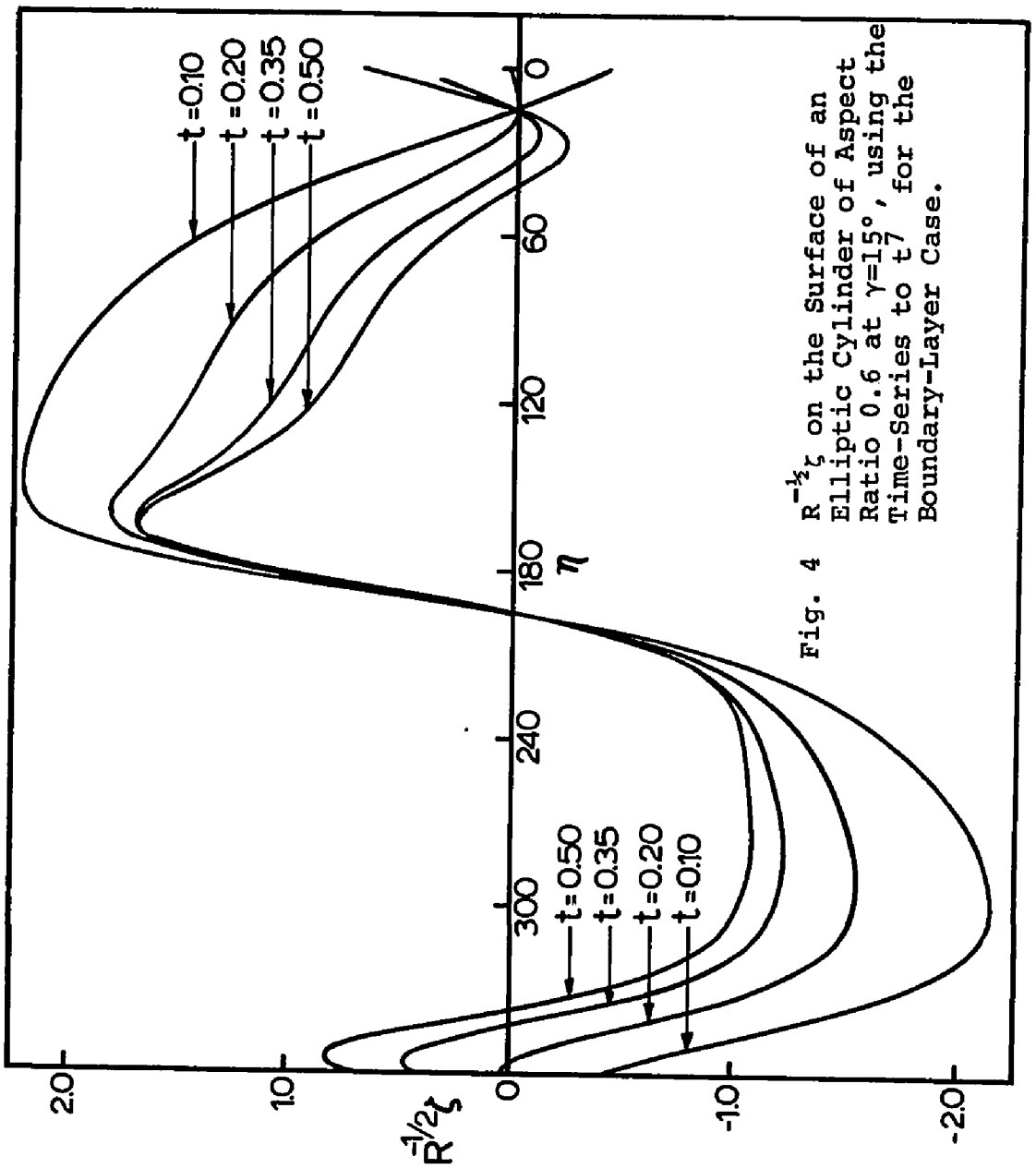

Fig. 4 $R^{-\frac{1}{2}}\zeta$ on the Surface of an Elliptic Cylinder of Aspect Ratio 0.6 at $\gamma=15°$, using the Time-Series to $t^{\frac{7}{2}}$ for the Boundary-Layer Case.

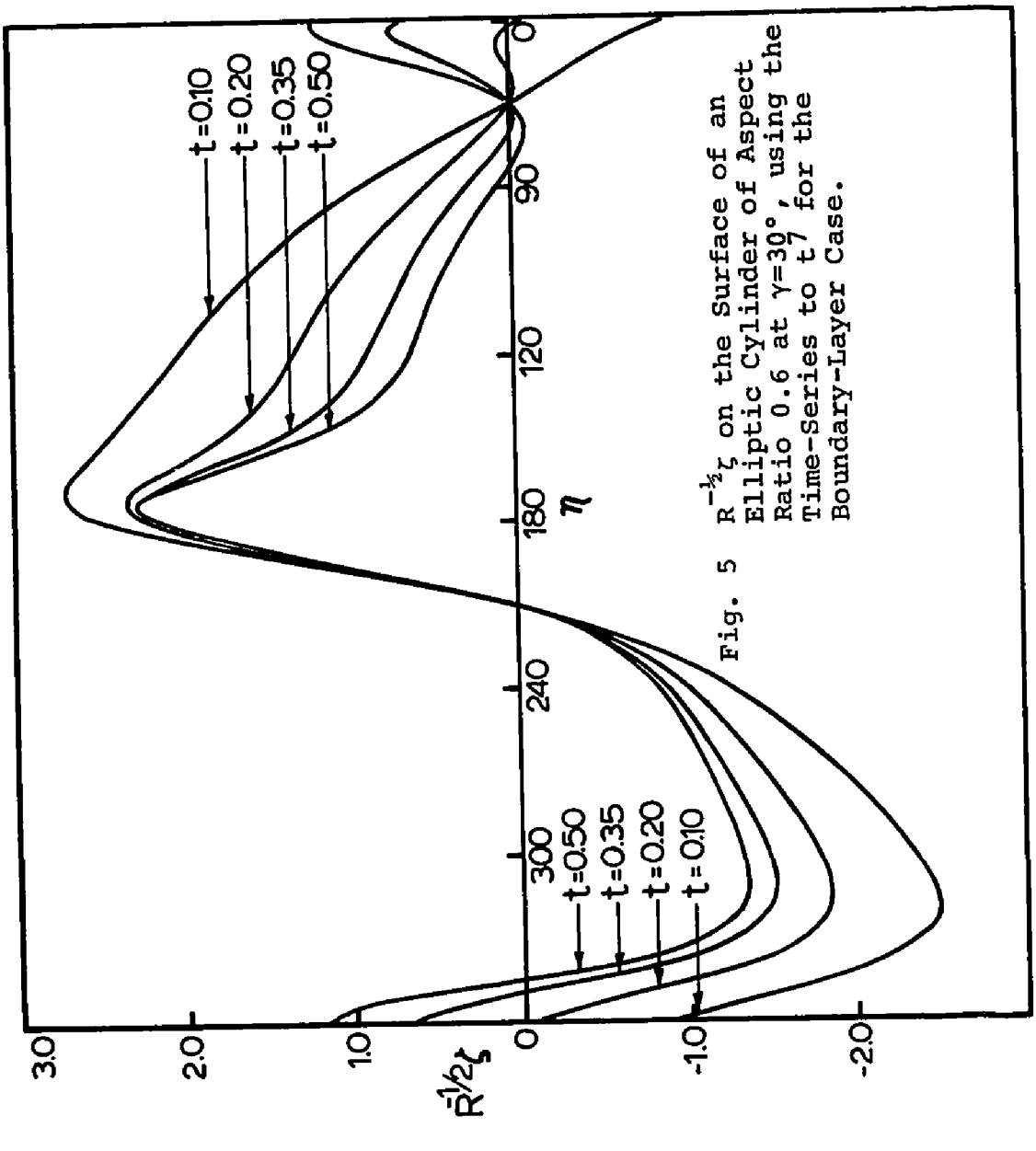

Fig. 5 $R^{-\frac{1}{2}}\zeta$ on the Surface of an Elliptic Cylinder of Aspect Ratio 0.6 at $\gamma=30°$, using the Time-Series to $t^{\frac{1}{7}}$ for the Boundary-Layer Case.

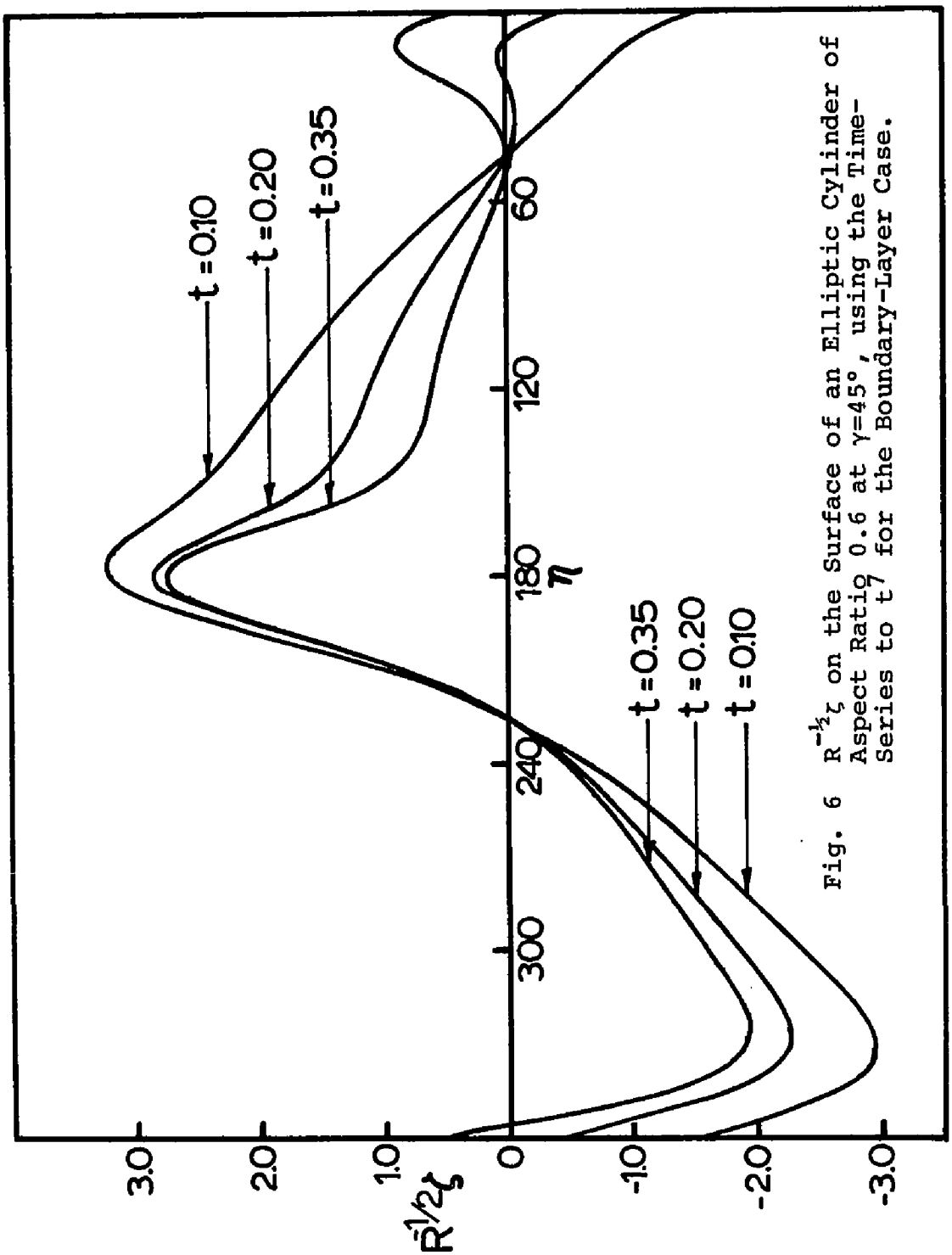

Fig. 6 $R^{-\frac{1}{2}}\zeta$ on the Surface of an Elliptic Cylinder of Aspect Ratio 0.6 at $\gamma=45°$, using the Time-Series to t^7 for the Boundary-Layer Case.

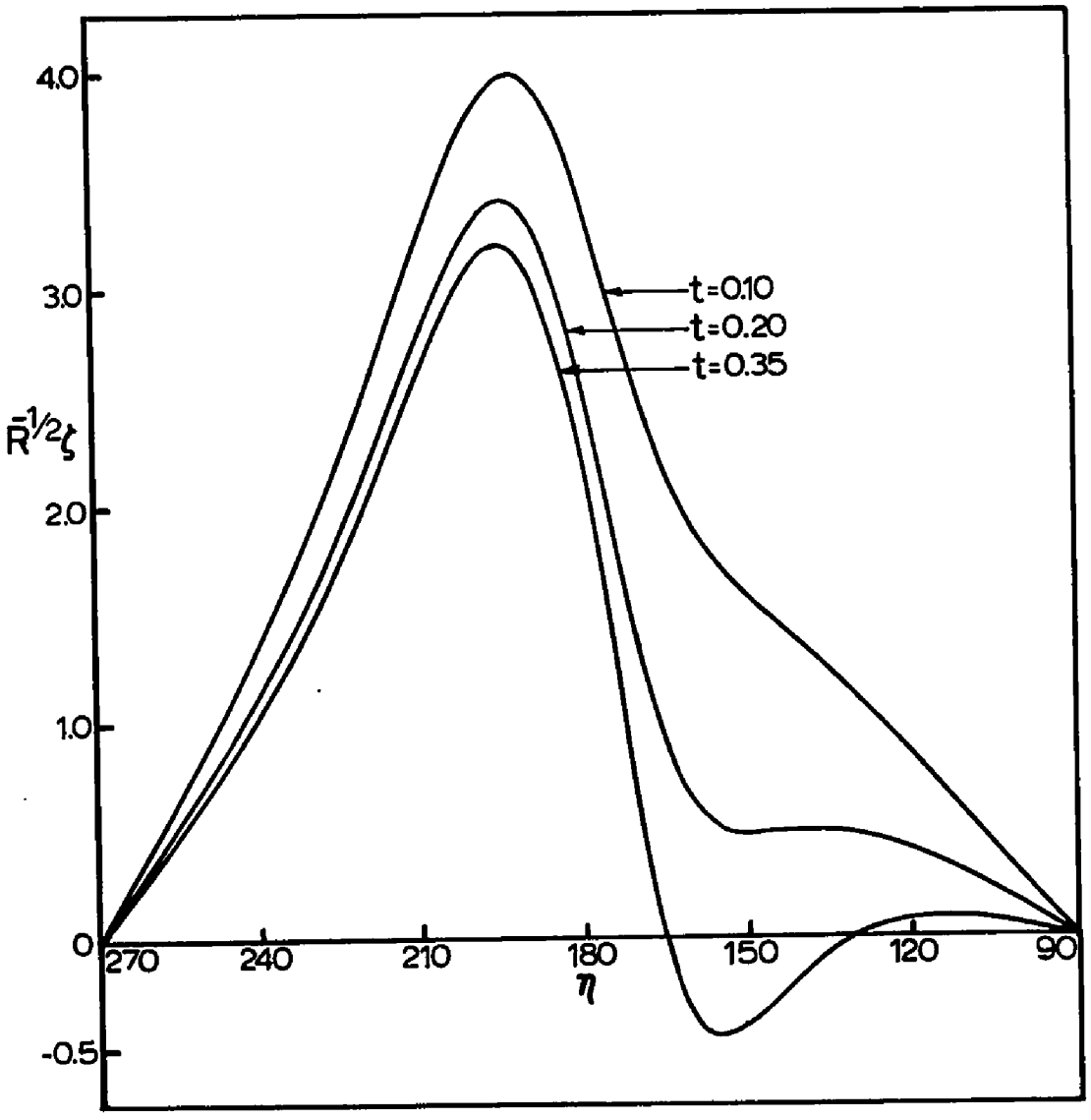

Fig. 7 $R^{-\frac{1}{2}}\zeta$ on the Surface of an Elliptic Cylinder of Aspect Ratio 0.6 at $\gamma=90°$, using the Time-Series to t^7 for the Boundary-Layer Case.

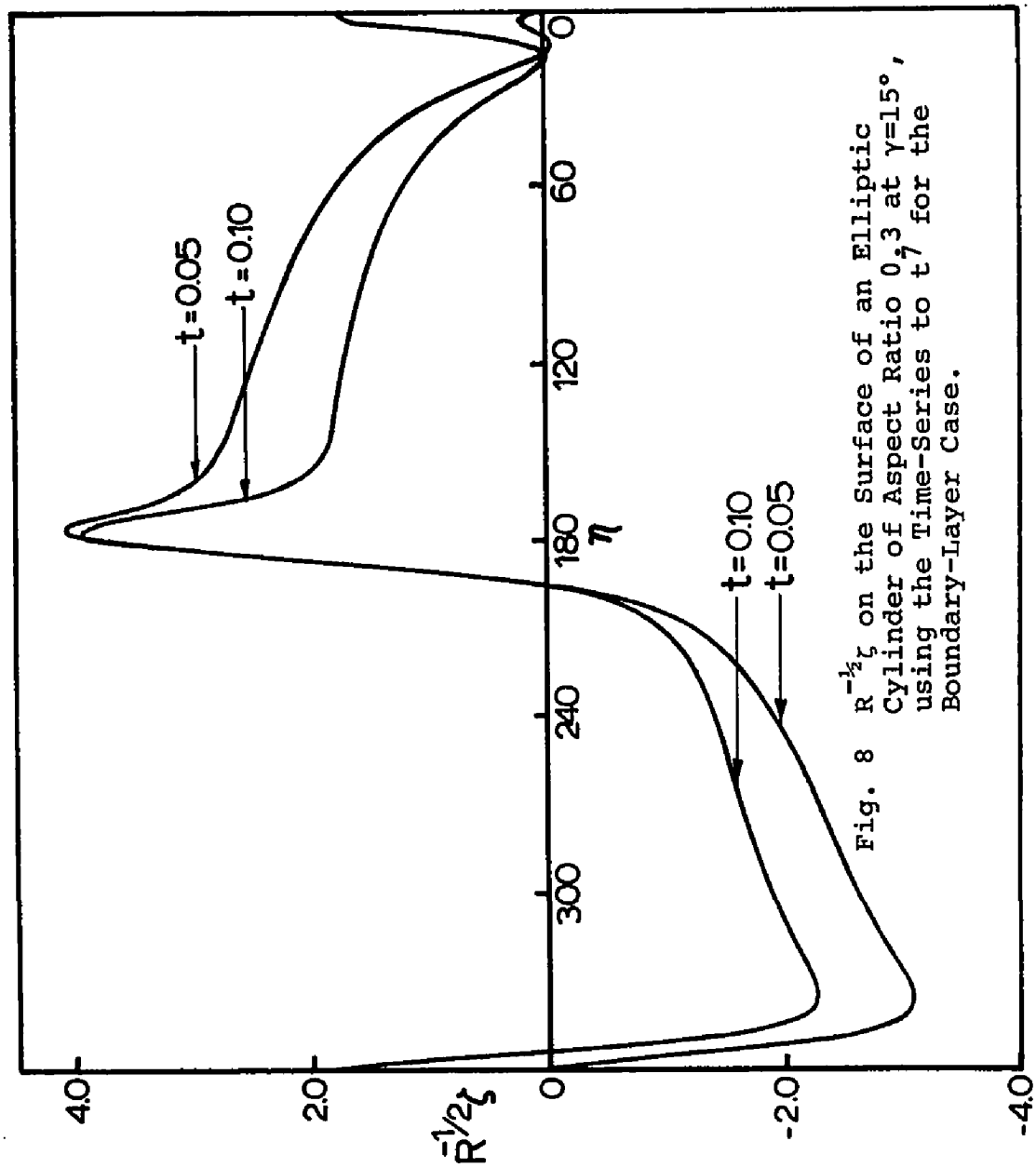

Fig. 8 $R^{-\frac{1}{2}}\zeta$ on the Surface of an Elliptic Cylinder of Aspect Ratio 0.3^3 at $\gamma=15°$, using the Time-Series to t^7 for the Boundary-Layer Case.

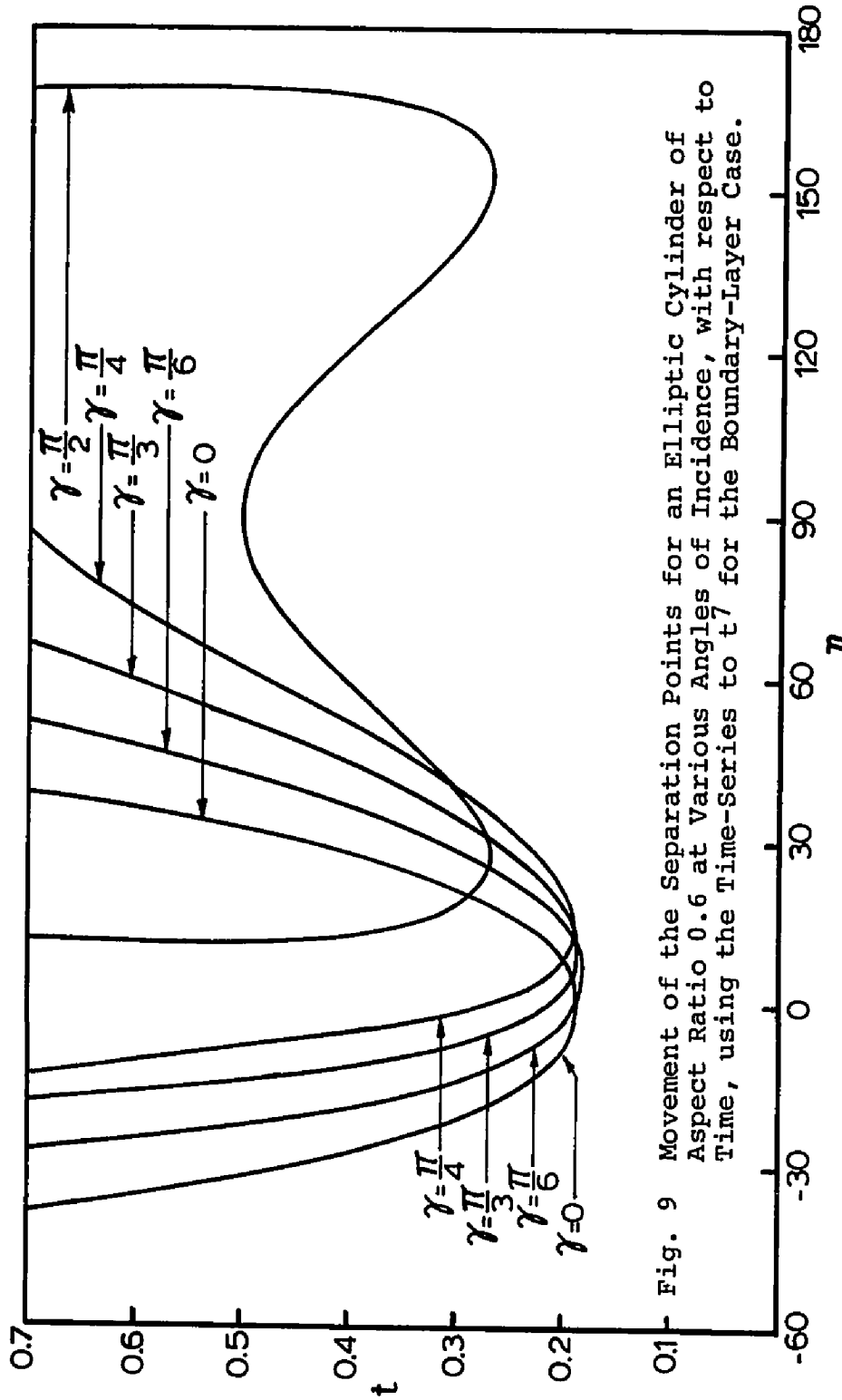

Fig. 9 Movement of the Separation Points for an Elliptic Cylinder of Aspect Ratio 0.6 at Various Angles of Incidence, with respect to Time, using the Time-Series to t^7 for the Boundary-Layer Case.

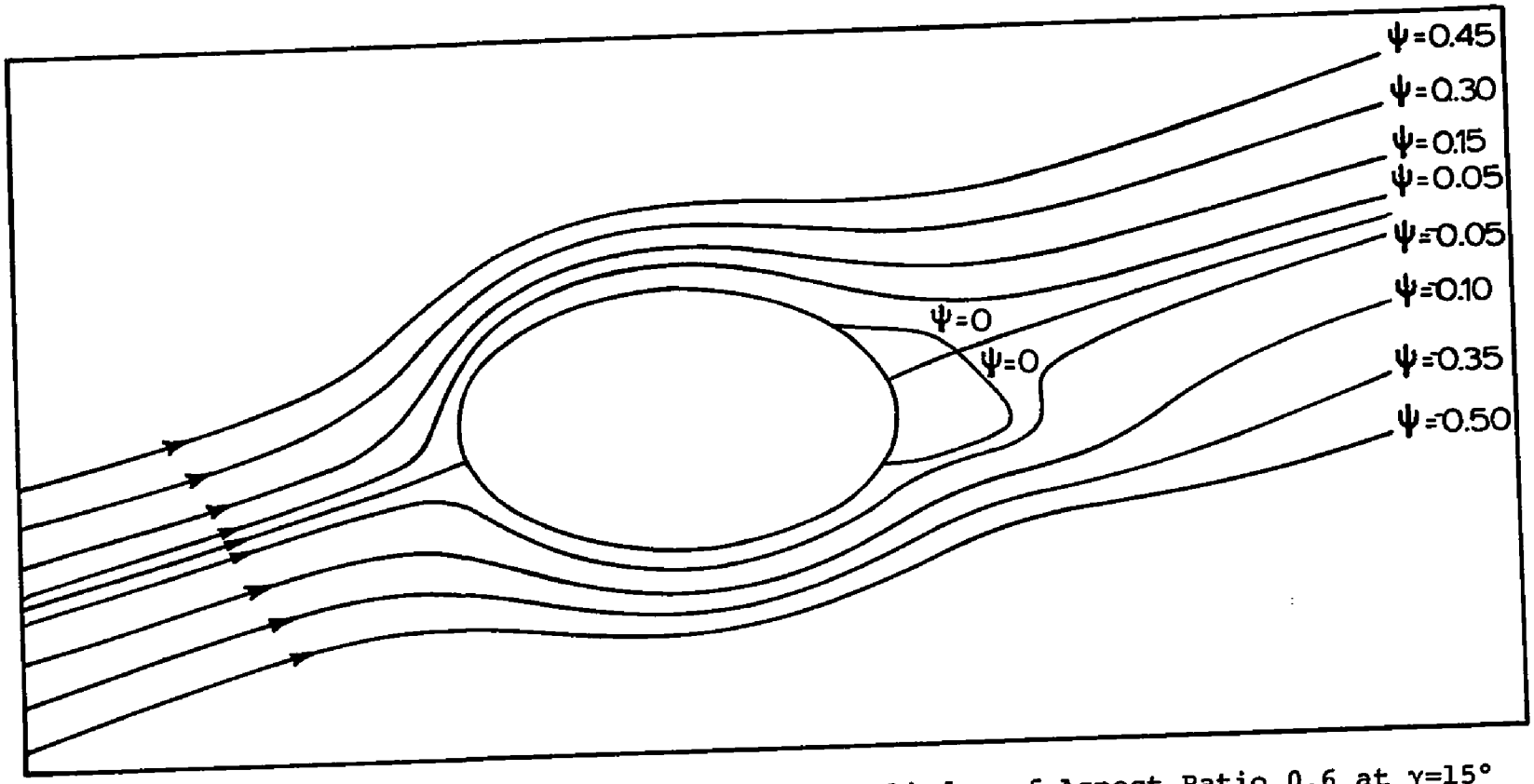

Fig. 10 Streamlines at t=0.5 for an Elliptic Cylinder of Aspect Ratio 0.6 at γ=15° as calculated from the Boundary-Layer Time Series to t^7 in k^0 with R set at 100.

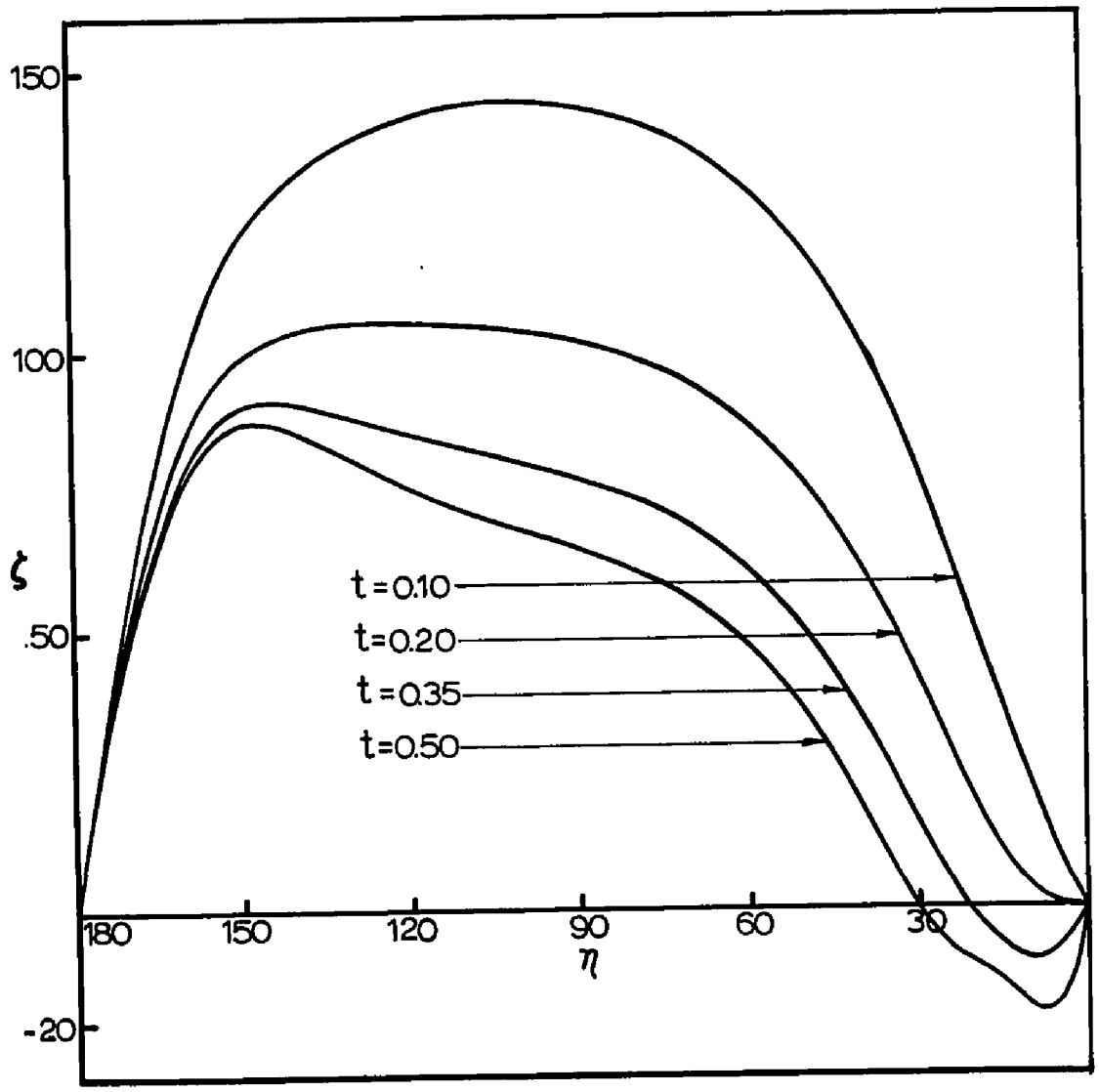

Fig. 11 ζ on the Surface of an Elliptic Cylinder of Aspect Ratio 0.6 at $\gamma=0°$ for R=5000 using the Time-Series to t^7 in k^0, t^5 in k^1 and t^0 in k^2.

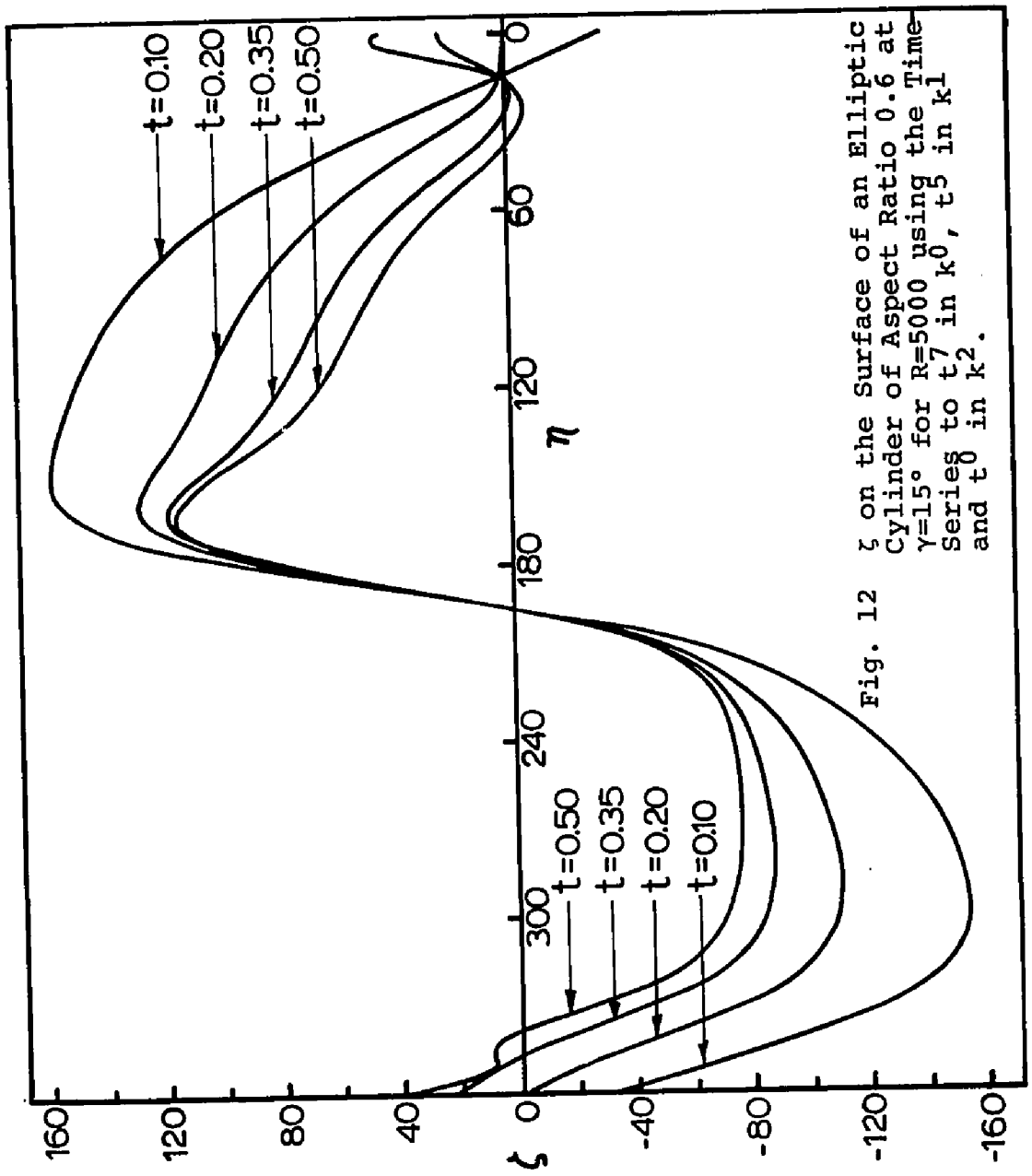

Fig. 12 ζ on the Surface of an Elliptic Cylinder of Aspect Ratio 0.6 at γ=15° for R=5000 using the Time Series to t^7 in k^0, t^5 in k^1 and t^0 in k^2.

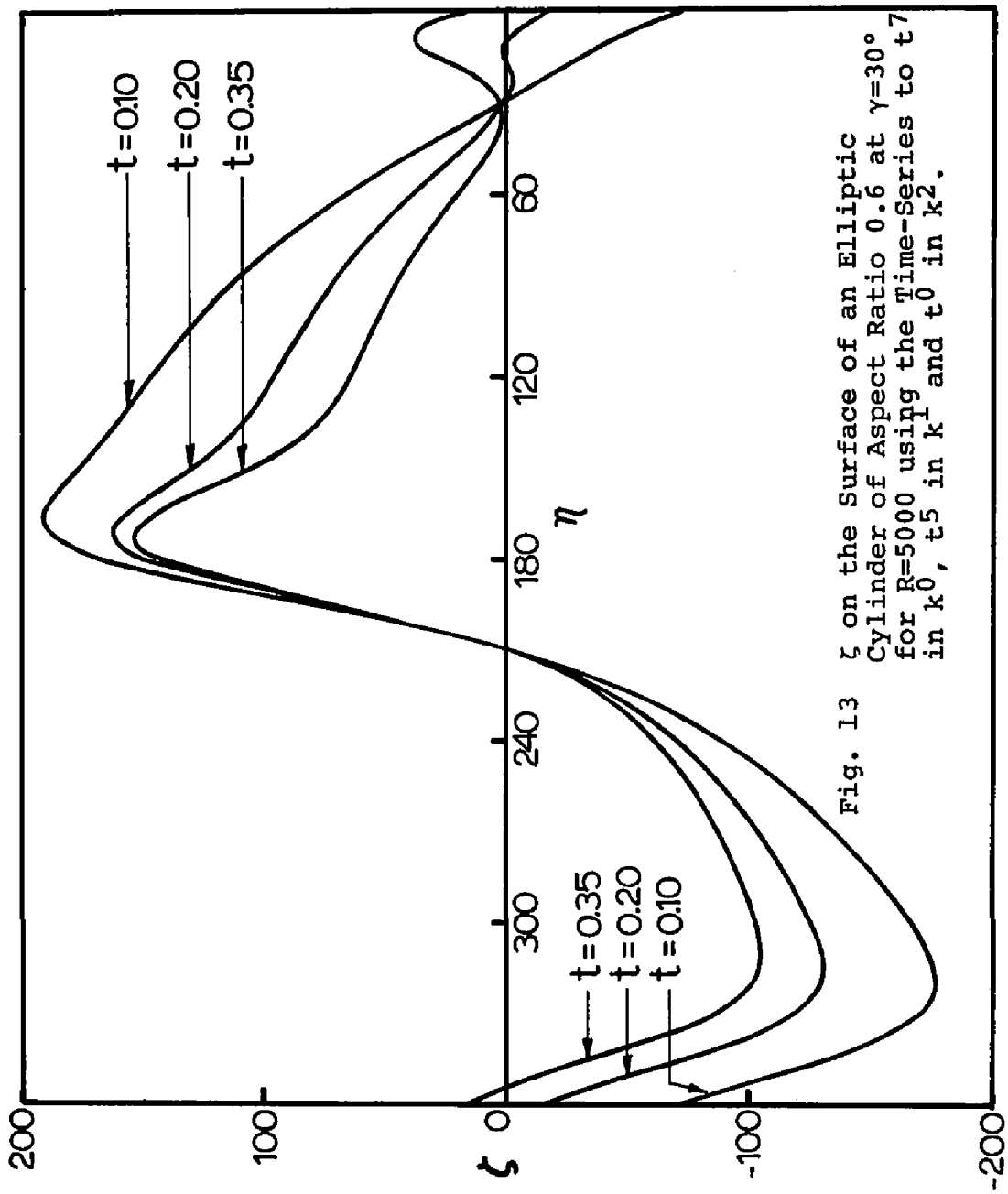

Fig. 13 ζ on the Surface of an Elliptic Cylinder of Aspect Ratio 0.6 at γ=30° for R=5000 using the Time-Series to t^7 in k^0, t5 in k^1 and t^0 in k^2.

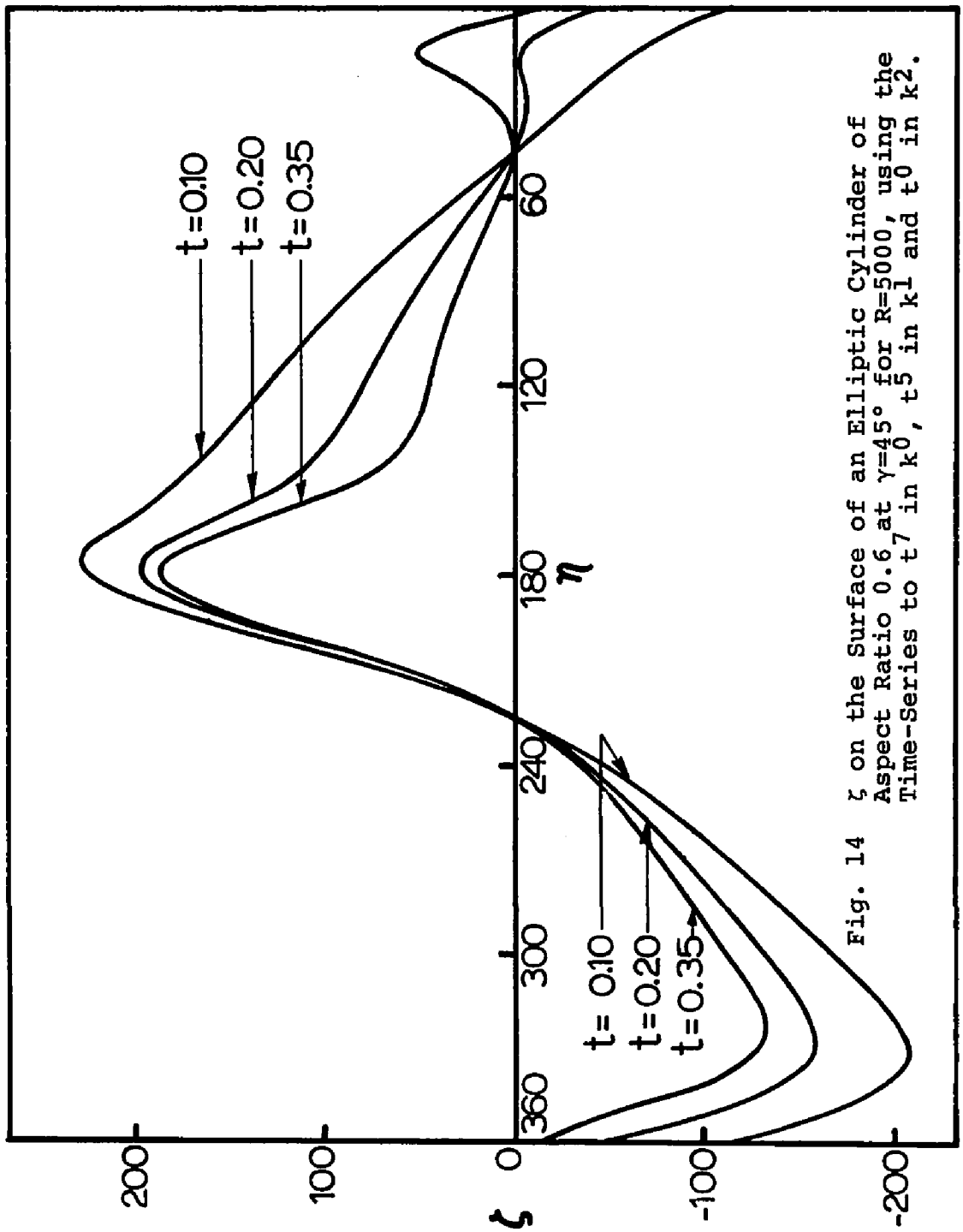

Fig. 14 ζ on the Surface of an Elliptic Cylinder of Aspect Ratio 0.6 at γ=45° for R=5000, using the Time-Series to t^7 in k^0, t^5 in k^1 and t^0 in k^2.

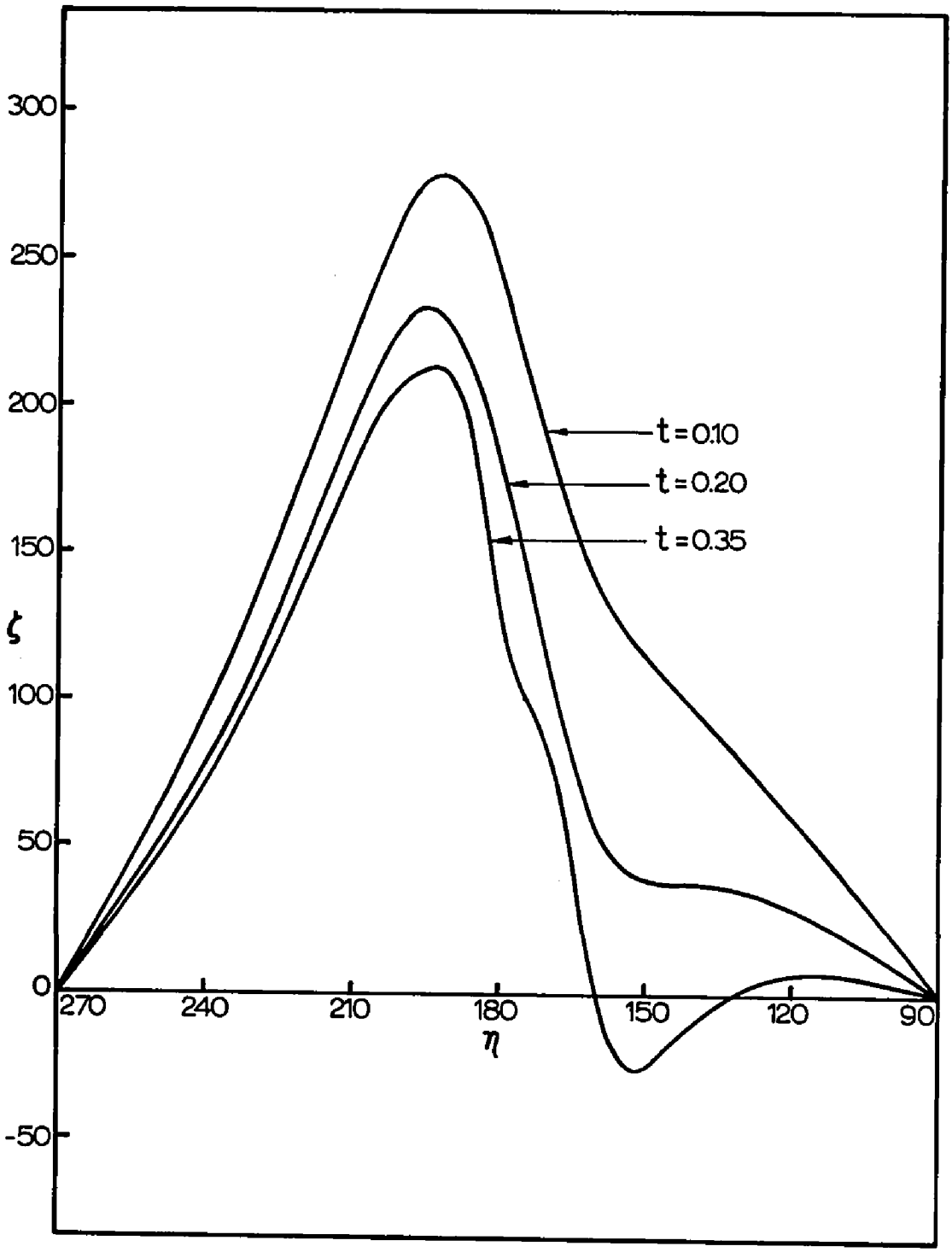

Fig. 15 ζ on the Surface of an Elliptic Cylinder of Aspect Ratio 0.6 at $\gamma=90°$ for R=5000, using the Time-Series to t^7 in k^0, t^5 in k^1 and t^0 in k^2.

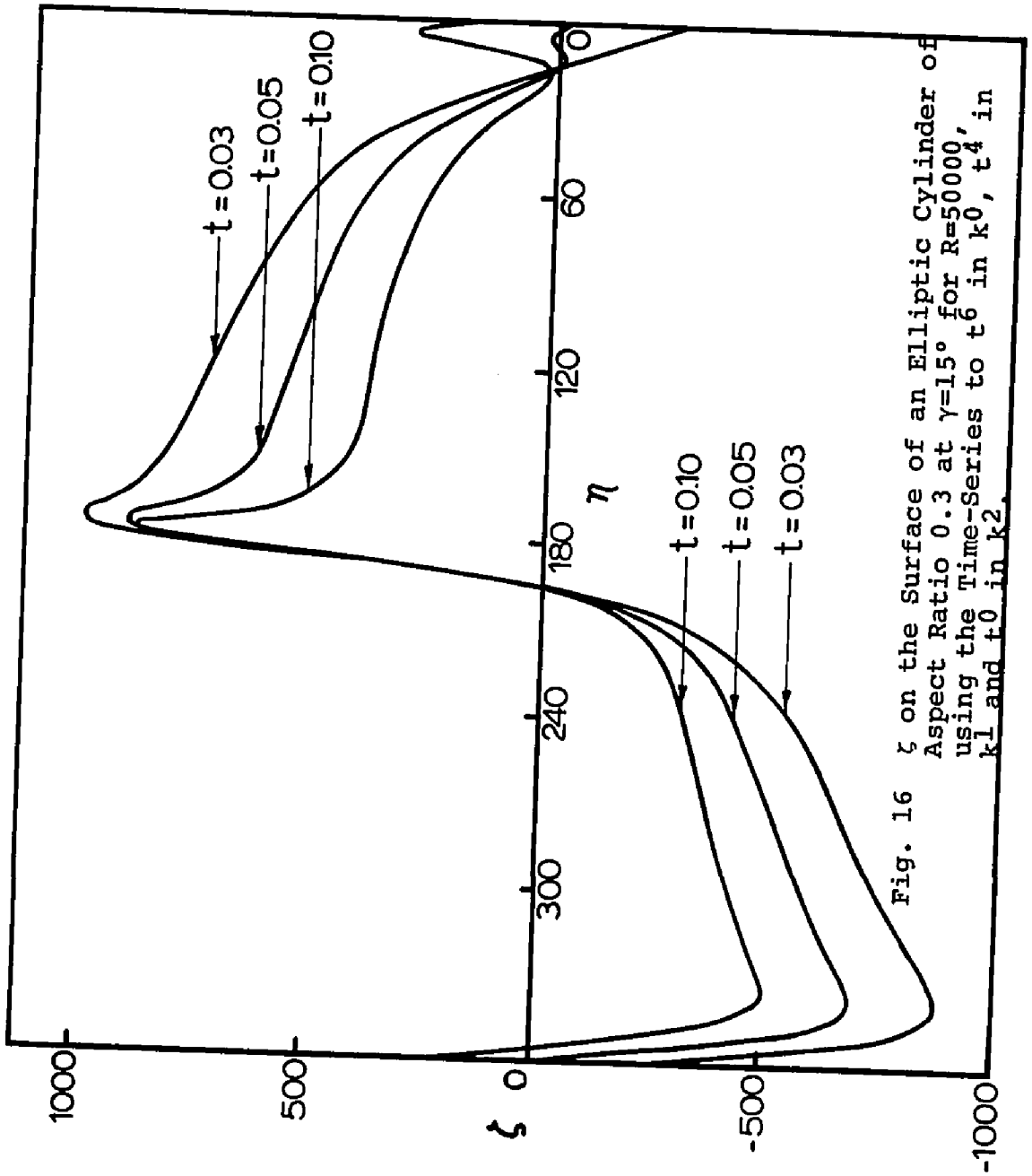

Fig. 16 ζ on the Surface of an Elliptic Cylinder of Aspect Ratio 0.3 at γ=15° for R=50000, using the Time-Series to t^6 in k^0, t^4 in k1 and t0 in k2.

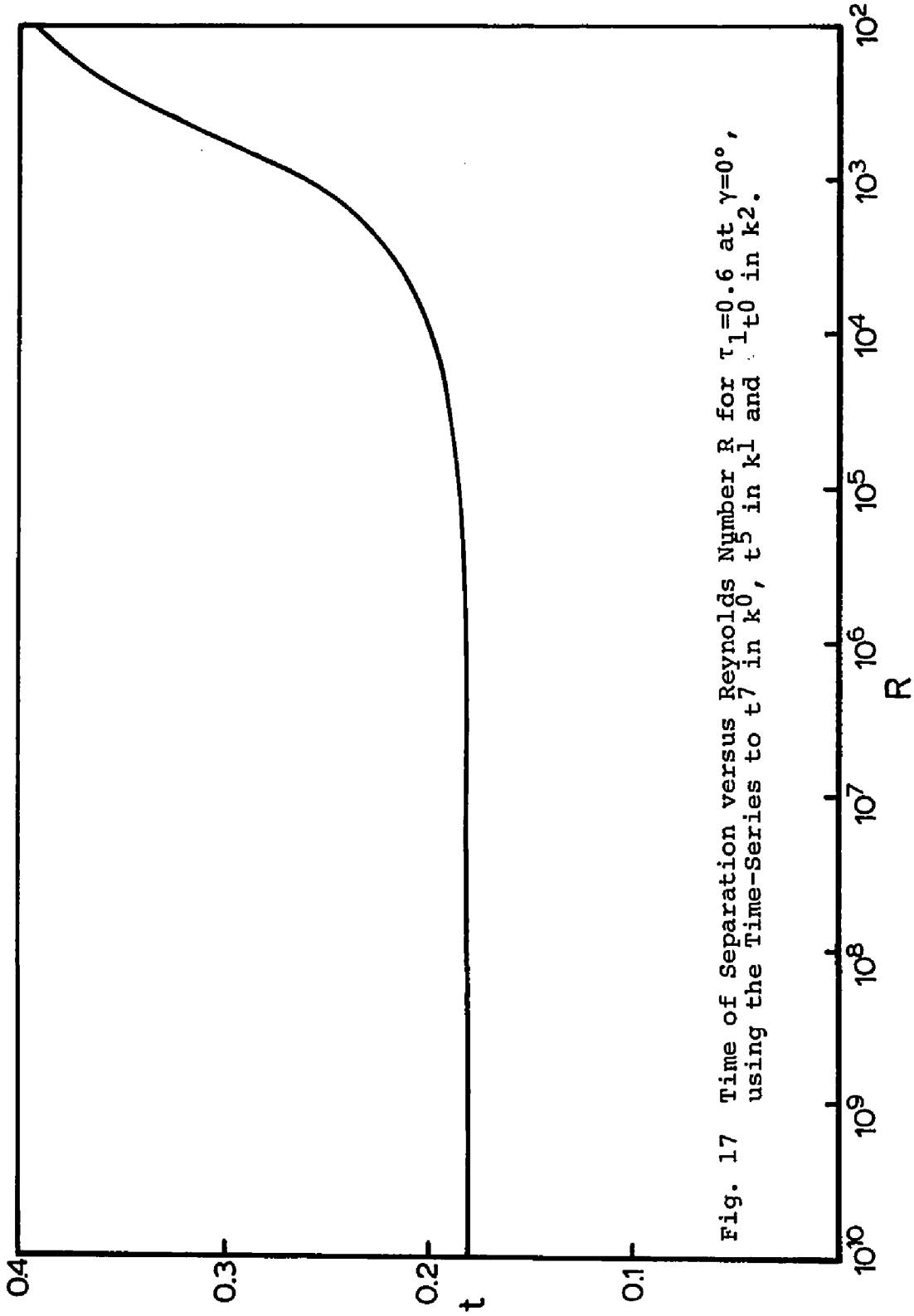

Fig. 17 Time of Separation versus Reynolds Number R for τ_1=0.6 at γ=0°, using the Time-Series to t^7 in k^0, t^5 in k^1 and t^0 in k^2.

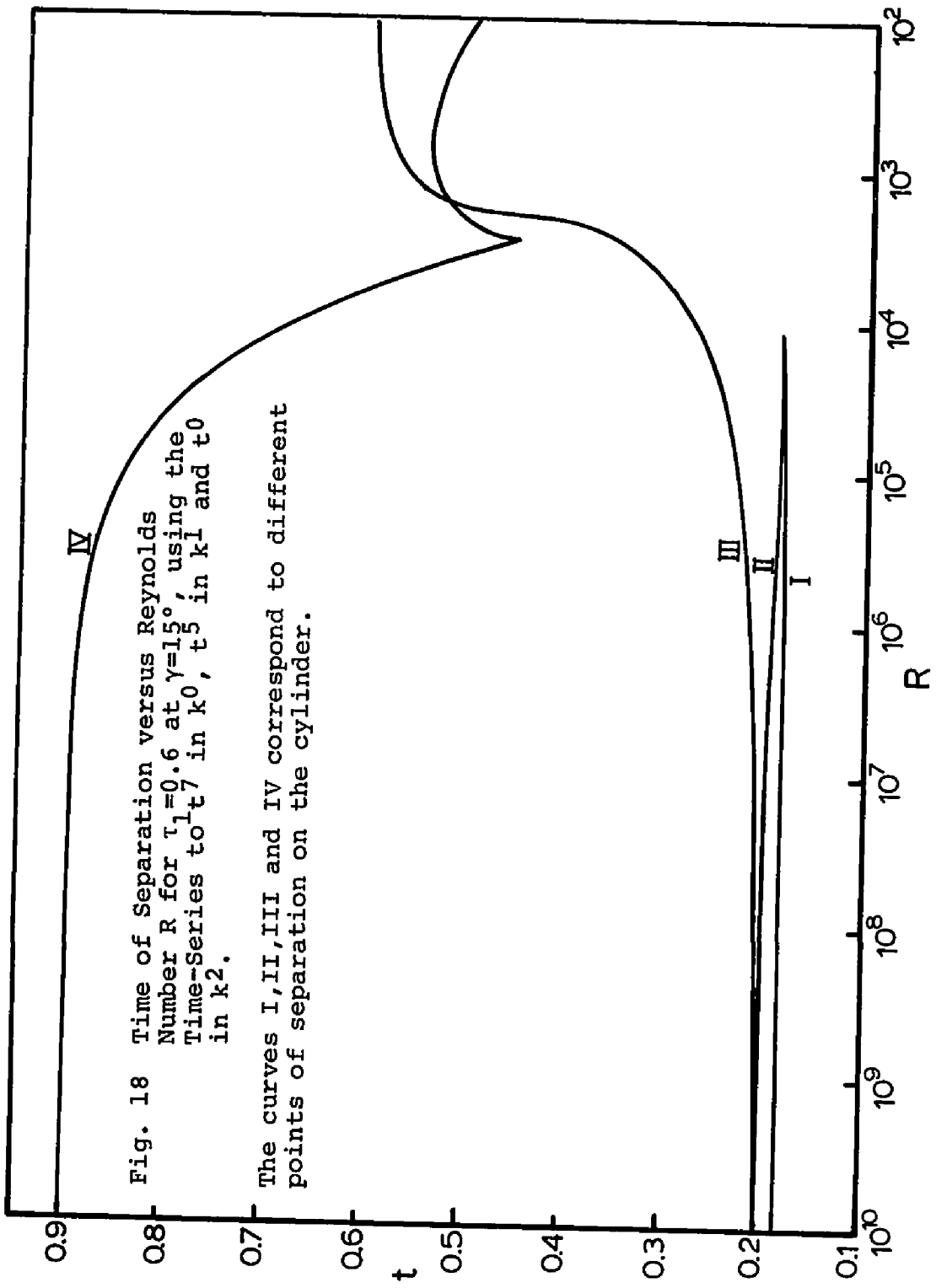

Fig. 18 Time of Separation versus Reynolds Number R for τ_1=0.6 at γ=15°, using the Time-Series t_o-t^7 in k^0, t^5 in k^1 and t^0 in k^2.

The curves I,II,III and IV correspond to different points of separation on the cylinder.

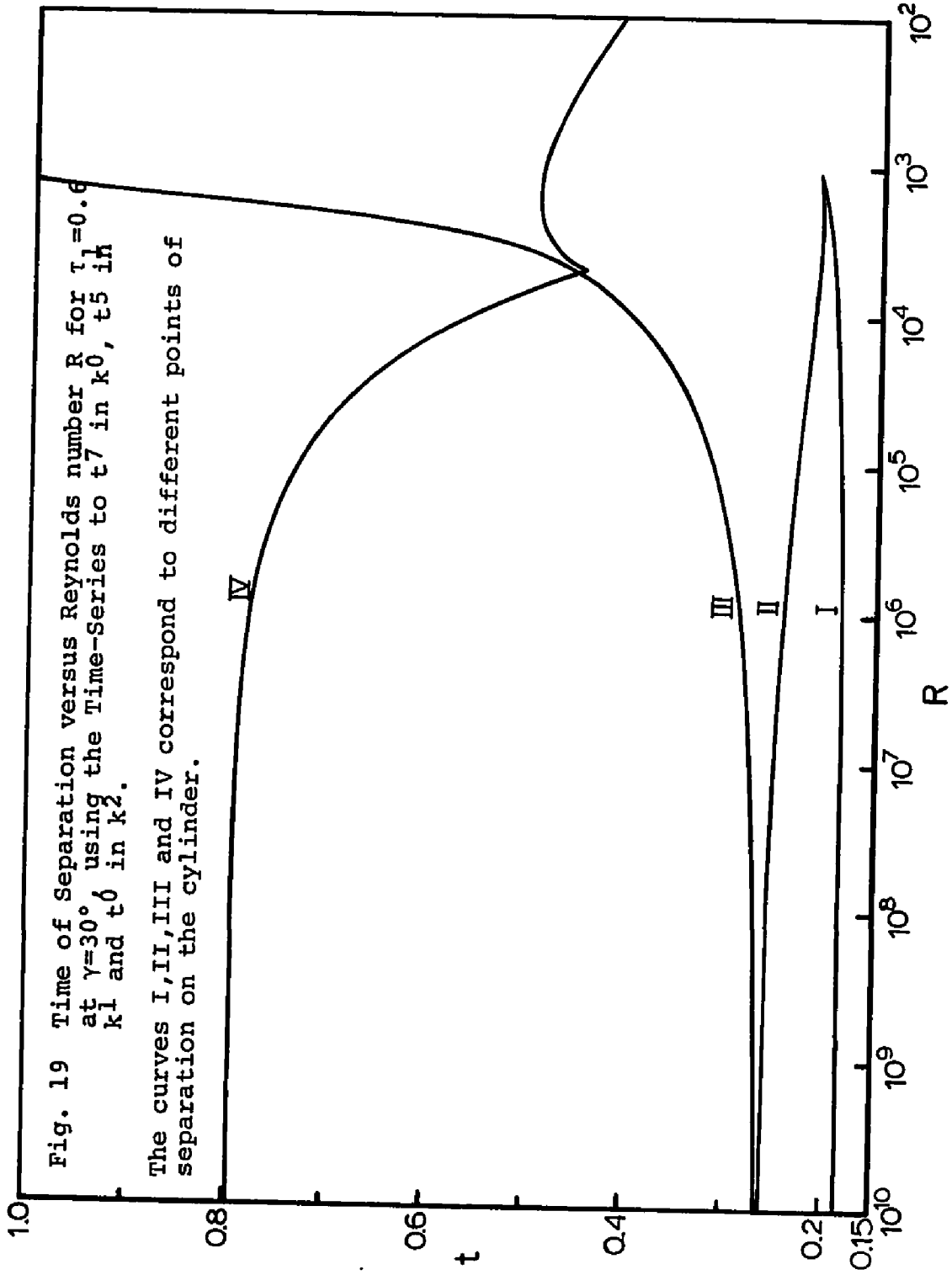

Fig. 19 Time of Separation versus Reynolds number R for $T_1=0.6$ at $\gamma=30°$ using the Time-Series to t7 in $k\overset{0}{,}$ t5 in $k\overset{1}{,}$ and $t\overset{0}{,}$ in $k\overset{2}{,}$.

The curves I,II,III and IV correspond to different points of separation on the cylinder.

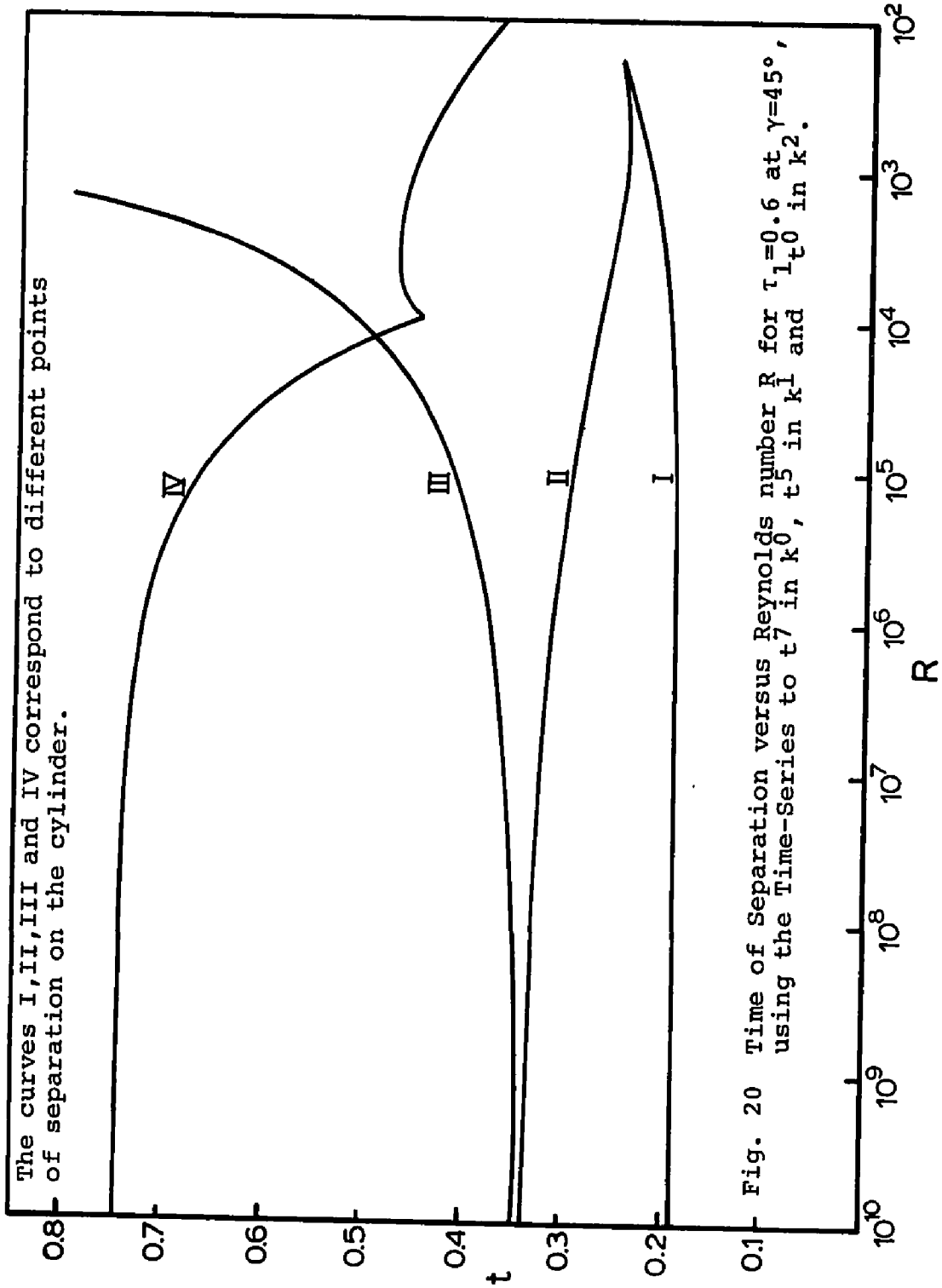

Fig. 20 Time of Separation versus Reynolds number R for τ_1=0.6 at γ=45°, using the Time-Series to t^7 in k^0, t^5 in k^1 and t^0 in k^2.

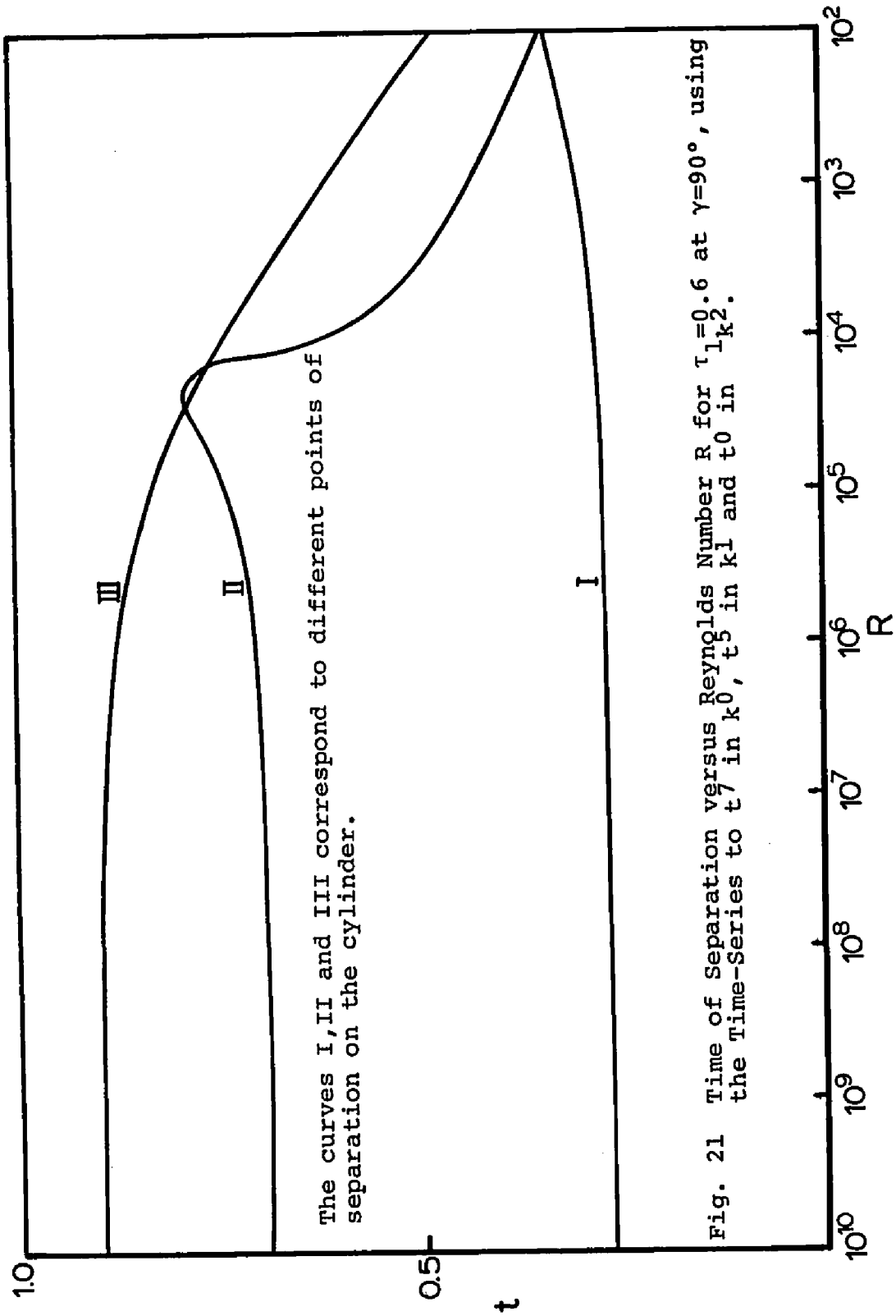

Fig. 21 Time of Separation versus Reynolds Number R for $\tau_1=0.6$ at $\gamma=90°$, using the Time-Series to t^7 in k^0, t^5 in k^1 and t^0 in k^2.

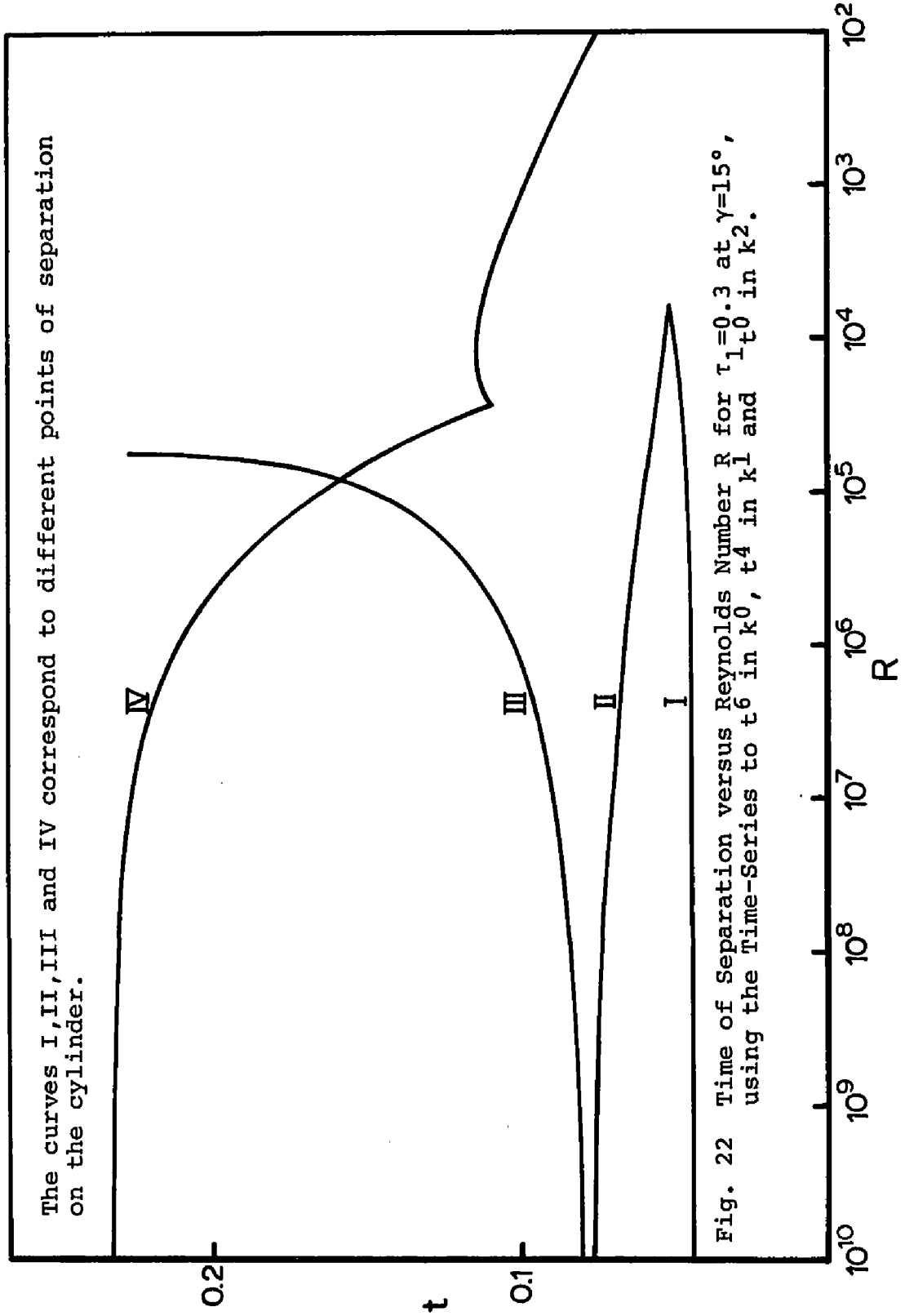

Fig. 22 Time of Separation versus Reynolds Number R for $\tau_1=0.3$ at $\gamma=15°$, using the Time-Series to t^6 in k^0, t^4 in k^1 and $_1t^0$ in k^2.

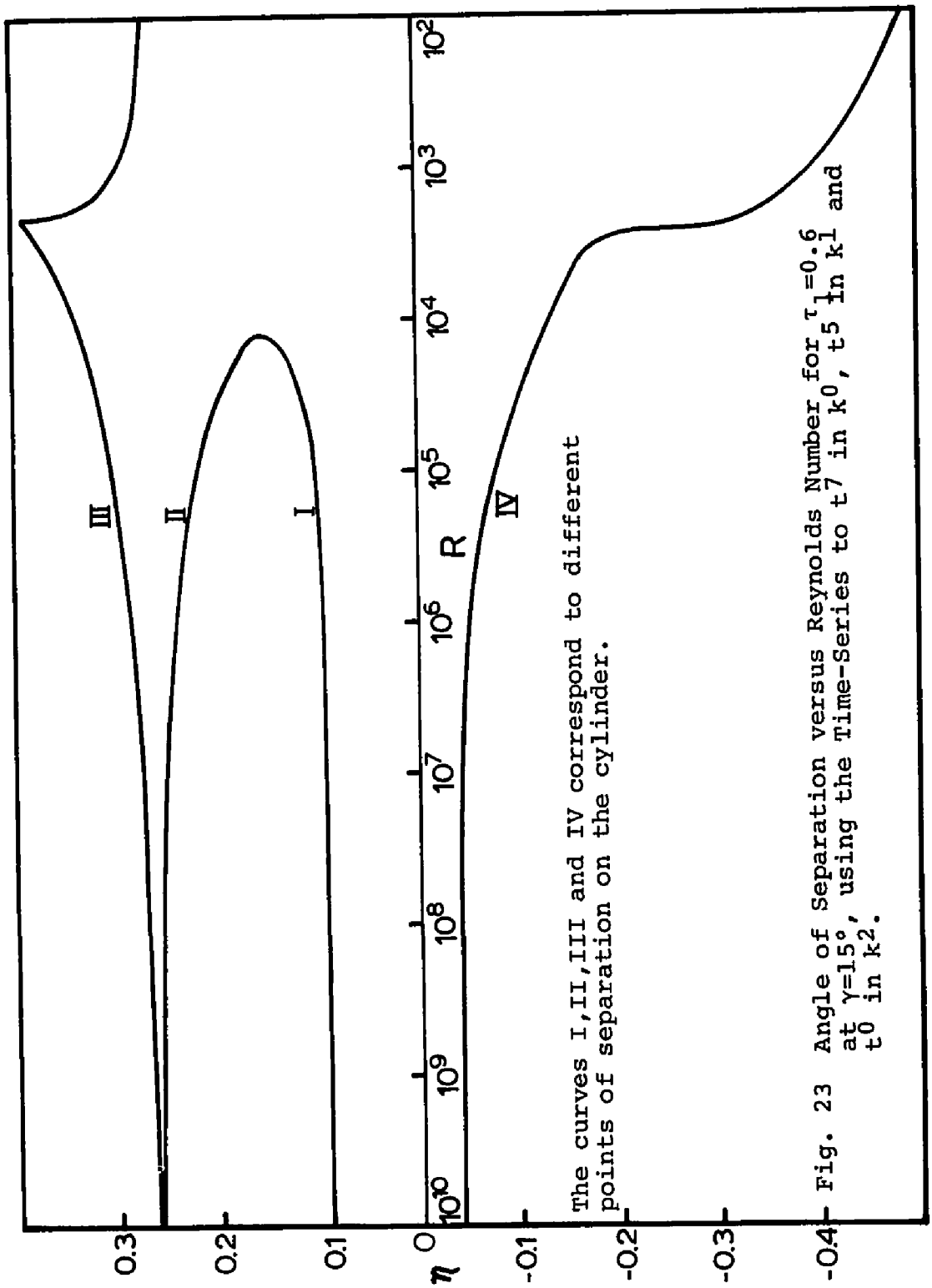

Fig. 23 Angle of Separation versus Reynolds Number for τ_1=0.6 at γ=15°, using the Time-Series to t^7 in k^0, t^5 in k^1 and t^0 in k^2.

The curves I,II,III and IV correspond to different points of separation on the cylinder.

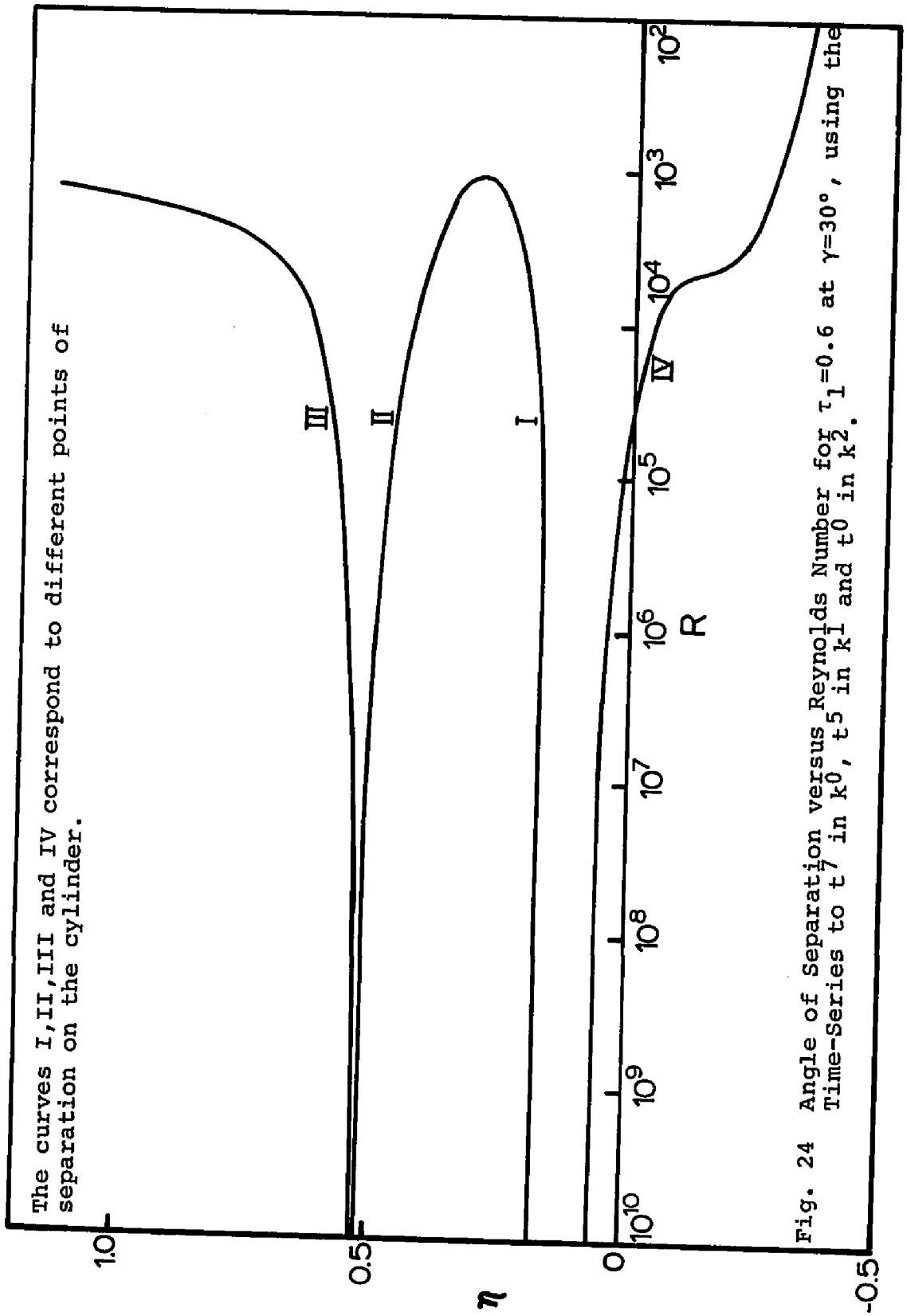

Fig. 24 Angle of Separation versus Reynolds Number for $\tau_1=0.6$ at $\gamma=30°$, using the Time-Series to t^7 in k^0, t^5 in k^1 and t^0 in k^2.

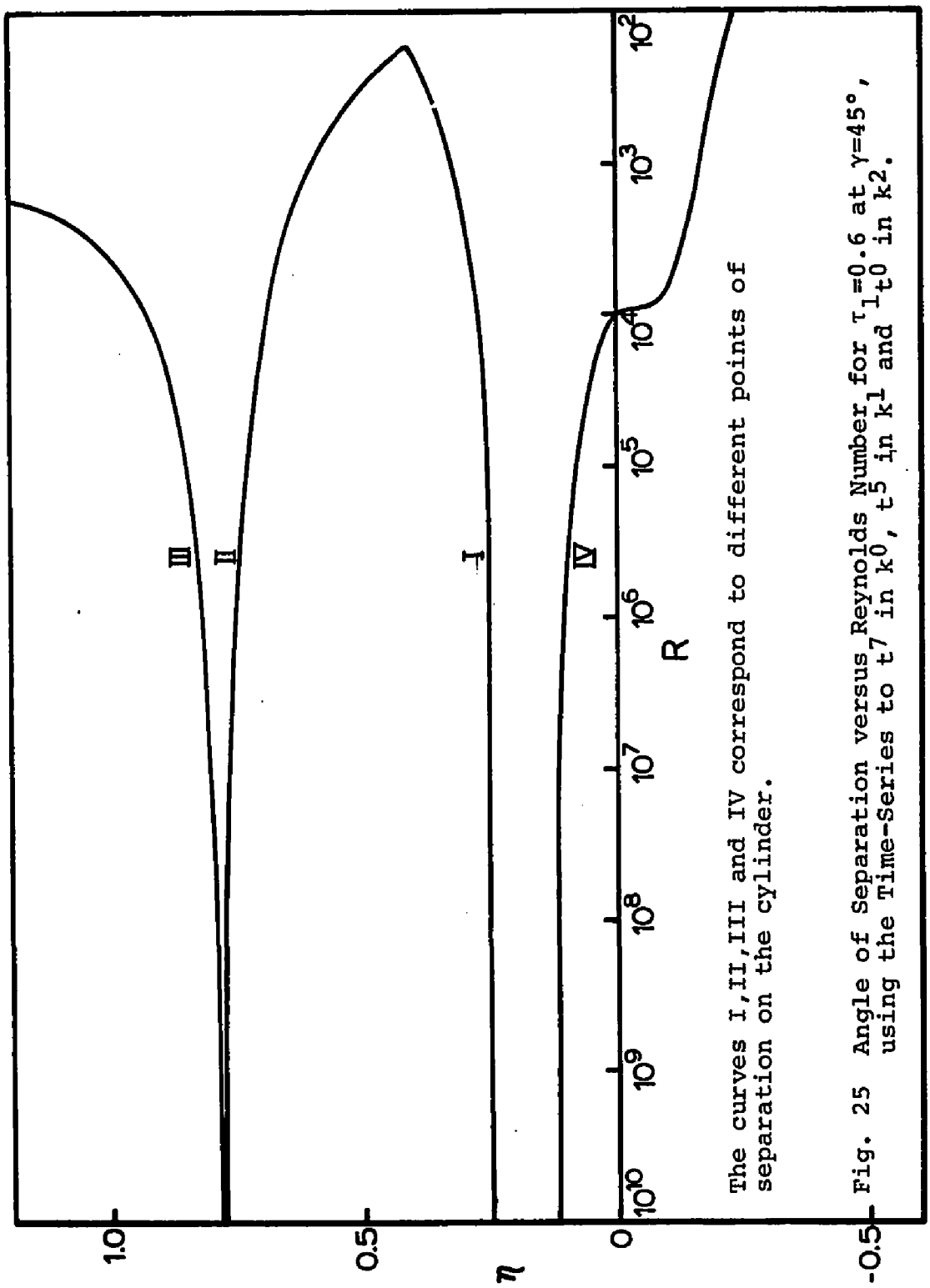

Fig. 25 Angle of Separation versus Reynolds Number for τ_1=0.6 at γ=45°, using the Time-Series to t^7 in k^0, t^5 in k^1 and t^0 in k^2.

The curves I,II,III and IV correspond to different points of separation on the cylinder.

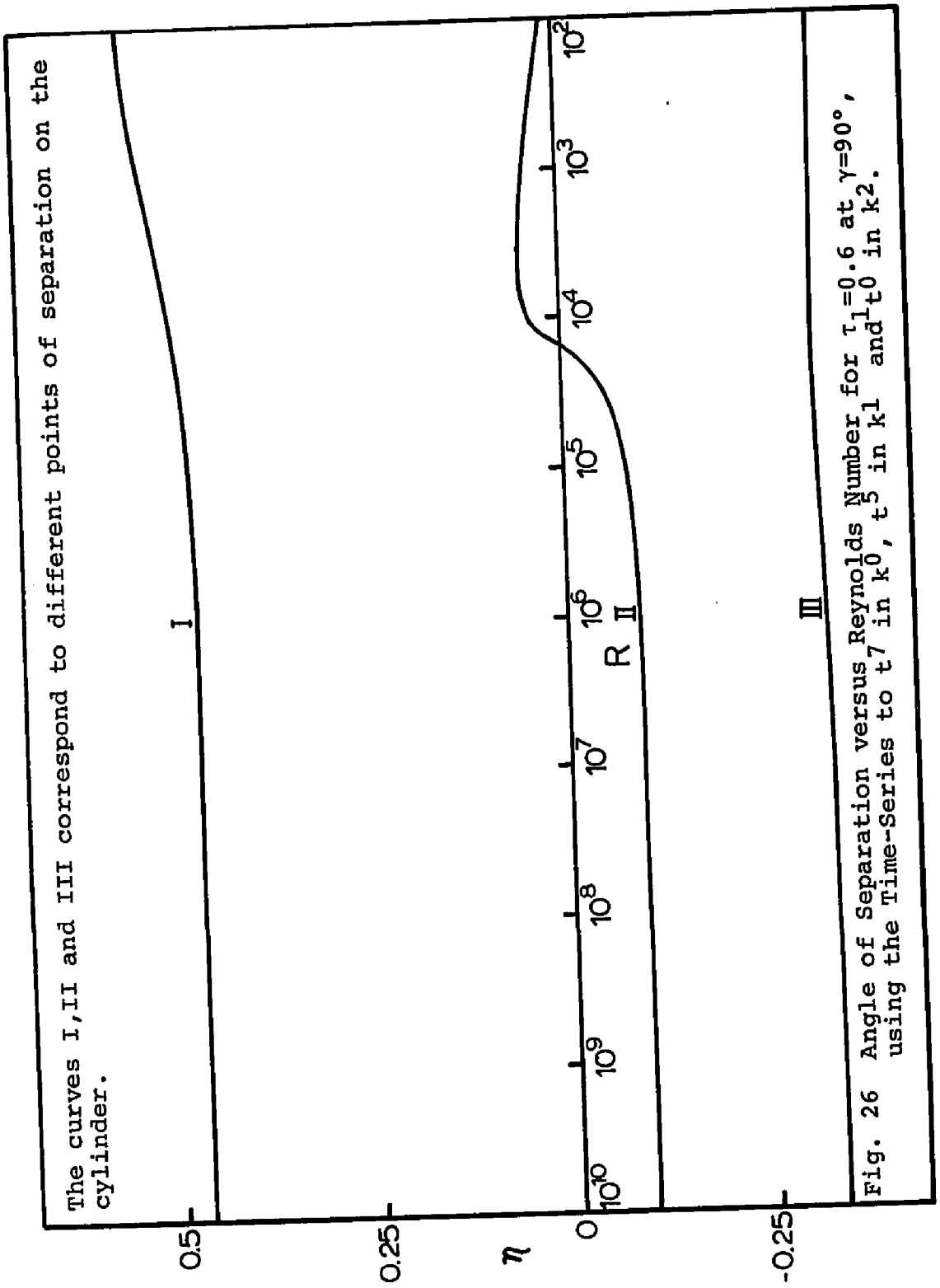

Fig. 26 Angle of Separation versus Reynolds Number for τ_1=0.6 at γ=90°, using the Time-Series to t^7 in k^0, t^5 in k^1 and $^1t^0$ in k^2.

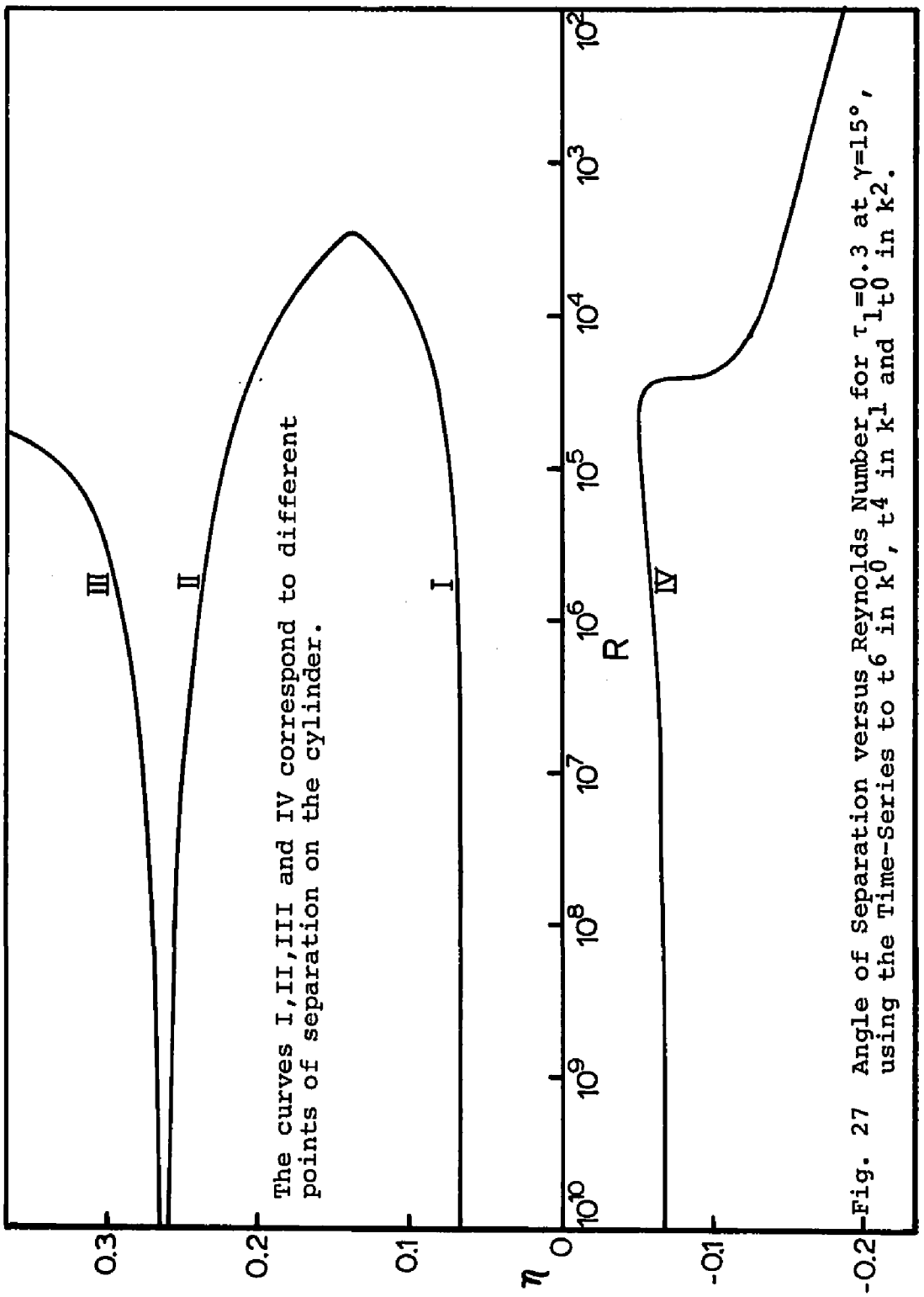

Fig. 27 Angle of Separation versus Reynolds Number for τ_1=0.3 at γ=15°, using the Time-Series to t^6 in k^0, t^4 in k^1 and $^1t^0$ in k^2.

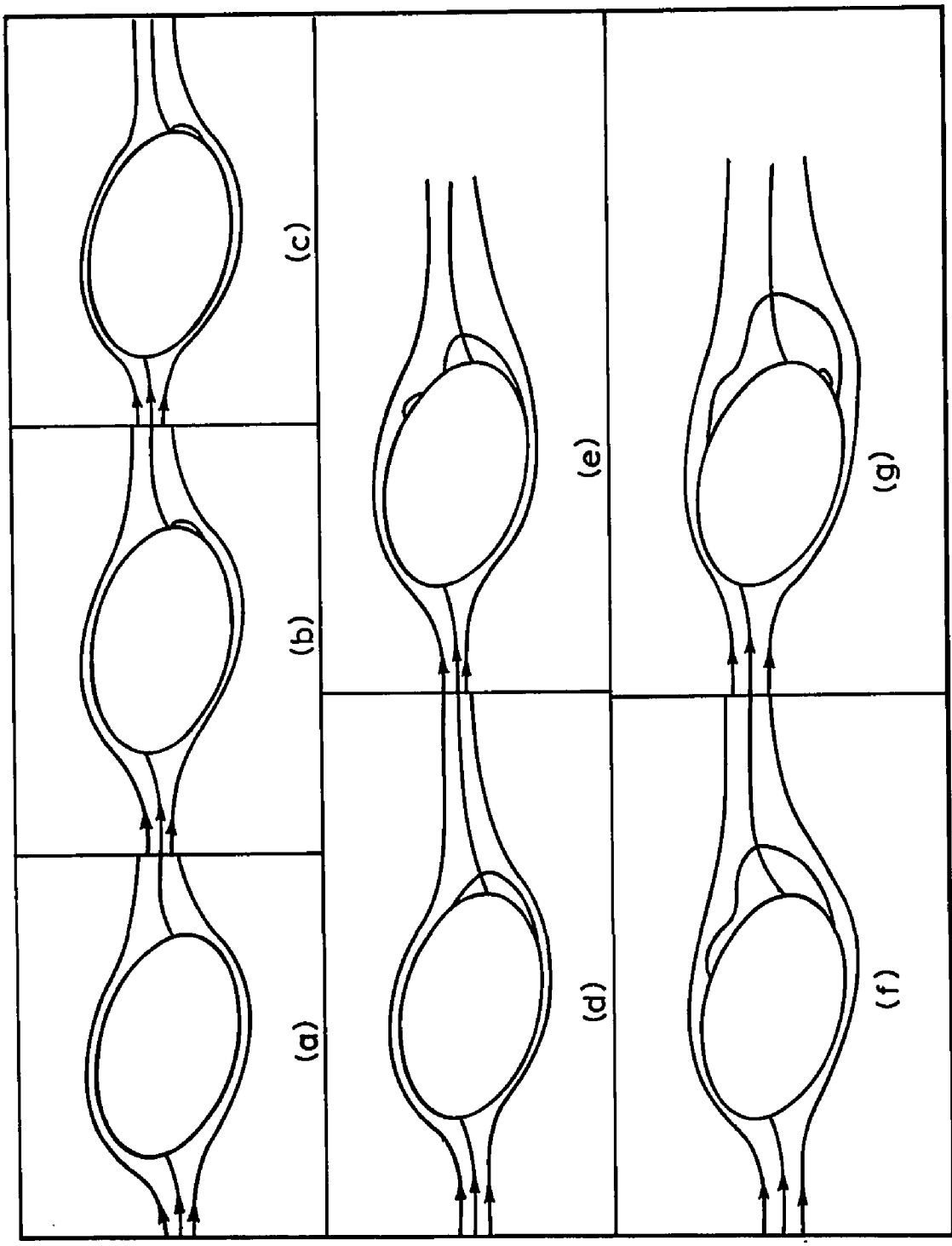

Fig. 28 Schematic Development of the Wake for R>13,000, where τ_1=0.6, γ=15°.

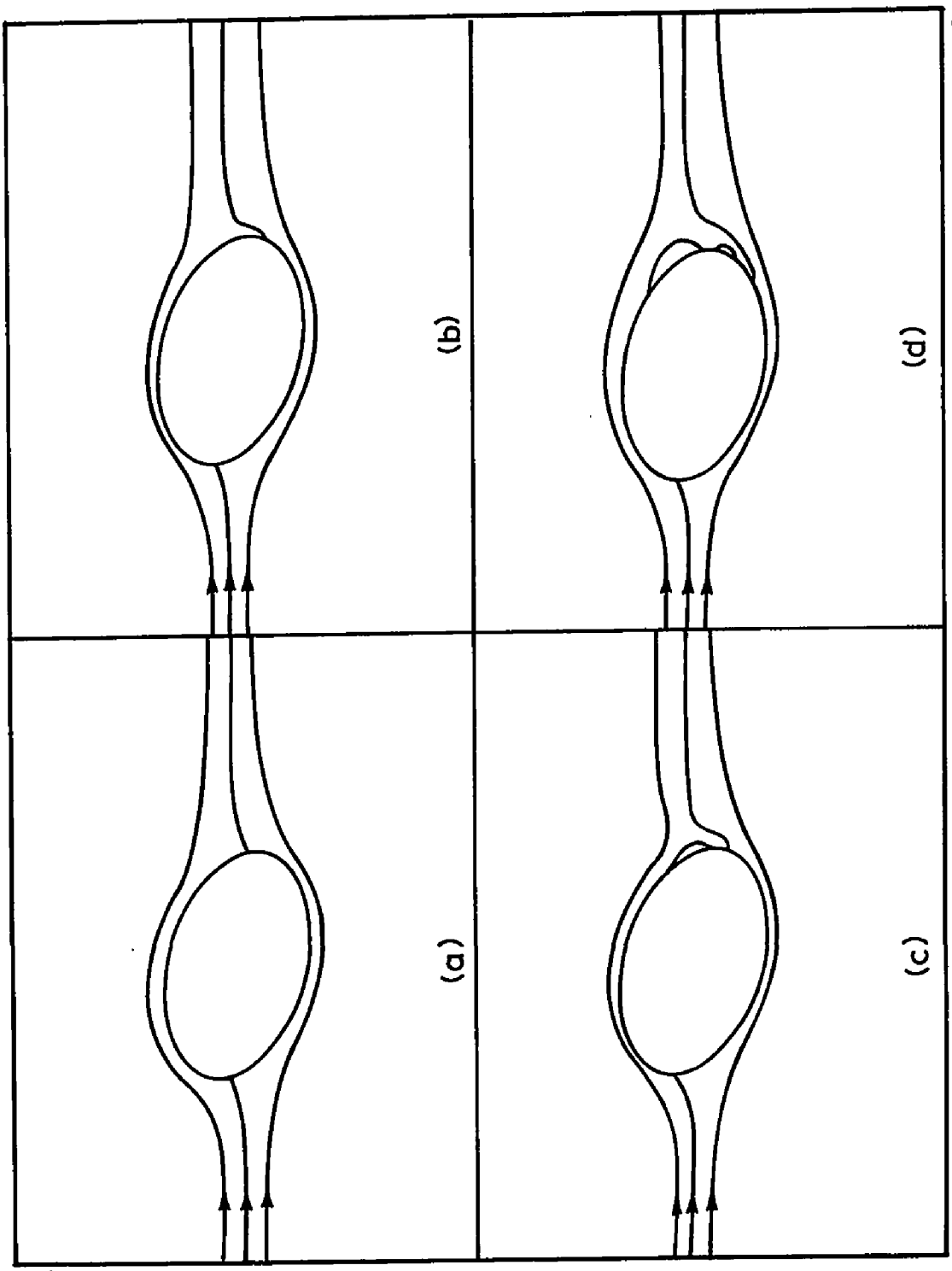

Fig. 29 Schematic Development of the Wake for 1700<R<13,000 where τ_1=0.6, γ=15°.

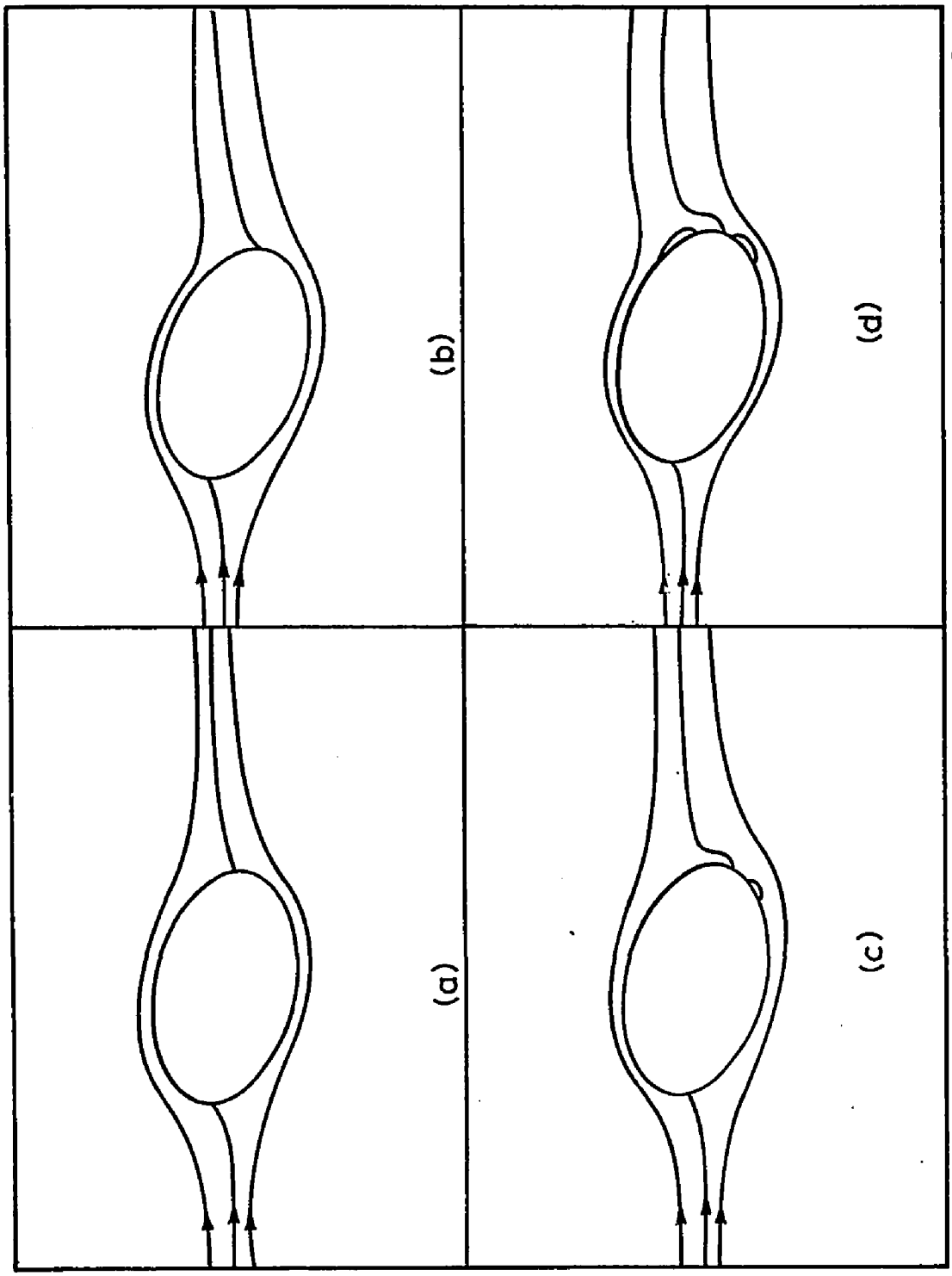

Fig. 30 Schematic Development of the Wake for R<1700 where τ_1=0.6,γ=15°.

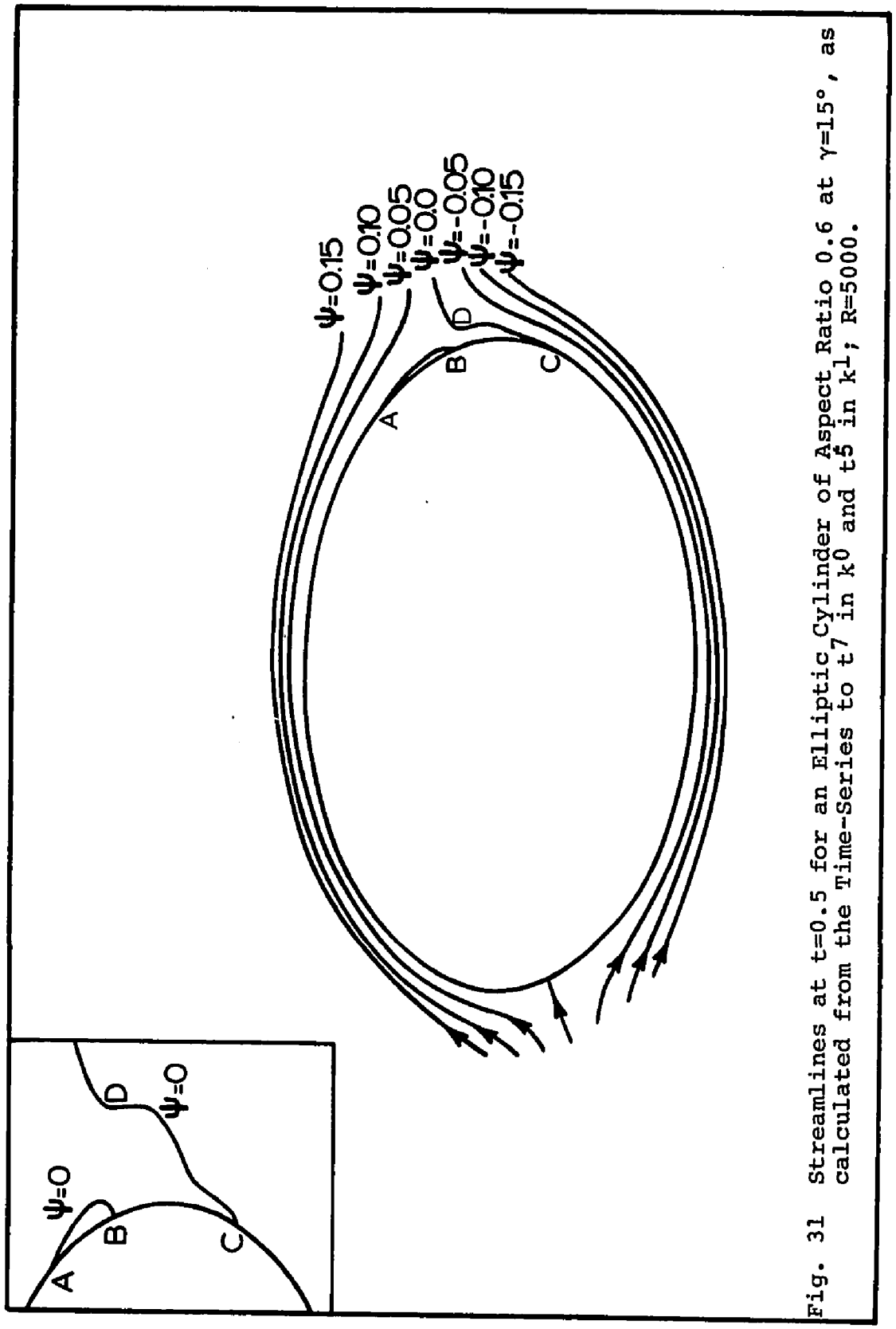

Fig. 31 Streamlines at t=0.5 for an Elliptic Cylinder of Aspect Ratio 0.6 at γ=15°, as calculated from the Time-Series to t^7 in k^0 and t^5 in k^1; R=5000.

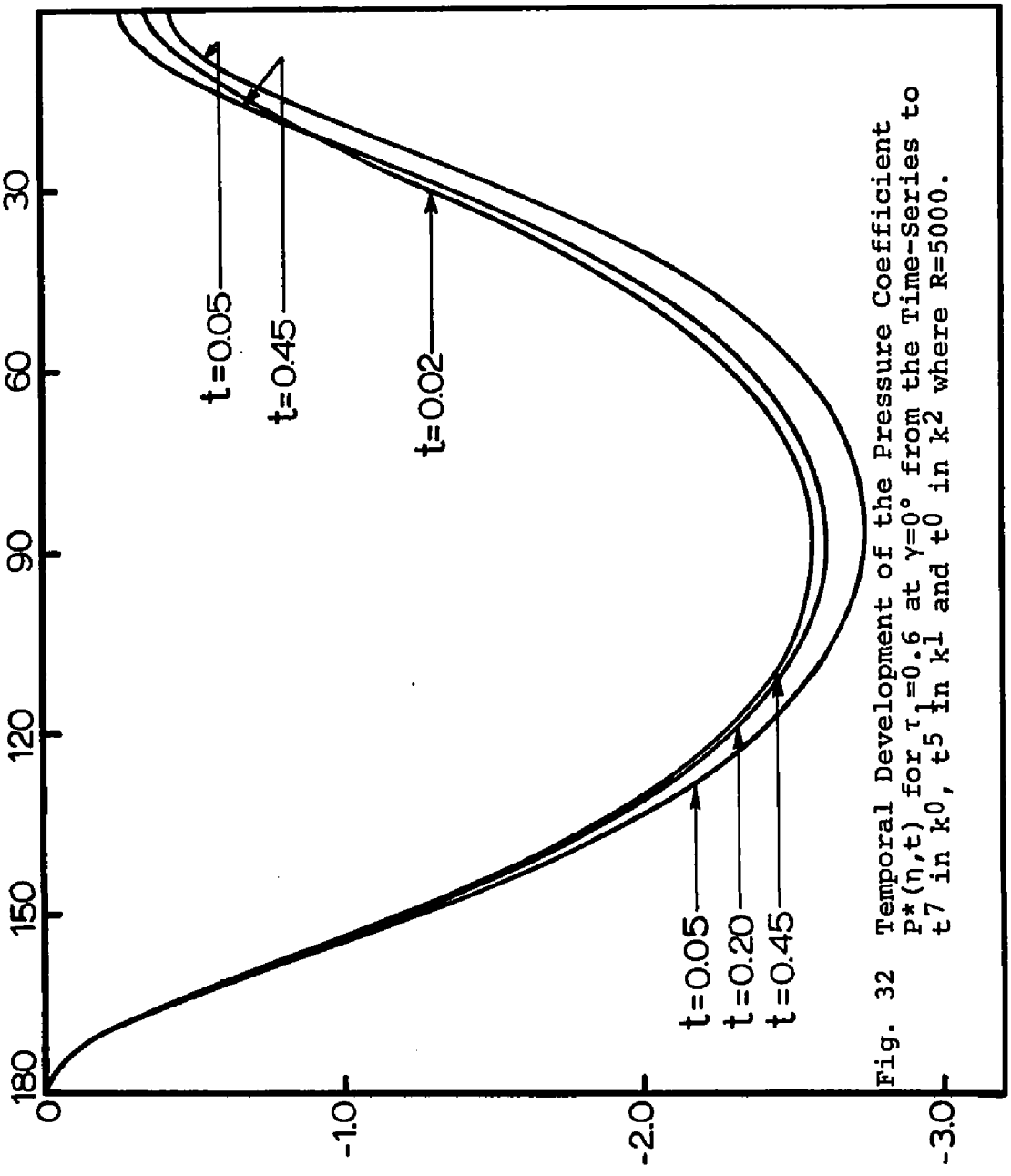

Fig. 32 Temporal Development of the Pressure Coefficient $P^*(\eta,t)$ for τ_1=0.6 at γ=0° from the Time-Series to t^7 in k^0, t^5 in k^1 and t^0 in k^2 where R=5000.

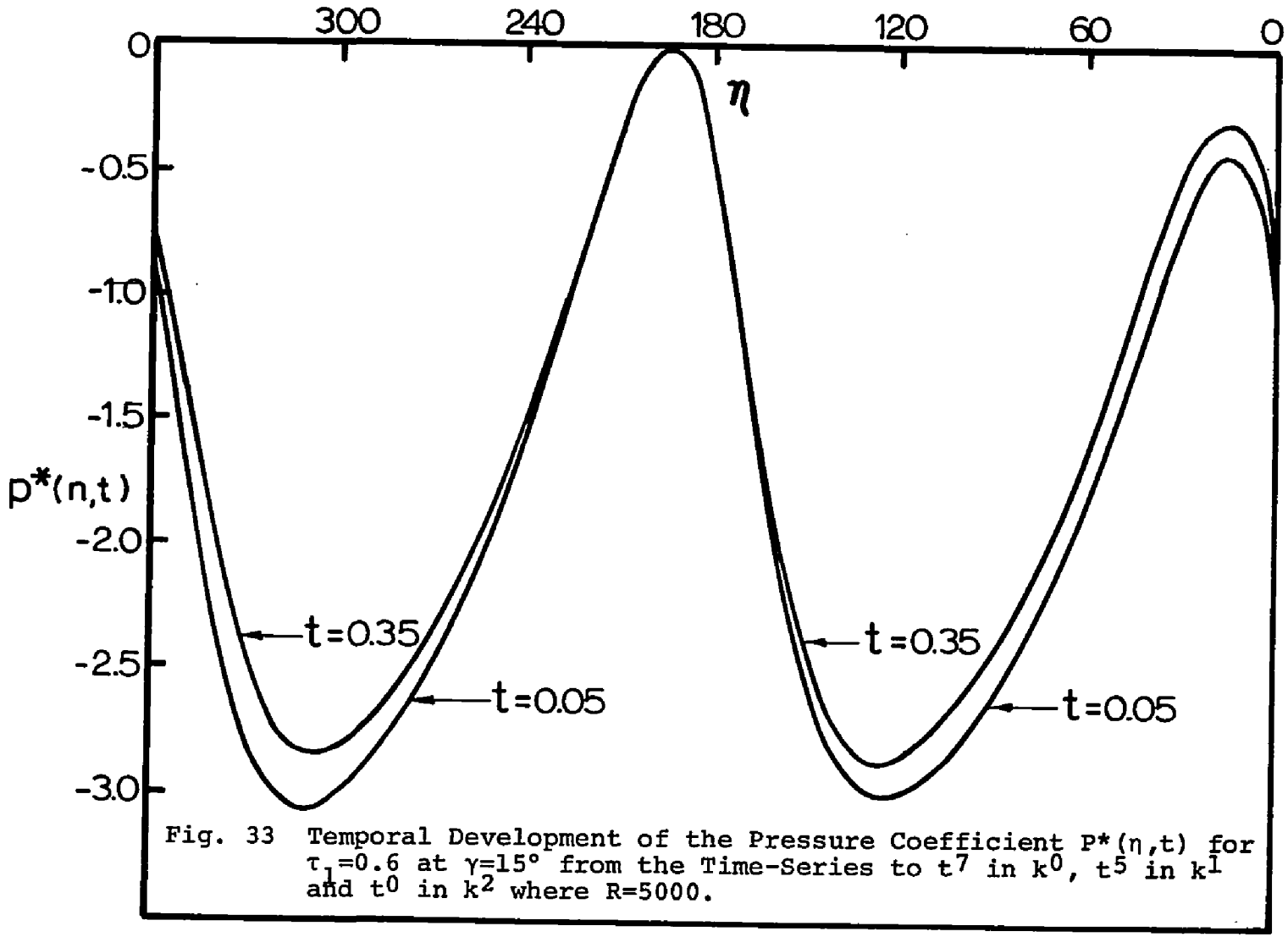

Fig. 33 Temporal Development of the Pressure Coefficient $P^*(\eta,t)$ for $\tau_1=0.6$ at $\gamma=15°$ from the Time-Series to t^7 in k^0, t^5 in k^1 and t^0 in k^2 where R=5000.

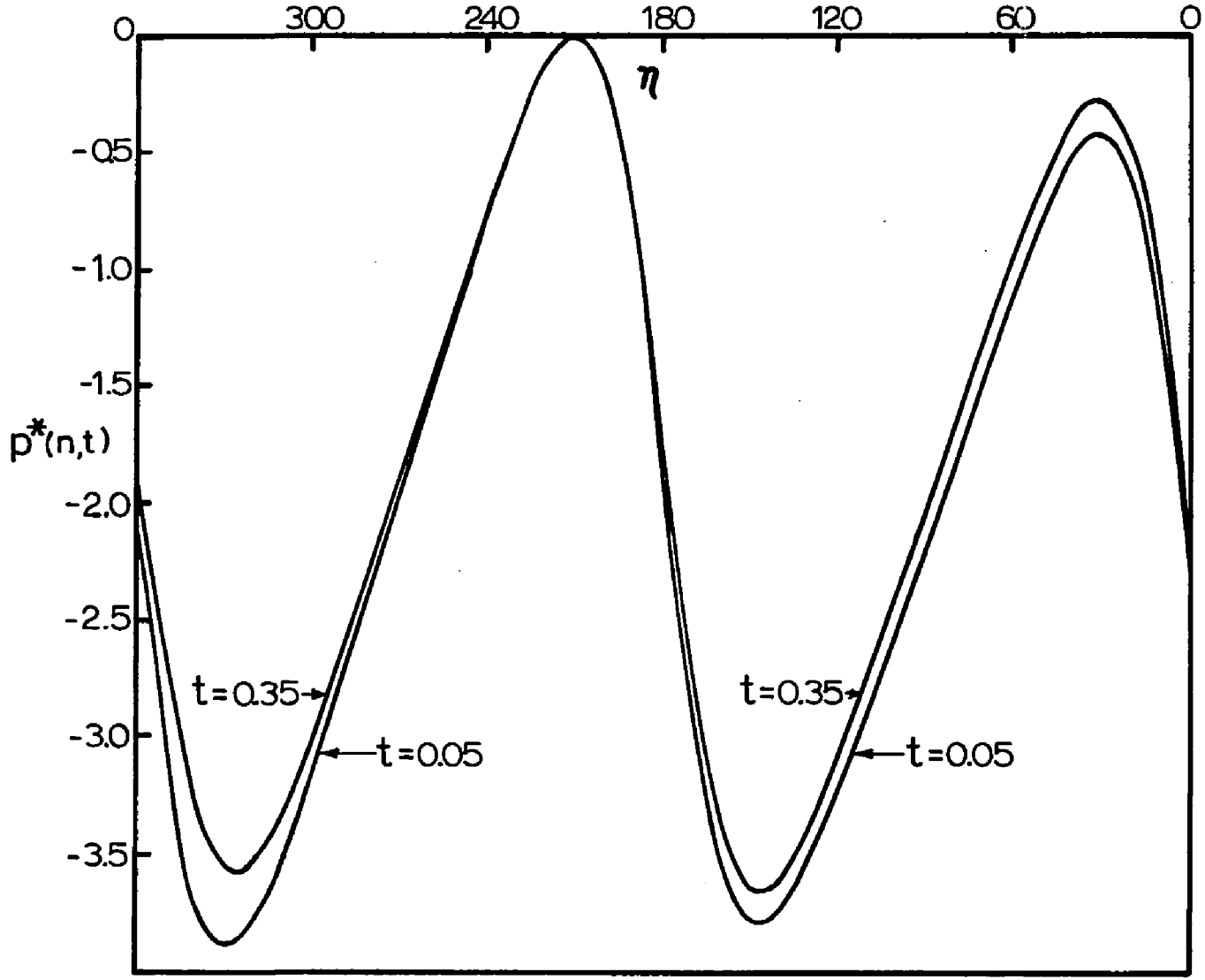

Fig. 34 Temporal Development of the Pressure Coefficient $P^*(\eta,t)$ for $\tau_1=0.6$ at $\gamma=30°$ from the Time-Series to t^7 in k^0, t^5 in k^1 and t^0 in k^2 where R=5000.

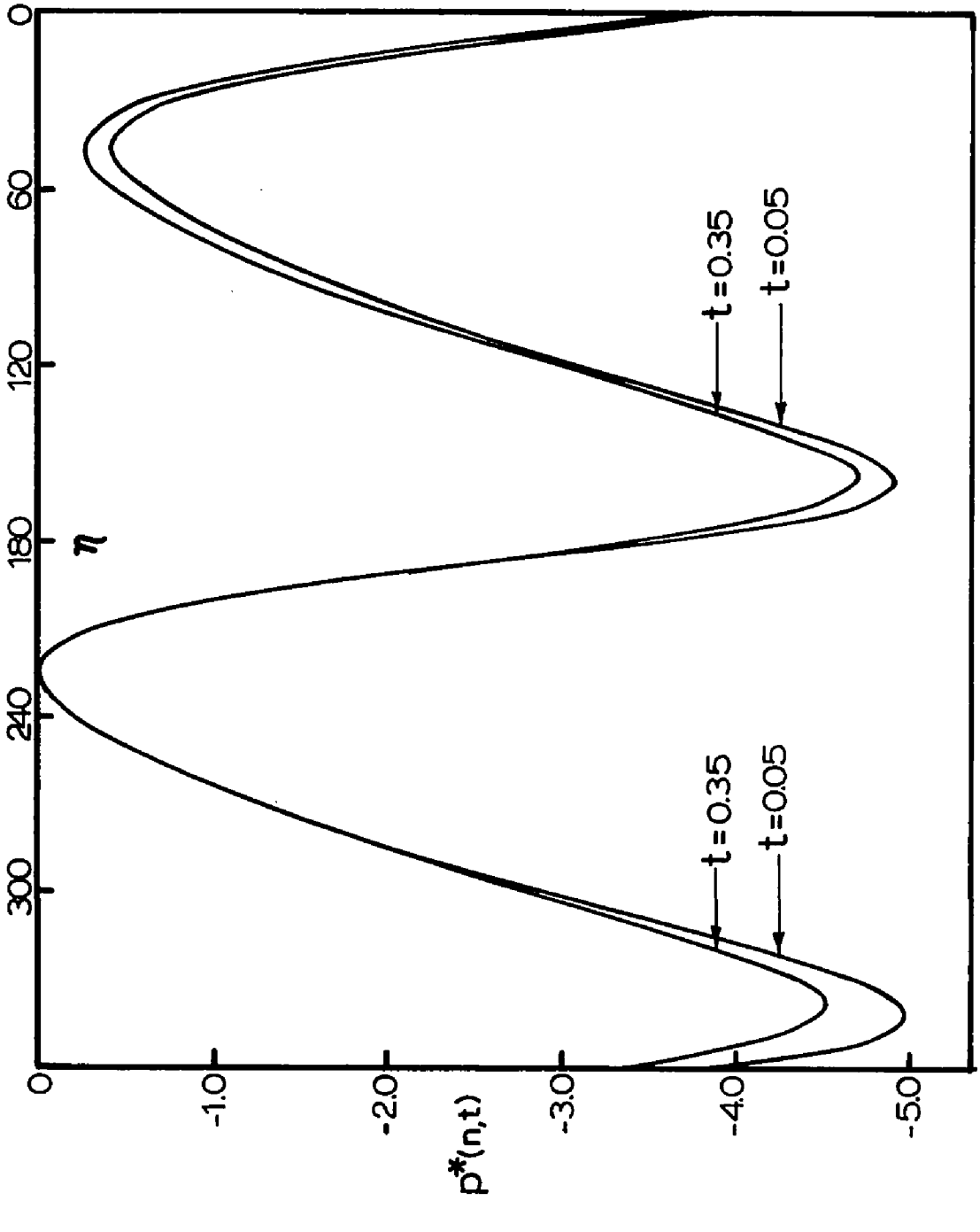

Fig. 35 Temporal Development of the Pressure Coefficient $p^*(\eta,t)$ for $\tau_1=0.6$ at $\gamma=45°$ from the Time-Series to t^7 in k^0, t^5 in k^1 and t^0 in k^2 where $^1R=5000$.

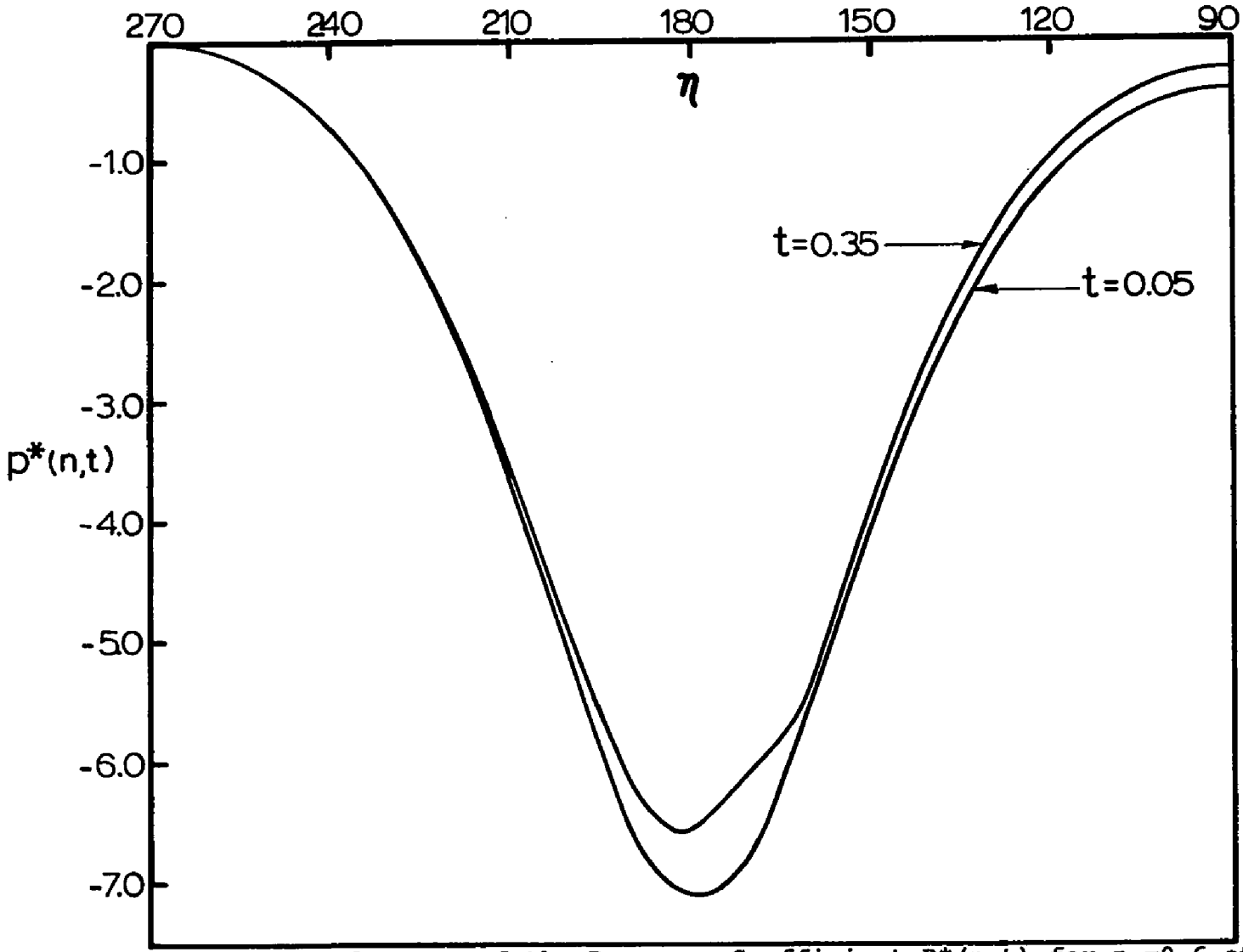

Fig. 36 Temporal Development of the Pressure Coefficient $P^*(\eta,t)$ for $\tau_1=0.6$ at $\gamma=90°$ from the Time-Series to t^7 in k^0, t^5 in k^1 and t^0 in k^2 where $^1R=5000$.

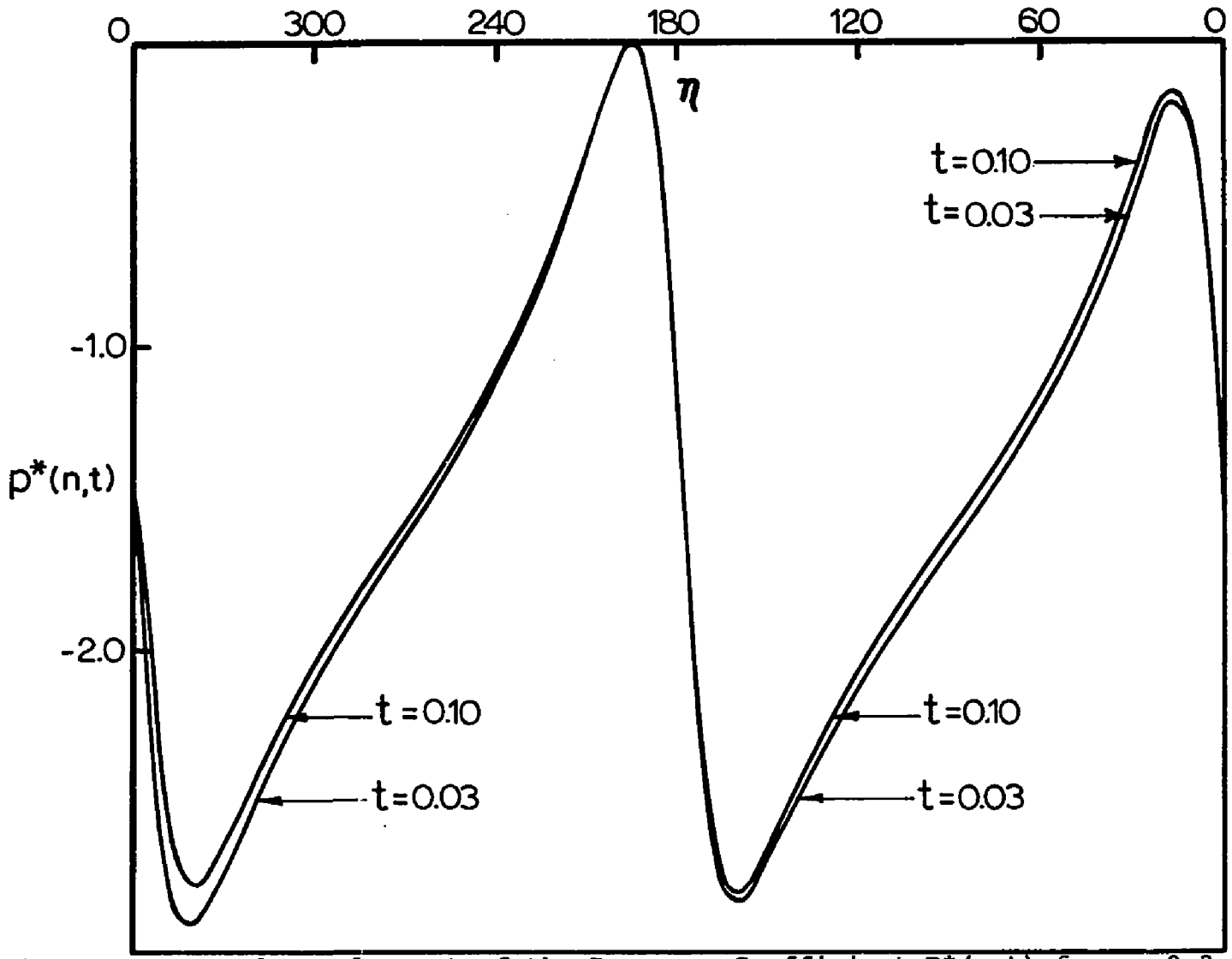

Fig. 37 Temporal Development of the Pressure Coefficient $P^*(\eta,t)$ for $\tau_1=0.3$ at $\gamma=15°$ from the Time-Series to t^6 in k^0, t^4 in k^2 and t^0 in k^2 where $^1R=50,000$.

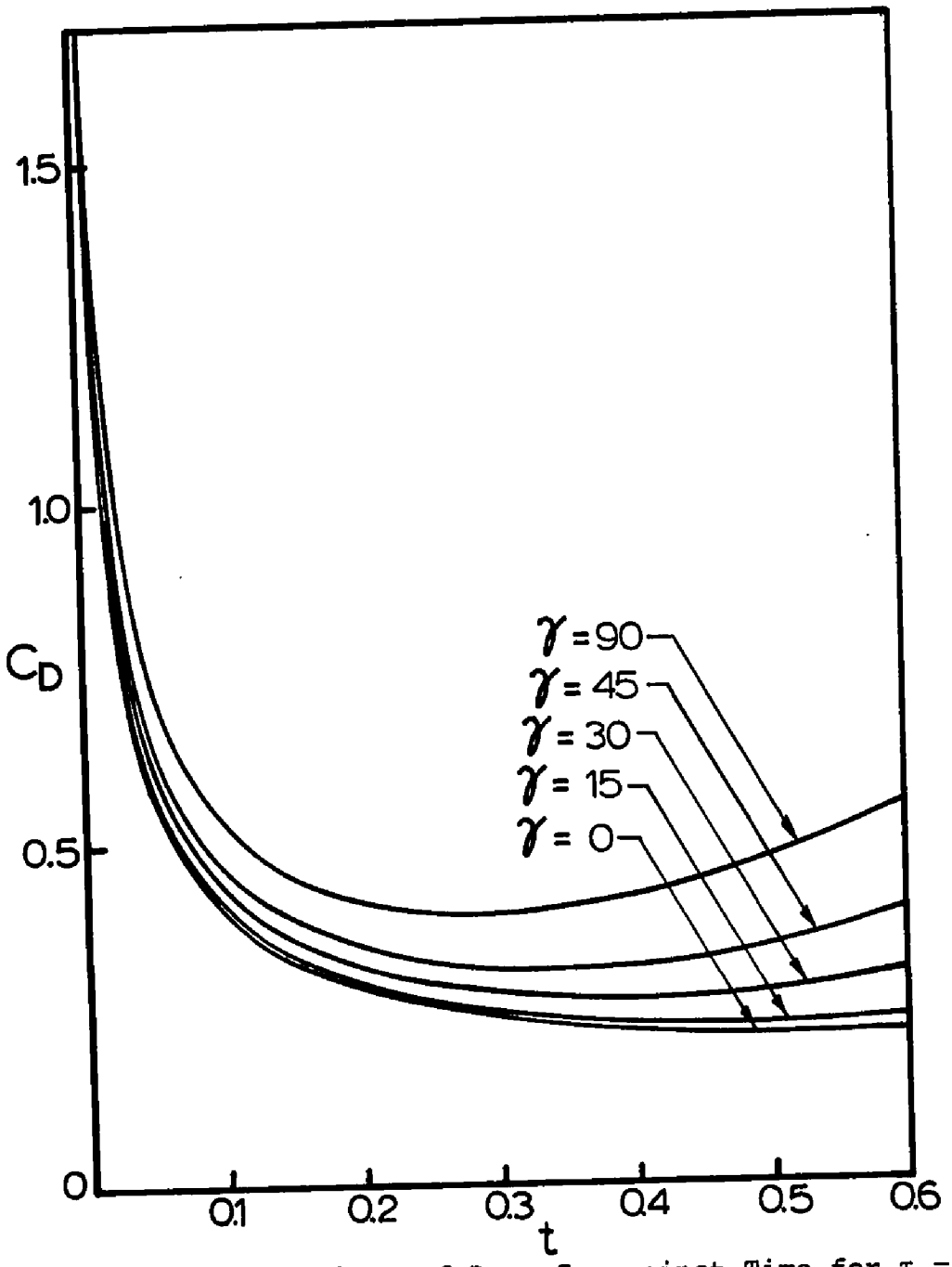

Fig. 38 Coefficient of Drag C_D against Time for $\tau_1=0.6$ and R=5,000 at Various Angles of Incidence using the Time-Series to t^7 in k^0, t^5 in k^1 and t^0 in k^2.

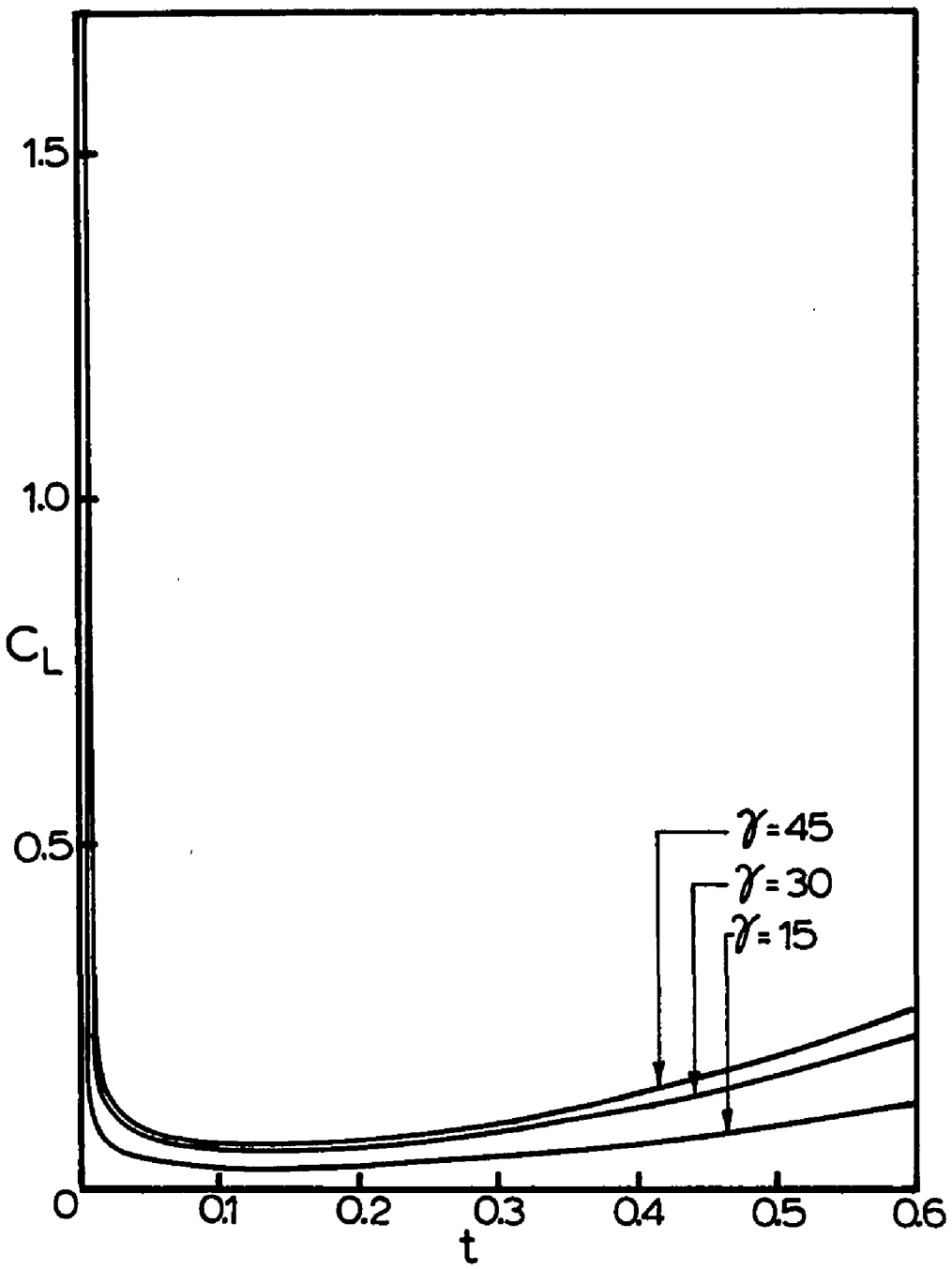

Fig. 39 Coefficient of Lift C_L against Time for τ_1=0.6 and R=5,000 at Various Angles of Incidence using the Time-Series to t^7 in k^0, t^5 in k^1 and t^0 in k^2.

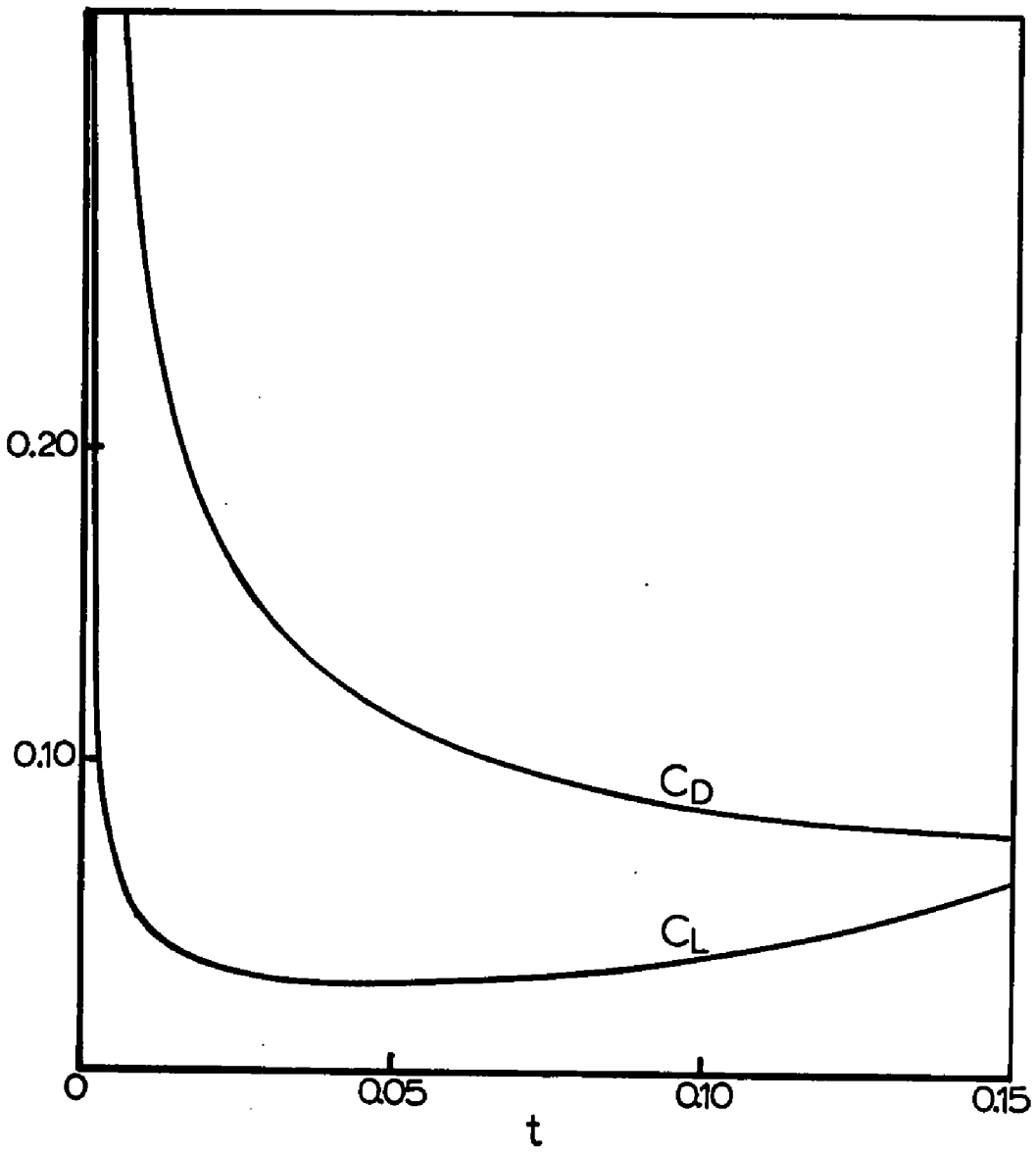

Fig. 40 Coefficients of Drag and Lift versus Time for τ_1=0.3 and R=50,000 at γ=15°, using the Time Series to t^6 in k^0, t^4 in k^1, and t^0 in k^2.

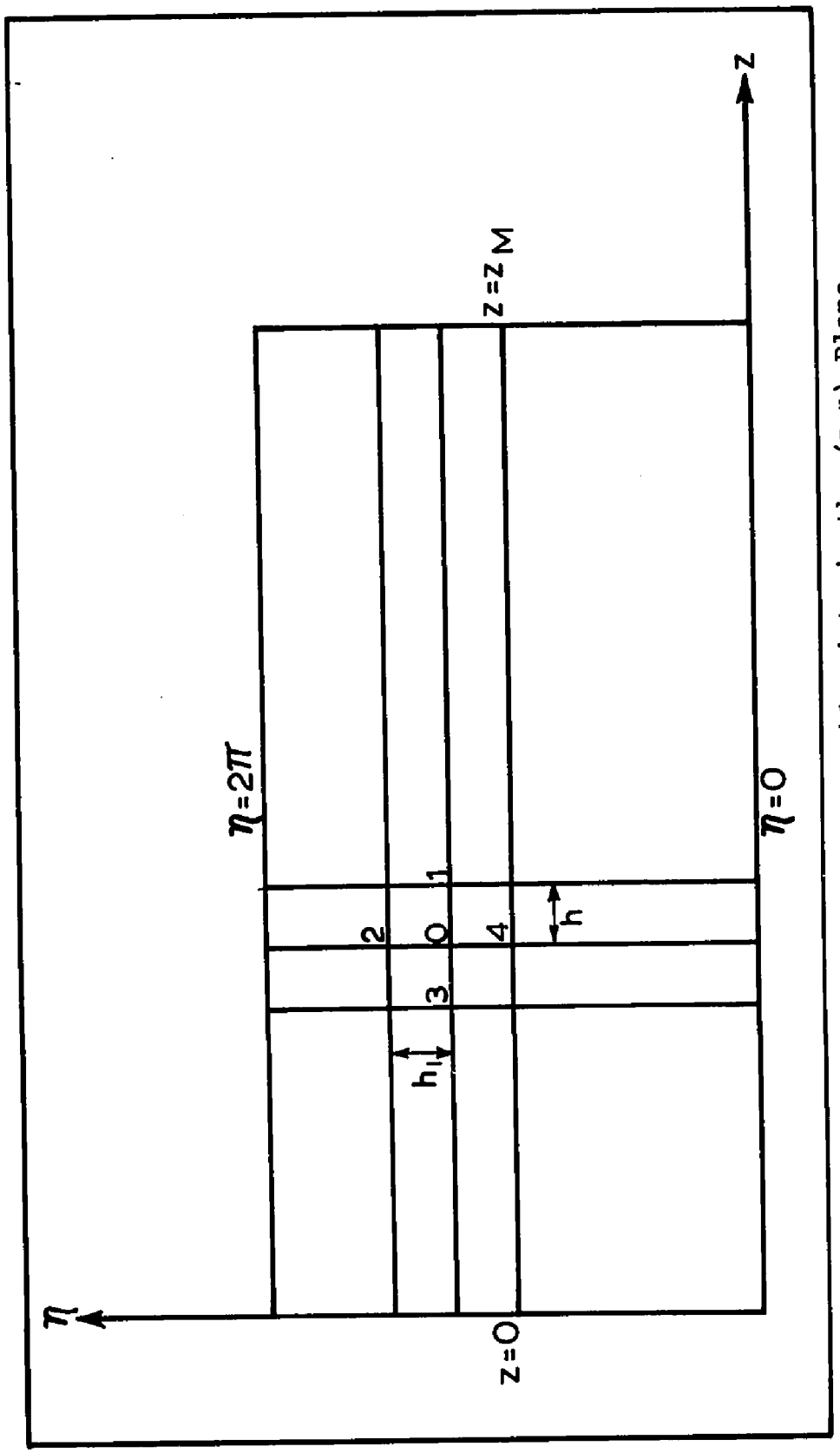

Fig. 41 The Convention for Labelling Grid Points in the (z-η) Plane.

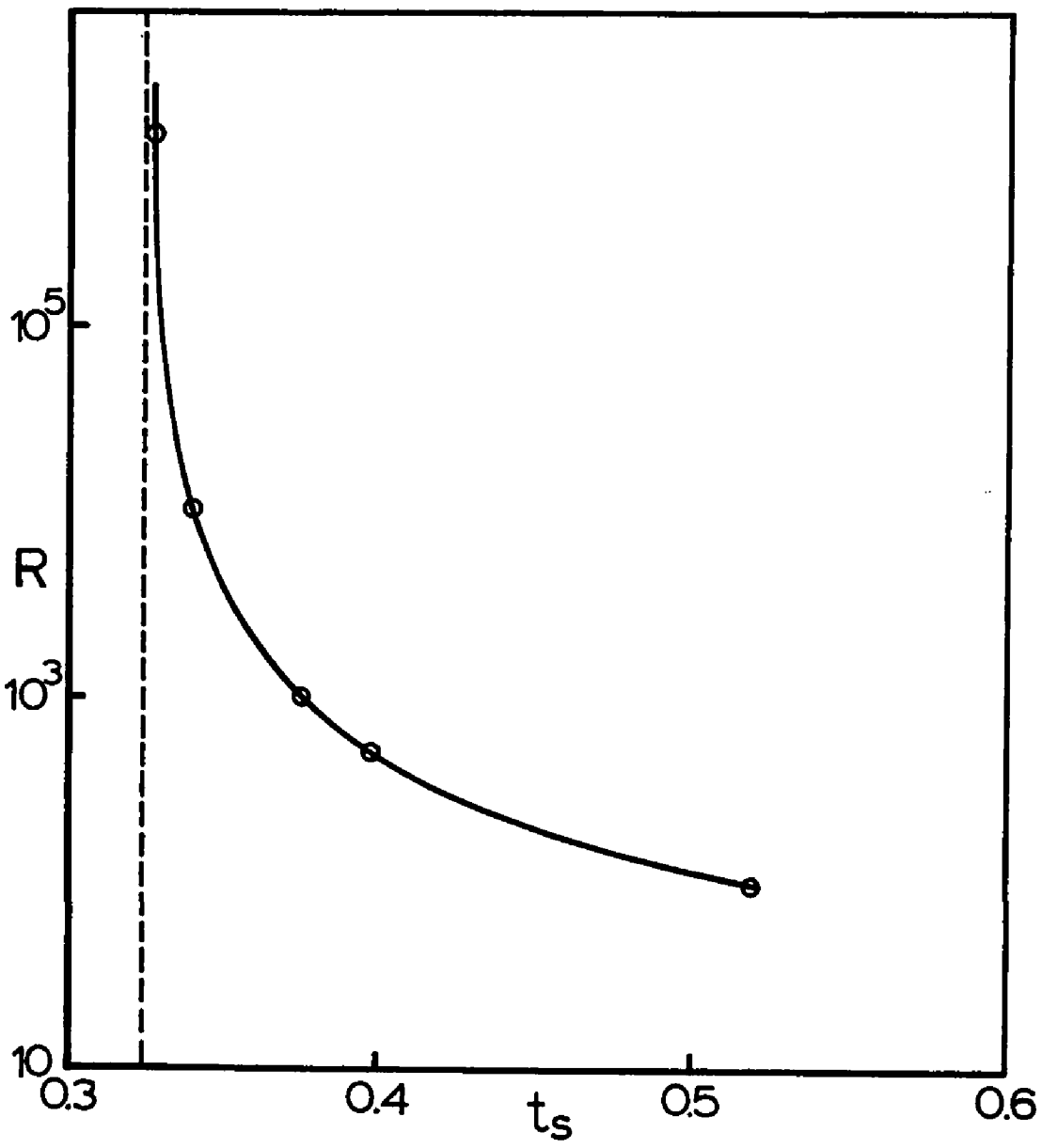

Fig. 42 Separation Time versus Reynolds Number for Flow Past a Circular Cylinder.

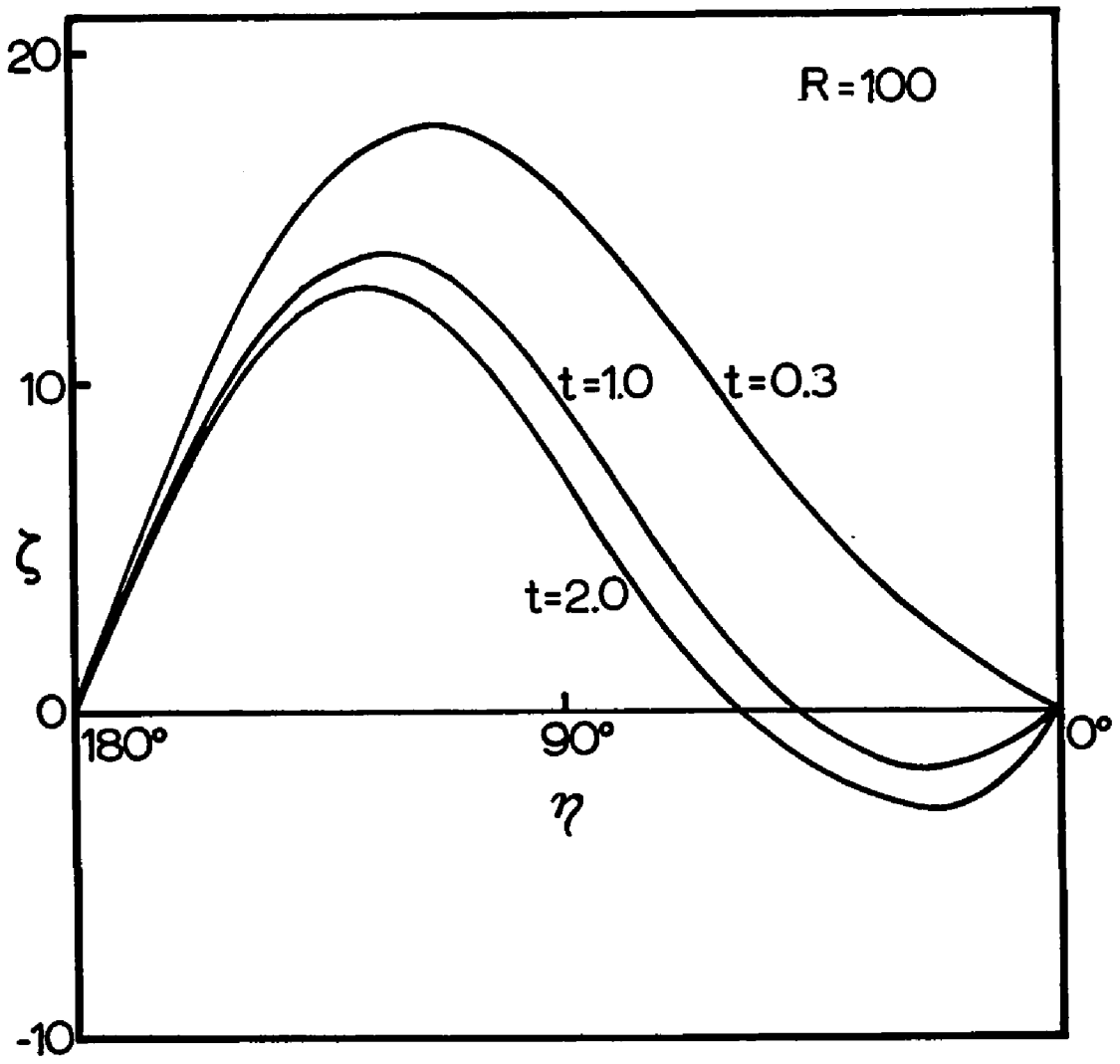

Fig. 43 Temporal Development of Surface Vorticity for Flow Past a Circular Cylinder at R=100.

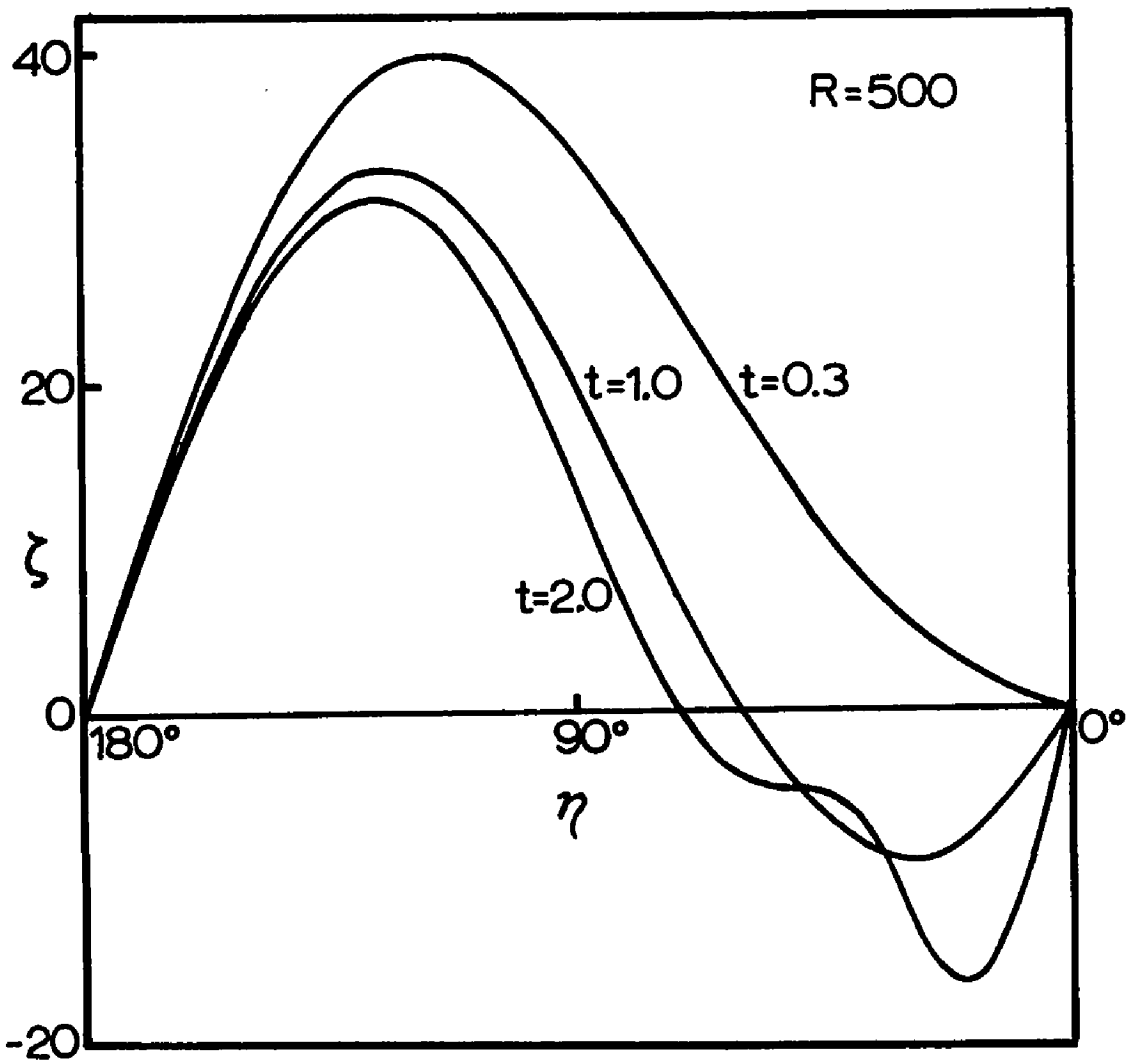

Fig. 44 Temporal Development of Surface Vorticity for Flow Past a Circular Cylinder at R=500.

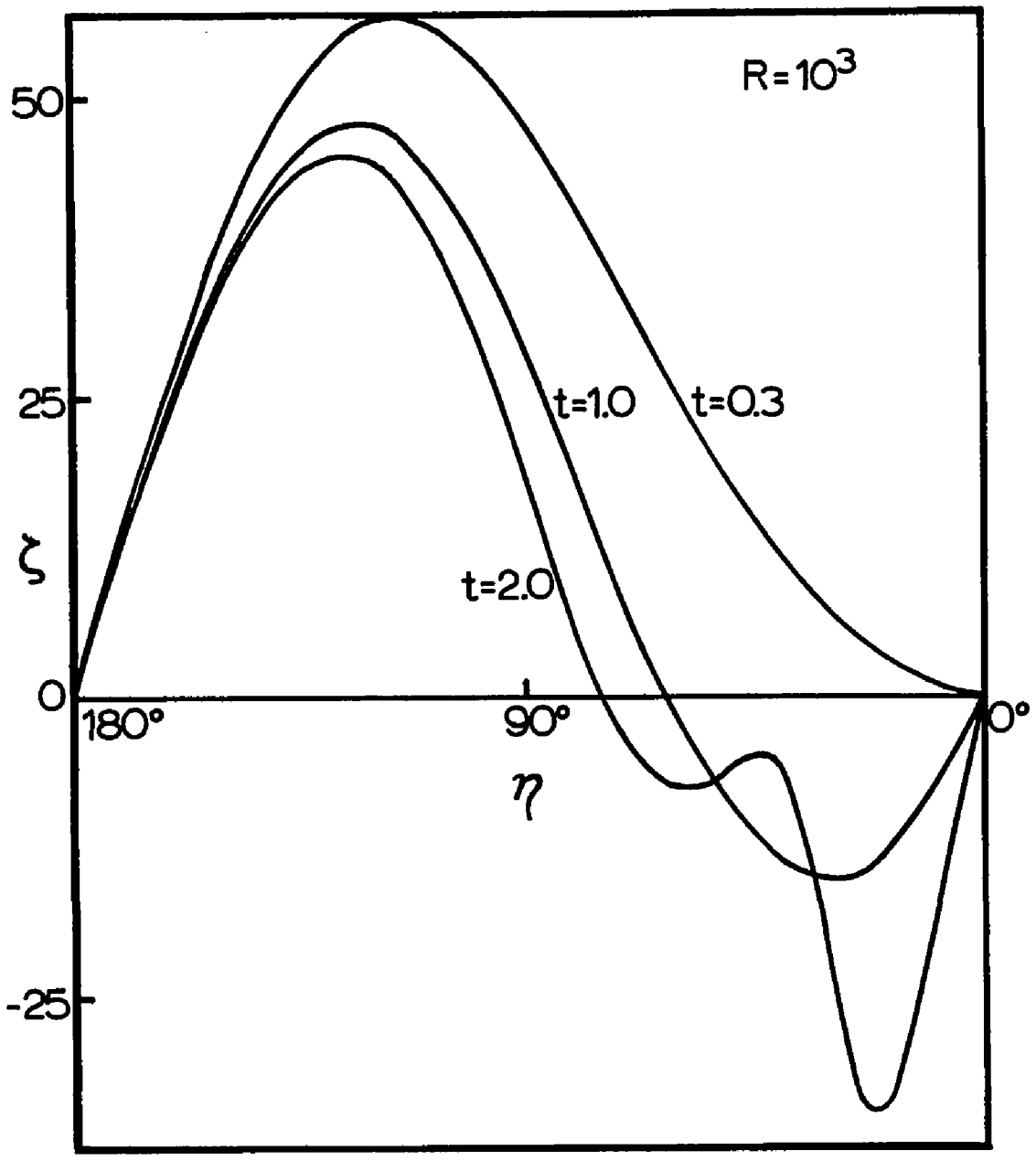

Fig. 45 Temporal Development of Surface Vorticity for Flow Past a Circular Cylinder at R=1000.

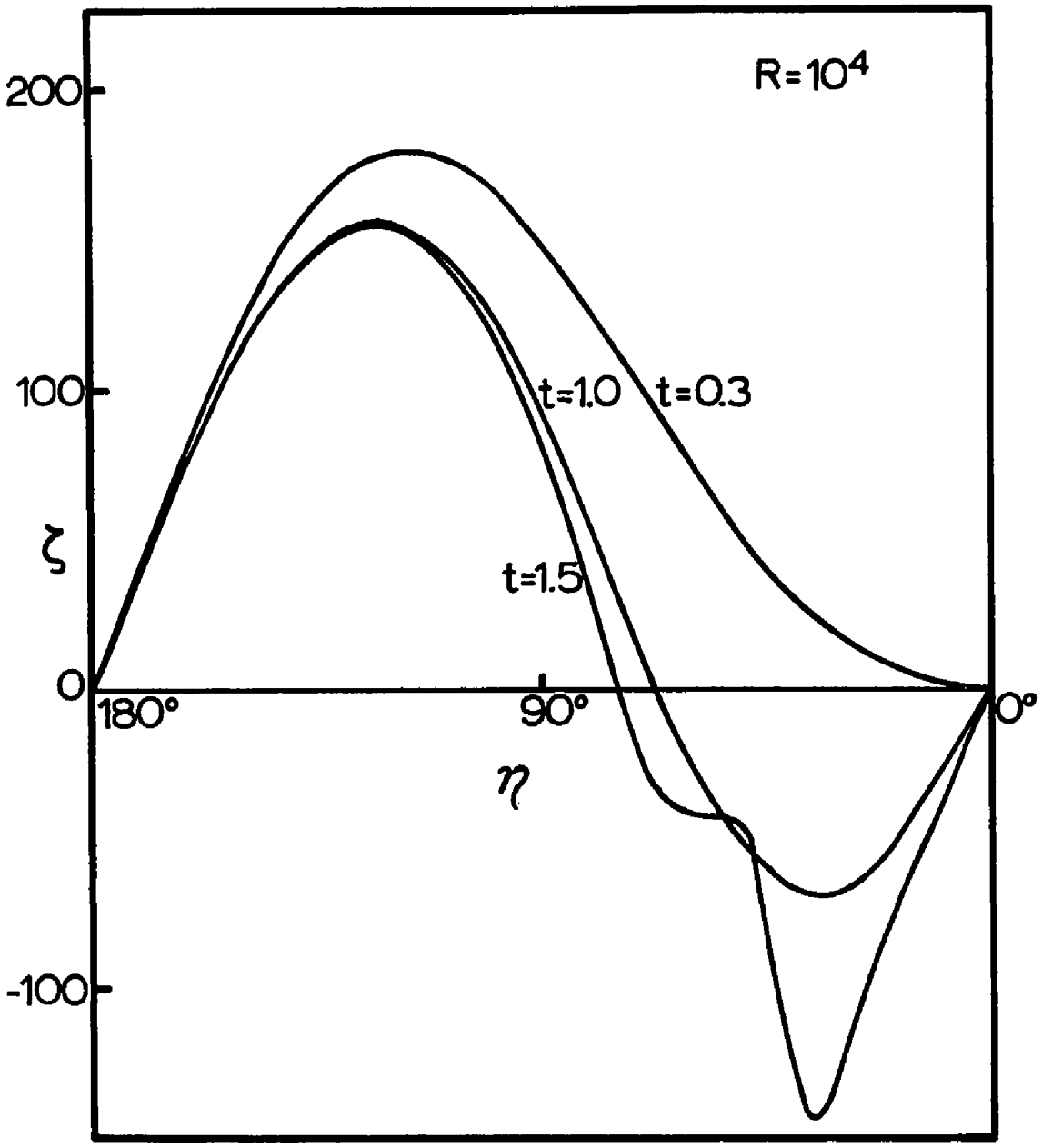

Fig. 46 Temporal Development of Surface Vorticity for Flow Past a Circular Cylinder at $R=10^4$.

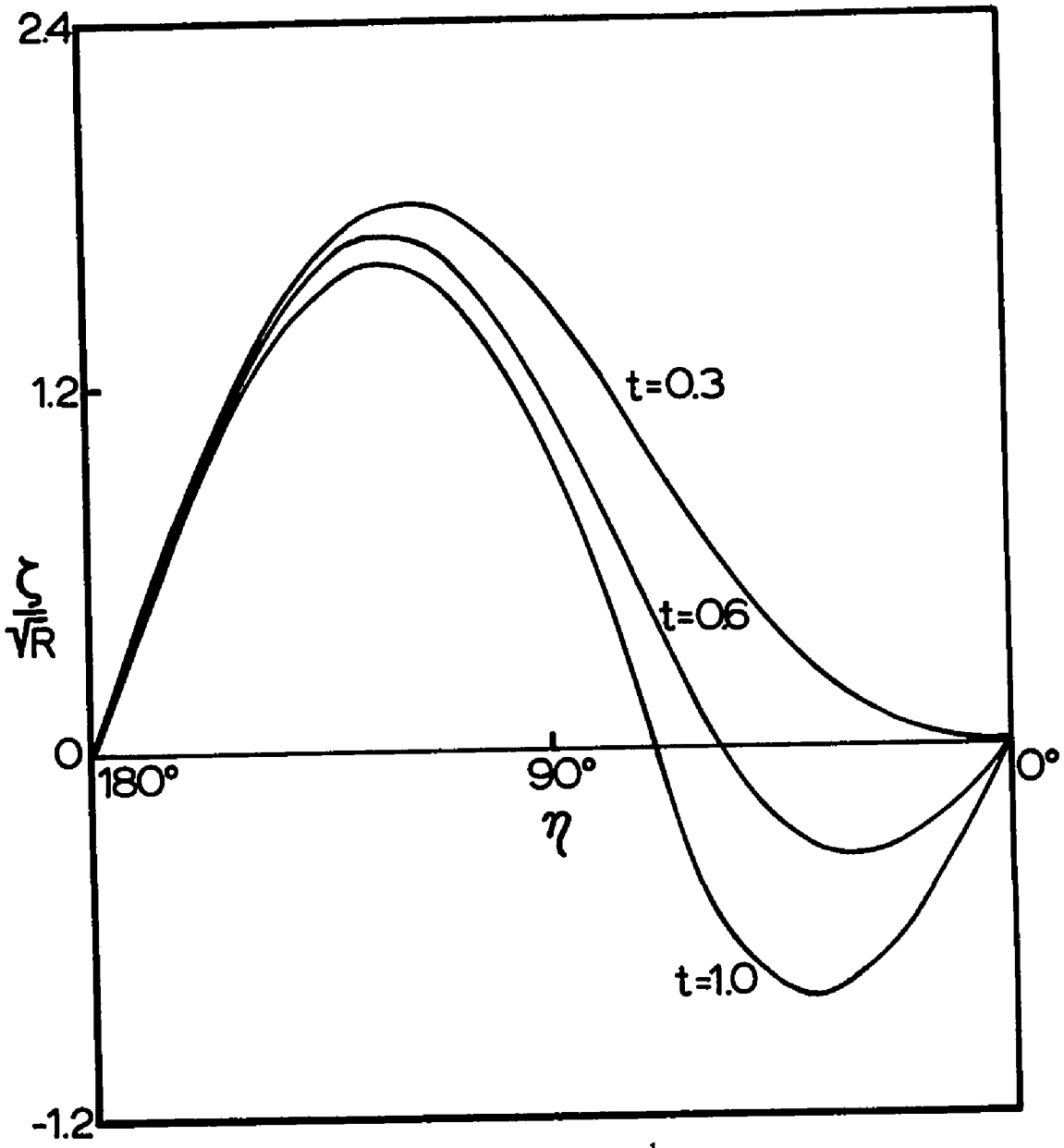

Fig. 47 Temporal Development of $R^{-\frac{1}{2}}\zeta$ for Flow Past a Circular Cylinder at l/R=0.

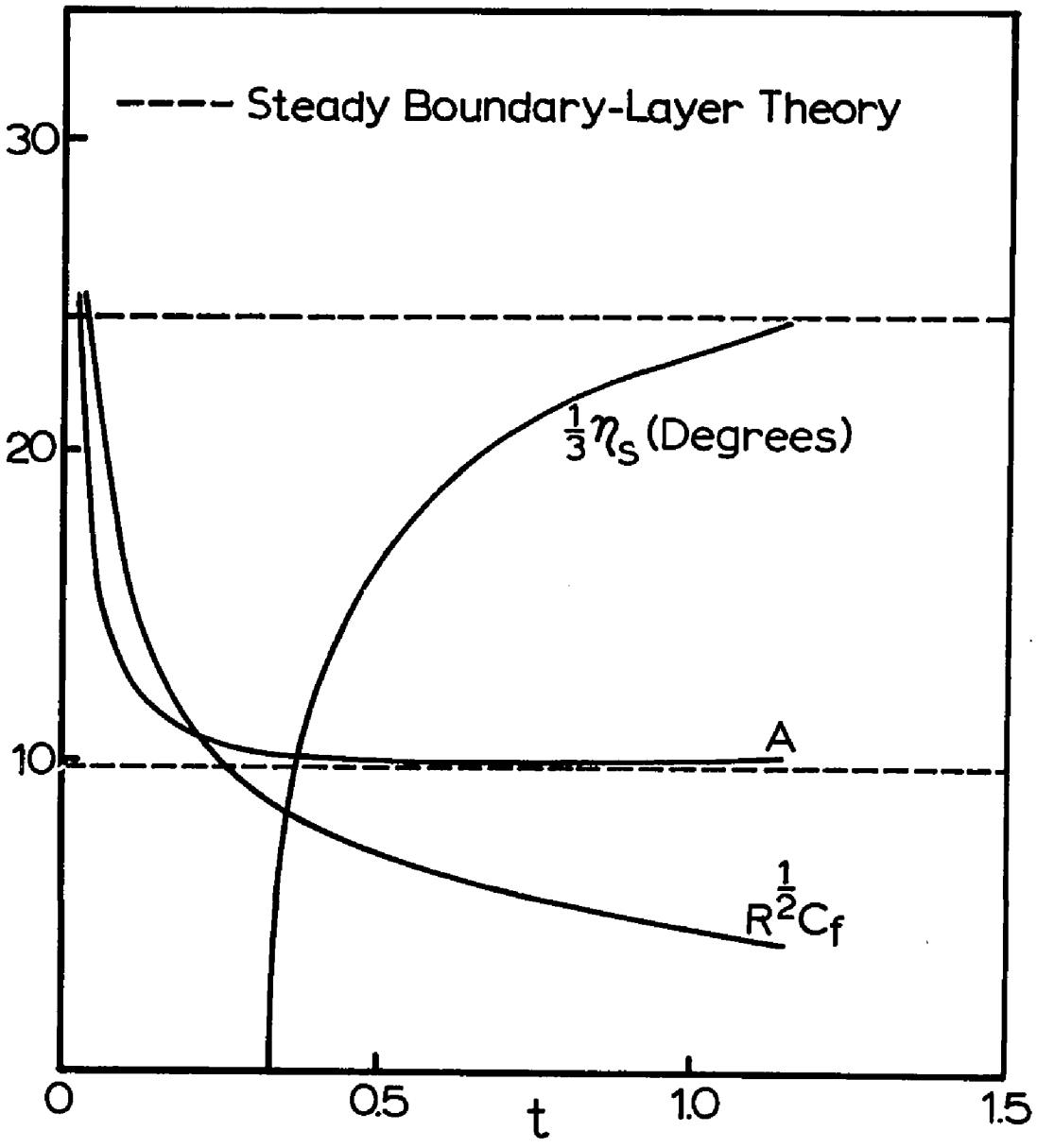

Fig. 48 Some Properties of the 1/R=0 Solution for Flow Past a Circular Cylinder.

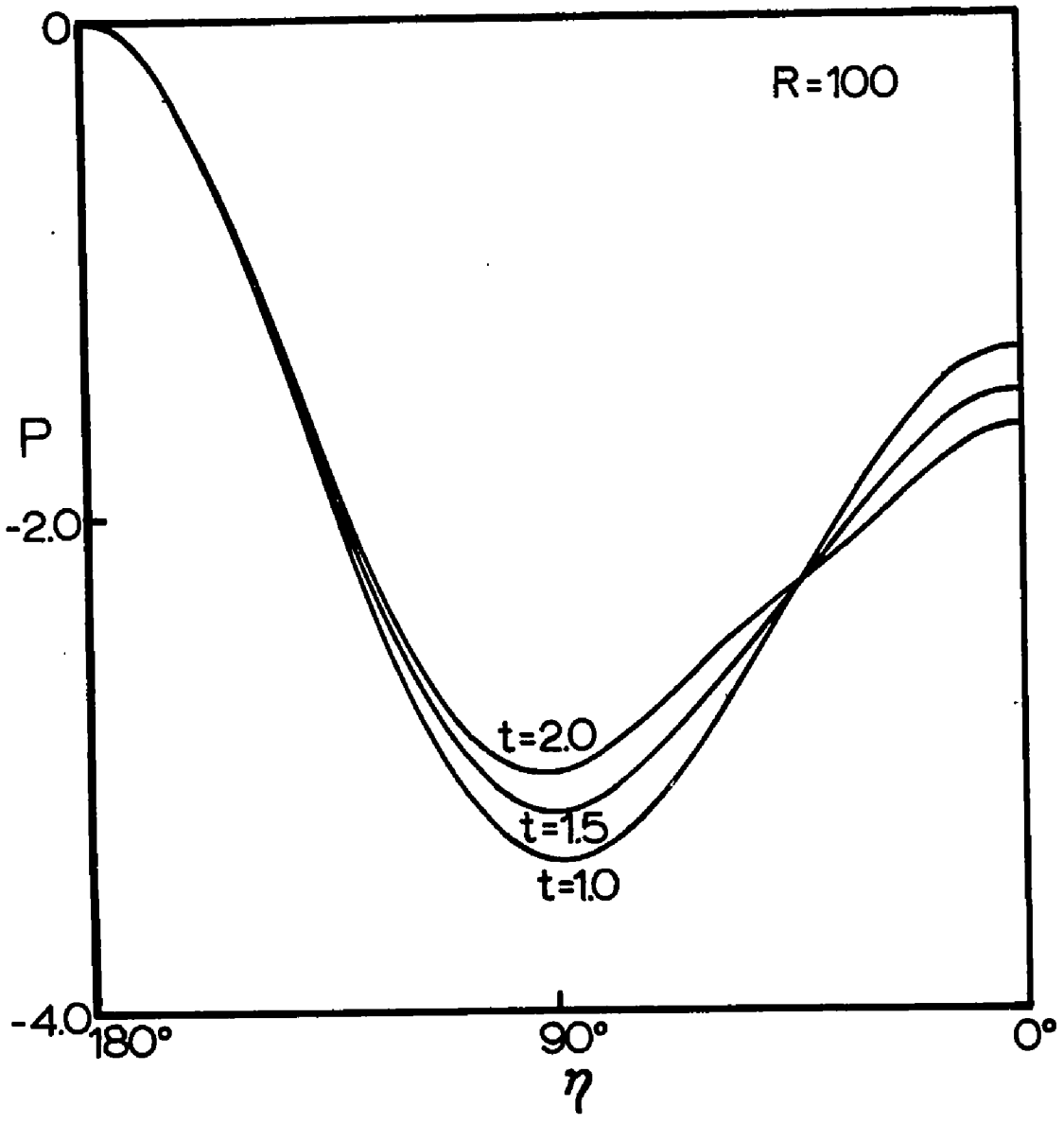

Fig. 49 Temporal Development of the Pressure Coefficient $p^*(\eta,t)$ for Flow Past a Circular Cylinder at R=100.

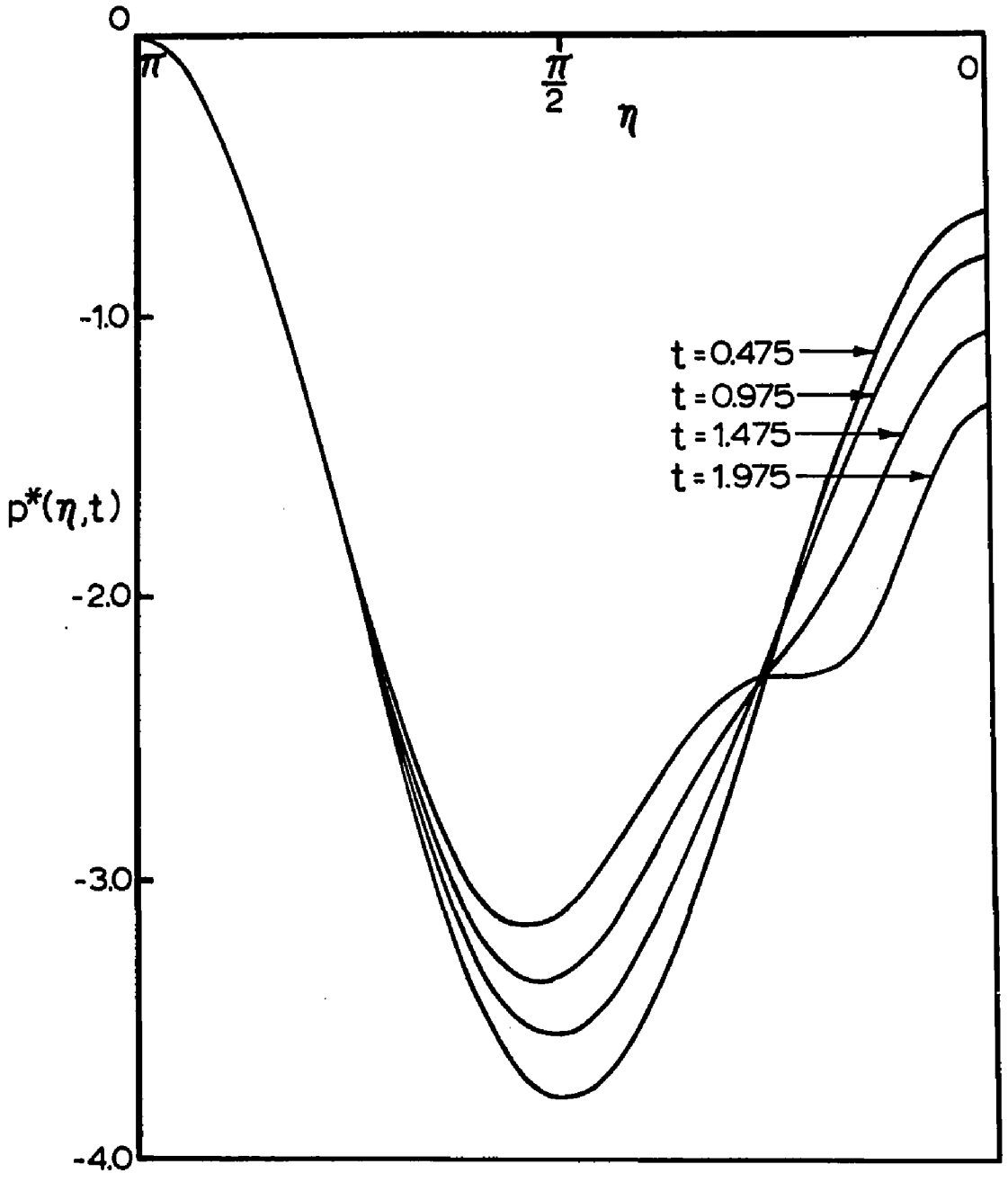

Fig. 50 Temporal Development of the Pressure Coefficient $P^*(\eta,t)$ for Flow Past a Circular Cylinder at R=500.

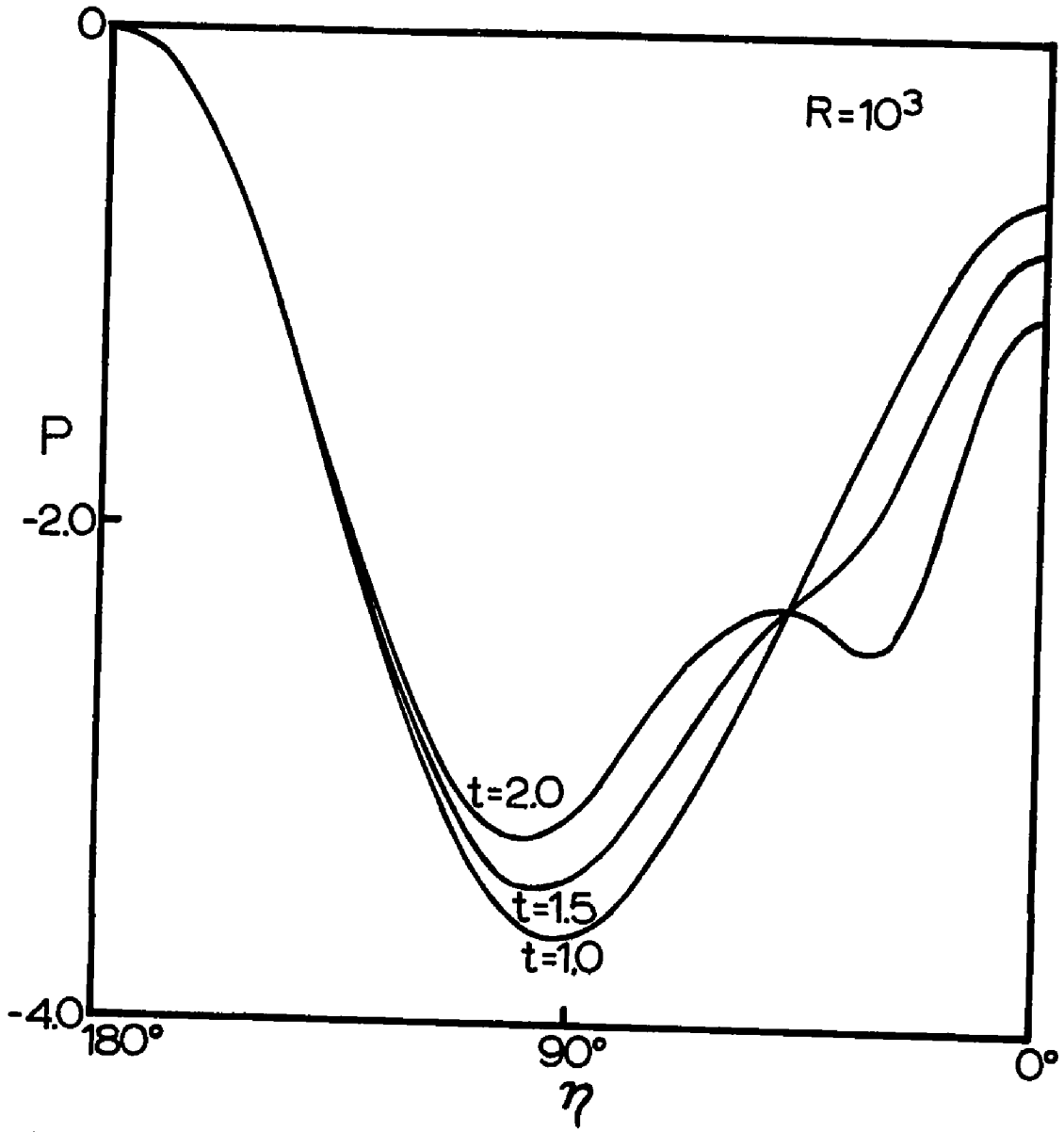

Fig. 51 Temporal Development of the Pressure Coefficient $P^*(\eta,t)$ for Flow Past a Circular Cylinder at R=1000.

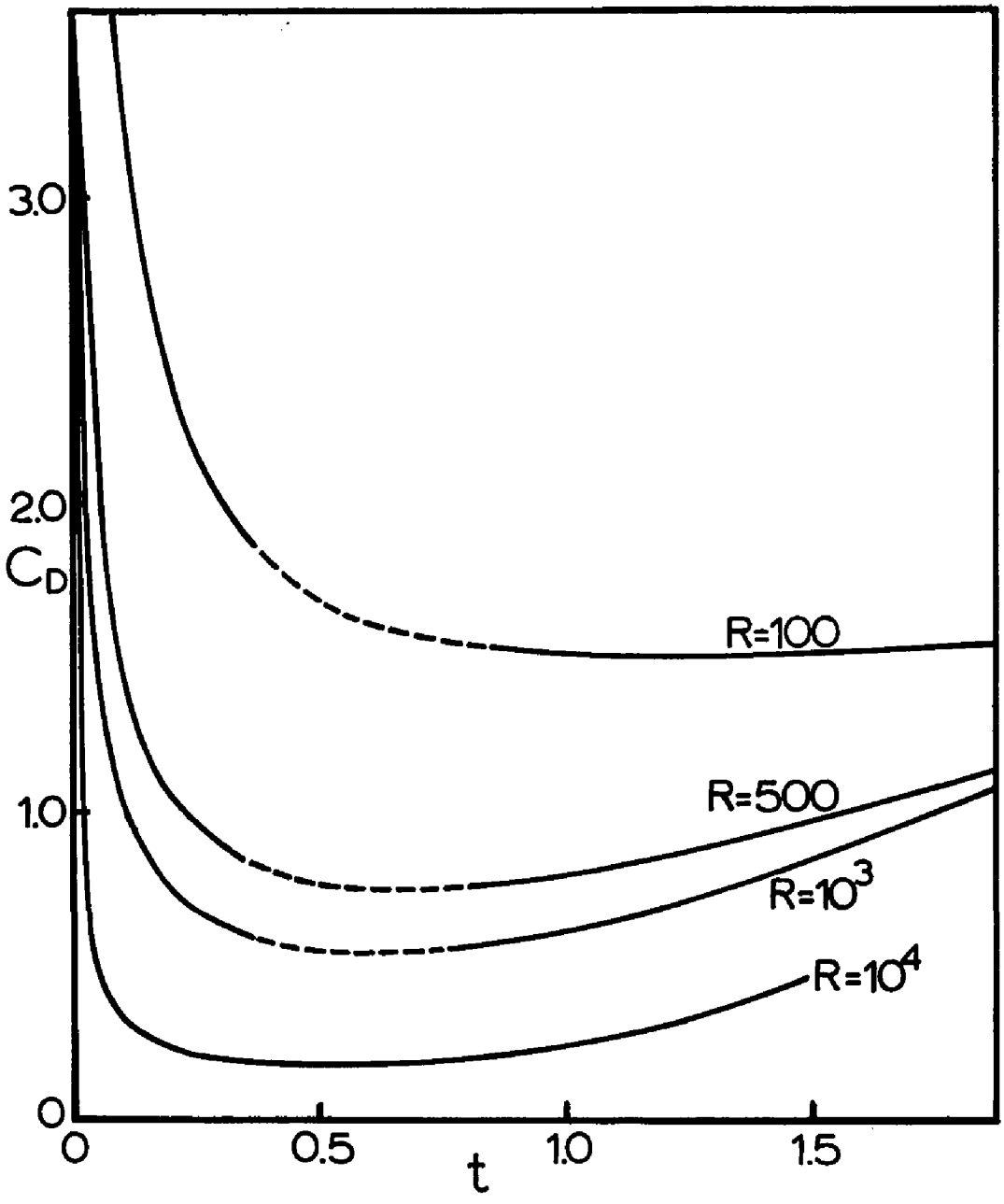

Fig. 52 Variation of the Total Drag Coefficient C_D for Flow Past a Circular Cylinder, as a Function of Time.

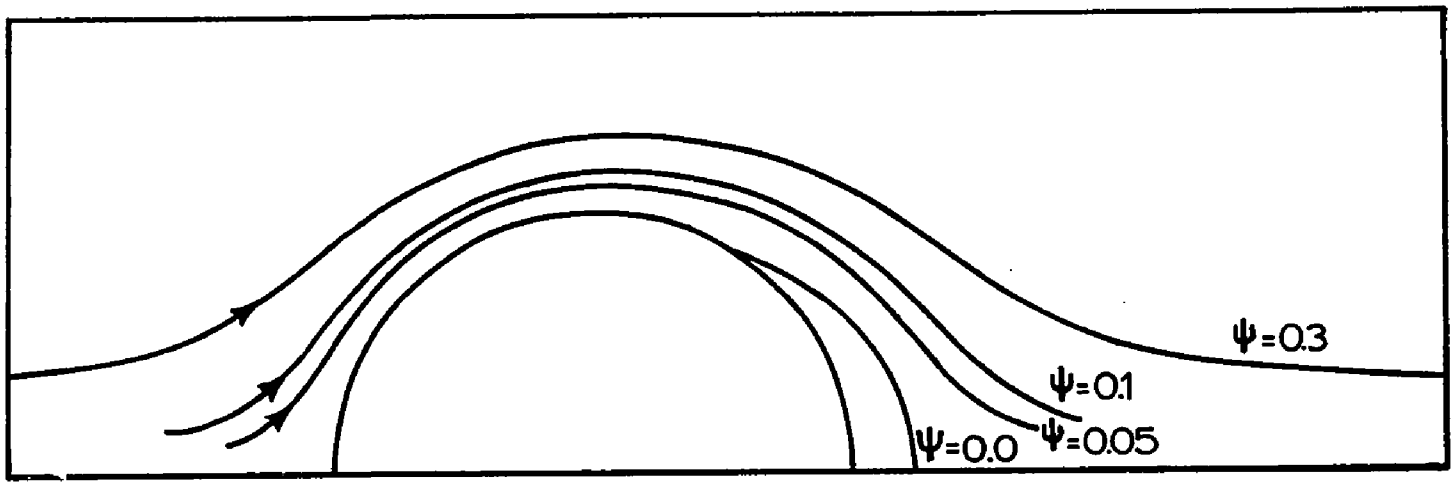

Fig. 53 Streamlines at t=1.0 for Flow Past a Circular Cylinder at R=100.

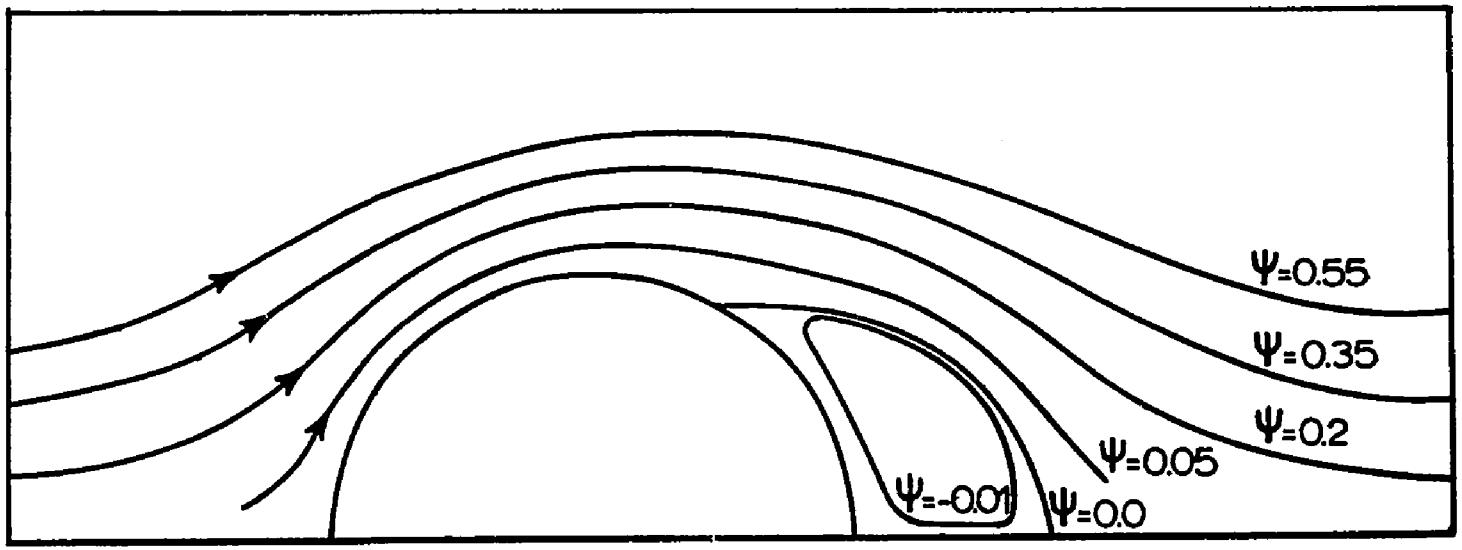

Fig. 54 Streamlines at t=?.0 for Flow Past a Circular Cylinder at R=100.

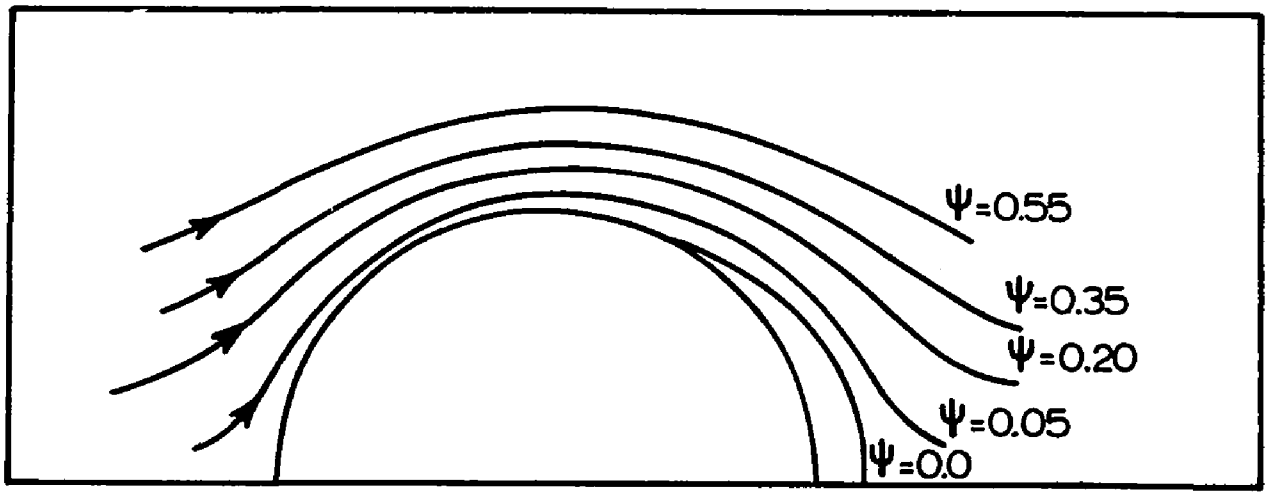

Fig. 55 Streamlines at t=1.0 for Flow Past a Circular Cylinder at R=500.

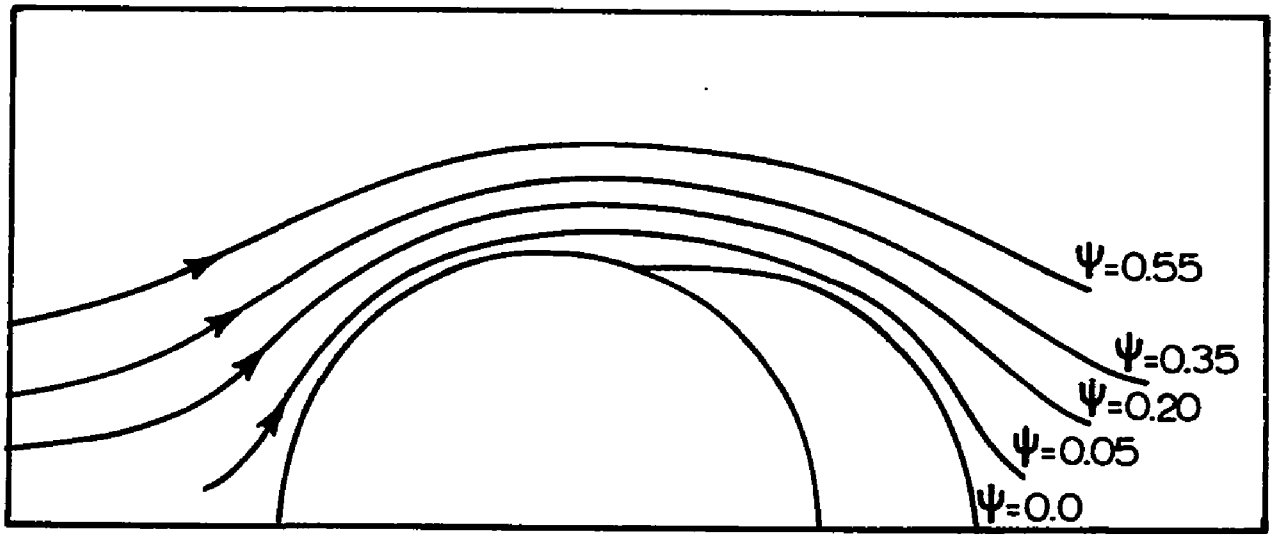

Fig. 56 Streamlines at t=2.0 for Flow Past a Circular Cylinder at R=1000.

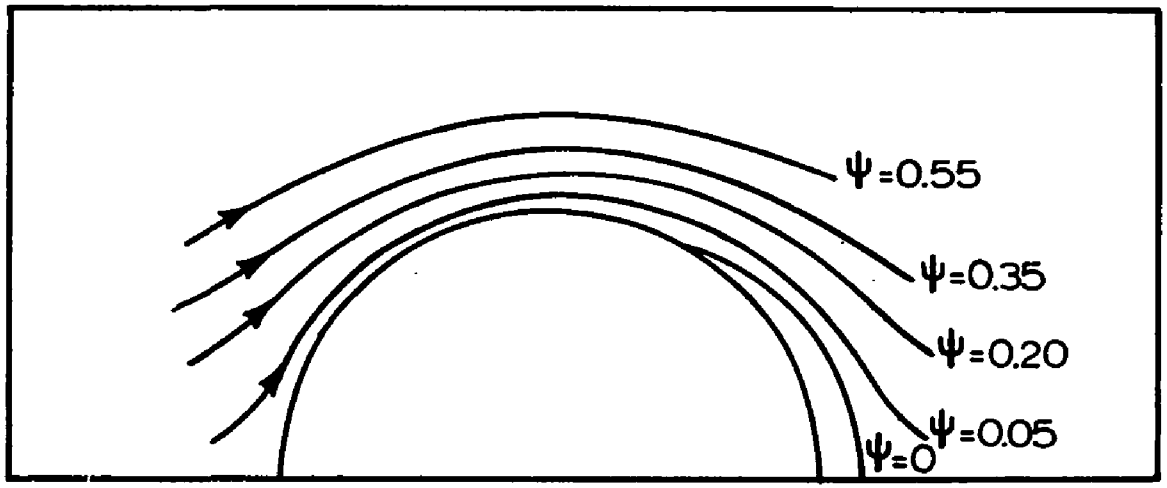

Fig. 57 Streamlines at t=1.0 for Flow Past a Circular Cylinder at R=1000.

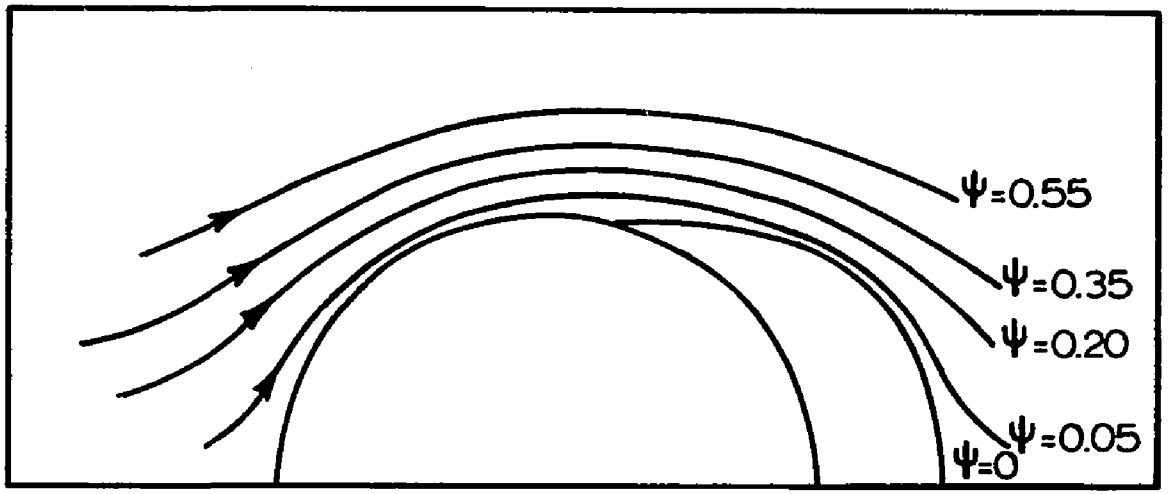

Fig. 58 Streamlines at t=2.0 for Flow Past a Circular Cylinder at R=1000.

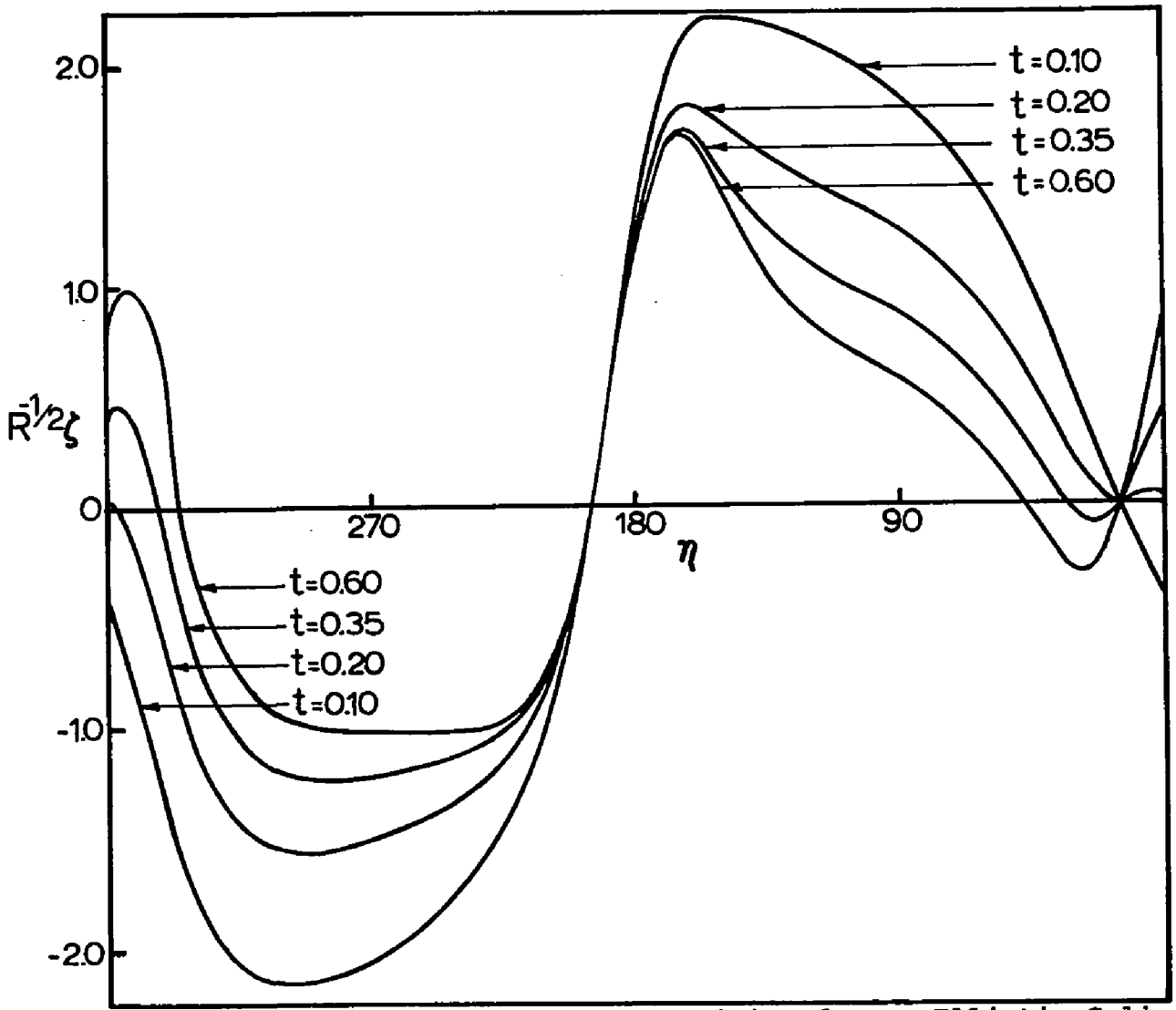

Fig. 59 Temporal Development of Surface Vorticity for an Elliptic Cylinder of Aspect Ratio 0.6 at γ=1.5° for the Boundary-Layer Solution obtained from the Fully-Numerical Procedure.

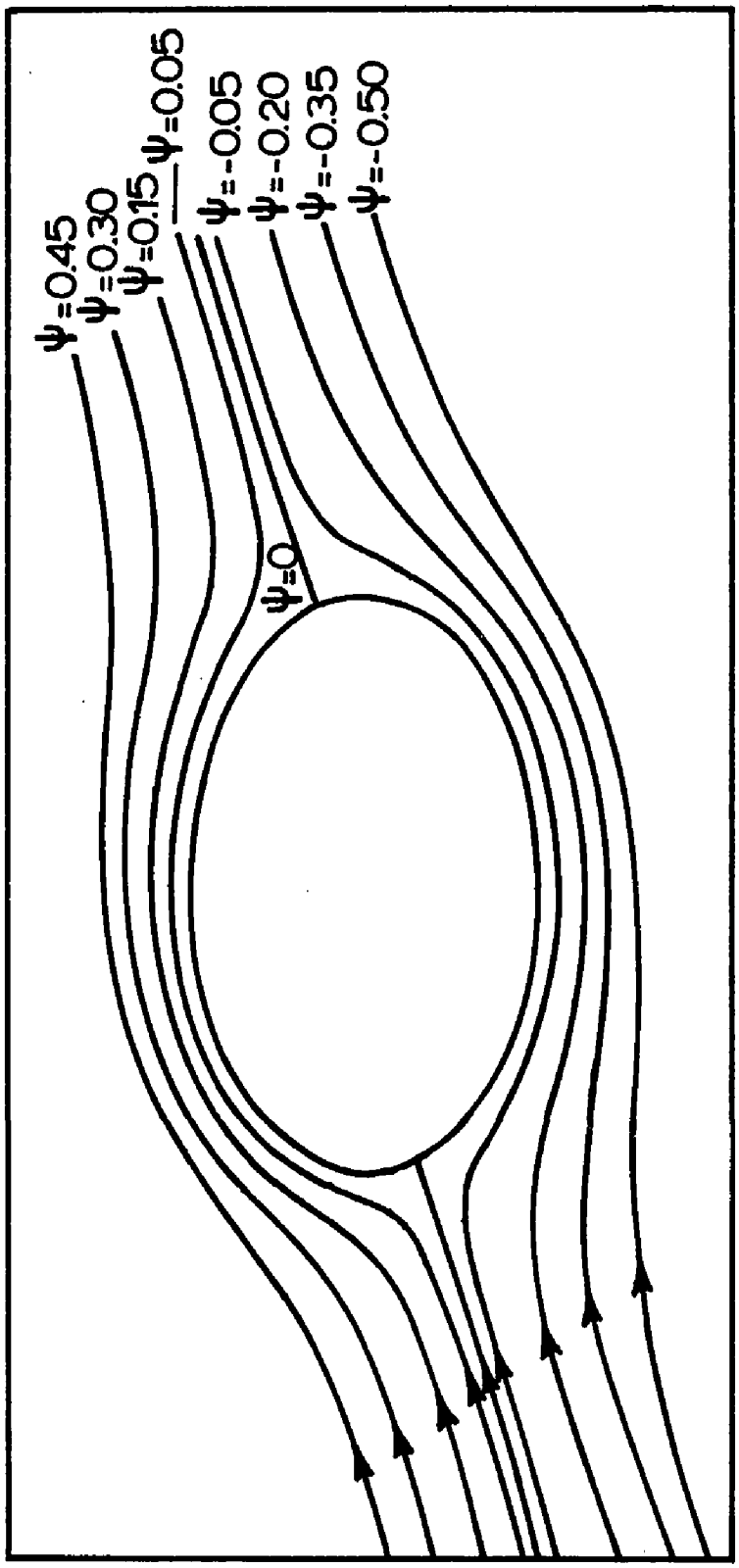

Fig. 60 Streamlines at t=0.15 for an Elliptic Cylinder of Aspect Ratio 0.6 at γ=15° from the Boundary-Layer Solution obtained by the Fully-Numerical Procedure; R set to 100.

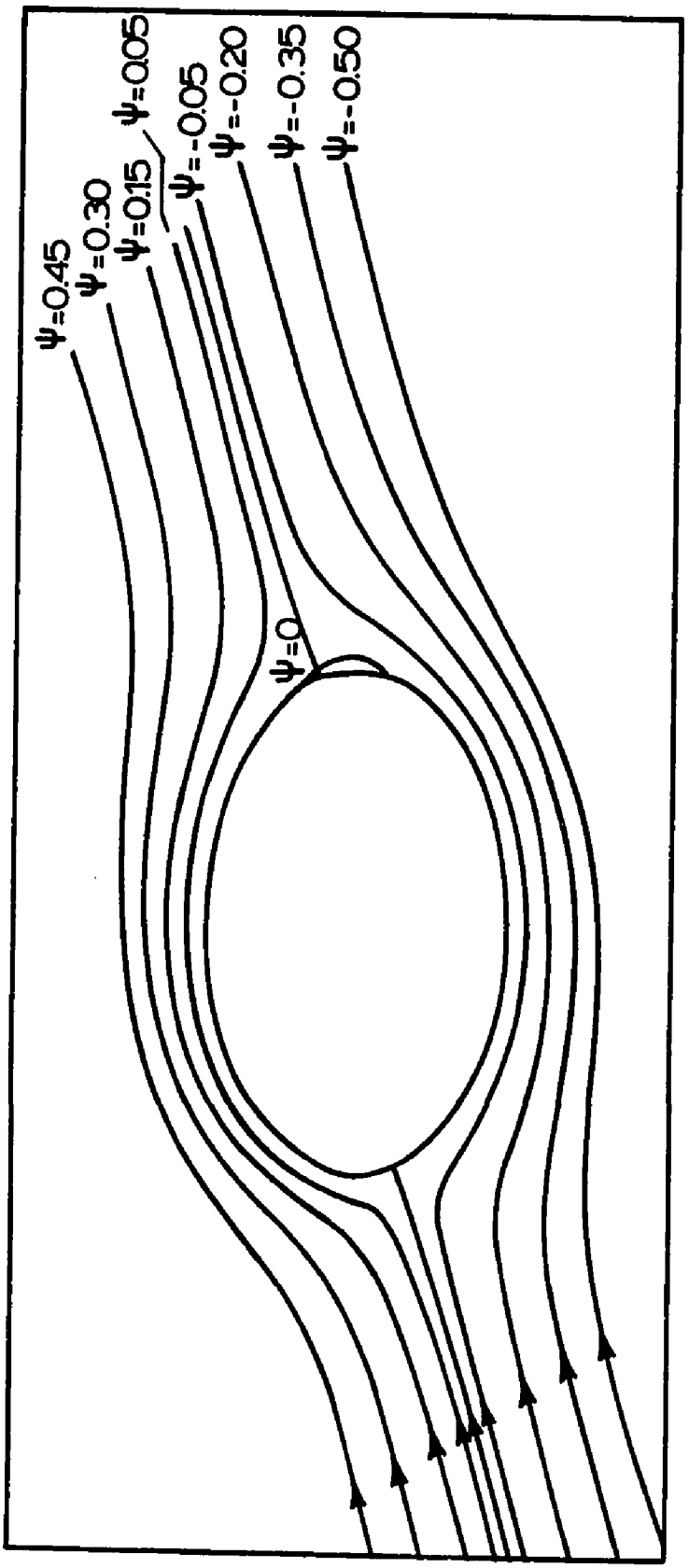

Fig. 61 Streamlines at t=0.25 for an Elliptic Cylinder of Aspect Ratio 0.6 at γ=15° from the Boundary-Layer Solution obtained by the Fully-Numerical Proc-dure; R set to 100.

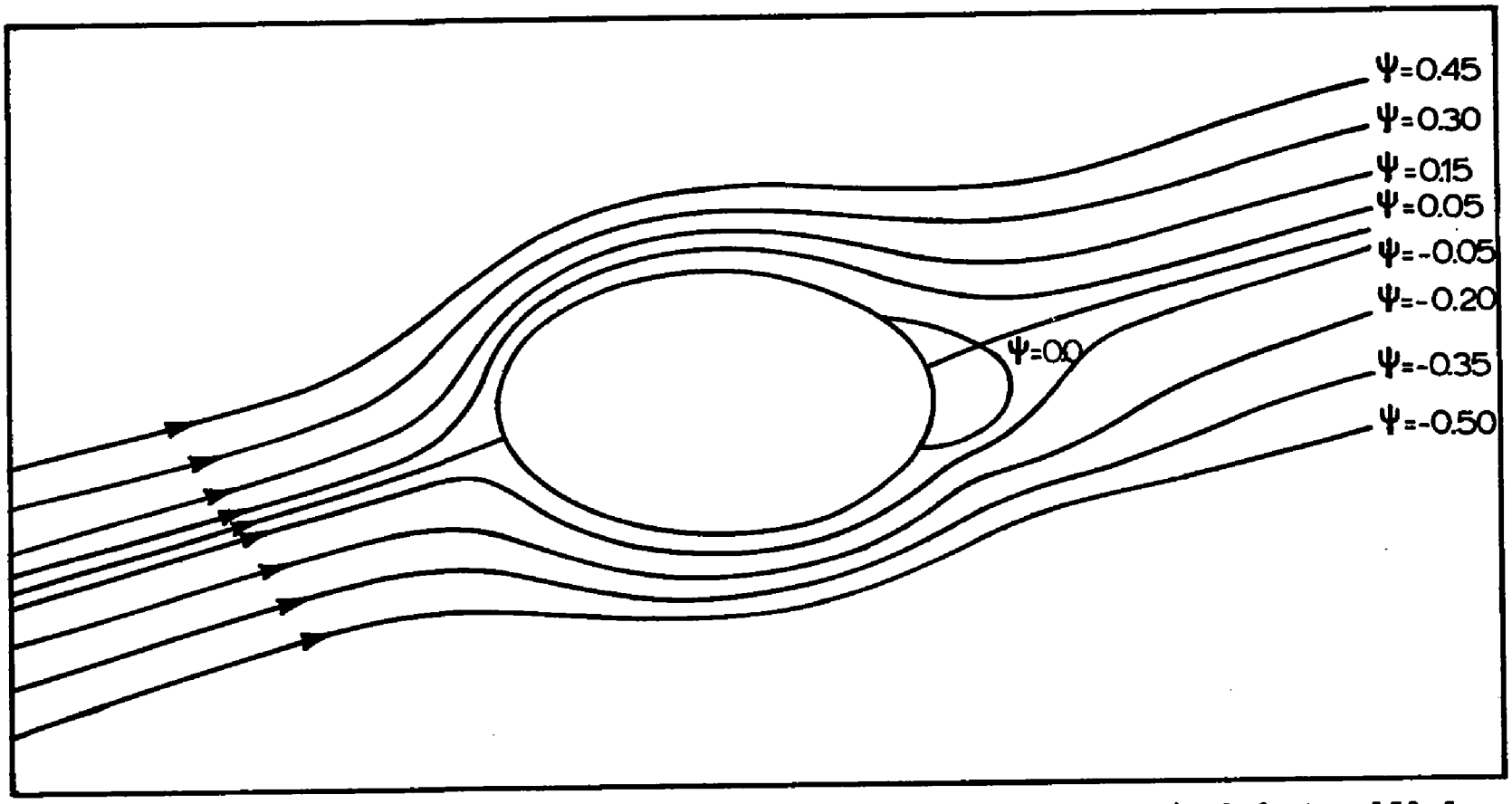

Fig. 62 Streamlines at t=0.45 for an Elliptic Cylinder of Aspect Ratio 0.6 at γ=15° from the Boundary-Layer Solution obtained by the Fully-Numerical Procedure; R set to 100.

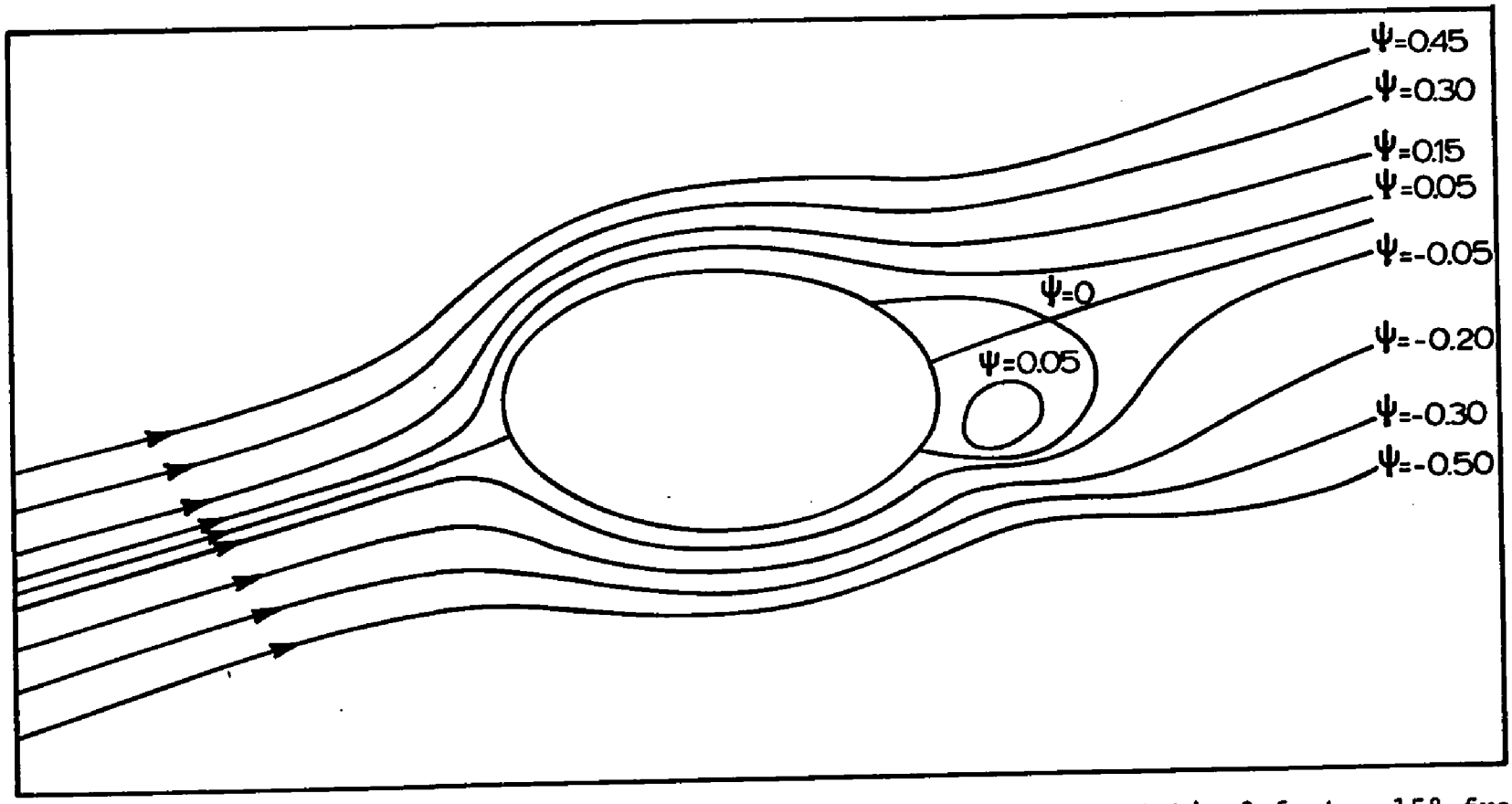

Fig. 63 Streamlines at t=0.60 for an Elliptic Cylinder of Aspect Ratio 0.6 at γ=15° from the Boundary-Layer Solution obtained by the Fully-Numerical Procedure; R set to 100.

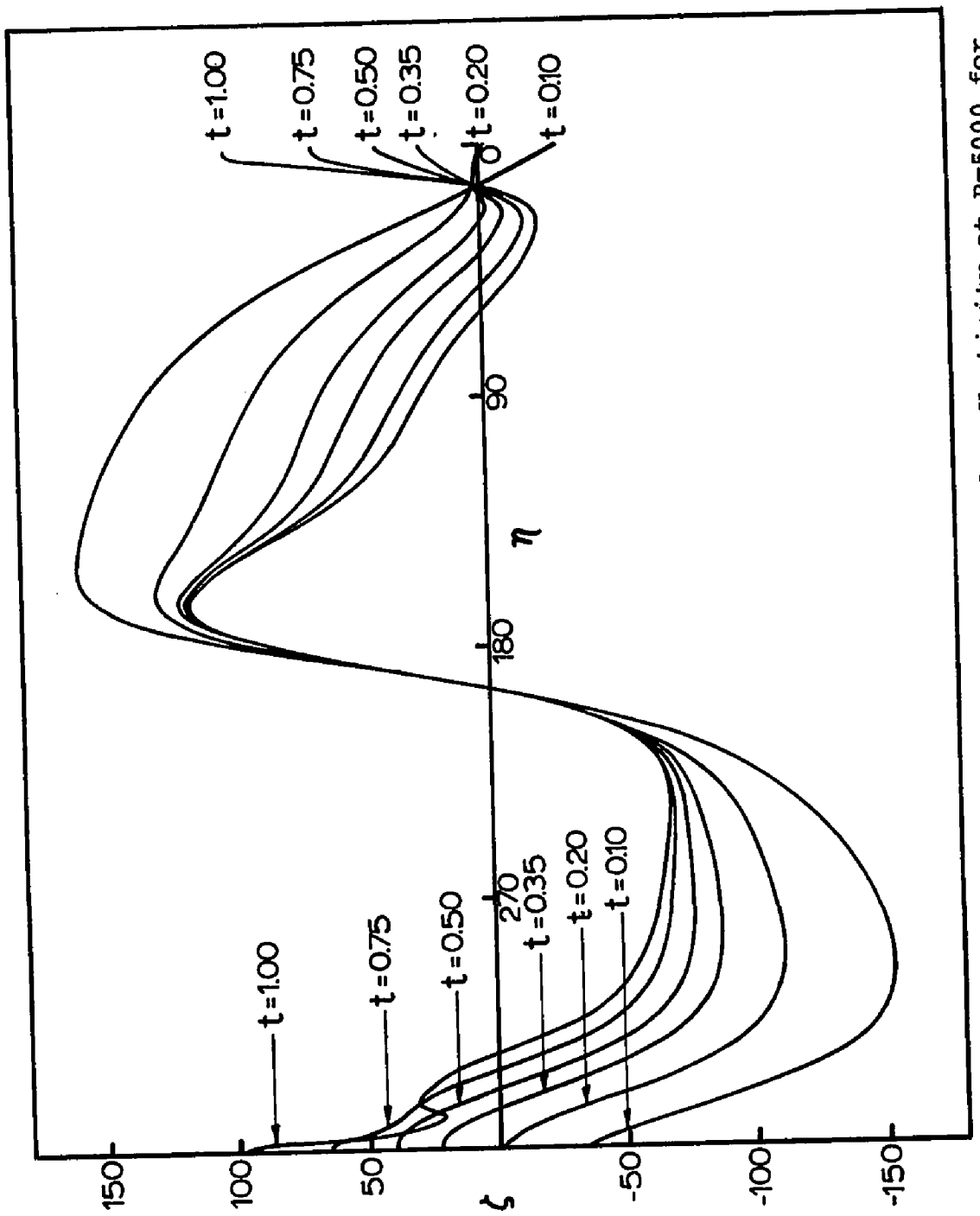

Fig. 64 Temporal Development of the Surface Vorticity at R=5000 for τ_1=0.6 at γ=15° using the Fully-Numerical Method.

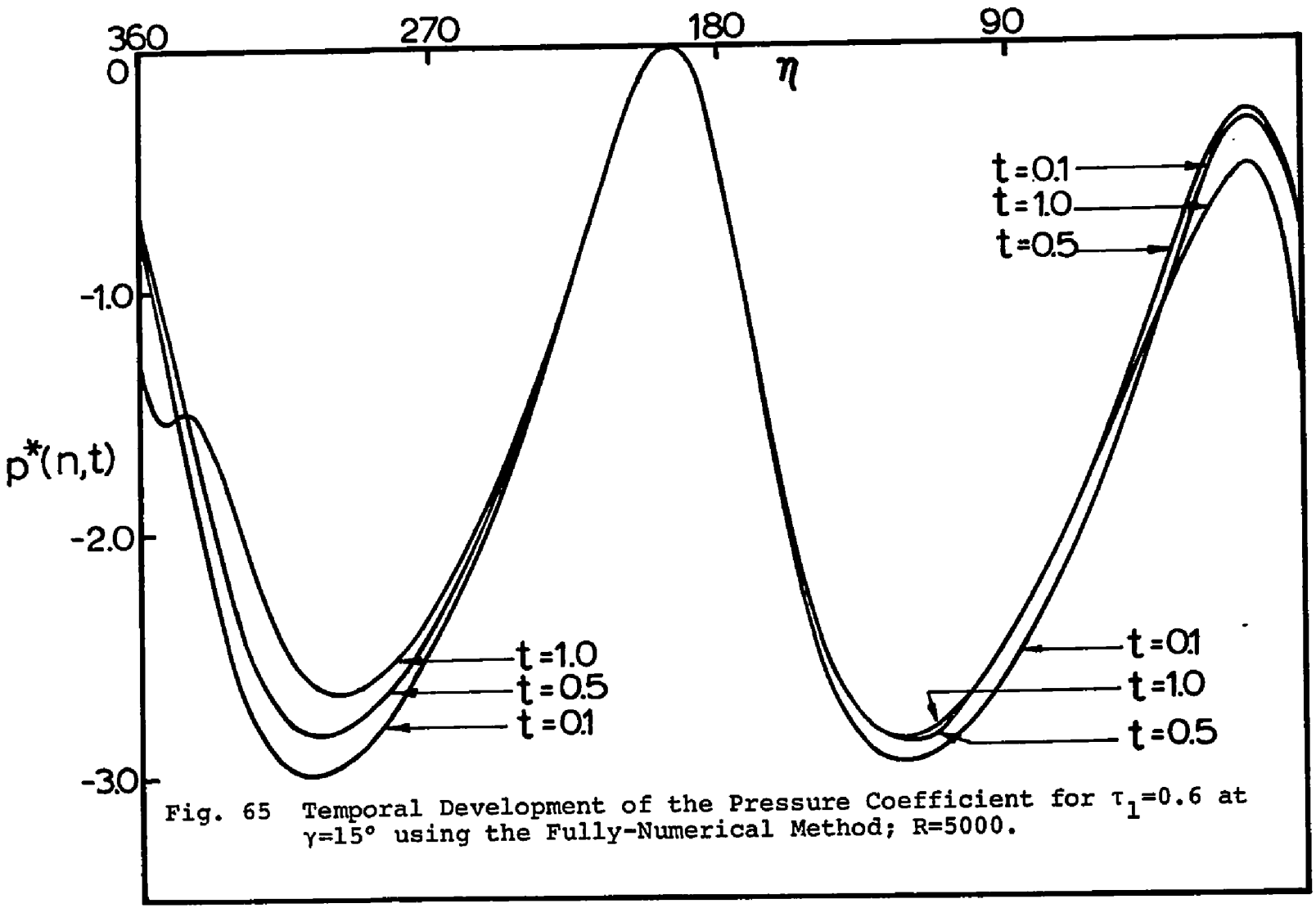

Fig. 65 Temporal Development of the Pressure Coefficient for τ_1=0.6 at γ=15° using the Fully-Numerical Method; R=5000.

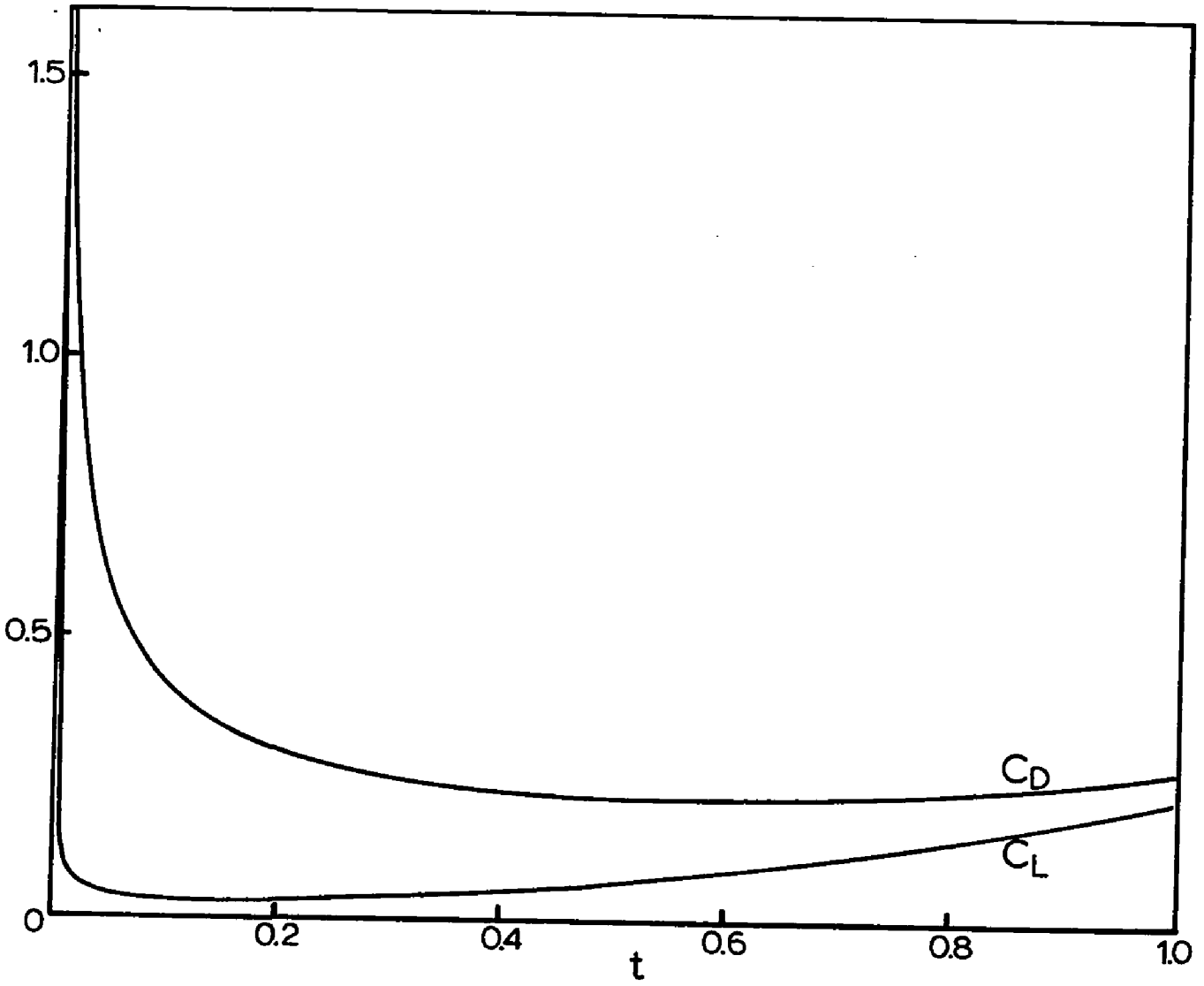

Fig. 66 Variation of the Drag and Lift Coefficients with Time for τ_1=0.6 at γ=15°, using the Fully-Numerical Method; R=5000.

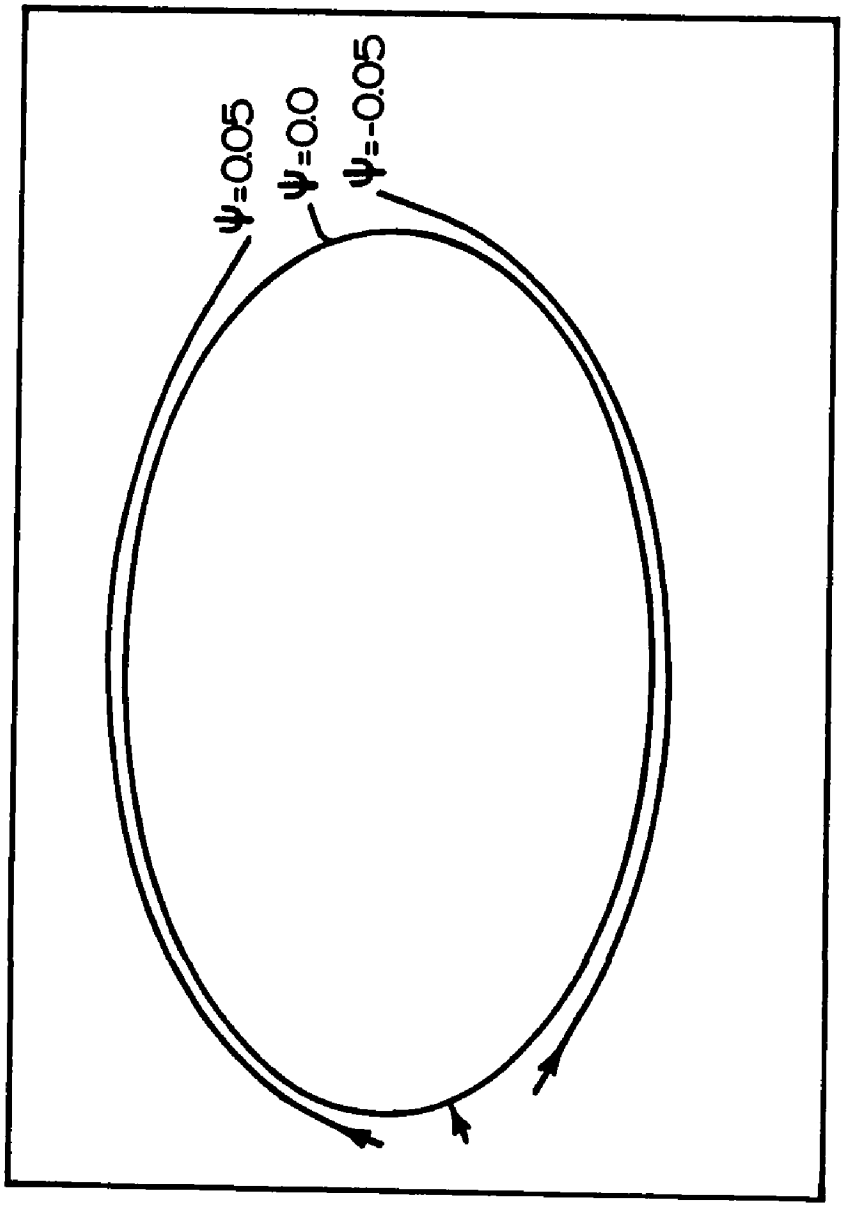

Fig. 67 Streamlines at t=0.2 for τ_1=0.6 at γ=15° using the Fully-Numerical Method; R=5000.

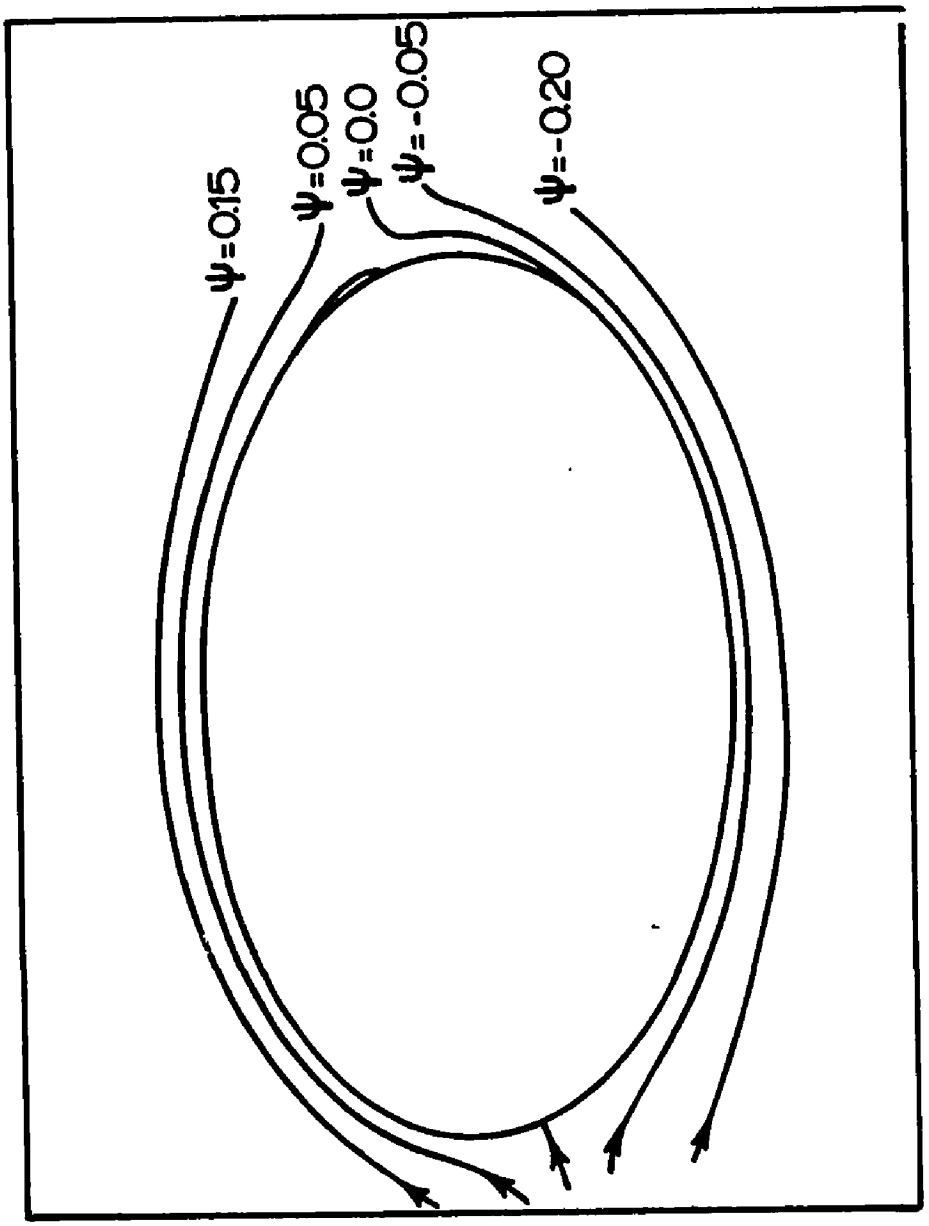

Fig. 68 Streamlines at t=0.6 for τ_1=0.6 at γ=15° using the Fully-Numerical Method; R=5000.

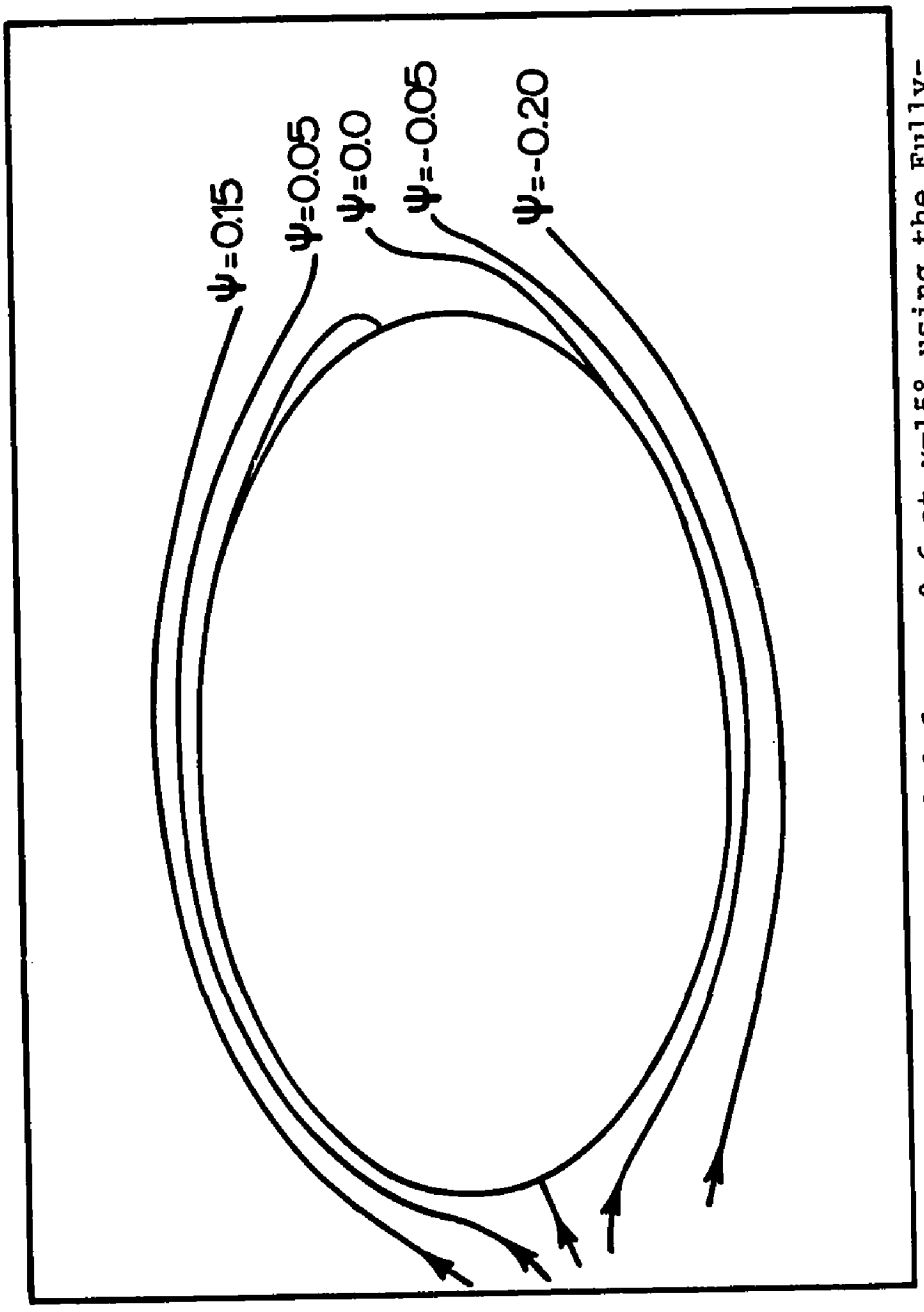

Fig. 69 Streamlines at t=1.0 for τ_1=0.6 at γ=15° using the Fully-Numerical Method; R=5000.